The biological evaluation of inhibitors of the Keap1-Nrf2 protein-protein interaction

Marjolein Charlotte Andrea Schaap

August 2015

A thesis submitted for the degree of Doctor of Philosophy of University College London

Department of Pharmaceutical and Biological Chemistry
UCL School of Pharmacy

Plagiarism statement

This thesis describes research conducted in the UCL School of Pharmacy, between 1st October 2011 and 1st March 2015 under the supervision of Dr. Geoff Wells. I certify that the research described is original and that any parts of the work that have been conducted by collaboration are clearly indicated. I also certify that I have written all the text herein and have clearly indicated by suitable citation any part of this dissertation that has already appeared in publication.

Signed…….. **Date……..**

Abstract

The Keap1-Nrf2 pathway has been identified as a key regulator of the cytoprotective response of cells when exposed to oxidative stress. The induction of detoxification gene products by increasing the activity of the transcription factor nuclear factor erythroid 2-related factor 2 (Nrf2) can be used as a chemopreventive approach to cancer treatment. Natural and synthetic agents can disrupt the interaction between the substrate adaptor protein Kelch-like ECH-associated protein 1 (Keap1) and Nrf2, which allows nuclear Nrf2 translocation and accumulation. The aim of this project was to characterize the behaviour of direct and indirect Nrf2 inducer molecules by applying several biological methods that were specifically optimised or developed for the Keap1-Nrf2 pathway. Potential inhibitors of the Keap1-Nrf2 complex were screened using a cellular NQO1 induction assay and an *in vitro* fluorescence polarisation (FP) assay for direct inhibitors. A novel *in vitro* Förster resonance energy transfer (FRET) assay was developed as an additional screening tool to identify Keap1 binding partners. Further biological evaluation was conducted with the most promising molecules using western blotting analysis and a new intracellular Nrf2 staining method for flow cytometry. The natural product and indirect Nrf2 inducer sulforaphane was used as a reference compound (NQO1 CD = 0.4 μM). From a library of Michael acceptor-containing cyclohexadienone analogues, a 3-chlorophenyl compound (**6.49**) was identified as a potent inducer (NQO1 CD = 1 μM). Stearoyl-capped Nrf2-derived peptides were potent inhibitors of the direct Keap1-Nrf2 protein-protein interaction and showed promising cell penetrating properties. Direct inhibitor small molecules included two bis-sulphonamide derivatives (**7A4**, NQO1 CD = 8 μM and **7B1**, NQO1 CD = 4 μM) and a 1,2,3-triazole derivative (**7C55**, NQO1 CD = 0.6 μM) with FP IC_{50} values in the nano- to micromolar range. The selectivity of the compounds was assessed by revealing potential aryl hydrocarbon receptor (AhR) transcription factor cross-talk.

Table of Contents

Abbreviations

ABC – ATP-binding cassette

AhR – Aryl hydrocarbon receptor

Akt – Alpha serine or threonine-protein kinase

α-MEM – Alpha modified eagle medium

AOS – Antioxidant

APS – Ammonium persulfate

ARE – Antioxidant Response Element

Arg – Arginine

ARNT– AhR nuclear translocator

ATCC – American Type Culture Collection

ATP – Adenosine triphosphate

Asp – Aspartate

BHA – Butylated hydroxyanisole

B_{max} – Maximum number of binding sites

BP – Band Pass

BRCA1/BRCA2 – Breast cancer type 1/2 susceptibility protein

BSA – Bovine serum albumine

BTB – Broad complex Tramtrack Bric-a-brac

bZIP – Basic Leucine Zipper Domain

CD – Concentration to double the NQO1 enzymatic activity

CDDO – 2-Cyano-3,12-dioxooleana-1,9(11)-dien-28-oic acid

cDNA – Complementary deoxyribonucleic acid

CER – Cytoplasmic extraction reagent

CNC – Cap ‘n’ collar

Cpds – Compounds

CUL3 – Cullin 3

CYP1A1 – Cytochrome P450, family 1, subfamily A, polypeptide 1

DAPI – 4',6-diamidino-2-phenylindole

DAS – Diallyl sulfides

DGR – Double glycine repeat

DMEM – Dulbecco's modified eagle medium

DMF – N,N’-dimethylformamide

DMSO – Dimethyl sulfoxide

DNA – Deoxyribonucleic acid

DSF – Differential scanning fluorimetry

DTT – Dithiothreitol

ECACC – European Collection of Cell Culture

eCFP – Enhanced cyan fluorescent protein

ECL – Enhanced chemiluminescence

EDTA – Ethylenedinitrilotetracetatic acid

EGCG – Epigallocatechin-3-gallate

ELISA – Enzyme-linked immune assay

EMEM – Eagle minimal essential medium

EMSA – Electrophorectic mobility shift assay

ERK – Extracellular-signal-regulated kinase

eYFP – Enhanced yellow fluorescent protein

FAD – Flavin adenine dinucleotide disodium salt hydrate

FBS – Fetal bovine serum

FD – Fold difference or fold change

FDA – Food and drug administration

FE – FRET efficiency

2D-FIDA – Two-dimensional fluorescence intensity distribution analysis

FITC – Fluorescein isothiocyanate

FP – Fluorescence polarisation

FRET – Förster resonance energy transfer

FSC – Forward scattered light

G – Gravitational force

GFP – Green fluorescent protein

Glu – Glutamate

GSH – Glutathione

GST – Glutathione S-transferase

G6P – Glucose-6-phosphate

G6PD – Glucose-6-phosphate dehydrogenase

HEK293 – Human embryonic kidney cells 293

HeLa – Henrietta Lacks

His – Histadine

HO-1 – Hemeoxygenase 1

HPLC – High-performance liquid chromatography

HRP – Horseradish peroxidase

Hsp90 – Heat shock protein 90

HTS – High throughput screening

IC_{50} – Inhibition constant

IMAC – Immobilised metal ion affinity chromatography

IPTG – Isopropylthio-β-D-galactosidase

ITC – Isothermal calorimetry

ITCs – Isothiocyanates

IVR – Intervening region

JNK – Jun N-terminal kinase

Kan – Kanamycin

K_d – Dissociation constant

Keap1 – Kelch-like ECH associated protein 1

LB – Luria Bertani

MAPK – Mitogen-Activated Protein Kinase

MCF-7 – Michigan Cancer Foundation-7

(n)MFI – (normalised) median fluorescence intensity

mRNA – Messenger ribonucleic acid

MTT – Thiazolyl blue tetrazolium Bromide

MWCO – Molecular weight cut off

NER – Nuclear extraction reagent

NMR – Nuclear Magnetic Resonance

NADP(H) – Nicotinamide adenine dinucleotide phosphate

NQO1 – NAD(P)H:quinone oxidoreductase 1

Nrf2 – Nuclear transcription factor erythroid 2p45 (NF-E2)-related factor

PAH – Polycyclic aromatic hydrocarbons

PBS – Phosphate buffered saline

PCR – Polymerase chain reaction

PFA – Paraformaldehyde

Pfu – Pyrococcus furiosus

PKC – Protein kinase C

PPI – Protein-protein interaction

PI3 – Phosphatidylinositol-4,5-bisphosphate 3-kinase

RNS – Reactive nitrogen species

ROS – Reactive oxygen species

RPM – Revolutions per minute

RT – Room temperature

SAR – Structure-activity relationship

SDS – Sodium dodecyl sulphate

SDS-PAGE – Sodium dodecyl sulphate polyacrylamide gel electrophoresis

SE – Sensitised emission

shRNA – Short hairpin ribonucleic acid

siRNA – Short interference ribonucleic acid

SPR – Surface plasmon resonance

SRB – Sulforhodamine B

SSC – Side scattered light

TAT – Transactivator of transcription

TBE – Tris-Borate-EDTA buffer

tBHQ – *tert*-Butylhydroquinone

TCA – Trichloroacetic acid

TCDD – 2,3,7,8-Tetrachlorodibenzo-p-dioxin

TEMED – *N*,*N*,*N*',*N*'-tetramethylethylene diamine

TEV – Tobacco Etch Virus

Tm – Melting temperature

TMB – Tetramethylbenzidine

Tris – Tris(hydroxymethyl)aminomethane

TS – Tris sodium

Tween®-20 – Polyethylene glycol sorbitan monolaurate

UGT – UDP-glucuronosyltransferase

USP15 – Ubiquitin specific peptidase 15

WT – Wild-type

XME – Xenobiotic-metabolizing enzymes

XRE – Xenobiotic response element

Acknowledgements

First of all, I would like to thank my supervisor Dr. Geoff Wells for his guidance and advice over the course of my PhD. In particular, his expertise in medicinal chemistry was invaluable in helping me with various aspects of the project. He has taught me to be critical of my own work and stimulated me to work autonomously. I wish to thank my second supervisor Dr. Andrew Wilderspin for his support in developing and optimising diverse biochemical methods. Thanks also to my group and lab members, past and present, for their support and companionship. I would like to thank my family and friends for their huge support and encouragement. To Mum and Dad, for always being there for me. To Ben, for his endless patience, motivation and for reminding me never to give up. To all my friends in the Netherlands and the UK, for listening to my trials and tribulations of my PhD and for making me laugh. And last but not least, thanks to Cancer Research UK for making this research project possible.

1. Introduction

1.1 Cancer statistics

Cancer is one of the key causes of world-wide mortality and was responsible for more than one in four deaths in the UK in 2011 [1]. Moreover, every two minutes in the UK somebody receives the diagnosis of cancer [2]. As a result of improvements in public awareness and screening methods, the overall mortality rate is decreasing [1]. However, the incidence rates have risen by 43% in females and 23% in males since the mid-1970s [3]. For example, the frequency of people diagnosed with cancers of the kidney, liver, skin, oral and womb have increased. These cancers could be associated with lifestyle habits, such as smoking and high alcohol, salt and fat intake [4]; poor lifestyle factors were related to 34% of cancers in 2010 in the UK [5]. A study from 2012 [6] predicted that the worldwide cancer incidence rate will rise from 12.7 million new cases in 2008 to 22.2 million by 2030. The cost of cancer care in the EU has been estimated to be 23.2 billion euros in 2009 alone [7]. Considering the widespread impact of this disease on individuals, their families and on society, there is a large research effort targeted at finding effective treatments.

1.2 Current cancer treatments

The choice of cancer therapy often depends on the type of cancer that is diagnosed, with surgery, chemotherapy and radiotherapy being the most common treatments [8]. Surgery can be used as a preventive measure to remove pre-cancerous tissue such as a mole that is changing in appearance or a polyp found in the colon [9]. Moreover, a mastectomy may prevent the development of breast cancer in women with inherited mutations in BRCA1 or BRCA2 genes [9]. Exploratory surgery can also be applied as a tool to diagnose or stage cancer [9]. Curative surgery is often used to remove cancerous tissue as well as normal tissue to minimise the risk of cancer relapse and is often practiced alongside chemo- or radiotherapy [9]. Chemotherapy was first used in the 1940s by administration of nitrogen mustards and antifolate drugs to treat Hodgkin's lymphoma [10]. However, modern chemotherapy has developed over the years into the use of different classes of cytotoxic drugs such as alkylating agents, antimetabolites, anthracyclines, topoisomerase inhibitors, mitotic inhibitors and additional agents such as corticosteroids [11]. Generally, cytotoxic

drugs used for chemotherapy elicit their effects by inhibition of the relatively high cellular proliferation rate of cancer cells. Yet, healthy dividing cells including hair follicles, bone marrow and the lining of the digestive tract, may also be affected by chemotherapy [12]. Radiation therapy uses ionising radiation that releases energy as it sensitises cancer cells. This energy causes DNA damage and thus prevents cellular proliferation of cancer [13]. Other treatments include immunotherapy, oncolytic virotherapy and gene transfer; immunotherapy aims to improve the effectiveness of the body's own immune system to target cancerous cells [14], oncolytic virotherapy destroys tumours by using viral particles that replicate inside cancerous cells and gene transfer makes use of the introduction of new genes into cancer cells that cause cell death [15]. Although, numerous successes have been achieved with current treatments, none of them are without risks or side effects; hence a preventive approach might be more suitable.

1.3 Carcinogenesis and chemoprevention

The process of carcinogenesis involves three different stages; initiation, promotion and progression [16] (Figure 1.1). The onset of the carcinogenic process, initiation, results from irreversible genetic damage by chemical carcinogens, ionising radiation or viral gene insertion (e.g. human papilloma virus). Chemical carcinogens and ionising radiation can generate reactive oxygen species (ROS) during their metabolism, thereby causing DNA damage [17]. The active proliferation and accumulation of mutated cells is recognised as the reversible process of promotion [16]. The final stage involves the irreversible conversion of pre-neoplastic cells to a malignant cell population and is characterised by the invasive and metastatic growth of a tumour [17].

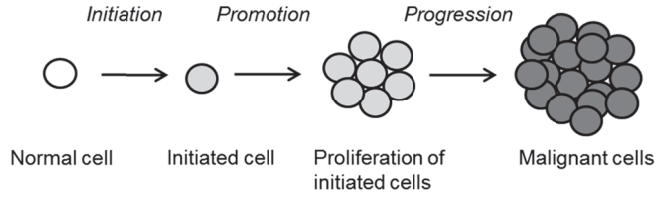

Figure 1.1: Schematic representation of the three stages of carcinogenesis.

Reactive oxygen species (ROS) are highly unstable and reactive molecules that are derived from the metabolic reduction of oxygen. They include species such as superoxide anion radicals ($O_2^{-\bullet}$), singlet oxygen (O_2), hydrogen peroxide (H_2O_2) and hydroxyl radicals ($OH^{\bullet}$), which can cause cell damage at sustained high concentrations [18]. Reactive nitrogen species (RNS) are nitric oxide and related superoxide derivatives that can be as reactive and damaging to cells as ROS. ROS can be a by-product of normal essential metabolic processes in the body, such as mitochondrial respiration and intracellular signalling [18]. They may also be derived from external sources including pollutants, tobacco smoke or UV exposure. Antioxidants (AOS) are naturally occurring stable molecules that can reduce ROS by donating an electron to a free radical, thus reducing potential cell damage [19]. A balance between ROS and antioxidants is important for maintaining physiological processes in the body. However, a state of oxidative stress originates from an imbalance between those two molecular species; hence, sustained levels of oxidative stress can cause disruptions in cellular signalling and may contribute to the development of cancer and other diseases (Figure 1.2).

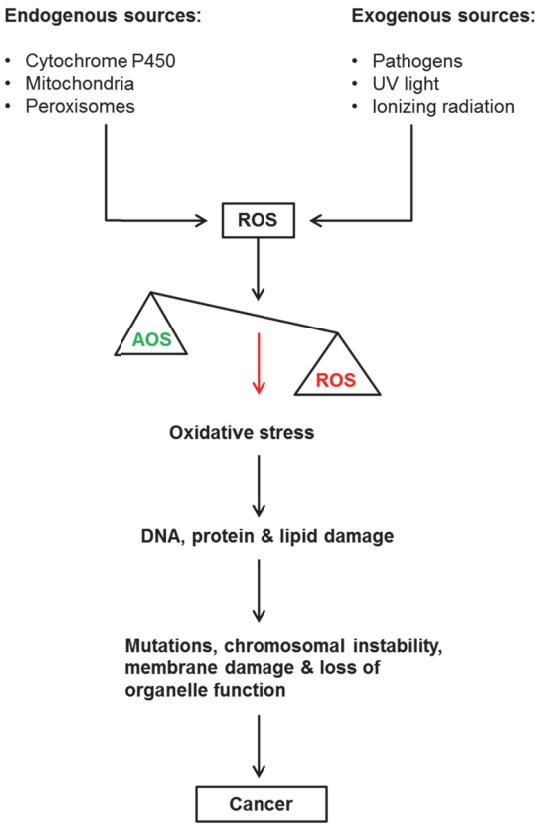

Figure 1.2: The relation between the production of ROS and the development of cancer. Adapted from [20].

The term chemoprevention was first used by Michael Sporn in 1976 and is described as the use of non-toxic chemicals of either natural or synthetic origin to inhibit, block or reverse carcinogenesis in its early stages [21]. The two types of chemopreventive agents are described as blocking or suppressing compounds [22] (Figure 1.3). Blocking agents inhibit cancer initiation by scavenging free radicals or by inducing antioxidant activity and thus reducing the level of mutations and cell damage. Suppressing agents prevent promotion and progression of initiated cells by inhibiting cell proliferation or inducing apoptosis [23-24].

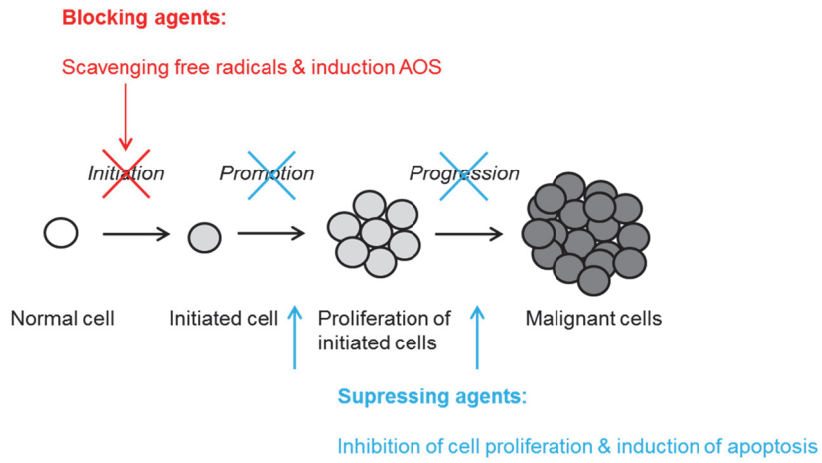

Figure 1.3: Mode of action of two types of chemoprevention: blocking and supressing agents.

Blocking agents prevent carcinogens from causing DNA damage by stimulating their detoxification, which is an aspect of the xenobiotic metabolism. It is proposed that the metabolism and excretion of foreign xenobiotic chemicals (e.g. drugs, pollutants and food substances) reduces their impact on host cells and limits their carcinogenic potential [25]. Phase I (hepatic) enzymes, such as the cytochrome P450s, are responsible for the bioactivation of xenobiotics via oxidation, reduction, hydrolysis and/or hydration processes [25]. Numerous carcinogens (or pro-carcinogens) require bioactivation via phase I metabolism. The arylhydrocarbon receptor (AhR) is a ligand dependent transcription factor that interacts with xenobiotic responsive elements (XREs), which lie upstream of ligand inducible genes encoding both phase I (e.g. CYP1A1) and phase II metabolic enzymes (e.g. NQO1) (Section 1.7). Transferase or phase II enzymes, such as glutathione *S*-transferases (GSTs), hemeoxygenase 1 (HO-1), glucoronidases, NAD(P)H:quinone oxidoreductase-1 (NQO1) and UDP-glucuronosyltransferase (UGT), along with

small molecules such as glutathione (GSH) are responsible for the conjugation of polar groups to the phase I activated metabolites [26]. Phase II enzymes are associated with the detoxification of xenobiotics by increasing their hydrophilic character and by preparing them for excretion via ATP-binding cassette (ABC) drug transporters found in the kidney, liver and intestine (phase III) [25]. Several blocking agents were found to increase the detoxification of pro-carcinogens by up-regulating the expression of phase II enzymes [27]. At the genetic level, the antioxidant response element (ARE) is a DNA sequence (5′-TGACNNNGC-3′) [28] that lies upstream of the promoter region of several phase II gene products, including GSTs, NQO1, UGT and HO-1 [27]. The transcription of ARE-driven genes is largely controlled by the transcription factor nuclear factor-erythroid 2-related factor 2 (Nrf2) and its regulator protein Kelch-like ECH-associated protein 1 (Keap1) [27, 29].

1.4 Keap1 – Nrf2 pathway

The nuclear factor erythroid 2-related factor 2 (Nrf2) (66 kDa) is a basic leucine zipper (bZip) transcription factor that is a member of the cap 'n' collar (CNC) family [30]. The basic leucine zipper domain is a DNA binding domain that is able to bind to AREs that are positioned in the upstream regulatory regions of cytoprotective genes. The bZip domain is part of the Neh1 domain of Nrf2. The transcription factor contains five other highly conserved domains, Neh2 – Neh6 (Figure 1.4). The Neh2 domain binds to the Kelch domain of Kelch-like ECH-associated protein 1 (Keap1) via high affinity motif ETGE and weaker affinity motif DLG, both Neh1 and Neh3 domains are responsible for the heterodimerisation with small musculoaponeurotic (Maf) proteins, the domains Neh3 - Neh5 recruit different co-activators for the activation of transcription [31-32] and the Neh6 domain mediates the degradation of Nrf2 via a redox insensitive mechanism [33]. Recently, it was found that Nrf2 protein levels are regulated by two β-transducin repeat-containing protein (β-TrCP) binding sites in the Nrf2-Neh6 domain [34]. Chowdry *et al*. [34] demonstrated a decrease in β-TrCP mediated ubiquitination of Nrf2 upon deletion of either recognition motif. Moreover, glycogen synthase kinase-3 (GSK-3), a serine/threonine protein kinase, showed to affect the activity of one of the β-TrCP binding sites [34].

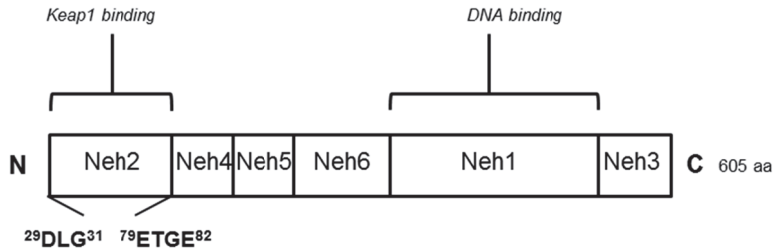

Figure 1.4: Nrf2 domain structure with indicated binding domains. The Neh2 domain contains the DLG motif (residues 29 – 31) and the ETGE motif (residues 79 – 82). Adapted from [35].

Keap1 (69 kDa) is a substrate adaptor protein for Cullin3 (Cul3)-based ubiquitin E3 ligase and contains three main domains; the Cullin3 binding broad complex, tramtrack and broad complex tramtrack bric-a-brac (BTB) homodimerisation domain, the cysteine rich intervening region (IVR) and the Nrf2 binding Kelch or double glycine repeat (DGR) domain [36-37] (Figure 1.5).

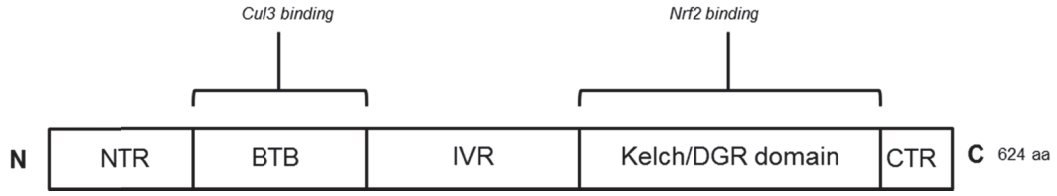

Figure 1.5: Keap1 domain structure with indicated binding domains. Adapted from [35].

Under basal conditions Keap1 negatively regulates Nrf2; the substrate adaptor protein sequesters the transcription factor in the cytoplasm and targets it for ubiquitination and 26S proteosomal degradation via the Cul3-Rbx1 E3 ubiquitin ligase complex [38] (Figure 1.6). This process results in the rapid degradation of the transcription factor, with Nrf2 demonstrating a half-life of only 20 minutes [39]. Following exposure to stressors; i.e. ROS, RNS or electrophiles, reactive cysteine residues (C151, C257, C273, C288, and C297) in the IVR of Keap1 [40] are modified. This modification is thought to cause a conformational change that reduces the binding affinity for Nrf2 [40]. Nevertheless, recent evidence has emerged that this cysteine modification does not affect the Keap1-Nrf2 PPI, but instead impairs the ubiquitination and proteosomal degradation of Nrf2 [41]. Besides the electrophilic modifications of cysteine residues in Keap1, Nrf2 also undergoes post-translational modifications, including PKC phosphorylation of serine residue 40 [42].

The transcriptional Nrf2 activation is under control of other signalling pathways such as, JNK, PI3K/Akt, ERK and p38/MAPK [43]. *De novo* produced Nrf2 translocates to the nucleus where it heterodimerises with members of the small Maf protein family. This heterodimer binds the ARE sequence and initiates the transcription of ~ 200 genes that play a role in lipid metabolism, gene transcription and cytoprotection (Table 1.1) [44]. Phase II enzyme induction is an important aspect of cytoprotection and includes enzymes such as NAD(P)H quinone oxidoreductase 1 (NQO1), heme oxygenase (HO-1), thioredoxin, glutathione-S-transferases (GSTs) and the subunits of gamma-glutamylcysteine synthetase [29].

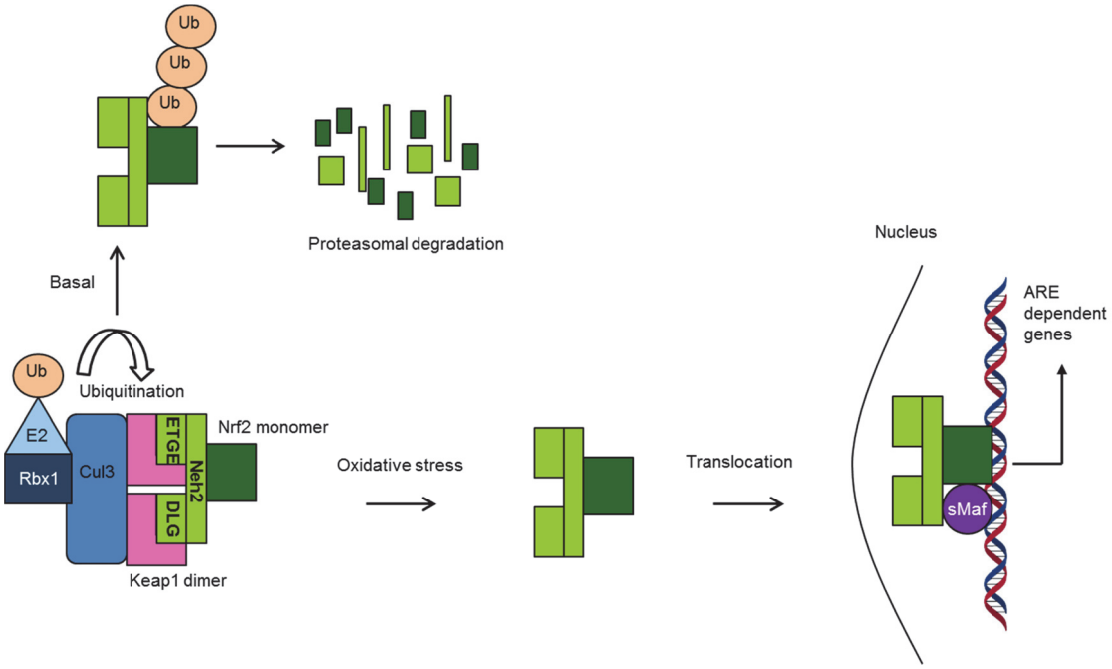

Figure 1.6: A schematic representation of the Keap1-Nrf2 pathway.

Table 1.1: Genes regulated by Nrf2 in mouse liver, lung and small intestine. Adapted from [44].

Biochemical Function	Name	Symbol
Antioxidant: GSH synthesis and inactivation of ROS	Cystine transporter	Slc7a11
	Glutamate cysteine ligase catalytic subunit	Gclc
	Glutamate cysteine ligase modifier subunit	Gclm
	Glutathione peroxidase 2	Gpx2
	Glutathione reductase 1	Gsr1
	Peroxiredoxin 1 and 6	Prxd1/6
Antioxidant: protein thiol homeostasis	Sulfiredoxin 1	Srx1
	Thioredoxin 1	Txn1
	Thioredoxin interacting protein	Txnip
	Thioredoxin reductase 1	TrxR1
NADPH regeneration enzymes	Glucose-6-phosphate dehydrogenase	G6pdh
	Malic enzyme 1	Me1
	6-Phosphogluconate dehydrogenase	Pgd
Metal-binding proteins	Ferritin heavy and light subunit	Fth/l
	Metallothionein 1 and 2	Mt1/2
General cytoprotection against stress	Heme oxygenase 1	Hmox1
	Heat shock protein 40/84/86	Hsp40/84/86
Receptors and transcription factors	Cluster of differentiation 36	CD36
	Very-low-density lipoprotein	VLDL
	MafF and K protein	MafF/K
	Nuclear factor-erythroid 2-like 2 and 3	Nrf2/3
	Arylhydrocarbon receptor	Ahr
	Peroxisome proliferator-activated receptor gamma and delta	PPARγ/δ
Phase I drug oxidation/reduction enzymes	Alcohol dehydrogenase 7	ADH7
	Aldehyde dehydrogenase-3	ALDH3
	Aldo-keto reductase 1B, 1C and 7A families	Akr1B/1C/7A
	Carbonyl reductase 1 and 3	Cbr1/3
	Carboxyl esterase	CES
	Cytochrome P450 2a4, 2a12, 4a10, 4a14, 2c39	Cyp450 2a4/2a12/4a10/4a14/2c39
	Flavin-containing mono-oxygenase 3	FMO3
	Microsomal epoxide hydrolase	Eph1
	NAD(P)H:quinone oxidoreductase 1	Nqo1
	Prostaglandin reductase 1	Ptgr1
Phase II drug-conjugating enzymes	Glutathione transferase class Alpha	Gsta1/2/3/4
	Glutathione transferase class Mu	Gstm1/2/3/4/5/6
	Glutathione transferase class Pi	Gstp1
	Glutathione transferase class Theta	Gstt1/2/3
	Microsomal glutathione transferase 3	MGST3
	Sulfotransferase 3A family	Sult3a
	UDP-glucuronosyl transferase 2B enzymes	UGT2B
Transporters	Multi-drug resistance-associated protein 2, 3, 4, 5 and 12	Mrp2/3/4/5/12
	Neutral amino acid transporter	mASCT1
	Solute carrier family 2, 5, 6, 39	SLC2/5/6/39
Protein degradation	α1-antitrypsin proteinase inhibitor	A1AT
	26S proteasome α subunits	Psma1/4/5/6
	26S proteasome β subunits	Psmb1/2/3/4/5/6
	Seqestosome-1	Sqstm1 or p62

The Keap1-Nrf2 protein-protein interaction (PPI) has been defined by molecular biology techniques and characterised structurally by NMR and X-ray crystallography methods (Figure 1.7). Two binding motifs in the Neh2 domain of Nrf2, the ^{23}LxxQDxDLG^{31} motif and the ^{77}DxETGE^{82} motif, were found to be responsible for binding to the Keap1 Kelch domain [45-46]. Both motifs form β-turn-like structures and make several electrostatic interactions with the bottom region of the *C*-terminal Kelch domain, predominantly via salt bridges between glutamate (Glu) and aspartate (Asp) residues in Nrf2 and arginine (Arg) residues 380, 415 and 483 in the Kelch domain of Keap1 [47]. The DLG motif demonstrates a 200-fold weaker affinity for Keap1 than the ETGE motif (K_d = 1000 nM *vs*. 5 nM) [47]. The acidic residues were found to be responsible for the difference in binding affinity of the DLG and ETGE motif [45]. However, both motifs are found to be essential for Keap1 driven ubiquitination of Nrf2 [48].

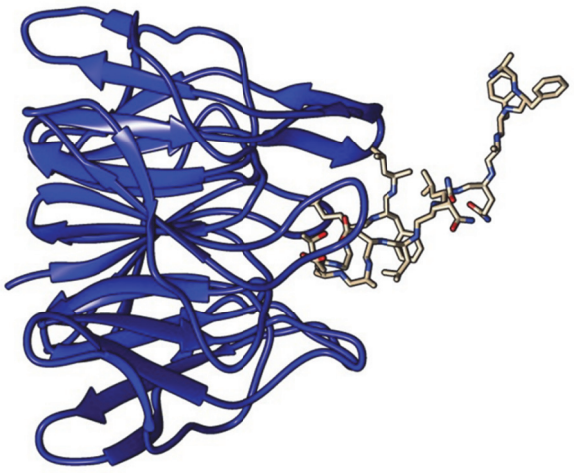

Figure 1.7: Crystal structure of the Kelch domain in complex with a 16-mer Nrf2 derived peptide containing an ETGE motif [46]. The Kelch domain is represented as a ribbon structure (blue) and the Nrf2 peptide is displayed as a stick structure (grey) (PDB code: 2FLU).

The most generally accepted mode of Nrf2 activation was proposed by Tong *et al.* [47]; a two-site substrate recognition model for the Keap1-Nrf2 interaction, the hinge and latch mechanism (Figure 1.8) [47, 49]. In this model, Keap1 forms a homodimer via interactions between the BTB domains of adjacent proteins. The BTB domain is connected to the Kelch domain via the IVR. One molecule of the Kelch domain interacts with the higher affinity motif ETGE (hinge) of the Nrf2 Neh2 domain and the weaker affinity motif DLG (latch) binds to another Kelch molecule (Figure 1.6).

The DLG motif is believed to facilitate the ubiquitination and degradation of Nrf2 by Keap1. Under the condition of oxidative stress, Nrf2 dissociates from its ubiquitination site (DLG motif), but remains bound to Keap1 via the ETGE motif.

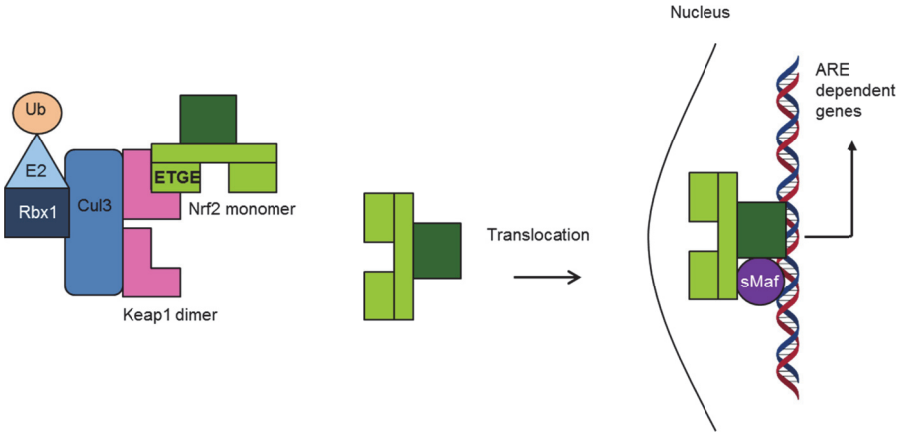

Figure 1.8: Hinge and latch model of the regulation of the Keap1-Nrf2 pathway in the induced state.

Other suggested models of Keap1-Nrf2 pathway regulation include the Keap1 nucleocytoplasmic shuttling, which involves the removal of nuclear Nrf2 by Keap1 under basal conditions. In this model, oxidative stress prevents the nuclear entry of Keap1 (Figure 1.9) [35].

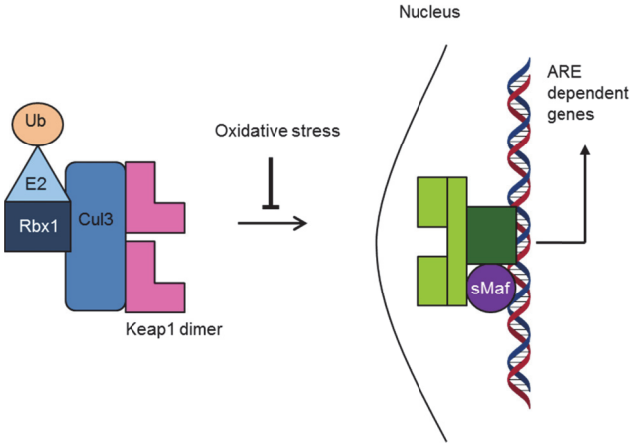

Figure 1.9: Nucleocytoplasmic shuttling model of the regulation of the Keap1-Nrf2 pathway in the induced state.

Another model for Nrf2 activation entails the dissociation of Keap1 from the Cullin3 ubiquitin ligase, hence preventing ubiquitination of Nrf2 (Figure 1.10) [43].

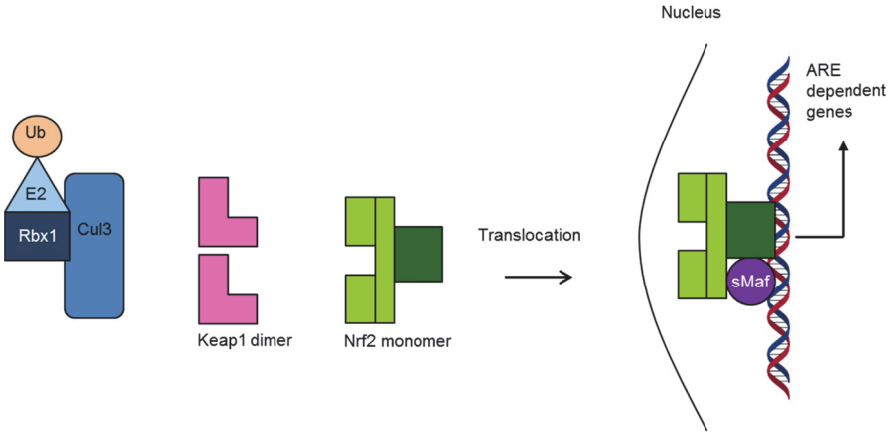

Figure 1.10: Dissociation of Keap1 and Cullin 3 model of the regulation of the Keap1-Nrf2 pathway in the induced state.

The shift from ubiquitination of Nrf2 to ubiquitination of Keap1 following exposure to oxidative stress may form an alternative mode of Nrf2 induction [35] (Figure 1.11). Villeneuve *et al.* [50] suggested that the deubiquitinating enzyme, USP15, plays a role in the regulation of this polyubiquitination switch. USP15 is thought to specifically target Keap1 for deubiquitination, thereby reducing Nrf2 activation [50].

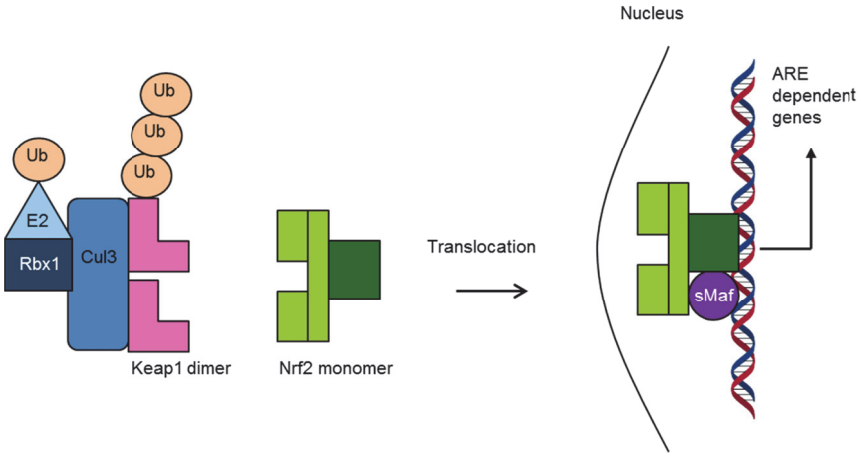

Figure 1.11: Ubiquitination of Keap1 model of the regulation of the Keap1-Nrf2 pathway in the induced state.

1.5 Induction or inhibition of the Keap1-Nrf2 pathway?

Studies with Nrf2-knockout and null mice have revealed the significance of this transcription factor in controlling ARE-mediated gene expression [27]. These mutant mice demonstrated reduced levels of detoxification enzymes, an increased level of DNA adduct formation and an increased predisposition towards the development of tumours following exposure to carcinogens [27, 51]. Moreover, the effectiveness of numerous chemopreventive agents is dependent on a fully functional Keap1-Nrf2 pathway [52]. Mutations in Nrf2 and/or Keap1 have been observed in certain (human) cancers, which were typically found in or near the DLG and/or ETGE motif in the Nrf2 Neh2 domain and in the Keap1 Kelch and/or IVR domain [53-55]. These mutations may compromise the Keap1-Nrf2 PPI and result in constitutive Nrf2 activation, which can prime resistance towards chemotherapy and radiotherapy [56-57]. Moreover, Nrf2 up-regulation in cancerous cells can increase the expression of drug efflux pumps, hence promoting chemotherapy resistance [58]. The dual function of Nrf2 in chemoprevention and tumourigenesis presents a challenge in Nrf2 research; induction of Nrf2 activity may be beneficial for non-cancerous cells by protecting them against cellular damage, whereas inhibition of its function may contribute to enhancing the effectiveness of chemo- and radiotherapy [59-61]. The research presented here only focusses on the role of Nrf2 in chemoprevention.

1.6 Inducers of the Keap-Nrf2 mediated cytoprotective response

The Keap1-Nrf2 pathway can be induced by numerous cellular stresses (e.g. oxidative stress, endoplasmic reticulum stress and shear stress) and both endogenous (ROS and RNS) and exogenous ARE inducer molecules [35]. The exogenous inducers are either from natural or synthetic origin. Keap1 acts as a sensor protein that contains highly reactive cysteine residues. Under basal conditions these residues are in a reactive state (S^- rather than SH) due to their low pKa values [40]. Most ARE inducers are indirect inhibitors of the Keap1-Nrf2 PPI by forming covalent adducts with the sulfhydryl groups of cysteines in Keap1 via alkylation or oxidation processes [52]. The soft electrophilic nature of these molecules makes them selective for reacting with soft nucleophiles (sulfhydryl groups of cysteine) rather than hard nucleophiles (amino and hydroxyl groups). Indirect Nrf2 inducers react with diverse cysteine residues in Keap1 depending on their structure. They are generally divided into ten distinct groups based on their chemical structure

and interaction or reaction with cysteine sulfhydryl groups: isothiocyanates (ITCs) and sulfoxythiocarbamates, dithiolethiones and diallyl sulfides (DAS), Michael acceptors, oxidizable diphenols and quinones, vicinal dimercaptans, trivalent arsenicals, selenium-based compounds, polyenes, hydroperoxides and heavy metals and metal complexes [52]. The most well-known indirect Nrf2 inducers include sulforaphane, oltipraz, tBHQ and CDDO and are currently undergoing clinical trials for their effectiveness as chemopreventive agents [52].

1.6.1 Sulforaphane

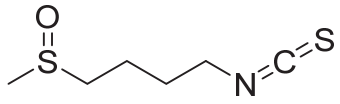

Figure 1.12: Chemical structure of sulforaphane [62].

As it was recognised that phase II enzyme upregulation is a key step in the prevention of cancer initiation [63-64], Prochaska and coworkers developed a cellular assay to identify inducers of the phase II enzyme NQO1 in Hepa1c1c7 cells [65]. NAD(P)H:quinone oxidoreductase-1 (NQO1) is a flavoprotein that facilitates the two-electron reduction of quinones to hydroquinones. Hydroquinones are subsequently subjected to glucuronidation (addition of a glucuronic acid), which increases their water solubility and allows for excretion from the body [65]. NQO1 is officially a phase I drug-metabolising enzyme according to the toxicological classification [66]. However, due to its cytoprotective properties the enzyme will be referred to as a phase II enzyme in this thesis. Up-regulation of NQO1 is associated with the induction of other phase II enzymes including, UDP-glucuronosyltransferase (UGT) and glutathione S-transferases (GSTs). The NQO1 enzyme induction assay was applied to screen extracts from diverse cruciferous vegetables for their ability to activate the phase II enzyme after epidemiological evidence emerged that suggested a positive correlation between the consumption of vegetables and a reduction in the occurrence of carcinogenesis [67]. Extracts from broccoli and brussel sprouts were found to be among the most potent inducers. Sulforaphane (Figure 1.12) was isolated and identified as the main compound responsible for the up-regulation of NQO1 [68]. Sulforaphane is released from disrupted plant cells by the enzyme myrosinase, which hydrolyses the sulforaphane precursor glucoraphanin, a glucosinolate [69]. Sulforaphane is part of the isothiocyanate (ITC) group of chemicals

in which the protective effect is thought to be derived from their electrophilic nature; the central carbon atom can react with the sulfhydryl groups of cysteine residues in Keap1 to form an adduct.

Evidence suggests that sulforaphane covalently modifies cysteine residues in Keap1, thereby allowing nuclear Nrf2 translocation [40, 70]. It is proposed that sulforaphane modifies cysteine residue C151 in the IVR domain of Keap1, thereby preventing the ubiquitination of Nrf2 [71]. Nuclear accumulation of Nrf2 by sulforaphane was abolished following mutation of C151 of Keap1 to a serine residue [71]. Moreover, it has been suggested that the reaction of sulforaphane with C151 is reversible [70]. Although sulforaphane has multiple targets and effects (apoptosis, cell cycle arrest, anti-angiogenesis and inhibition of metastasis) it reacts most readily with Keap1 at a low concentration range [72]. Sulforaphane is a monofunctional inducer of Nrf2 because it activates phase II enzymes without involvement of the AhR-dependent CYP450 enzyme battery [68]. Numerous case control and cohort studies have shown a reduction in the development of various cancers following the consumption of broccoli preparations [73]. Consequently, the use of sulforaphane as a chemopreventive compound is currently under investigation in several phase II clinical trials [73]. As sulforaphane was one of the first Nrf2 inducers to be discovered, it is one of the most extensively studied molecules. Hence, sulforaphane was chosen as a reference compound or positive control for the evaluation of other Nrf2 inducers in this project.

1.6.2 Oltipraz

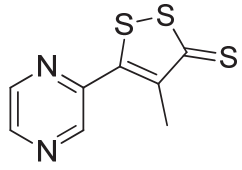

Figure 1.13: Chemical structure of oltipraz [62].

Oltipraz or 5-(2-pyrazinyl)-4-methyl-1,2-dithiol-3-thione (Figure 1.13) is a synthetic dithiolethione that shares structural similarities with natural occurring dithiolethiones. Initially, oltipraz was brought onto the market as an anti-schistosomiasis drug [74]. Evidence emerged that the compound exhibited cytoprotective properties by up-regulation of phase II enzymes including, UDP-glucoronosyltransferase, glutathione

S-transferases, GSH and glutamate cysteine synthetase [75]. Moreover, it was found that oltipraz is protective against the development of cancer in mammary, lung, hepatocellular and colon tumour models [75]. Moon *et al.* [76] demonstrated a reduction in carcinogenesis of the bladder in mice, but this effect was not observed in Nrf2-null mice, which indicates the involvement of the Keap1-Nrf2 pathway. Dithiolethiones such as oltipraz, are sulphur containing compounds that are associated with enhanced phase II enzyme levels, through their reactivity towards thiols [52]. However, this mode of action has not yet been confirmed for oltipraz [77]. Miao *et al.* [78] showed that oltipraz induced both phase I and phase II enzymes in rat hepatoma cells and suggested oltipraz to act as a bifunctional inducer (acting via the Nrf2 and AhR pathways). In addition, a study by Zhang *et al.* [77] demonstrated the production of cellular ROS by oltipraz, which may contribute to Nrf2 activation. Although some positive outcomes were shown, results of phase I and phase II clinical trials were inconclusive and associated with negative side effects including gastrointestinal irritation, paresthesia in fingertips and flatulence [73]. Hence, preclinical testing was terminated.

1.6.3 tBHQ

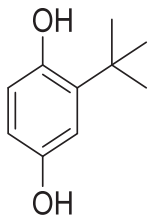

Figure 1.14: Chemical structure of tBHQ [62].

Tert-butylhydroquinone (tBHQ) (Figure 1.14), a metabolite of butylated hydroxyanisole (BHA) [79], is a synthetic phenolic compound that is used as a food preservative. Diverse studies have demonstrated the protective effect of tBHQ against inducers of oxidative stress including dopamine [80], alcohol [81], glutamate [82] and hydrogen peroxide [83]. Dinkova-Kostova *et al.* [40] showed that the cytoprotective activity of tBHQ is mediated through the Keap1-Nrf2 pathway. Diphenols such as tBHQ require bio-oxidation to electrophilic quinones containing Michael acceptor - groups to react with cysteine residues of Keap1, which results in nuclear Nrf2 translocation [84] [85]. Michael acceptors are olefins or acetylenes conjugated to

electron-withdrawing groups, which are subjected to Michael addition with nucleophiles [52, 86]. Michael acceptors are thought to react with cysteine residues of Keap1. Although, chemopreventive effects have been attributed to tBHQ, chronic exposure to the compound is associated with carcinogenicity [87]. This may be due to the production of e.g. ROS, GSH-conjugates and CYP1A1 activation [87].

1.6.4 CDDO

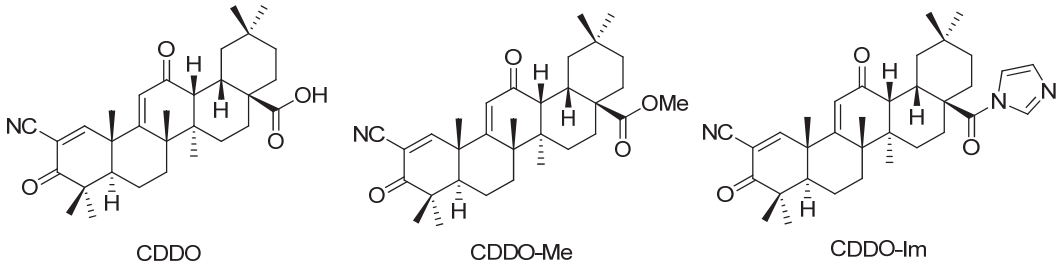

Figure 1.15: Chemical structures of CDDO, CDDO-Me and CDDO-Im [62].

The synthetic triterpenoid, 2-cyano-3,12-dioxooleana-1,9(11)-dien-28-oic acid (CDDO) (Figure 1.15), is derived from naturally occurring oleonolic acid and displays various anti-inflammatory and anti-cancer activities [88]. CDDO was found to up-regulate phase II enzymes, which was shown to be dependent on the involvement of Nrf2 [89]. Moreover, the CDDO structure is one of the most potent Nrf2 inducers [90] (Table 1.2).

Table 1.2: The NQO1 induction potencies of synthetic triterpenoids in Hepa1c1c7 cells [89] (CD value, Section 1.8.1.1).

Compound	NQO1 CD value (μM)
CDDO	0.0023
CDDO-Me	0.0010
CDDO-Im	0.0033

Dinkova-Kostova *et al.* [89] demonstrated the reactivity of CDDO towards cysteine residues of Keap1. The analogues CDDO-Me and CDDO-Im also showed the ability to activate the Keap1-Nrf2 pathway [91]. Several phase I clinical trials have been conducted with CDDO-Me and revealed promising anti-cancer effects [92]. However, a phase III trial was terminated prematurely due to adverse off-target effects [93].

1.6.5 Other indirect Nrf2 inducers

Phenolic compounds are found in many types of plants and are another important group of Nrf2 indirect inducers. Well-known examples are quercetin, epigallocatechin-3-gallate (EGCG), curcumin, resveratrol and flavonoids (flavones, flavonols, flavanones, flavanols, chalcones, anthocyanins, and isoflavones) [86]. Quercetin, EGCG, resveratrol and flavonoids are polyphenols; they can be oxidised to quinones, which contain Michael acceptors [52, 94]. Curcumin contains two Michael acceptors and is able to induce the expression of Nrf2 regulated gene products [94]. Recently, dimethyl fumarate (DMF), a novel compound for the treatment of multiple sclerosis (approved by the FDA in 2013), has been reported to induce nuclear Nrf2 translocation [95]. DMF has been shown to modify key cysteine residues of Keap1 [73] and demonstrated to have potential as an anti-cancer drug for diverse types of cancer [96]. Although both DMF and triterpenoids CDDO-Im and CDDO-Me are indirect Nrf2 inducers, a recent study found that they initiated the up-regulation of different Nrf2 target genes and Nrf2 independent genes [97]. Moreover, in a carcinogen-induced model of lung cancer the triterpenoids prevented the progression of cancer, whereas DMF induced the growth and numbers of tumours [97]. DMF and the triterpenoids contain thiol reactive Michael acceptor sites (α,β-unsaturated carbonyl group) that can interact with diverse cysteine residue containing target proteins including STAT3, PI3K/Akt, IKK, mTOR, HER2 and Keap1 [97]. The biological effect of each compound may be a result of activation of the Keap1-Nrf2 pathway and/or other pathways, which is dependent on the dose and the cellular context (dual role of Nrf2 described in Section 1.5).

1.6.6 Direct inhibition of the Keap1-Nrf2 PPI

An alternative strategy to avert the process of cysteine modification and its associated cytotoxicity is by direct inhibition of the Keap1-Nrf2 PPI. Potential advantages of direct Nrf2 inducers over indirect Nrf2 inducers include enhanced specificity of the interaction with the target, reduced off-target effects, reversibility due to a non-covalent interaction and the potential for relatively low cytotoxicity [98]. Direct Nrf2 inducers include Nrf2-derived (short) peptides or small molecules that can compete with Nrf2 for Keap1 binding sites. These inducers have been identified by screening compound or fragment-based libraries or via *in-silico* docking studies. Sequences of other Keap1 interactors may also provide a basis for the development

of direct Nrf2 inducer molecules. P62 or sequestosome-1 targets ubiquitinated protein cargo for autophagy, which is a process responsible for the degradation of proteins [99]. Evidence has emerged that p62 positively regulates Nrf2 and induces Nrf2 downstream target genes in response to oxidative stress [100]. P62 has been reported to bind to the Keap1 Kelch domain via a DPSTGE motif that is similar to the DEETGE sequence of Nrf2, hence competing with Nrf2 for Keap1 binding sites [100]. This knowledge has been used by our group to develop peptides with sequences based on the p62 protein, which demonstrated increased binding affinities compared to peptides containing the native Nrf2 ETGE containing sequence in a fluorescence polarisation assay [101].

1.7 Transcription factor cross-talk: Nrf2 and AhR

The aryl hydrocarbon receptor (AhR), a ligand dependent transcription factor, is responsible for the up-regulation of genes under the control of the xenobiotic response element (XRE) (Figure 1.16). These genes form the AhR battery and encode both phase I (e.g. CYP1A1, 1A2 and 1B1) and phase II enzymes (e.g. NQO1, GSTA2, UGT1A1 and UGT1A6), also referred to as xenobiotic-metabolizing enzymes (XMEs) [102]. Up-regulation of phase I enzymes such as CYP1A1 can result in the development of reactive metabolites and oxidative stress, which may eventually induce carcinogenesis [103]. Examples of well-known AhR ligands are 2,3,7,8-tetrachlorodibenzo-*p*-dioxin (TCDD) and polycyclic aromatic hydrocarbons (PAHs). Under basal conditions the AhR is sequestered by two Hsp90 proteins in the cytoplasm [102]. Following ligand binding, the AhR dissociates from Hsp90 and translocates to nucleus where it interacts with ARNT (AhR nuclear translocator) [102]. Subsequently, the AhR-ARNT hetereodimer binds to the XRE of AhR battery genes and induces the transcription and translation of XMEs [102].

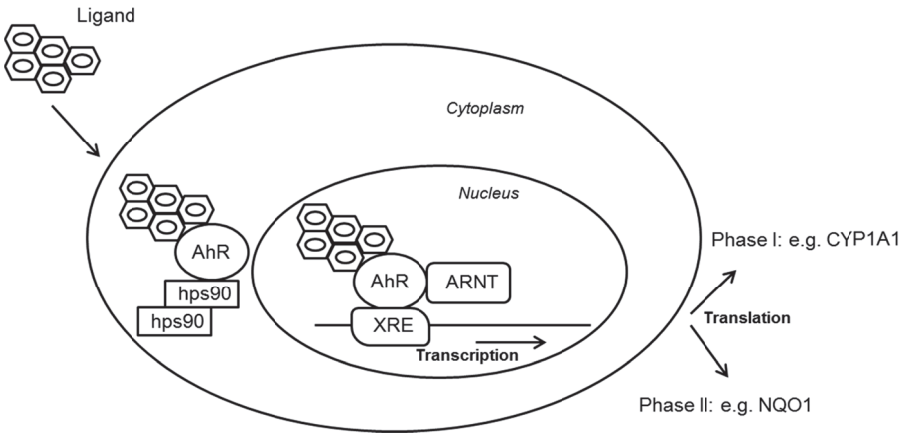

Figure 1.16: Schematic representation of the AhR pathway [102]: AhR is localised in the cytoplasm where it is bound to two Hsp90 proteins. Upon ligand binding, the AhR dissociates from Hsp90 and translocates to the nucleus where it interacts with ARNT. The heterodimer binds to the XRE, which lies upstream of certain genes. Transcription and translation of phase I and phase II enzymes follow.

It has been recognised that there is cross-talk between transcription factors AhR and Nrf2 [103]. Several mechanisms have been proposed to explain this complex linkage (Figure 1.17). Nrf2 is a target gene of the AhR; the Nrf2 and AhR promoters contain both ARE and XRE motifs [103-104]. Moreover, in the NQO1 promoter, ARE and XRE have been identified [103]. Evidence has accumulated that AhR ligands up-regulate NQO1 expression via AhR, ARNT and Nrf2 [105]. Another possibility involves indirect Nrf2 induction via ROS production by CYP1A1. Furthermore, there may be a direct interaction of AhR/XRE and Nrf2/ARE pathways. A recent study by Wang *et al.* [105] has suggested that TCDD is capable of inducing binding of Nrf2 to ARE and AhR to XRE in the promoter region of the NQO1 gene in Hepa1c1c7 cells using a chromatin immunoprecipitation (ChIP) assay. Moreover, TCDD induced a more rapid binding of AhR to XRE compared to Nrf2 to ARE [105]. Co-immunoprecipitation experiments revealed protein-protein interactions between Nrf2-AhR and Keap1-AhR in Hepa1c1c7 cells stimulated by TCDD [105]. In addition, Shin and *et al.* [106] demonstrated with a luciferase reporter and ChIP assay that Nrf2 regulates AhR expression by Nrf2 binding to the ARE positioned in the -230 bp region of the AhR promoter in MEF cells. Following treatment with CDDO-Im, activation of the AhR promoter by Nrf2 – ARE binding was largely abolished by mutation of the -230 bp ARE [106].

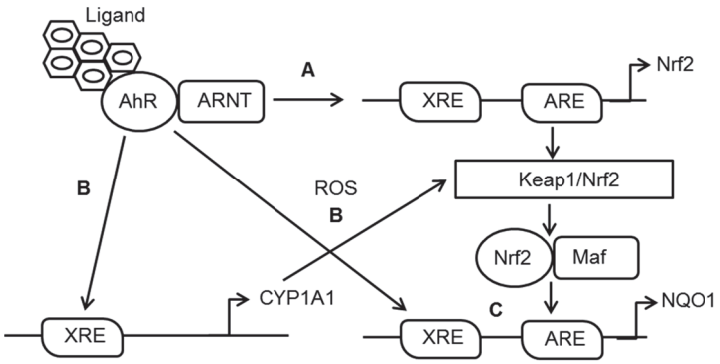

Figure 1.17: Proposed mechanisms for cross-talk between AhR and Nrf2: A. Nrf2 is an AhR target gene; B. Indirect Nrf2 induction by CYP1A1 generated ROS; C. Direct interaction between AhR/XRE and Nrf2/ARE pathways. Adapted from [103].

The identified linkage and cross-talk between AhR and Nrf2 signalling pathways has important consequences for the development of inducers and/or inhibitors of these transcription factors; the AhR plays an important role in the bio-activation of xenobiotics, whereas Nrf2 is associated with detoxification and cytoprotection processes. Hence, potent Nrf2 inducers need to be evaluated for potential AhR – XRE cross-talk. In this respect, monofunctional inducers are believed to upregulate phase II enzyme activity via the ARE without induction of phase I enzymes [107]. Bifunctional inducers activate phase II enzymes via the XRE with induction of phase I enzymes [107].

1.8 Biological evaluation of Nrf2 inducers

Numerous assays and techniques have been employed to screen and identify Nrf2 inducer molecules. They can be subdivided into cellular and *in vitro* (cell-free) based methods. The cell-based assays and techniques are generally aimed at studying the effect of Nrf2 inducer compounds on the nuclear translocation of Nrf2 and on the up-regulation of downstream phase II target genes in cells. Diverse *in vitro* methods have been developed and applied to examine the effectiveness of direct Nrf2 inducers to disrupt the Keap1-Nrf2 PPI. In this section the most commonly used methods are discussed.

1.8.1 Cell-based assays and techniques

1.8.1.1 NQO1 assay

One of the first developed methods for screening potential Nrf2 inducers is a cellular assay, described by Prochaska *et al.* [65], to measure the activity of the phase II enzyme NQO1 in murine hepatoma cells. The NQO1 assay is currently widely applied to measure the NQO1 induction ability of numerous compounds [108]. The principle of this assay is based upon the non-enzymatic reduction of 3-(4,5-dimethylthiazol-2-yl)-2,5-diphenyltetrazolium bromide (MTT) by menadione to a blue/purple colored formazan, which can be solubilised in DMSO and determined colourimetrically at a wavelength of λ = 595 nm (Figure 1.18). The menadiol for the reaction is generated by the action of NQO1 on menadione (the rate-limiting step). Glucose-6-phosphate and glucose 6-phosphate dehydrogenase are added to convert NADP to NADPH which acts as a co-factor for the reaction. The NQO1 induction potencies are often expressed as the dose required to double the NQO1 enzymatic activity (CD) after a 24 hour incubation with the test compound. Since CD values alone may not provide a complete picture for comparison of the various potencies of Nrf2 inducers (no indication of maximum NQO1 induction or potential cytotoxicity), compounds may first be examined at fixed doses and further evaluated in dose response experiments, which allows the ranking of molecules based on their induction potencies.

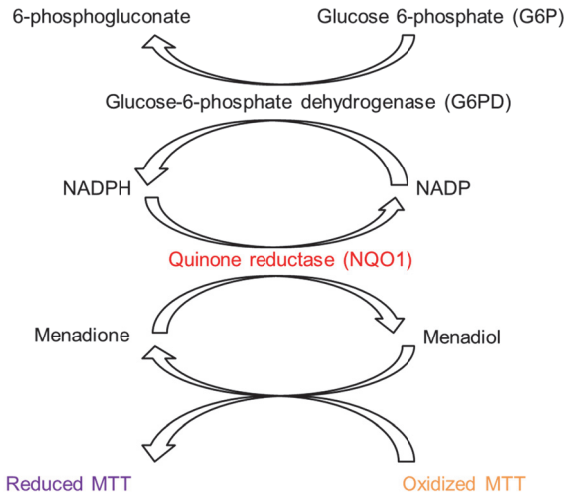

Figure 1.18: Principle of the NQO1 enzymatic assay. Adapted from [65].

The murine hepatoma cell line Hepa1c1c7 was used for this assay as its NQO1 protein is highly inducible [109]. Besides NQO1 induction, the assay can also be employed to estimate the cytotoxicity of potential phase II enzyme inducers. Certain compounds may induce phase II enzymes co-ordinately with phase I enzymes, which could result in carcinogenic bio-activation. The BpRc1 cell line is a variant of the Hepa1c1c7 cell line with a defective ARNT (aryl hydrocarbon receptor, AhR, nuclear translocator), thereby preventing the transcription factor AhR from accumulating in the nucleus [110]. Monofunctional inducers are able to induce the NQO1 enzyme in both the Hepa1c1c7 and BpRc1 cell lines and are generally preferable chemopreventive agents.

1.8.1.2 Luciferase reporter assays: ARE-luciferase assay

The first stable ARE reporter cell line was created by Boerboom *et al.* [111] using the mouse hepatoma Hepa1c1c7 cell line. This cell line was stably transfected with a luciferase gene controlled by a functional ARE sequence of the human NQO1 gene. Wang *et al.* [112] reported in 2007 the generation of a stable MCF-7 - derived ARE reporter cell line, AREc32. The luciferase gene in this cell line is under control of multiple ARE copies, which showed increased activity compared to Boerboom's reporter cell line containing only a single ARE [111]. Nrf2 overexpression resulted in an increase in luciferase activity, whereas Nrf2 knockdown reduced the expression of the luciferase protein [112]. Well-known Nrf2 inducer compounds such as sulforaphane and t-BHQ, were found to induce ARE-luciferase activity [112]. This assay has been used to study numerous putative Nrf2 inducer compounds [113-114] and was adapted by Wu *et al.* [115] to suit high-throughput screening (HTS).

1.8.1.3 Luciferase reporter assays: Neh2- luciferase assay

Inspired by the ARE- reporter cell line, Smirnova *et al.* [116] used the Nrf2 Neh2 domain to develop a Neh2-luciferase reporter system. In this method the Neh2 domain is fused to firefly luciferase (Neh2 – luciferase) and competes with endogenous Nrf2 for Keap1 binding sites. Nrf2 inducing compounds avert the Nrf2 fusion protein from degradation and increase its accumulation. The intensification of the luciferase signal is proportional to the Nrf2 inducing capability of the compound. The main advantage of this assay compared to the ARE based assays is that

compounds can be screened for their ability to disrupt the Keap1-Nrf2 PPI directly. Moreover, the Neh2 – reporter assay was found to be suitable for HTS [116].

1.8.1.4 PathHunter Nrf2 translocation assay

The principle of the PathHunter Nrf2 translocation assay (DiscoveRx) is based on enzyme fragment complementation [117]. A recombinant cell line contains two inactive β-galactosidase enzyme fragments of which one is fused to the Nrf2 protein and the other fragment is located in the nucleus. Upon activation of the Keap1-Nrf2 pathway, Nrf2 translocates to the nucleus where it reconstitutes functional β-galactosidase enzyme. A chemiluminescent galactose-derived substrate is used to determine enzyme activity. Well-known Nrf2 inducers CDDO and t-BHQ have been used as positive controls in this assay [117-118]. A small molecule inhibitor, (*SRS*)-5, of the Keap1-Nrf2 PPI was found to induce Nrf2 nuclear translocation in this assay [119].

1.8.1.5 EMSA and ELISA based methods

Electrophoretic mobility shift assay (EMSA) and enzyme-linked immune assay (ELISA) based methods have been developed to study the ARE-specific binding affinity of Nrf2. In an Nrf2-specific EMSA, radiolabeled ARE sequences are incubated with nuclear extracts, before the mixture is separated using electrophoresis [120]. The Nrf2 protein that is present in the nuclear extract will bind to the ARE DNA sequence, which causes a shift to a higher molecular weight on the polyacrylamide gel compared to the control containing only the DNA fragment [120]. In an Nrf2-specific ELISA, the ARE DNA sequence is immobilised in the wells of a 96-well microtitre plate. Nuclear extracts containing Nrf2 will bind to the ARE and can be detected by a specific Nrf2 primary antibody and a horseradish peroxidase (HRP)-conjugated secondary antibody [121-122]. These methods can be applied to study the ARE-specific Nrf2 inducing abilities of various compounds. The ELISA method developed by Assay Biotechnology detects Nrf2 by fixing cells on a plate and incubating them with a specific primary antibody against Nrf2 and a HRP conjugated secondary antibody [123]. A 3,3′,5,5′-tetramethylbenzidine (TMB) substrate system is used to quantify the amount of Nrf2 present. This system works via the oxidation of TMB to the blue TMB diimine by the HRP enzyme [123].

1.8.1.6 Expression, transcription and translation of Nrf2 (target) genes

The potency of compounds to induce the expression, transcription and translation of Nrf2 (target) genes can be measured using diverse methods. Real-time quantitative PCR is a technique that is commonly used to quantify gene expression. It is based on the hybridisation of a (fluorescently) labelled oligonucleotide probe that can intercalate with double stranded DNA [124]. The nuclease cleavage of the probe by Taq DNA polymerase during PCR extension generates a fluorescence signal, which is used to detect gene amplification [124]. Real-time quantitative reverse transcription PCR entails reverse transcription of mRNA to cDNA followed by quantitative PCR, which allows the measurement of real time mRNA levels [125]. Western blotting is the most frequently used technique to assess protein expression levels [126]. This method involves the separation of proteins based on their molecular weight using electrophoresis, transfer to a membrane (blotting) and incubation with labelled antibodies to visualise the protein of interest [126].

1.8.2 In-vitro assays and techniques

1.8.2.1 Fluorescence polarisation (FP)

Fluorescence polarisation (FP) is a homogenous method that can be used to identify direct inhibitors of the Keap1-Nrf2 PPI [127]. When a rapidly tumbling fluorescently labelled Nrf2 derived peptide is excited with polarised light, the emission light is depolarised, which results in a low polarisation value. Following binding of the fluorescent Nrf2 probe to the Keap1 Kelch domain, the tumbling of the complex decreases. This results in an increase in the emission of polarised light and consequently an increase in the polarisation value. Addition of an unlabelled inhibitor compound disrupts the binding of the fluorescent probe to the Keap1 Kelch domain, resulting in a decrease in polarisation, which can be measured. Diverse FP assays have been developed and successfully applied for the screening of small molecule inhibitors of the Keap1-Nrf2 PPI [52, 128-129]. More details of this assay are discussed in Section 3.1.

1.8.2.2 Surface plasmon resonance (SPR)

The principle of Surface Plasmon Resonance (SPR) is based on a change in refractive index upon association of a ligand with an immobilised binding partner. The degree of change can be measured over time at variable ligand concentrations, which enables the establishment of a binding affinity profile [130]. The SPR technique can be used to screen for compounds that directly inhibit the Keap1-Nrf2 PPI. In such an assay the Nrf2 derived peptide is immobilised on a sensor chip whilst the Keap1 Kelch domain flows in solution over the chip [52]. Upon association, the refractive index changes and as a result affects the angle of reflected polarised light. Several research groups have reported the use of this method to identify *de novo* inhibitors of the Keap1-Nrf2 PPI [52, 118, 131]. More details of this assay are discussed in Section 3.1.

1.8.2.3 Isothermal calorimetry (ITC)

ITC has been used to characterise the binding interaction between Keap1 and Nrf2 [52, 55, 132]. This method generates valuable information on interaction thermodynamics: binding affinity and binding stoichiometry, enthalpy and entropy and Gibbs free energy [133]. The principle of this technique is based on a heat-flux calorimeter that determines the amount of energy needed to maintain equal temperatures between a reference cell, containing buffer, and a sample cell, containing the macromolecule in the same buffer [133]. The amount of heat exchanged (an exothermic or endothermic reaction) upon association of the Keap1 and Nrf2 proteins is measured as one of the components is titrated into the sample cell containing the protein binding partner [133]. The assay can be carried out in a competition format in which the binding profile changes upon addition of inhibitors to the solution cell. More details of this assay are discussed in Section 3.1.

1.8.2.4 Confocal fluorescence anisotropy

This method makes use of two-dimensional fluorescence intensity distribution analysis (2D-FIDA) and a polarisation cube and is similar to the FP approach [134]. A fluorescent Nrf2-derived peptide and an unlabelled Keap1 Kelch domain can be used to determine the binding affinity [135]. IC_{50} values can be obtained following the addition of varying concentrations of unlabelled inhibitors to the protein mixture.

1.8.2.5 Differential scanning fluorimetry (DSF)

The principle of differential binding fluorimetry (DSF) is based on the binding of a fluorescent dye to the hydrophobic parts of a protein. Following heating of the protein-dye sample, the protein unfolds and exposes buried hydrophobic regions of the protein that can associate with the dye, which results in a change in fluorescence intensity [136-137]. Binding of an interacting ligand increases the stability of Keap1 and hence affects its denaturing temperature, resulting in modified fluorescence values [138]. Using this technique, binding affinity profiles can be created for Keap1 interactors [118, 139].

1.8.3 Selection of screening and evaluation methods

In this project several methods have been selected for the screening and evaluation of inhibitors of the Keap1-Nrf2 PPI. The cellular enzymatic NQO1 induction assay was chosen as an initial screening method to identify putative Nrf2 inducing molecules. This assay is one of the most widely used methods for studying the potency of direct and indirect Nrf2 inducer compounds to up-regulate the phase II enzyme NQO1 in Hepa1c1c7 cells. Potential bifunctional inducers were also examined in the ARNT-deficient BpRc1 cell line, where time allowed. Direct disrupters of the Keap1-Nrf2 PPI were additionally screened in an FP based assay, which was validated previously [101]. In this assay a fluorescein-labelled 7-mer Nrf2 peptide (FITC-β-DEETGEF-OH) was used as a fluorescent probe and the Keap1 Kelch domain as a target protein. Competition experiments were carried out with unlabelled peptides and small molecules to evaluate their potential for disrupting the fluorescent peptide – protein complex. Both NQO1 and FP screening assays were initially performed at fixed doses to identify potent molecules. This was followed by dose response assays for promising structures. An additional *in vitro* screening assay was developed based on the principle of Förster resonance energy transfer. In the past decade, *in vitro* FRET assays have been developed to study several PPIs [140-141]. However, there was no record of a Keap1-Nrf2 specific *in vitro* FRET assay when this work was carried out. Hence, a steady state FRET assay was developed to identify inhibitors of the Keap1-Nrf2 PPI [142] (development and validation described in Chapter 3). In this assay the binding of an eCFP fluorophore conjugated 16-mer Nrf2 derived peptide to an eYFP fluorophore fused Keap1 Kelch domain generates a FRET signal.

This signal can be disrupted by unlabelled peptides or small molecules upon their addition to the protein mixture. Both fixed dose and dose response profiles were created to identify and examine potent compounds. The most promising molecules were evaluated further by western blotting analysis to study their ability to up-regulate the expression of nuclear Nrf2 and the cytoplasmic detoxification enzymes, HO-1 and NQO1. Potential bifunctional compounds were also assessed for the induction of nuclear AhR and cytoplasmic CYP1A1 proteins using both western blotting technique and a bioluminescent CYP1A1 activation assay (P450-Glo CYP1A1, Promega). Western blotting provides good qualitative information on protein induction levels and to lesser extent quantitative information. However, there is no universally standardised method for the quantification of Nrf2 activation. The flow cytometry based method in Chapter 4 describes a novel Nrf2 intracellular staining technique, which can be applied to quantify (inducible) Nrf2 protein levels in cells. The main advantage of this quantification method is the ability to determine the Nrf2 protein expression in individual cells, whereas western blotting provides an average for the protein expression in a whole cell population. Potential cellular ROS production upon exposure to promising Nrf2 inducer molecules was measured using a fluorescence dye and flow cytometry. Although the cellular NQO1 induction assay provides an insight into compounds cytotoxicity levels, the sulforhodamine B (SRB) assay, which measures cellular protein content, was used as a supportive tool in the dose dependent cytotoxicity evaluation.

1.9 Project aims

This project focusses on the use of Nrf2 inducers as a chemopreventive strategy in cancer treatment. The main aim is to characterise the behaviour of various classes of Nrf2 inducer compounds by:

- Screening all types of Nrf2 inducers for their ability to up-regulate the phase II enzyme NQO1 in a cellular enzymatic assay. The NQO1 assay pioneered by Prochaska *et al.* is the most widely used method to evaluate the NQO1 enzyme inducibility by various compounds.
- Applying other existing cellular techniques (i.e. western blotting) to evaluate the ability of Nrf2 inducers to up-regulate Nrf2 and downstream target enzymes.
- Developing a novel flow cytometry based assay to quantify inducible Nrf2 protein levels in cells as an additional method to existing approaches (i.e. western blotting). As the flow cytometry technique relies on single-cell analysis rather than population analysis, the determination of Nrf2 protein levels is anticipated to benefit from increased reproducibility and reliability.
- Screening of direct Nrf2 inducers for their ability to disrupt the Keap1-Nrf2 pathway using *in vitro* methods including a FP assay that was previously developed in our group [143].
- Developing a novel FRET based assay as another approach to screen direct inhibitors of the Keap1-Nrf2 PPI. This method benefits from fusing stable fluorophores to the interacting protein pair, which makes the assay more durable than FP-based assays.

2 Materials & Methods

2.1 Bacterial strains, culture medium & preparation of competent cells

XL-1 blue bacteria were a kind gift from Dr. Colin James, UCL School of Pharmacy. The strain-specific genotype is: *recA1 endA1 gyrA96 thi-1 hsdR17 supE44 relA1 lac [F´ proAB lacIqZΔM15 Tn10 (Tetr)].*

Rosetta 2 (DE3) bacteria from Novagen were supplied by MerckMillipore. The strain-specific genotype is: $F^- ompT\ hsdS_B(r_B^- m_B^-)\ gal\ dcm\ (DE3)\ pRARE2\ (Cam^R)$.

Bacteria were grown in:

- Luria-Bertani (LB) Broth (in 1 L): 10 g NaCl, 10 g tryptone and 5 g yeast extract. Autoclave solution, cool down to hand-warm and add appropriate antibiotics solution.

- LB agar (in 1 L): 10 g NaCl, 10 g tryptone and 5 g yeast extract, 1.5 g agar. Autoclave solution, cool down to hand-warm and add appropriate antibiotics solution.

Growth media was supplemented with antibiotic solution where appropriate: a final concentration of 12.5 µg/mL tetracycline, 20 µg/mL chloramphenicol, 30 µg/mL kanamycin

Competent bacteria were prepared using the $CaCl_2$ method: 0.5 mL of 10 mL overnight grown bacteria culture was added to 500 mL LB Broth (added tetracycline for XL-1 blue cells and chloramphenicol for Rosetta 2 (DE3) cells). Bacteria were grown until OD_{600nm} = 0.6 and pelleted at 4°C. After the supernatant was discarded, cells were resuspended in 500 mL ice-cold 0.1 M $CaCl_2$ and left to incubate on ice for 45 min. Cells were pelleted at 4°C and resuspended in 10 mL of 20% glycerol in $CaCl_2$. Competent cells were aliquoted at 0.25 mL/vial in pre-cooled Eppendorf tubes before flash-freezing them in liquid nitrogen. Competency was tested by plasmid transformation of the cells.

2.2 The bacterial expression vector, pET28c

The pET28c bacterial expression system enables the rapid production of a large quantity of proteins when activated. In bacterial cells, the cloned gene is under control of the viral T7 promoter, which ensures strong levels of transcription when T7 RNA polymerase is present and not repressed by the lac operator [144]. The host Rosetta 2 (DE3) bacterial cell strain contains an isopropylthio-β-D-galactosidase (IPTG) dependent promoter. When IPTG is added to the bacterial host strain, the lac repressor is removed from the operator and proteins can be expressed [144]. The pET28c plasmid (Novagen) also contains a kanamycin resistance gene and an N-terminal hexahistadine sequence to allow for affinity purification (Figure 2.1).

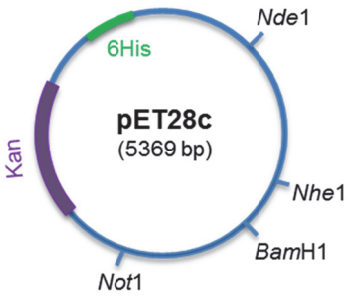

Figure 2.1: Vector map of the pET28c plasmid (Novagen) showing the used restriction sites.

2.3 cDNA cloning

The pET28c plasmid (Novagen), contains a kanamycin (kan) selective marker. The plasmids pET28c-eCFP-TEV-CTAD and pET28c-eYFP-p300, which were kindly provided by Dr. Andreia.Guimaraes (UCL School of Pharmacy), were used to generate plasmids pET28c-eCFP-TEV-Nrf2 (-wild-type, -E78P/F83L, -E79Q, -T80K and -E82D) and pET28c-eYFP-TEV-Kelch (Chapter 3, Figure 3.5). The plasmids encode enhanced yellow fluorescent protein (eYFP) or enhanced cyan fluorescent protein (eCFP). The pET28c-eYFP and pET28c-eCFP-TEV-eYFP plasmids were kindly provided by Dr. Edwin Nkansah (UCL School of Pharmacy).

2.3.1 pET28c – eYFP- TEV- Kelch plasmid

The cDNA encoding the human Keap1 Kelch domain (residues 321 – 609) was amplified from the pET15b – human Kelch plasmid (gift from Dr. Tadayuki Tsujita, University of Dundee) by PCR using the forward primer 5'-AAAA**GGATCC**GCGCCCAAGGTGGGCCG-3' and reverse primer 5'AAAA**GCGGCCGC**TTAGGTGACAGCCACGCCCAC-3', introducing a *Bam*H1 site at the 5'-end and a *Not*1 site at the 3'-end. The restriction endonuclease sites are shown in bold. Each oligonucleotide primer contains additional bases at the 5' end to aid the binding of the restriction enzymes. Forward and reverse primers were purchased from Eurofins MWG Operon and HPLC purified by the manufacturer. The amplified product and pET28c-eYFP-TEV plasmid were digested with *Bam*H1 and *Not*1 (NEB) (Section 2.4) and ligated (Section 2.6), creating pET28c-eYFP-TEV-Kelch.

The PCR primers for the amplification of the human Keap1 Kelch domain were designed using the following criteria [145-147]:

- The melting temperature (Tm) was calculated using the Wallace equation [148]:

$$Tm = 64.9 + 41 * \frac{yG + zC - 16.4}{wA + xT + yG + zC}$$

Where w,x,y,z are the number of the bases A,T,G,C in the amplification sequence respectively.

- The melting temperature of the primer pair is designed to be within 5 °C of each other.
- The optimal annealing temperature is 5 °C below the estimated Tm.
- The optimal primer length is between 18-22 bases.
- Primers were designed with a maximum of 4 identical bases.
- Primers do not have complementary sequences (palindromes) within themselves or with the other primer in the pair.

For the PCR amplification of the Keap1 Kelch cDNA, a mastermix was prepared for use in minimal 6x PCR reactions (50 µL/reaction):

7 µL Template DNA (pET15-humanKelch)

35 µL Pfu 10x buffer (NEB)

3.5 µL Forward primer

3.5 µL Reverse primer

7 µL dNTP mix

7 µL Pfu DNA polymerase (NEB)

287 µL dH2O

350 µL mastermix volume (50 µL/reaction)

All reactions were cycled using a Techne TC-3000G Thermal Cycler (Bibby Scientific) using the conditions in Table 2.1.

Table 2.1: PCR reaction scheme for amplification of the Keap1 Kelch cDNA.

Step	Cycles	Temperature	Time
1: Initial denaturation	1	95°C	5 min
2: Denaturation	30	95°C	45 sec
3: Annealing		54.2°C – 67.1°C	30 sec
4: Extension		72°C	4 min and 15 sec
5: Extension	1	72°C	10 min
6: PCR product	NA	4°C	On hold

The PCR products were separated according to size by electrophoresis on a 1% agarose gel (Section 2.5). The desired 864 basepair PCR product was most visible at the highest annealing temperature of 67.1 °C and was excised from the gel. The PCR product was gel purified (Section 2.5) and used in subsequent cloning steps.

2.3.2 pET28c – eCFP- TEV- Nrf2 (wild-type, E78P/F83L, E79Q, T80K and E82D) plasmids

The Nrf2 wild-type (WT) and Nrf2 mutant DNA sequences (E78P/F83L, E79Q, T80K and E82D) were only 48 base pairs long and did not require PCR. They were made by annealing forward and reverse oligonucleotide sets (Table 2.2), introducing a *Bam*H1 site at the 5'-end and a *Not*1 site at the 3'-end. The nucleotides which were mutated to generate the Nrf2 mutant peptide sequences are shown in bold within each oligonucleotide sequence. All oligonucleotide sets were purchased from Eurofins MWG Operon and HPLC purified by the manufacturer. Oligos were dissolved in dH_2O to make up 1 mM stocks. Next, 20 µl of each oligo set was combined with 100 mM NaCl (final concentration) in a total volume of 100 µl and incubated at 100 °C for 5 min. The double stranded DNA was allowed to cool down to RT and stored at - 20°C. The annealed products and the pET28c-eCFP-TEV plasmid were digested with *Bam*H1 and *Not*1 (Section 2.4) and ligated (Section 2.6) generating the pET28c- eCFP-TEV-Nrf2 expression plasmids.

Table 2.2: Nrf2 primers used to generate pET28c – eCFP- TEV- Nrf2 plasmids: wild-type (WT), E78P/F83L, E79Q, T80K and E82D.

Nrf2	Primer set #	Nucleotide sequence (5' → 3')
WT	1 FP	GATCCGCGTTCTTCGCGCAGCTGCAGCTGGACGAAGAAACCGGTGAATTCCTGGC
WT	1 RP	GGCCGCCAGGAATTCACCGGTTTCTTCGTCCAGCTGCAGCTGCGCGAAGAACGCG
WT	Peptide sequence	Ala Phe Phe Ala Gln Leu Gln Leu Asp Glu Glu Thr Gly Glu Phe Leu
Mutant E78P/ F83L	2 FP	GATCCGCGTTCTTCGCGCAGCTGCAGCTGGAC**CCG**GAAACCGGTGAA**CTG**CTGGC
Mutant E78P/ F83L	2 RP	GGCCGCCAG**CAG**TTCACCGGTTTC**CGG**GTCCAGCTGCAGCTGCGCGAAGAACGCG
Mutant E78P/ F83L	Peptide sequence	Ala Phe Phe Ala Gln Leu Gln Leu Asp **Pro** Glu Thr Gly Glu **Leu** Leu
Mutant E79Q	3 FP	GATCCGCGTTCTTCGCGCAGCTGCAGCTGGACGAA**CAG**ACCGGTGAATTCCTGGC
Mutant E79Q	3 RP	GGCCGCCAGGAATTCACCGGT**CTG**TTCGTCCAGCTGCAGCTGCGCGAAGAACGCG
Mutant E79Q	Peptide sequence	Ala Phe Phe Ala Gln Leu Gln Leu Asp Glu **Gln** Thr Gly Glu Phe Leu
Mutant T80K	4 FP	GATCCGCGTTCTTCGCGCAGCTGCAGCTGGACGAAGAA**AAA**GGTGAATTCCTGGC
Mutant T80K	4 RP	GGCCGCCACCAATTCACC**TTT**TTCTTCGTCCAGCTGCAGCTGCGCGAAGAACGCG
Mutant T80K	Peptide sequence	Ala Phe Phe Ala Gln Leu Gln Leu Asp Glu Glu **Lys** Gly Glu Phe Leu
Mutant E82D	5 FP	GATCCGCGTTCTTCGCGCAGCTGCAGCTGGACGAAGAAACCGGT**GAC**TTCCTGGC
Mutant E82D	5 RP	GGCCGCCAGGAA**GTC**ACCGGTTTCTTCGTCCAGCTGCAGCTGCGCGAAGAACGCG
Mutant E82D	Peptide sequence	Ala Phe Phe Ala Gln Leu Gln Leu Asp Glu Glu Thr Gly **Asp** Phe Leu

2.4 Restriction endonuclease digestion

Restriction digests were performed for both the cloning of PCR and annealed double stranded DNA products and for clone verification purposes. For cloning purposes, 1 – 2 µg plasmid DNA, 1 µL *Bam*H1, 1 µL *Not*1 and 1x concentrated restriction NEB endonuclease buffer 4 (50 mM Potassium Acetate, 20 mM Tris-acetate pH 7.9, 10 mM Magnesium Acetate, 1 mM DTT) made to a total volume of 15 or 20 µL with dH_2O was combined in a sterile 0.5 mL centrifuge tube. The mixture was incubated at 37°C for 2 h. The digested DNA was separated on a 1% agarose gel by electrophoresis, gel purified (Section 2.5), and used for ligation reactions (Section 2.6). Control restriction digests with *Bam*H1 or *Not*1 were performed separately to ensure complete digestion by both enzymes. For clone verification purposes, 0.5 µg mini-prepped DNA (Section 2.7), 0.5 µL *Nde*1, 0.5 µL *Not*1 and 1x concentrated restriction NEB endonuclease buffer 4, made to a total volume of 10 µL with dH_2O was combined in a sterile 0.5 mL centrifuge tube.

The mixture was incubated at 37°C for 2 h. The digested DNA was separated on a 1% agarose gel by electrophoresis, stained with SYBR Safe (Life Technologies) and analysed. Control restriction digests with *Nde*1 or *Not*1 were performed separately to ensure complete digestion by both enzymes.

2.5 Agarose gel electrophoresis and DNA purification

DNA products were separated by electrophoresis through a submerged gel (1% (w/v) agarose, 1 x SYBR Safe (Life Technologies) in DMSO in TBE buffer). Samples were mixed with 1x volume gel loading dye (NEB), loaded into sample wells and electrophoresed at 80V for 1.5 h. The DNA was visualised using a blue light transilluminator gel. Agarose containing DNA fragments generated by restriction enzyme digestion were excised from the gel and the DNA purified using the Qiagen kit for DNA gel extraction according to manufacturer's instructions.

2.6 Ligation reactions

The amount of insert for a 6:1 molar ratio with plasmid or vector needed for the ligation reactions was determined by the following equation:

$$\text{Amount of insert (ng)} = \frac{\text{x ng of vector}}{\text{size in kb of vector}} * 0.005 \text{ kb of insert} * 6$$

In a sterile 0.5 mL centrifuge tube were combined: typically 150 ng of restriction endonuclease digested vector, the previous calculated amount of restriction endonuclease digested insert, 1.5 µL T4 DNA ligase (NEB) and 1x concentrated T4 DNA ligase buffer (50 mM Tris-HCl pH 7.5, 10 mM $MgCl_2$, 1 mM ATP, 10 mM DTT), which was made to a total volume of 15 µL with dH_2O. Ligations were carried out at RT for 1 h and at 4°C for 30 min.

2.7 Bacterial transformation and plasmid purification

70 µL of competent XL-1 blue cells were transformed with ligation products and incubated on ice for 45 min. The cells were heat-shocked at 42°C for 90 sec then returned to ice for 2 min. Following the addition of 400 µL of LB-broth, cells were incubated at 37 °C for 45 min whilst shaking (220 rpm). 100 µL of the cell culture was dispersed on LB-kan agar plates and incubated at 37 °C overnight.

Colonies were picked and grown in 5 mL LB-kan medium at 37°C overnight whilst shaking at 220 rpm. 2.5 mL of overnight cultures were harvested by centrifugation and purified using the Mini-Prep spin column system (Qiagen) according to the manufacturer's instructions. The purified DNA was eluted in 30 µL sterile dH_2O. The recovery of plasmid with an insert and confirmation of no additional introduced mutations was verified by restriction enzyme digest analysis (Section 2.4) and DNA sequencing respectively, using T7 forward and reverse primers (Eurofins MWG Operon). Large-scale plasmid DNA preparations were generated using the Maxi-Prep Kit (Qiagen) according to manufacturer's instructions. Recovered plasmid DNA was quantified by measuring the absorbance values (OD_{260nm}) on the NanoVue Plus Spectrophotometer. The concentration of DNA in the sample was calculated using the following equation: OD_{260nm} x 50 ng/µg. Estimation of the purity of the plasmid DNA was carried out by measuring the ratio of OD_{260nm}/OD_{280nm}. A ratio of 1.8 - 2.0 indicated that the sample did not contain protein.

2.8 Glycerol stocks of transformed XL-1 blue or Rosetta 2 (DE3) cells

A single colony of transformed cells was picked from a selective agar plate and used to inoculate 5 mL of LB – broth containing the appropriate antibiotic. The cell culture was grown at 37°C overnight whilst shaking at 220 rpm. The next day 500 µL of cell culture was supplied with 500 µL of glycerol and mixed. The glycerol stocks were flash frozen in liquid nitrogen before storage at - 80°C.

2.9 Protein expression, purification & storage

All plasmid constructs (pET28c- eCFP-TEV-Nrf2-WT, pET28c- eCFP-TEV-Nrf2-E78P/F83L, pET28c- eCFP-TEV-Nrf2-E79Q, pET28c- eCFP-TEV-Nrf2-T80K, pET28c- eCFP-TEV-Nrf2-E82D, pET28c-eYFP-TEV-Kelch, pET28c-eYFP and pET28c-eCFP-TEV-eYFP) were used to transform 50 µL of competent Rosetta 2 (DE3) cells as described in Section 2.7. Transformed cells were dispersed on LB-kan agar plates and incubated at 37°C overnight. One single colony was picked and grown overnight in LB-kan medium at 37°C whilst shaking at 220 rpm. 1 mL of overnight grown culture was added to 1 L of LB-kan and incubated at 37°C until the cells reached the exponential growth phase (OD_{600nm} = 0.4-0.6). The 1 L bacterial culture was induced with IPTG (1 mM final concentration) and incubated at 21°C for 16 h. Cells were pelleted (6,000 x g at 4°C for 30 min) and kept on ice for further purification or stored at - 80°C.

Bacterial pellets were resuspended in extraction buffer (20 mM Tris-HCl pH 7.4, 150 mM NaCl, 30 mM imidazole, 0.5 mM DTT, 0.5 mM EDTA, 5% glycerol and 50 µL protease inhibitor cocktail (AEBSF, bestatin, E-64, pepstatin A and phosphoramidon, Sigma-Aldrich) / gram of bacterial pellet and sonicated for 5 min on ice with 15 sec of rest between each 15 sec cycle of sonication. After the cell debris and insoluble proteins in the bacterial suspension were pelleted at 27,000 x g at 4°C for 40 min, the supernatant was filtered with a 0.22 µM filter to remove any remaining insoluble particles.

2.10 Affinity purification of hexahistadine tagged proteins

The hexahistidine tagged proteins were affinity purified using immobilised metal ion affinity chromatography (IMAC), which is based on the binding affinity of histadine to nickel ions. A range of increasing concentrations of imidazole competitively displaces the hexahistadine tagged proteins from the nickel loaded column.

The filtered supernatant (Section 2.9) was then applied to a 5 ml His-Trap FF column (GE Healthcare Life Sciences), which was washed with 30 mL degassed dH_2O and equilibrated with 30 mM imidiazole in purification buffer (20 mM Tris-HCl

pH 7.4, 0.5 M NaCl and 0.5 mM DTT). After washing the column with 50 mL of 30 mM imidazole in purification buffer and 10 mL of 50 mM imidazole in purification buffer, the proteins were eluted with 10 mL of a gradient of purification buffer containing 100 – 300 mM imidazole. To monitor purification, samples were removed from each stage and subjected to SDS-PAGE (Section 2.14) followed by Coomassie Brilliant Blue staining (Section 2.15). The eluted proteins were transferred to a pre-boiled dialysis membrane (SpectrumLabs). Dialysis was carried out in 2 L dialysis buffer (20 mM Tris-HCl pH 7.4, 150 mM NaCl, 0.5 mM DTT and 1 mM EDTA, adapted from [149]) at 4 °C for 16 – 24 h whilst stirring. The dialyzed protein elutes were concentrated to a 1 mL volume using Amicon Ultra-15 centrifugal filter units MWCO 10K spin columns (MerckMillipore) for the eCFP-TEV-Nrf2 (WT and mutants) and eYFP proteins and MWCO 30K spin columns for the eYFP-TEV-Kelch and eCFP-TEV-eYFP proteins. Aliquots of the eYFP-TEV-Kelch protein were supplemented with 1.0x Halt protease inhibitor cocktail (AEBSF, aprotinin, bestatin, E-64, leupeptin, pepstatin, EDTA, Thermo Scientific). Protein aliquots were supplemented with 10% glycerol to prevent ice-crystals from forming upon freezing. The proteins were flash-frozen in liquid nitrogen and stored at - 80°C.

2.11 eYFP-TEV-Kelch protein stability

eYFP-TEV-Kelch protein samples were prepared with increasing amounts of Halt protease inhibitor cocktail (+ 0.0x, + 0.5x, +1.0 x or +10 x concentrated). Next, the protein samples were either stored at 4°C, RT or 37°C. Samples were taken after 0 days (T = 0), 3 days (T = 3), 5 days (T = 5) and 7 days (T = 7). The stability of the eYFP-TEV-Kelch protein samples was assessed by SDS-PAGE gel electrophoresis (Section 2.14).

2.12 Protein quantification by intrinsic GFP absorbance

All YFP-Kelch and CFP-Nrf2 or CFP-Nrf2 mutant protein concentrations were determined by UV/visible spectroscopy, using wavelengths of 514 nm and 435 nm for eYFP and eCFP respectively and the extinction coefficients 83400 $M^{-1}cm^{-1}$ (eYFP) and 28750 $M^{-1}cm^{-1}$ (eCFP). The Beer-Lambert law was applied to calculate the protein concentrations:

$A = \varepsilon lc$

Where A = absorbance, ε = extinction factor ($M^{-1}cm^{-1}$), l = optical cell length (cm) and c = concentration (M).

The stored protein concentrations were adjusted for the dilution factor of the measured solutions.

2.13 Protein quantification by Bio-Rad protein assay

Protein content of crude, cytoplasmic and nuclear lysate samples was measured using the Bio-Rad protein assay (Section 2.21). This assay is based upon the Bradford method for determining protein concentration [150] and was carried out according to the manufacturer's protocol. A range of BSA (1 - 20 µg) was used to produce a standard curve. Samples were diluted where necessary and made up to 20 µL with dH_2O. Then 5 µL of the samples was transferred to a flat-bottom 96-well plate (NUNC) and 200 µL of 5x diluted Bio-Rad protein assay reagent was added to each well before measurement on a spectrophotometer plate-reader (PerkinElmer Envision or BMG Spectrostar) at a wavelength of 595 nm. The protein concentration was calculated with the BSA standard curve.

2.14 SDS-Polyacrylamide gel electrophoresis (SDS-PAGE)

2.14.1 Preparation of protein samples for SDS-PAGE

Protein samples were prepared by mixing 5 volumes of sample with 1 volume of 6x SDS sample loading buffer (375 mM Tris-HCl pH 6.8, 12% SDS, 30% sucrose and 0.012% bromphenol blue) and 100 mM DTT (final concentration). The samples were mixed and incubated at 95°C for 10 min.

2.14.2 SDS-PAGE

Proteins were separated by electrophoresis using the Mini-PROTEAN Tetra Cell system (Bio-Rad). Two glass plates (spacer plate and short plate) were assembled in a casting frame. The 10% polyacrylamide gels were prepared according to Table 2.3. Polymerisation of the resolving gel was initiated by the addition of 10% ammonium persulfate (APS). The resolving gel mixture was dispensed into the gap between the glass plates and dH_2O was overlaid onto the resolving gel to prevent drying out of the gel surface. Following polymerisation of the resolving gel, the dH_2O was discarded and the stacking gel mixture was overlaid onto the resolving gel.

A comb was placed inside the stacking gel mixture. After the stacking gel had polymerised, the wells were rinsed with SDS running buffer (0.125 M Tris-base, 0.626 M Glycine and 0.5% SDS) prior to loading the samples and a molecular weight marker (7-175 kDa, NEB). Electrophoresis was carried out at 40V – 150V for 1 – 2 h.

Table 2.3: Constituents of a single resolving and a single stacking gel.

	Resolving gel	**Stacking gel**
dH_2O	1.6 mL	1.2 mL
1M Tris – HCl	2.5 mL (pH 8.8)	225 µL (pH 6.8)
30% Acrylamide (Protogel)	2 mL	289 µL
10% SDS	50 µL	17.3 µL
N,N,N',N'-tetramethylethane-1,2-diamine (TEMED)	5 µL	1.7 µL
10% ammonium persulfate (APS)	500 µL	17.3 µL

2.15 Detection of proteins by Coomassie blue staining

Proteins separated by SDS-PAGE were visualised by Coomassie blue staining. Gels were rinsed with dH_2O before being submerged into patented Coomassie stain, Instant Blue (Expedion), and incubated for 1 – 2 h at RT on a rocking

platform. The gels were rinsed again with dH2O and dried between wetted cellophane membranes on a gel drier (Bio-Rad).

2.16 Detection of protein by western blotting

Proteins were separated by SDS-PAGE and then transferred onto a nitrocellulose membrane (Amersham) for western blotting analysis. Fibre pads, 3 MM paper, and the nitrocellulose membrane were first prepared by soaking in western transfer buffer (25 mM Tris, 119 mM glycine and 20% methanol). Electroblotting was carried out at 150 mA for 1.5 h using a Mini-Trans-Blot Electrophoretic Transfer Cell (Bio-Rad). Following protein transfer, the nitrocellulose membrane was incubated in blocking buffer (1% skimmed milk powder (Marvel) in Tris-salt (TS) buffer: 10 mM Tris-HCl pH 7.0, 150 mM NaCl) at RT for 1 h on a rocking platform. The membrane was incubated with primary antibodies (Table 2.4) in blocking buffer supplemented with 0.1% non-ionic, non-denaturing detergent, igepal CA-630 (Sigma Aldrich) at 4°C overnight on a rocker. The membrane was washed with 1x TS, 2x TS/0.1% igepal CA-630 and 1x TS buffer for 10 min each, for a total of 40 min. After washing, the membrane was incubated with secondary antibodies, conjugated to horseradish peroxidase (HRP) (Table 2.4) in blocking buffer supplemented with 0.1% igepal CA-630 at RT for 2 h. The membrane was washed as described previous before the protein-bound HRP was visualised using enhanced chemiluminescence (ECL) reagents (ThermoScientific) as directed by the manufacturer, together with a Bio-Rad imager.

Table 2.4: Overview of all antibodies used and their respective concentrations.

Antibodies	Clonality	Manufacturer details	Dilution
Primary anti – Nrf2	Rabbit polyclonal	H-300, sc-13032, SantaCruz	1:1000
Primary anti – Nrf2	Rabbit monoclonal	D1Z9C XP, Cell Signalling	1:1000
Primary anti – NQO1	Mouse monoclonal	A-5, sc-271116, SantaCruz	1:100
Primary anti – HO-1	Rabbit polyclonal	H-105, sc-10789, SantaCruz	1:1000
Primary anti – AhR	Rabbit polyclonal	BML-SA210-0100, Enzo Life Sciences	1:2500
Primary anti – CYP1A1	Rabbit polyclonal	H-70, sc-20772, SantaCruz	1:100
Primary anti – Keap1	Mouse monoclonal	1B4 ab119403, Abcam	1:1000
Primary anti – GFP	Rabbit polyclonal	ab6556, Abcam	1:1000
Primary anti – β-actin	Rabbit polyclonal	R-22, sc-130657, SantaCruz	1:250
Secondary ECL anti– rabbit IgG HRP conjugated	Donkey polyclonal	NA9340, GE Healthcare	1:1000
Secondary ECL anti– mouse IgG HRP conjugated	Sheep polyclonal	NA931, GE Healthcare	1:1000

2.17 Förster Resonance Energy Transfer (FRET)

2.17.1 Fluorescence spectra

All fluorescence spectra were acquired using a single sample unit PerkinElmer LS 55 luminescence spectrometer (5 nm slit width, 1 nm interval, 1 second integration) and an excitation wavelength of 435 nm. Fluorescence emission spectra were recorded from 400 to 600 nm. Samples were measured in cuvettes (3.5 mL volume, 10 mm path length, Sarstedt). The samples were diluted in FRET buffer (20 mM Tris-HCl pH 7.4 buffer containing, 0.5 mM DTT, 100 mM NaCl, 5 mM $MgCl_2$, 0.1 mM EDTA and 5% v/v glycerol) to a final volume of 3 mL. The cuvettes were sealed with parafilm and inverted 10 times. Fluorescence emission spectra of the FRET pair and eCFP-TEV-Nrf2 and eYFP-TEV-Kelch were recorded separately. All samples were measured in duplicate.

2.17.2 FRET efficiency and sensitised emission

The observed decrease in donor emission at 475 nm of the donor and acceptor pair relative to that of the donor alone was used to calculate the efficiency of energy transfer (FRET efficiency or FE) between the fluorescent fusion proteins:

$$FE = 1 - \frac{F^{da}}{F^{d}}$$

Where da = donor emission in the presence of the acceptor and d = donor emission in the absence of the acceptor.

The observed increase in acceptor emission at 527 nm of the donor and acceptor pair relative to that of the acceptor alone was used to calculate the sensitised emission (SE) of the acceptor fluorescence:

$$SE = \frac{F^{ad}}{F^{a}} - 1 * \frac{(\varepsilon a * ca)}{(\varepsilon d * cd)}$$

Where ad = acceptor emission in the presence of the donor, a = acceptor emission in the absence of the donor, εa or εd = extinction coefficient of the acceptor or donor respectively and ca or cd = molar concentration of the acceptor or donor respectively.

2.17.3 FRET eCFP-TEV-eYFP validation: ProTEV protease

A series of 100 µL reactions were prepared in duplicate containing increasing amounts of ProTEV protease (Promega) (0.5, 1.0, 1.5, 2.0, 2.5, 5.0 and 10 units). Each reaction contained 20 µg purified eCFP-TEV-eYFP protein, 1x ProTEV buffer and 1 mM DTT, which was made to a total of 100 µL with dH_2O. The mixture was vortexed and pelleted at 13,000 x g for 10 sec. A control reaction containing the fusion protein but no ProTEV protease was prepared in parallel. Both test and control reactions were incubated at 30 °C for 30 min. After incubation, 20 µL aliquots of the reaction mixtures were removed for SDS-PAGE analysis (2.14) and stored at - 20 °C. The remaining 80 µL reaction mixtures were transferred to cuvettes containing FRET buffer.

2.17.4 FRET pair: eCFP-TEV-Nrf2 and eYFP-TEV-Kelch titration

Following the determination of the eCFP-TEV-Nrf2 and eYFP-TEV-Kelch protein concentrations, the protein mixtures were diluted as appropriate in FRET buffer. Final concentrations of 0.05, 0.07, 0.09, 0.11, 0.20, 0.30, 0.40, 0.50, 0.60, 0.70 and 0.80 μM eYFP-TEV-Kelch or unconjugated eYFP were added to a final concentration of 0.11 μM eCFP-TEV-Nrf2. Protein samples containing either the donor or acceptor were prepared separately.

Emission spectra were recorded and FRET efficiencies and sensitised emissions were calculated for each protein combination. Binding curves were fitted by nonlinear regression using SigmaPlot software (ligand binding, one site saturation) and K_d and B_{max} values were determined.

In addition, the emission intensity values at 527 nm were plotted for eCFP-TEV-Nrf2 titrated with unconjugated eYFP and for direct excitation of eYFP-TEV-Kelch. Linear regression was used to connect the data points and generate slope values:

$y = ax+b$

Where y represents the emission at 527 nm, a is the extent of emission increase upon titration of eCFP-TEV-Nrf2 with increasing concentration of unconjugated eYFP or as a result of the direct excitation of eYFP-TEV-Kelch and b is the emission at 527 nm when the concentration of unconjugated eYFP or eYFP-TEV-Kelch (x) is 0 μM (y intercept).

2.17.5 FRET buffer system optimisation: NaCl

A series of solutions were made containing increasing amounts of NaCl (0, 50, 100 and 150 mM) in the original FRET buffer (without NaCl where appropriate). Each mixture contained 0.11 μM eCFP-TEV-Nrf2 and 0.30 μM eYFP-TEV-Kelch. Fluorescence emission spectra were recorded.

2.17.6 FRET pair: eCFP-TEV-Nrf2 and eYFP-TEV-Kelch validation: ProTEV protease

A series of 100 µL reactions were prepared containing increasing amounts of ProTEV protease (2.5, 5.0, 7.5 and 10 units). Each reaction contained 8.9 µg eCFP-TEV-Nr2 and 24.3 µg eYFP-TEV-Kelch, 1x ProTEV buffer, 1 mM DTT and dH_2O. The mixture was vortexed and pelleted at 13,000 x g for 10 sec. A control reaction containing the fusion proteins but no ProTEV protease was prepared in parallel. The reactions were incubated at 30°C for 30 min. Following incubation, 20 µL aliquots of the reaction mixtures were removed for SDS-PAGE analysis (Section 2.14) and stored at - 20°C. The remaining 80 µL reaction mixtures were transferred to cuvettes containing FRET buffer. Fluorescence emission spectra were recorded.

2.17.7 Inhibition of FRET between FRET pair: eCFP-TEV-Nrf2 and eYFP-TEV-Kelch

Vehicle (DMSO) concentration

A series of solutions in FRET buffer were made containing increasing percentages of DMSO (0, 1, 5 and 10%). Each mixture contained 0.11 µM eCFP-TEV-Nrf2 and 0.30 µM eYFP-TEV-Kelch. Fluorescence emission spectra were recorded.

Nrf2 peptide inhibitor

Solutions in FRET buffer were made containing 0.11 µM eCFP-TEV-Nrf2 and 0.30 µM eYFP-TEV-Kelch in the presence or absence of 10 µM of an unlabelled Nrf2 derived peptide inhibitor (in 0.1% DMSO). Fluorescence emission spectra were recorded.

2.17.8 FRET - multi-well plate format

All fluorescence spectra were acquired using a Pherastar BMG Labtech microplate reader (excitation filter: 430 nm, dual emission filters: 480 nm and 530 nm). The

samples were diluted in FRET buffer (20 mM Tris-HCl pH 7.4 buffer containing, 0.5 mM DTT, 0.1 mM EDTA and 5% v/v glycerol) to a final volume of 100 µL.The untreated black 96-well microtiter plates (Corning) were covered with aluminium foil to protect the fluorophore-fused proteins from light and incubated at 800 rpm on a plate shaker for 4 min. Fluorescence emission spectra of the FRET pair and eCFP-TEV-Nrf2 and eYFP-TEV-Kelch were recorded separately. All samples were measured in triplicate.

2.17.9 FRET titration - multi-well plate format

Following the determination of the eCFP-TEV-Nrf2 and eYFP-TEV-Kelch protein concentrations, the protein mixtures were diluted as appropriate in FRET buffer. Final concentrations of 0.01, 0.03, 0.05, 0.07, 0.09, 0.11, 0.20, 0.30, 0.40 and 0.50 µM eYFP-TEV-Kelch were added to a final concentration of 0.11 µM

eCFP-TEV-Nrf2 or eCFP-TEV-Nrf2 mutant proteins. Emission intensity values at 480 nm and 530 nm were recorded and FRET efficiencies were calculated for each protein combination. Binding curves were fitted by nonlinear regression using SigmaPlot software (ligand binding, one site saturation) and K_d and B_{max} values were determined.

2.17.10 FRET competition – multi-well plate format

In this multi-well plate format concentrations of 0.11 µM eCFP-TEV-Nrf2 and 0.20 µM eYFP-TEV-Kelch were used (~ 80% of maximal FE). Assays were performed with increasing concentrations of peptide inhibitor (0.001 – 100 µM) at a final volume of 100 µL and a final DMSO concentration of 0.1% v/v. All measurements were carried out in triplicate. Plates were read directly after mixing the components. The percentage inhibition was determined using:

$$\% \text{ FE} = 1 - \frac{\text{FE}^{\text{vehicle}} - \text{FE}^{\text{inhibitor}}}{\text{FE}^{\text{vehicle}}} * 100$$

Inhibition curves were fitted to a standard four-parameter logistic function using SigmaPlot and IC_{50} values were determined.

2.17.11 Calculation of Z′ value

The suitability of this assay for high throughput screening (HTS) was assessed by determining the Z′ value. This parameter is used as a measure of assay performance, based on the maximal and minimal fluorescence intensity at 480 nm. The Z′ value was calculated using the equation:

$$Z' = 1 - \frac{3SD_{maxFRET} - 3SD_{minFRET}}{maxFRET_{480nm} - minFRET_{480nm}}$$

Where min $FRET_{480nm}$ = the minimal fluorescence intensity observed in the absence of any inhibitor, max $FRET_{480nm}$ = the maximal fluorescence intensity observed in the presence of an inhibitor, and SD = the standard deviation of the fluorescence emissions at 480 nm. For both minimal and maximal fluorescence signal 0.11 µM eCFP-TEV-Nrf2 and 0.20 µM eYFP-TEV-Kelch was pipetted into the wells. The min $FRET_{480nm}$ condition was obtained using a final concentration of 0.1% v/v DMSO and the max $FRET_{480nm}$ condition was acquired using 100 µM of the 7-mer stearic acid (St) conjugated peptide St-DPETGEL in a final concentration of 0.1% v/v DMSO. The fluorescence emission at 480 nm of both the minimal and maximal fluorescence signal was measured in 48 wells of a 96-well plate. Triplicate experiments were performed.

2.18 Mammalian tissue culture and reagents

Alpha Modified Eagle Medium nucleotide free (α-MEM), Dulbecco's Modified Eagle's medium (DMEM), foetal bovine serum (FBS), 200 mM glutamine, Dulbecco's phosphate buffered saline without Ca^{2+}/Mg^{2+} (DPBS-), trypsin-EDTA and 10,000 units and 10,000 µg/ml penicillin and streptomycin were purchased from Invitrogen. Eagle's minimal essential medium (EMEM) was supplied by Lonza via VWR.

The murine hepatoma Hepa1c1c7 cell line was obtained from the European Collection of Cell Culture (ECACC). The BpRc1 cells are a Class II variant of the Hepa1c1c7 cell line and were purchased from the American Type Culture Collection (ATCC). The human epithelial carcinoma HeLa cell line was kindly provided by

Istvan Kovacs (UCL Cancer Institute and Wolfson Institute for Biomedical Research), the human epithelial mammary gland/breast MCF-7 cell line was a gift from Professor Stephen Neidle (UCL School of Pharmacy) and the HEK293 cells were provided by Professor Anne Stephenson (UCL School of Pharmacy). The cells were grown as monolayers and maintained by regular passage in α-MEM (Hepa1c1c7 cell line) or DMEM (BpRc1, HeLa and HEK293 cell line) or EMEM (MCF-7 cell line) supplemented with 2 mM L-glutamine, 100 units per mL penicillin and 100 µg mL-1 streptomycin and 10% heat-inactivated FBS, cultured at 37°C in a water vapour saturated atmosphere with 5% CO_2. Cells were grown in T-75 cm^2 or T-150 cm^2 tissue culture flasks (Helena Biosciences). All manipulations were performed in a sterile environment, with disposable plasticware and glassware reserved specifically for the purpose.

2.19 Sub-culturing of mammalian cell lines

When the mammalian cell lines appeared to be ~ 70% confluent, they required sub-culturing. Cell lines were sub-cultured at least 2 times a week. Cell culture media was aspirated and the cells were gently washed with PBS, which was pre-warmed to 37°C. The PBS was aspirated and 1 mL (for T-75 cm^2 tissue culture flasks) or 3 mL (for T150 cm^2 tissue culture flasks) of pre-warmed 0.25% trypsin-EDTA (1x) (Life Technologies) was added onto the cells and incubated at 37°C for 1 - 5 min. The tissue culture flasks were gently tapped to dislodge the cells and 5 mL (for T-75 cm^2 tissue culture flasks) or 10 mL (for T-150 cm^2 tissue culture flasks) of pre-warmed cell culture medium with FBS was added to inactivate trypsin. Cells were mixed by resuspension. A 20 µL sample of the cell suspension was taken and 20 µL of trypan blue was added (2x dilute sample). A 10 µL sample of the trypan blue mixture was taken and added to a haemocytometer before counting the cells in the counting chambers. After cell counting, an appropriate volume of the original cell suspension was added to a new tissue culture flask with 10 mL (for T-75 cm^2 tissue culture flasks) or 20 mL (for T-150 cm^2 tissue culture flasks) of pre-warmed cell culture medium. The density of cells added was 4 x 10^5 cells/T-75 cm^2 and 8 x 10^5 cells/T-150 cm^2 for ~ 70% confluency after 3 days and 2 x 10^5 cells/T-75 cm^2 and 4 x10^5 cells/T-150 cm^2 for ~ 70% confluency after 4 days. The flasks were incubated at 37°C and 5% CO_2 until ~ 70% confluency after which cells were used for subsequent experiments or sub-cultured as above.

2.20 Storage & revival of mammalian cells in liquid nitrogen

Mammalian cell lines that had reached a ~ 70% confluency, were used to make liquid nitrogen stocks. Cells were harvested using the method as described in Section 2.19. The cell suspension was centrifuged at 500 x g for 5 min at 4°C in a sterile 15 mL centrifuge tube. The supernatant was aspirated and the pellet was resuspended in pre-warmed PBS. Cells in the PBS suspension were counted as described in Section 2.19. The cell suspension was centrifuged and the supernatant was aspirated before adding 1 mL of serum free cell freezing media, Bambanker (Anachem)/1 x 10^6 cells. The cell suspension was transferred to cryotubes (Nunc) and placed in liquid nitrogen for future use.

A vial of frozen cells was taken from the liquid nitrogen storage container and rapidly defrosted in a water bath at 37°C. When the cells were completely thawed, they were transferred to 10 mL of culture medium and centrifuged at 500 x g at 4°C for 5 min. The supernatant was aspirated and 1 mL of culture medium was added to the pellet. Cells were resuspended and transferred to a T-75 cm^2 tissue culture flask with 10 mL pre-warmed cell culture medium. The flasks were incubated at 37°C and 5% CO_2. The following day the media was aspirated and replaced with new pre-warmed culture medium. The cells were grown until they had reached ~ 70% confluency before sub-culturing.

2.21 Crude, cytoplasmic and nuclear lysate fractions

The cells were grown until 70% confluence before they were dissociated with 1.5 – 3 mL trypsin for 1 – 2 min, resuspended in PBS, counted and pelleted. Crude cell lysates were obtained by adding 100 µL/ 4 x 10^6 cells RIPA buffer (100 mM Tris-HCl pH 7.5, 150 mM NaCl, 1mM EDTA, 1% igepal, 0.1% SDS, 0.1% deoxycholic acid, 10 mM DTT and 1x Halt protease inhibitor (AEBSF, aprotinin, bestatin, E-64, leupeptin, pepstatin, EDTA, Thermo Scientific). The mixture was incubated on ice for 30 min and centrifuged at 16,000 x g at 4°C for 15 min. The supernatant, containing the crude cell lysate, was stored at - 20°C. Nuclear and cytosolic lysate fractions were separated by NE-PER Nuclear and Cytoplasmic Extraction Reagents (Thermo Scientific). Ice-cold 100 µL/1x10^6 cells CER I + 1x Halt protease inhibitor was added to the pellet. The tube was vortexed for 15 sec and incubated on ice for

10 min. Ice-cold 5.5 µL/1x10^6 cells CER II was added to the mixture, vortexed for 15 sec and incubated on ice for 1 min. The suspension was then pelleted at 16,000 x g at 4°C for 5 min. The supernatant, containing the cytoplasmic lysate fraction, was transferred to a pre-chilled tube and stored at - 20°C. Next, ice-cold 50 µL/1x10^6 cells NER was added to the pellet, vortexed for 15 sec and incubated on ice for 10 min. This procedure was repeated for a total time of 40 min before the suspension was pelleted at 16,000 x g at 4°C for 10 min. The supernatant, containing the nuclear lysate fraction, was transferred to a pre-chilled tube and stored at - 20°C.

2.22 NQO1 induction assays

Hepa1c1c7 or BpRc1 cells were seeded in tissue-culture treated 96-well plates with a cell density of 2 x 10^4 cells/200 µL per well and incubated overnight in a 37°C incubator. The cells were treated with compound or vehicle (0.1% DMSO final concentration) and incubated for a further 24 h. The culture medium was aspirated and cells were lysed using 50 µL per well lysis buffer (0.1% Tween20 in 2 mM EDTA) and the plate shaken at RT for 15 min. An enzyme reaction was initiated by adding 200 µL of mixture to each well: 0.067% bovine serum albumin (BSA), 0.01% Tween20, 5 µM flavin adenine dinucleotide disodium salt (FAD), 1 µM glucose-6-phosphate (G6P), 30 µM β-nicotinamide adenine dinucleotide phosphate hydrate (NADP), 40 units G6P dehydrogenase, 0.03% thiazolyl blue tetrazolium bromide (MTT) and 50 µM menadione in 25 mM Tris-HCl pH 7.5.

After incubation at RT for 5 min, 40 µL of stop solution (10% SDS, 1.5% final concentration) was added to each well. The plate was shaken briefly before measuring the absorbance at 595 nm on a PerkinElmer EnVision or a BMG Pherastar plate reader. The background optical density was measured using wells containing tissue culture medium, lysis buffer, and enzyme and stop solutions without Hepa1c1c7 or BpRc1 cells. The optical density values at 595 nm were averaged and the background corrected ratio of optical densities was calculated:

$$\text{Ratio optical density} = \frac{OD_{595nm}^{\text{compound treated}}}{OD_{595nm}^{\text{vehicle treated}}}$$

The concentration of compound causing a doubling of NQO1 activity (change in optical density) relative to the vehicle was estimated from a plot of change in optical density versus concentration (CD value).

2.23 SRB cytotoxicity assays

Hepa1c1c7 or BpRc1 cells were seeded in tissue-culture treated 96-well plates with a cell density of $2x10^4$ cells/200 µL per well and incubated overnight in a 37°C incubator. The cells were treated with compound or vehicle (0.1% DMSO final concentration) and incubated for a further 24 or 48 h. The culture medium was aspirated and cells were fixed by adding 100 µL of ice-cold trichloroacetic acid (TCA, Sigma Aldrich) to each well. After incubation at 4°C for 1 h, wells were washed five times with 200 µL of dH_2O and dried in a hot-air oven. TCA fixed cells were stained with 100 µL of 0.4% w/v sulphorhodamine B (SRB, Sigma Aldrich) in 1% acetic acid at RT for 30 min. SRB was removed before the wells were washed five times with 200 µL of 1% acetic acid and dried in a hot-air oven. To dissolve the SRB dye, 100 µL of 10 mM Tris was added to each well and incubated at RT for 10 min on a plate shaker. The optical density values at 564 nm (BMG Spectrostar plate reader) were averaged and the background corrected percentage viability was calculated:

$$\% \text{ Cell viability} = 1 - \frac{OD_{564nm}^{\text{vehicle}} - OD_{564nm}^{\text{compound treated}}}{OD_{564nm}^{\text{vehicle}}} * 100$$

2.24 CYP1A1 induction assay

Hepa1c1c7 cells were seeded in tissue-culture treated 96-well plates with a cell density of $2x10^4$ cells/200 µL per well and incubated overnight in a 37°C incubator. The cells were treated with compound or vehicle (0.1% DMSO final concentration) and incubated for a further 6 or 24 h. The culture medium was aspirated and cells were washed with PBS before addition of culture medium containing luciferin substrate. After cells were incubated at 37°C for 3 h, 25 µL of the culture medium was transferred to a white luminometer plate. Subsequently, 25 µL of luciferin detection reagent was added to each well and incubated at RT for 15 min in the

dark. CYP1A1 activity was measured using a luminescence filter with the BMG Pherastar plate reader. Next, the cells were fixed in 10% TCA and stained with SRB (Section 2.23). The percentage cell viability was calculated and used to correct the luminescence values on an individual well basis.

2.25 Flow cytometry

All flow cytometry samples were analysed on a MACSQuant Analyzer (Miltenyi Biotec) using MACSQuantify software. Calibration checks were performed daily. The MACSQuant Analyzer has 3 lasers (405 nm, 488 nm and 635 nm) and 9 detectors: 2 for light scatter and 7 for fluorescence. MACSQuant running buffer, washing solution, storage solution and bleach solution were purchased from Miltenyi Biotec.

2.25.1 Intracelllular Nrf2 staining assay

Hepa1c1c7, HeLa and MCF-7 cells were seeded in tissue-culture treated T-75 cm^2 flasks and grown until 70% confluence. The cells were treated with 10 μM sulforaphane or other Nrf2 inducer compound for different periods of time and incubated at 37°C at 5% CO_2 before dissociation with trypsin. Cells were pelleted and resuspended in PBS and used for western blotting (Section 2.16) or flow cytometric analysis.

2.25.1.1 Standard protocol

The ‘standard protocol’ was developed as an initial intracellular staining method for the detection of Nrf2. Unstimulated and stimulated Hepa1c1c7 cells were fixed by adding 40 μL 36.5 - 38% in H_2O formaldehyde solution (Sigma Aldrich) to 1 mL PBS to obtain a final concentration of ~ 1.5 % formaldehyde. Cells were incubated at RT for 10 min and pelleted. After a centrifugation step, cells were resuspended in the residual 100 μL PBS. The cells were then permeabilised by slowly adding 900 μL of ice-cold 100% methanol (Sigma Aldrich) and incubated on ice for 30 min or stored

up to 1 week at - 80°C. Permeabilised cells were washed with 0.5 mL flow buffer (0.5% BSA/2 mM EDTA in PBS buffer) before blocking in 0.5 mL flow buffer at RT for 10 min. Subsequently, cells were stained with 5 µL of polyclonal rabbit anti-Nrf2 primary antibody (H-300, sc-13032, SantaCruz) in 0.5 mL flow buffer and incubated at 4°C overnight. After primary antibody staining, cells were washed with 1 mL flow buffer and pelleted. Cells were then incubated with 1 uL of polyclonal goat anti-rabbit IgG FITC conjugated secondary antibody (sc-2012, SantaCruz) or isotype control normal rabbit IgG (sc-3888, SantaCruz) in 0.5 mL flow buffer at RT for 1 h. Finally, cells were washed with 1 mL flow buffer, pelleted and resuspended in 0.3 mL flow buffer before being analysed on a flow cytometer.

2.25.1.2 Adapted standard protocol – 'whole' cells and isolated nuclei

The 'adapted standard protocol' was implemented to quantify Nrf2 using flow cytometry after examination of a range of parameters to improve the 'standard protocol'. Hepa1c1c7, HeLa and MCF-7 cells were handled as described above and processed as whole cells or isolated nuclei. To obtain intact nuclei, cells were pelleted in PBS and resuspended in 100 µL/1 x 10^6 cells CER I (+ Halt protease inhibitor) (NE-PER kit, Thermo Scientific). After incubating the mixture on ice for 10 min, 5.5 µL/1 x 10^6 cells CER II (NE-PER kit, Thermo Scientific) was added and left on ice for 1 min. Nuclei were pelleted and resuspended in 1 mL PBS. Isolated nuclei were checked for their integrity by staining an aliquot of the nuclei suspension with trypan blue. Nuclei look round and blue, whole cells do not get stained and cell debris appears as blue irregular shaped particles. Cells and nuclei were fixed by adding 40 µL 36.5-38% in H_2O formaldehyde solution (Sigma Aldrich) to 1 mL PBS to obtain a final concentration of ~ 1.5 % formaldehyde. Cells were incubated at RT for 10 min. After a centrifugation step, cells and nuclei were resuspended in the residual 100 µL PBS. Subsequently, 1 mL of ice-cold 100% methanol was added. Cells and nuclei were left to incubate on ice for 30 min or stored up to 1 week at -80°C. Permeabilised cells and nuclei were washed with 0.5 mL flow buffer before a 10 min blocking step in 0.5 mL flow buffer. Next, 0.5 µL monoclonal rabbit anti-Nrf2 primary antibody (D1Z9C) XP (Cell Signalling) was added and the cell/nuclei – antibody mixture was left to incubate at 4°C overnight. After a washing step in 1 mL flow buffer, cells and nuclei were pelleted and resuspended in 0.5 mL flow buffer. They were incubated with 2.5 µL polyclonal goat anti-rabbit IgG FITC conjugated

secondary antibody (sc-2012, SantaCruz) or isotype control normal rabbit IgG (sc-3888, SantaCruz) in 0.5 mL flow buffer at RT for 1 h. After a washing step with 1 mL flow buffer, cells and nuclei were resuspended in 0.3 mL flow buffer and analysed on a flow cytometer.

2.25.1.3 Analysis

Fluorochrome emission was captured for FITC conjugates using a Band Pass (BP) filter 525/50 and a laser excitation of 488 nm. All samples (10.000 events/sample) were measured with the same protocol setting 150V FSC, 300V SSC, 300V FITC.

FITC fluorescence histograms, which graphically summarise the distribution of univariate data sets, were normalised by height and smoothed using predefined algorithms with the MACS Quantify software.

Data was analysed by normalizing the median fluorescence intensity (MFI) to an internal staining control (nMFI):

$$\text{nMFI} = \frac{\text{MFI}_{\text{sample}}}{\text{MFI}_{\text{internal staining control}}}$$

The internal staining controls are cells stained with the secondary antibody only. nMFI is representing shifts in the population's fluorescence intensity without being affected by outliers. The fold change was calculated using the nMFI of stimulated (S) and the nMFI of unstimulated (US) samples:

$$\text{Fold change} = \frac{\text{nMFI}_{\text{S}}}{\text{nMFI}_{\text{US}}}$$

2.25.2 ROS detection

Hepa1c1c7 cells were seeded in tissue-culture treated 6-well plates with a cell density of $2x10^5$ cells/2 mL per well and incubated overnight in a 37°C incubator. The cells were treated with compound or vehicle and incubated at 37°C for 1 h. The culture medium was removed and CellROX reagent diluted in culture medium was added and incubated at 37°C for 30 min. Culture medium was aspirated and cells were washed with PBS. Cells were dislodged by adding 0.25% trypsin-EDTA,

incubation at 37°C for 1 min and adding culture medium to neutralise the enzymatic reaction. The cells were pelleted and washed with PBS before they were resuspended in 0.5 mL PBS and analysed on a flow cytometer. The fluorescence emission of the CellROX deep red reagent was measured using a band-pass (BP) filter 655/730 and a laser excitation of 635 nm. All samples (10,000 events/sample) were measured with the same protocol settings 150V FSC, 300V SSC, 250V APC. Data was analysed using the median fluorescence intensity (MFI).

2.25.3 Uptake fluorescently labelled peptides

Hepa1c1c7 cells were seeded in tissue-culture treated 6-well plates with a cell density of $2x10^5$ cells/2 mL per well and incubated at 37°C overnight. The cells were treated with 1 µM fluorescently labelled peptide (0.1% DMSO final concentration) and incubated at 37°C for 5, 10, 30, 60 or 120 min. The culture medium was removed and cells were washed twice with PBS. Cells were incubated with 0.25% trypsin-EDTA at 37°C for 15 min. The cells were pelleted and washed twice with PBS before they were resuspended in 0.3 mL PBS and analysed on a flow cytometer. The fluorescence emission of the FITC labelled peptides was detected using a BP filter 525/50 and a laser excitation of 488 nm. All samples (10,000 events/sample) were measured with the same protocol settings 150V FSC, 300V SSC, 300V FITC. Data was analysed using the median fluorescence intensity (MFI).

2.26 Confocal Laser Scanning Microscopy (CLMS)

Confocal microscopy was used to image peptide uptake and sub-cellular distribution in fixed and live Hepa1c1c7 cells. A LSM 710 was used (Zeiss, Germany) with a Plan-Apochromat 63x/1.40 Oil DIC M27 immersion objective. The fluorescent labelled cells were excited with an Argon at 488 nm, a Diode at 405 nm and a Helium-Neon at 633 nm, all lasers were set at 2% total laser power. A number averaging of 4, a scan speed of 8 – 10, a bit depth of 12 and frame size of 1024 x 1024 were used to obtain the images. The range indicator was used to indicate regions of over- and undersaturation. The areas with blue (undersaturation) and red

(oversaturation) were adjusted accordingly using the digital offset and gain. Image conditions were kept constant when comparing test and control samples.

2.26.1 Cellular uptake of fluorescently labelled peptides in fixed cell samples

Hepa1c1c7 cells were seeded on glass cover slips in tissue culture treated 6-well plates with a cell density of 2 x 10^5 cells/ 2 mL and grown at 37°C overnight. The cells were treated with 1 µM or 10 µM fluorescently labelled peptide (0.1% DMSO final concentration) and incubated at 37°C for 1 h. The culture medium was removed and the cells were washed twice with PBS and submerged in 1x CellMask plasma membrane stain (Invitrogen, Life Technologies) diluted in PBS. After incubation at 37°C for 5 min, the staining solution was removed and the cells were washed twice with PBS. The cells were fixed in 2 mL of freshly prepared 2% paraformaldehyde (PFA) at RT for 10 min. The cells were washed twice with PBS and mounted on glass microscope slides (Thermo Scientific) with mounting medium containing DAPI stain (Hardset, Vectashield). Prepared slides were left to dry at RT for 30 min before they were imaged on a confocal laser scanning microscope.

2.26.2 Cellular uptake of fluorescently labelled peptides in live cell samples

Hepa1c1c7 cells were seeded in glass bottom dishes (Matek) with a cell density of 2 x 10^5 cells/ 2 mL and grown at 37°C overnight. The cells were treated with 1 µM or 10 µM fluorescently labelled peptide (0.1% DMSO final concentration) and incubated at 37°C for 1 h. The culture medium was removed and the cells were washed twice with PBS. The cells were incubated with 2 mL of 5 µg/mL Hoechst DNA dye diluted in culture medium (in 0.1% DMSO final concentration) at 37°C for 25 min. The Hoechst DNA dye was removed and cells were washed twice with PBS. The cells were submerged in 1x CellMask plasma membrane stain diluted in PBS. After incubation at 37°C for 3 min, the staining solution was removed and the cells were washed twice with PBS. The cells were replenished with fresh 2 mL culture medium and imaged on a confocal laser scanning microscope in a temperature and CO_2 controlled chamber (37°C and 5% CO_2).

3 Development of a steady-state FRET-based assay to identify inhibitors of the Keap1-Nrf2 protein-protein interaction

3.1 Introduction

The expression of *ARE* driven gene products can be modulated by molecules that possess electrophilic properties. These compounds increase Nrf2 activity by modifying reactive cysteine residues within Keap1, thereby blocking the ubiquitination process and stabilising Nrf2. An alternative approach to modulate *ARE* activation is by direct disruption of the Keap1-Nrf2 PPI. Potential advantages include increased target specificity and the reversible nature of these Nrf2 inducers. Several studies have shown that peptides and small molecules with sequences based on the Nrf2 - high affinity ETGE motif (residues 79-82) are able to bind to the Keap1 Kelch domain, thereby perturbing the strength of the Keap1-Nrf2 PPI [52, 135, 143, 151].

The aim of this chapter is to establish a steady-state FRET assay to study the Keap1 – Nrf2 PPI. This assay can be used to identify and evaluate potential Keap1 binding partners. Furthermore, the binding behaviour of inhibitors can be studied.

Theodor Förster was one of the founding fathers of FRET, hence the technique is also referred to as Förster resonance energy transfer [152]. FRET is based on Jablonski's theory: the non-radiative energy transfer from an excited donor fluorophore to an acceptor fluorophore by dipole-dipole interactions [153-154] (Figure 3.1). This involves the direct transfer of a proportion of the donor's excitation energy to the acceptor fluorophore. Energy transfer only ensues when the separating distance between both fluorophores is less than 10 nm (100 Å) [155]. This is within the distance range that two conjugated fluorophores may enter when two proteins interact i.e. the proteins involved in the PPI interact closely and the tethered fluorophores are within 10 nm of each other depending on the size of the proteins and the locations of their C- and N-termini. Furthermore, the donor and acceptor fluorophores should have a significant overlap in their fluorescence spectra and a favourable alignment to allow an optimal energy transfer [155]. In a mixture of both

donor and acceptor, FRET can be quantified by determining the extent of an increase in acceptor emission (sensitised emission) or the decrease in donor emission (FRET efficiency) following energy transfer [155-156]. These changes in fluorescence are compared to the fluorescence emission of the donor or acceptor fluorophore measured alone. Sensitised emission and FRET efficiency are calculated as described in Section 2.17.2.

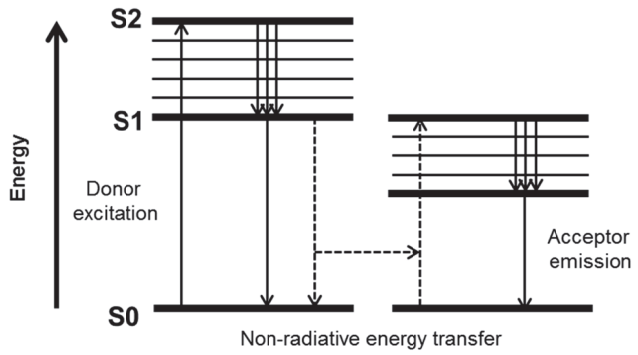

Figure 3.1:Jablonski diagram [153] showing the non-radiative transfer between a donor and an acceptor fluorophore. Excitation of the donor molecule results in the transition from the ground vibrational state (S0) to higher vibrational states (S1 or S2) (↑).This is followed by vibrational relaxation, where the excited donor fluorophore relaxes to lower vibrational levels (↓↓↓). Non-radiative energy transfer occurs when a vibrational state of an excited molecule is coupled to a vibrational state in the acceptor molecule (dashed arrows). Subsequent vibrational relaxation and energy emission from the acceptor molecule occurs at a longer wavelength (↓).

Cyan Fluorescent Protein (CFP, Y66W mutation) and Yellow Fluorescent Protein (YFP, T203Y mutation) are derivatives of green fluorescent protein (GFP) and have a good degree of spectral overlap (Figure 3.2) [157]. This makes the fluorescent proteins an ideal FRET pair. To study PPIs they can be conjugated to two interacting proteins. Moreover, CFP and YFP are highly stable fluorophores, which makes this technique relatively robust. The enhanced versions of the fluorescent proteins, eCFP and eYFP, have additional mutations that increase the quantum yield of the fluorophores [158-159].

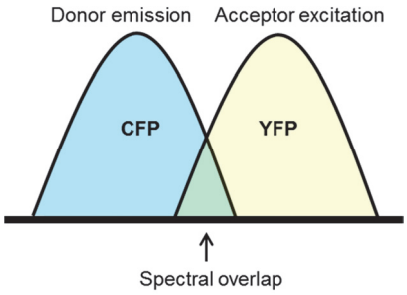

Figure 3.2: Schematic representing the spectral overlap of donor, CFP, and acceptor, YFP. FRET can only occur when both fluorophores are in close proximity of each other and there is significant spectral overlap.

In this study, the donor fluorophore eCFP is fused to an ETGE motif-containing 16-mer Nrf2-derived peptide and the acceptor fluorophore eYFP is conjugated to the Keap1 Kelch domain. X-ray crystallography studies of the complex formed between the human Keap1 Kelch domain and a 16-mer Nrf2 peptide suggested that when the two proteins interact, the distance between the N- or C-terminus of the Keap1 Kelch domain would be within 6 – 8 nm of the N- or C-terminus of the 16-mer Nrf2 peptide [46] (Figure 3.3). Since the C-terminus of the 16-mer Nrf2 peptide is located near to the PPI site, conjugation of a fluorescent protein to the peptide at this position could potentially introduce steric hindrance following the formation of the protein-peptide complex, hence the N-terminus of the peptide was favoured for conjugation. In addition, plasmids were available containing a convenient cloning site downstream of the coding sequence for eCFP or eYFP respectively. As a result, the N-terminus of both proteins was chosen for the fusion of the fluorophores (Figure 3.4).

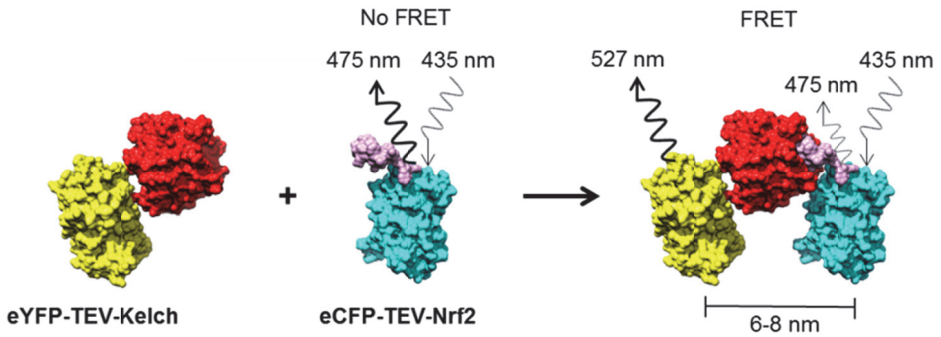

Figure 3.3: Molecular model demonstrating FRET between eYFP-TEV-Kelch and eCFP-TEV-Nrf2. The FRET pair is generated from the human Keap1 Kelch domain (red) and the 16-mer Nrf2 derived peptide (pink) complex (PDB ref: 2FLU) and the fluorophores eYFP (yellow; PDB ref: 1YFP) and eCFP (cyan; PDB ref: 2WSN). Chimera software was used to estimate the separation between the eCFP and eYFP fluorophores in the fusion protein complex [160]. The distance was found to be 6 – 8 nm, which is suitable for FRET (< 10 nm). FRET can be observed as a decrease in donor emission at 475 nm and a concomitant increase in acceptor emission at 527 nm. Adapted from [142].

Figure 3.4: Schematic diagram of the eYFP-TEV-Kelch and eCFP-TEV-Nrf2 constructs. Adapted from [142].

Several other assays have been developed to study potential inhibitors of the Keap1-Nrf2 PPI [132, 161-162] (Figure 3.5). Isothermal calorimetry (ITC) determines the thermodynamic properties of a protein-protein interaction (Figure 3.5 A) [163]. This label-free technique measures the heat exchanged upon binding of ligands to a particular protein and can be used to establish a binding profile [164-166]. Surface Plasmon Resonance (SPR) is another label-free technique that can be used to determine binding kinetics in real-time [133]. Upon association of a ligand with an immobilised binding partner on a sensor chip the angle of reflected polarised light changes (Figure 3.5 B). The extent of the change is a measure of binding affinity and can be used to study different binding partners.

Fluorescence polarisation (FP) is based on the association of fluorescent labelled molecules with larger macromolecules (proteins) [133]. When the small and rapidly rotating labelled ligand is excited with polarised light, the emission is depolarised resulting in a low polarisation value (Figure 3.5 C). Upon binding to a macromolecule, the rate of rotation of a fluorophore-conjugated molecule lowers. The slower rotation increases emission of polarised light and results in a high polarisation value in the bound state. The determined change in polarisation can be used to investigate various protein binding partners [167]. The relative merits of the FRET methodology in relation to previously applied techniques are discussed in Section 3.3.

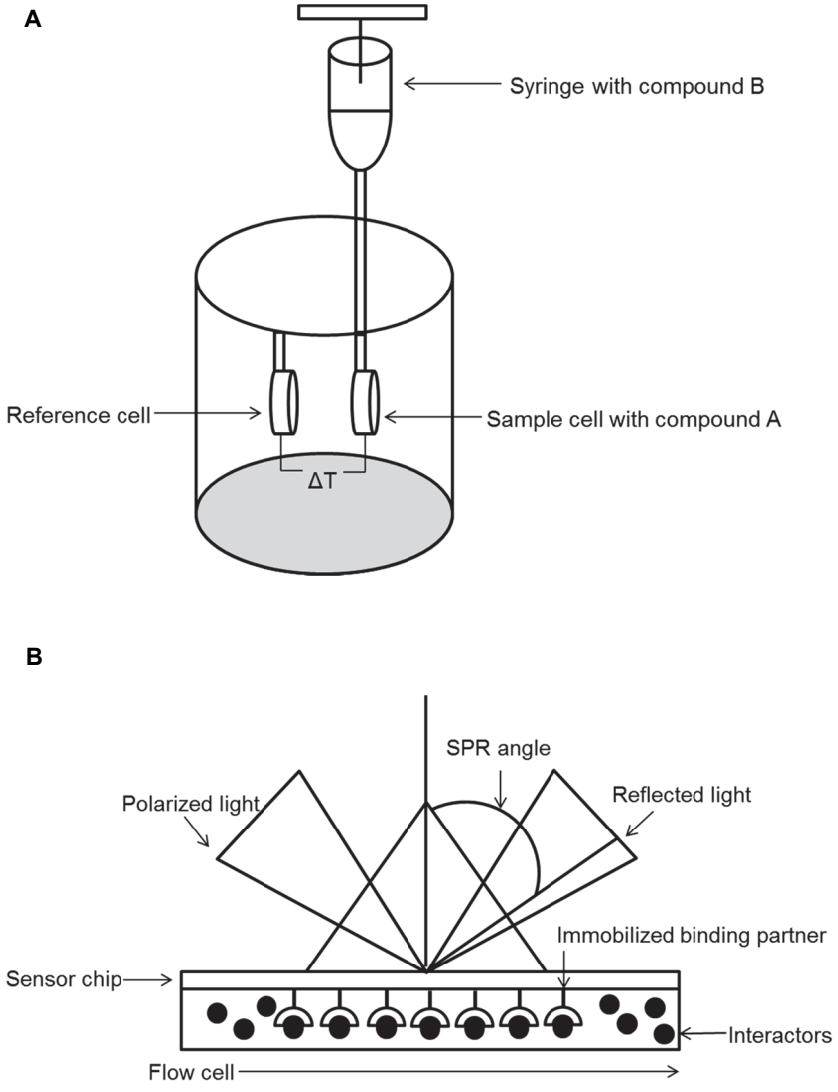

C

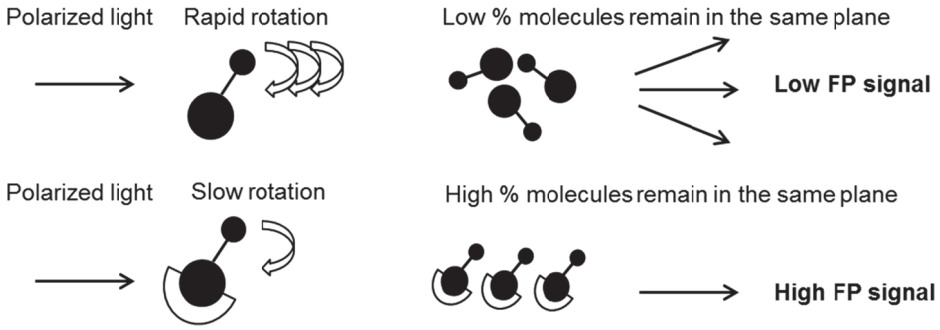

Figure 3.5: Three alternative assays to study potential Keap1-Nrf2 PPI inhibitors. (A) The isothermal calorimetry (ITC) instrument: the sample cell contains one binding partner (compound A) in buffer and the syringe the other binding partner (compound B) in buffer. Following addition of compound B the temperature difference (Δ T) is measured between the sample cell and the reference cell (containing only buffer) and is converted into enthalpy change (Δ H). (B) The inside of a surface plasmon resonance (SPR) instrument: polarised light is applied to the sensor chip that contains an immobilised binding partner. The polarised light is reflected at a certain angle. This angle changes upon binding of interactors to the immobilised binding partner on the sensor chip and can be measured. (C) The fluorescence polarisation (FP) principle: fluorescently labelled molecules are excited with polarised light. During excitation, unbound molecules rotate rapidly, resulting in a low percentage of molecules in the same plane and a relative low FP signal. The rotation of the molecules slows down upon binding to interactors, resulting in a high percentage of molecules in the same plane and a higher FP signal. The difference in FP signal between bound and unbound molecules can be determined.

3.2 Results

3.2.1 Plasmids

Conjugation of proteins to fluorophores provides interesting tools to examine a variety of PPIs found in cancer pathways, both in cell-based and cell-free assays. The sub-cellular localisation of the protein can be observed in cell-based assays, while the protein binding affinity for ligands (proteins, peptides and small molecules) and competition analysis can be studied in cell-free systems. Previously, a protein-protein interaction assay for the HIF1α/p300 interaction using GFP conjugates was developed in our laboratory. The pET28c bacterial expression system was used to produce the eCFP-TEV-HIF1α and eYFP-TEV-p300 proteins [168]. In this respect, the pET28c-eCFP-TEV-HIF1α and pET28c-eYFP-TEV-p300 plasmids [168] were used to generate the plasmids pET28c-eCFP-TEV-Nrf2 and pET28c-eYFP-TEV-Kelch (Figure 3.6) (details in Section 2.3).

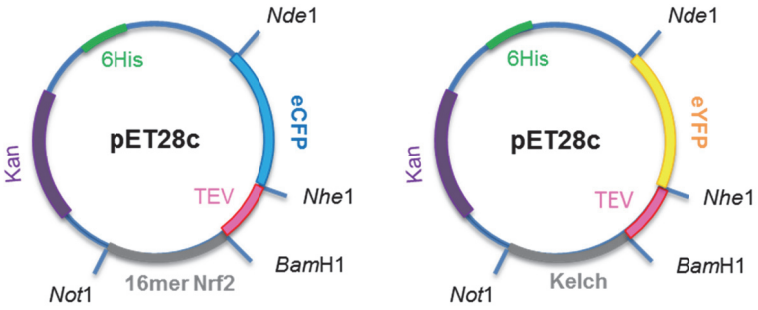

Figure 3.6: The pET28c plasmid constructs containing a kanamycin (Kan) resistance gene, a 6-histadine tag (6His), a Tobacco Etch Virus (TEV) recognition site and eCFP or eYFP and a 16-mer Nrf2 or a Keap Kelch domain respectively.

The plasmids contain constructs to express an eCFP protein conjugated to an ETGE motif-containing 16-mer Nrf2 derived peptide (eCFP-TEV-Nrf2) and an eYFP protein conjugated to the Keap1 Kelch domain (residues 321 – 609) (eYFP-TEV-Kelch). The pET28c-eYFP and pET28c-eCFP-TEV-eYFP plasmids were previously created by Dr. Edwin Nkansah [169] and were used to express unconjugated eYFP

and eCFP-TEV-YFP proteins respectively. The fluorescent protein conjugates have a Tobacco Etch Virus (TEV) recognition site between the C-terminus of the fluorescent tag and the N-terminus of the protein that forms a linker to allow flexible positioning of the fluorophore relative to the protein or peptide.

3.2.2 Purification of eCFP-TEV- eYFP, eCFP-TEV- Nrf2, eYFP-TEV-Kelch and eYFP proteins

Following transformation of *Escherichia coli* Rosetta 2 (DE3) with the pET28c plasmid constructs, the bacteria were induced with IPTG to express the eCFP-TEV-eYFP, eCFP-TEV-Nrf2, eYFP-TEV-Kelch and eYFP proteins (Sections 2.7 and 2.9). The proteins were purified using immobilised metal ion affinity chromatography (IMAC) as described in Section 2.10. Samples of the expressed proteins were analysed by SDS-PAGE (Section 2.14) at each stage of the purification process, which was followed by visualisation of the separated proteins by Coomassie Brilliant Blue staining (Section 2.15). An example of the purification stages for the eCFP-TEV-eYFP protein is shown in Figure 3.7. Lanes 1 & 2 show a predominant expression of the fluorescent fusion protein in the insoluble and soluble part of the crude cell lysate. Lanes 6 – 8 illustrate that the protein expression is even more prominent after IMAC. This enabled the isolation of the protein fractions for the development of subsequent assays.

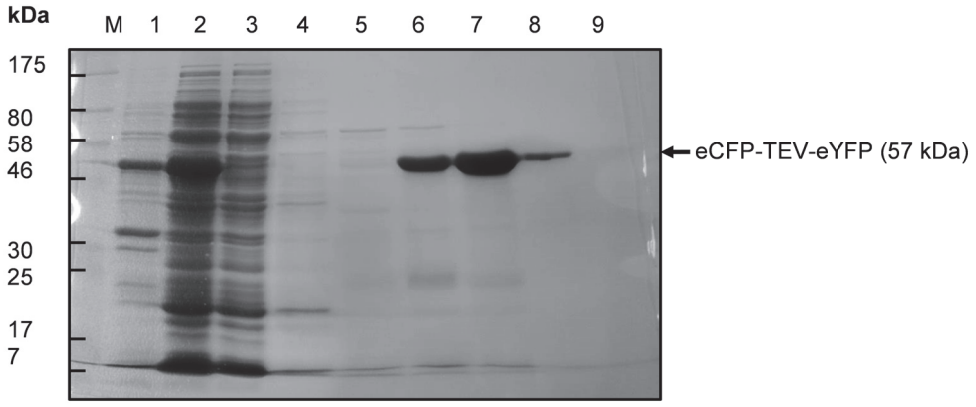

Figure 3.7: The purification stages of the eCFP-TEV-eYFP protein (57 kDa) analysed on a 10% SDS-PAGE gel. Lane M: marker 7 – 175 kDa as labelled, lane 1: insoluble protein in pellet, lane 2: soluble protein, lane 3: unbound protein, lane 4 – 9 proteins eluted with 30, 100, 200, 300, 400 and 500 mM imidazole respectively.

Figure 3.8 shows the purified eCFP-TEV-Nrf2, eYFP-TEV-Kelch and eYFP proteins. Although there are some non-specific protein-bands present in lane 3, the eYFP protein is the major component isolated in the purification process.

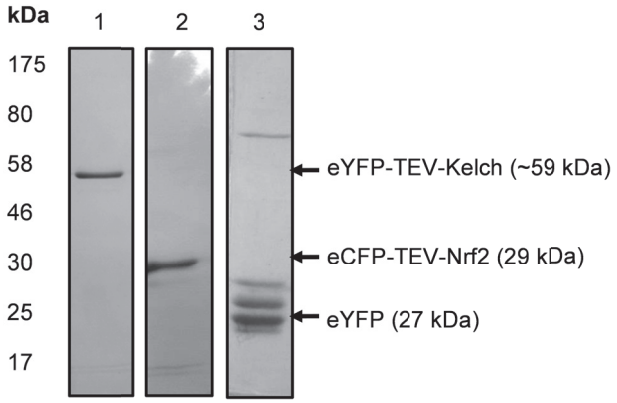

Figure 3.8: A representative example of the purified eYFP-TEV-Kelch (~ 59 kDa) (lane 1), eCFP-TEV-Nrf2 (29 kDa) (lane 2) and eYFP (27 kDa) (lane 3) proteins analysed on a 10% SDS-PAGE gel.

3.2.3 Validation of eCFP and eYFP fluorophores as FRET donor-acceptor pair

The spectral overlap of eCFP and eYFP proteins makes them ideally suited to form a good donor-acceptor pair for FRET. Initially, we demonstrated FRET between the donor (eCFP) and acceptor (eYFP) fluorophores using the eCFP-TEV-eYFP protein. FRET should occur since the distance between the two covalently linked fluorophores is approximately 3.8 nm, which is within the Förster distance of 10 nm. As the fluorescent fusion protein contains a TEV recognition sequence, the initial observed FRET should decrease rapidly upon addition of functional TEV protease (ProTEV protease). Figure 3.9 demonstrates that excitation of the donor, eCFP, at 425 nm results in donor emission at 475 nm and acceptor emission at 527 nm. Subsequently, eCFP-TEV-eYFP protein mixtures were prepared with increasing concentrations of ProTEV protease (0.5 – 10 units). Upon incubation of the reaction mixtures at 30°C for 30 min, the donor emission progressively increased as the acceptor emission similarly decreased. This observation suggests that FRET occurs when the donor, eCFP, and the acceptor, eYFP, are in close proximity (~ 3.8 nm apart) and is lost when the eCFP-TEV-eYFP is exposed to the proteolytic activities of ProTEV protease. The loss of FRET due to cleavage of the fusion protein by ProTEV protease is further supported by SDS-PAGE analysis.

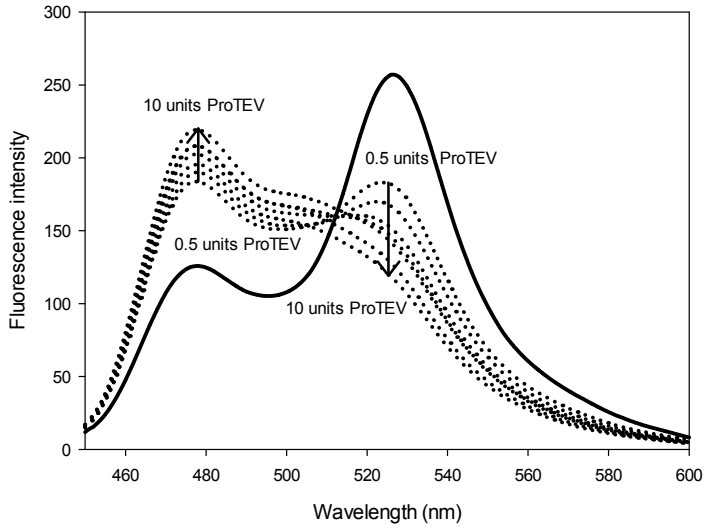

Figure 3.9: Demonstration of (disrupted) FRET between the donor and acceptor molecules of the eCFP-TEV-eYFP protein construct. The solid line represents the emission spectrum of the eCFP-TEV-eYFP protein demonstrating FRET before addition of ProTEV protease. The dotted lines illustrate the decreasing FRET after addition of increasing amounts of ProTEV protease (0.5, 1.0, 1.5, 2.0, 2.5, 5.0 and 10 units). The arrows indicate the decrease in acceptor emission and coinciding increase in donor emission upon addition of increasing concentrations of ProTEV protease. The shown emission spectra are the mean specific emissions from duplicate readings in a representative experiment.

The SDS-PAGE gel in Figure 3.10 demonstrates a decreasing band intensity of eCFP-TEV-eYFP protein (57 kDa) and a simultaneous increasing band intensity of the eCFP and eYFP proteins (27 kDa) with cumulative concentrations of ProTEV protease (48 kDa) after incubation of the reaction mixtures. When comparing the band intensities of the eCFP-TEV-eYFP protein and eCFP and eYFP proteins in lane 1 and lane 8 it is evident that the observed decrease in the fusion protein is due to TEV proteolysis. In addition, a weak band, representing one of the degradation products, is present in lane 1, which suggests a small amount of proteolysis upon cell lysis.

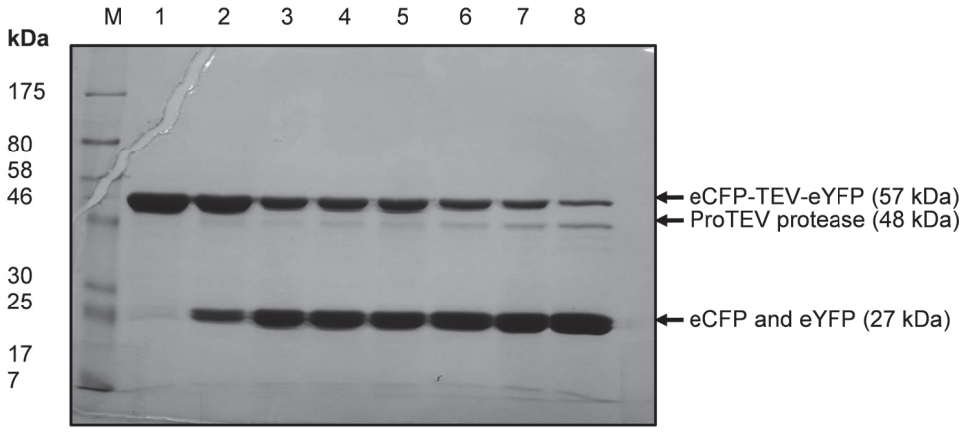

Figure 3.10: The eCFP-TEV-eYFP protein construct was incubated with increasing amounts of ProTEV protease and analysed on a 10% SDS-PAGE gel. Lane M: marker 7 – 175 kDa as labelled, lane 1: eCFP-TEV-YFP before addition of ProTEV protease, lane 2-8: eCFP-TEV-eYFP with increasing amounts of ProTEV protease (0.5, 1.0, 1.5, 2.0, 2.5, 5.0 and 10 units). Shown is a gradual decrease of eCFP-TEV-eYFP (57 kDa) and a concomitant appearance of the protein degradation products eCFP and eYFP (27 kDa) and the ProTEV protease (48 kDa).

3.2.4 Demonstration of FRET between eYFP-TEV-Kelch and eCFP-TEV-Nrf2

To demonstrate FRET as a result of the Keap1-Nrf2 protein-protein interaction, emission spectra were measured after the addition of increasing concentrations of eYFP-TEV-Kelch (0.05 – 0.80 µM) to a fixed concentration of eCFP-TEV-Nrf2 (0.11 µM), following excitation of the protein solutions at 425 nm. The titration concentration range was initially adopted from [140], which resulted in saturation of the fluorescence signal. Hence, in subsequent experiments, a ten-fold lower concentration range was used. Direct excitation of the donor and acceptor fusion proteins was monitored by recording the emission spectra of control reactions containing only the donor or acceptor fusion protein. To verify whether any observed FRET is due to a specific protein-protein interaction between Keap1 and Nrf2, increasing concentrations of unconjugated eYFP (0.05 – 0.80 µM) were added to a fixed concentration of eCFP-TEV-Nrf2 (0.11 µM) to account for non-specific interactions.

Upon addition of increasing concentrations of eYFP-TEV-Kelch to eCFP-TEV-Nrf2, the donor emission intensities at 475 nm gradually decreased with a corresponding increase in acceptor emission intensities at 527 nm (Figure 3.11 A). Although the acceptor fluorescence was amplified by addition of increasing amounts of unconjugated eYFP to eCFP-TEV-Nrf2, no concurrent decrease in donor emission was evident (Figure 3.11 B).

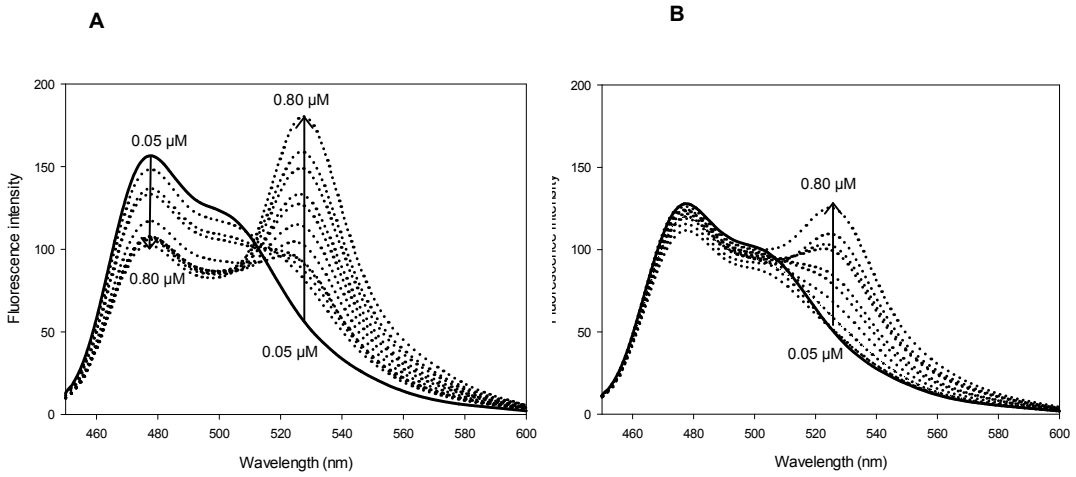

Figure 3.11: Emission spectra of 0.11 µM eCFP-TEV-Nrf2 titrated with 0.05, 0.07, 0.09, 0.11, 0.20, 0.30, 0.40, 0.50, 0.60, 0.70 and 0.80 µM: (A) eYFP-TEV-Kelch or (B) unconjugated eYFP. The solid line represents the donor alone before titration and the dotted lines show the addition of increasing amounts of the acceptor. The arrows indicate the increase in acceptor emission (in A and B) and concomitant decrease in donor emission (only in A) upon addition of increasing concentrations of the acceptor. The shown emission spectra are the mean specific emissions from duplicate readings (in A and B) in representative experiments.

Next, the eYFP emission wavelength maximum at 527 nm was plotted against the eYFP concentration, using linear regression, to explore the extent of acceptor emission increase upon titration of eCFP-TEV-Nrf2 with increasing concentrations of unconjugated eYFP. The emission of eYFP-TEV-Kelch, as a result of direct excitation, was plotted in parallel. Both datasets display a linear increase in eYFP emission wavelength maximum vs. concentration and comparable slope values; 110.97 e.u (emission units)/µM for the titration of eCFP-TEV-Nrf2 with eYFP and 118.23e.u/µM for the direct excitation of eYFP-TEV-Kelch (Figure 3.12).

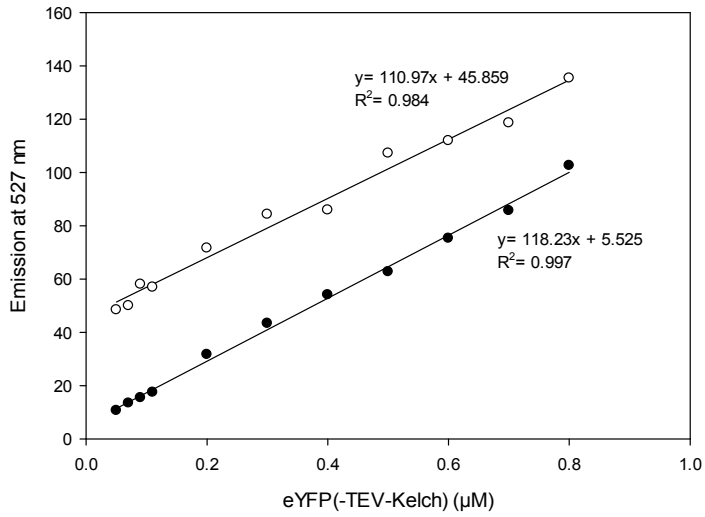

Figure 3.12: Emission intensities at 527 nm of 0.11 µM eCFP-TEV-Nrf2 titrated with 0.05 - 0.80 µM unconjugated eYFP (●) and the emission of increasing concentrations eYFP-TEV-Kelch (0.05 – 0.80 µM) upon direct excitation of the acceptor (○). Linear regression analysis was applied to produce the slope of both curves. The emission intensities shown are from representative experiments.

To examine whether FRET occurred between the two fluorescent fusion proteins, both FRET efficiency (FE) and sensitised emission (SE) values were calculated. The data were fitted by non-linear regression using an equation for ligand binding:

$$\text{Ligand binding} = \frac{B_{max} * \text{abs}(x)}{K_d + \text{abs}(x)} + Ns * x$$

A gradual increase in both FE and SE values was evident when increasing concentrations of eYFP-TEV Kelch were added to a fixed concentration of eCFP-TEV-Nrf2 (Figure 3.13).

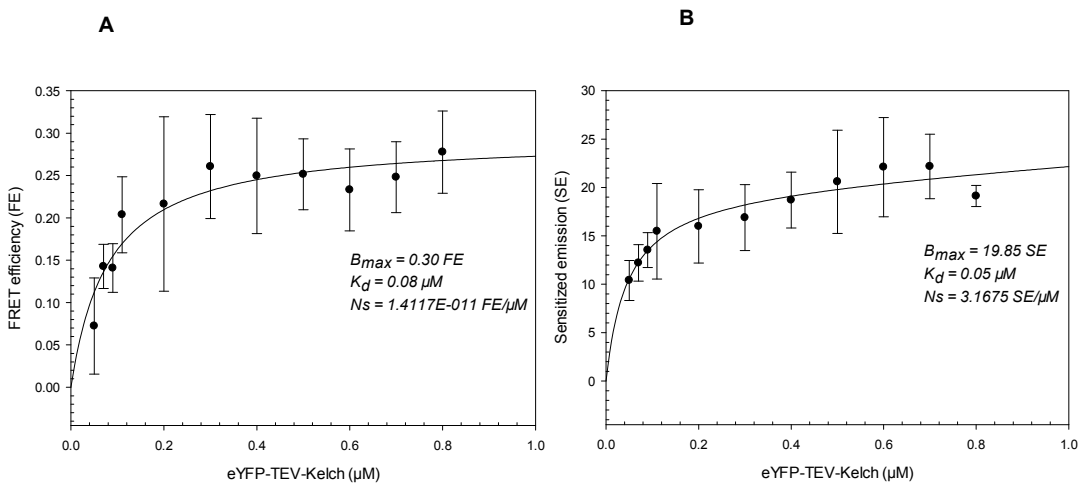

Figure 3.13: FRET efficiency (A) and sensitised emission (B) of 0.11 µM eCFP-TEV-Nrf2 titrated with increasing concentrations of eYFP-TEV-Kelch (0.05 – 0.80 µM). Binding curves were fitted by non-linear regression: ligand binding, one site saturation + non-specific binding. The error bars represent the standard deviation of n = 3 independent experiments.

The FRET signal started to plateau after approximately 0.30 µM eYFP-TEV-Kelch was added to 0.11 µM eCFP-TEV-Nrf2 (for FE: B_{max} = 0.30 FE, K_d = 0.08 µM, for SE: B_{max} = 19.85 SE, K_d = 0.05 µM). This protein ratio was consequently used in subsequent experiments unless mentioned otherwise. Substitution of eYFP-TEV-Kelch for unconjugated eYFP resulted in no significant increase in FE and SE (Figure 3.14).

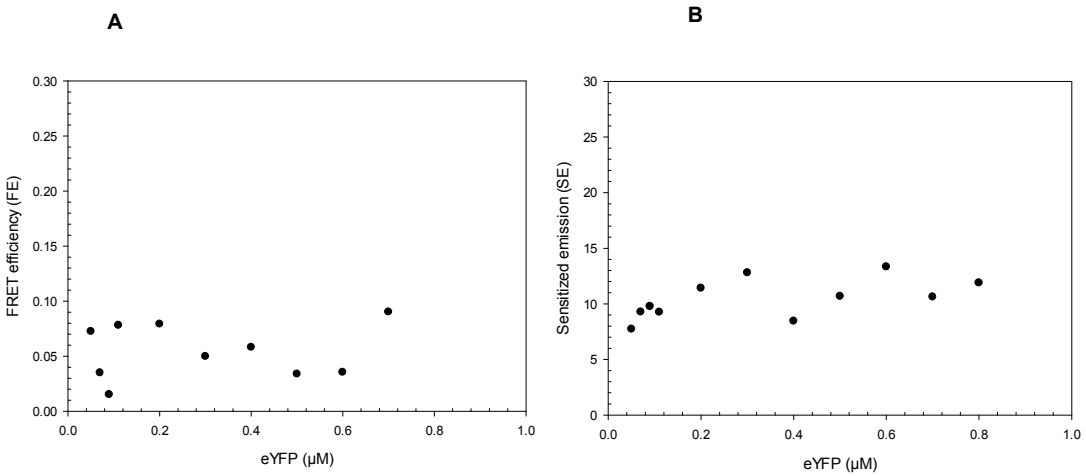

Figure 3.14: FRET efficiency (A) and sensitised emission (B) of 0.11 μM eCFP-TEV-Nrf2 titrated with increasing concentrations of unconjugated eYFP (0.05 – 0.80 μM). The data shown are from a representative experiment.

Because of the spectral overlap of the absorption spectra of the donor and acceptor fluorophores, the acceptor fluorophore can be excited directly with light at the excitation wavelength of the donor (excitation crosstalk). Likewise, donor fluorescence can leak into the detection channel for acceptor emission (emission crosstalk) [155]. Since the donor emission can normally be observed without acceptor emission bleed-through, FRET efficiency was used to determine the amount of FRET present in further studies.

3.2.5 Buffer system optimisation

Initial FRET buffer conditions (20 mM Tris-HCl pH 7.4 buffer containing, 0.5 mM DTT, 100 mM NaCl, 5 mM $MgCl_2$, 0.1 mM EDTA and 5% v/v glycerol) were adopted from Dr. Andreia Guimarães [168]. Preliminary experiments showed that increasing the viscosity of the buffer with > 5% glycerol didn't improve the FRET signal. Furthermore, no benefits were attributed to the $MgCl_2$ component. Other factors affecting the FRET efficiency were examined by varying the NaCl concentrations in the buffer system. X-ray crystallography studies of the protein-protein interaction between the Keap1 Kelch domain and the ETGE-containing Nrf2 peptide have

shown that salt bridge formation is an important component of the binding interaction [47]. It was hypothesised that high salt concentrations in the buffer may screen charge-charge interactions between Glu/Asp residues in the Nrf2 peptide and Arg residues in the Kelch binding site. Reaction mixtures of eYFP-TEV-Kelch and eCFP-TEV-Nrf2 were prepared in buffers with NaCl concentrations of 0, 50, 100 and 150 mM. Control reactions, containing either the donor or the acceptor in buffer supplemented with matching NaCl concentrations, were prepared in parallel. Emission spectra of the protein mixtures were recorded upon excitation at 425 nm and the FE values were calculated. Figure 3.15 demonstrates that the FE decreased to 0 in buffer containing 150 mM NaCl (vs. FE ~ 0.30 in buffer without NaCl). As a consequence, subsequent experiments were performed with FRET buffer containing 20 mM Tris-HCl pH 7.4, 0.5 mM DTT, 0.1 mM EDTA and 5% v/v glycerol with no added NaCl.

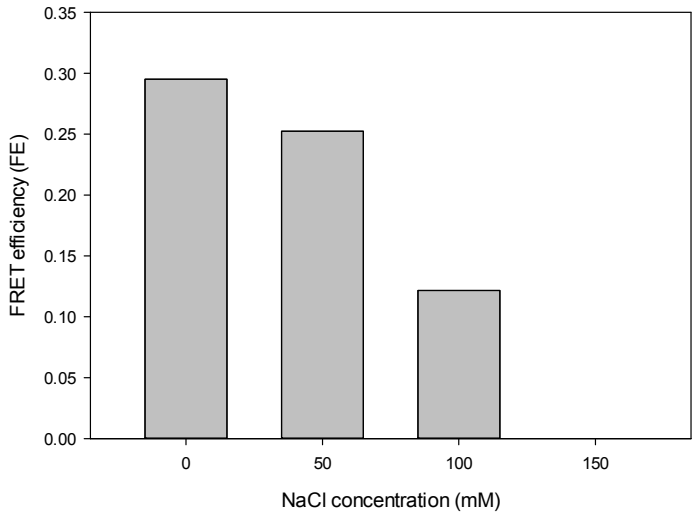

Figure 3.15: Demonstration of the effect of NaCl on the FRET efficiency (FE) between eCFP-TEV-Nrf2 and eYFP-TEV-Kelch. The FE values were plotted against increasing NaCl concentrations (0, 50, 100 & 150 mM). The data shown are from a representative experiment.

3.2.6 Validation of FRET between eYFP-TEV-Kelch and eCFP-TEV-Nrf2

As both fluorescent fusion proteins possess a TEV recognition site between the fluorescent tag and the protein, energy transfer should be abolished upon addition of ProTEV protease to the protein mixture. FRET between the eYFP-TEV-Kelch and eCFP-TEV-Nrf2 proteins is demonstrated in Figure 3.16.

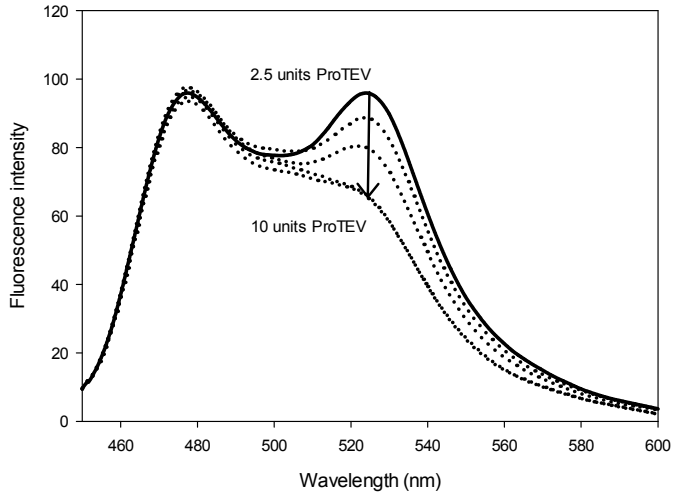

Figure 3.16: Demonstration of (disrupted) FRET between eCFP-TEV-Nrf2 and eYFP-TEV-Kelch. The solid line reflects the emission spectrum of the fusion proteins demonstrating FRET before addition of ProTEV protease. The dotted lines show the decreasing FRET following addition of increasing amounts of ProTEV protease (2.5, 5.0, 7.5 and 10 units). The arrow indicates the decrease in acceptor emission following addition of increasing concentrations of ProTEV protease. The shown emission spectra are the mean specific emissions from duplicate readings in a representative experiment.

Following incubation of the protein reaction mixture at 30°C for 30 min with ProTEV protease, a formation of precipitate was observed. Addition of increasing concentrations of ProTEV protease resulted in a decrease in acceptor emission at 527 nm. However, the donor emission at 475 nm was not altered. Nevertheless, SDS-PAGE analysis demonstrates supporting evidence of cleavage of the two fluorescent fusion proteins by ProTEV protease. Increasing concentrations of ProTEV protease (0 – 10 units) reveals a concomitant decrease of eYFP-TEV-Kelch

(~ 59 kDa) and eCFP-TEV-Nrf2 (29 kDa) proteins and an increase of eCFP, eYFP (27 kDa) and Kelch (~ 32 kDa) proteins (Figure 3.17). The 16-mer Nrf2 peptide degradation product (1.8 kDa) is not visible on the SDS-PAGE gel as a result of its relative small size. The eYFP-TEV-Kelch protein appears as a smaller band on the gel (~ 54 kDa) than its predicted biological size (59 kDa). Similarly, the Kelch protein degradation product presents a smaller protein band (~ 29 kDa) than its predicted biological size (32 kDa).

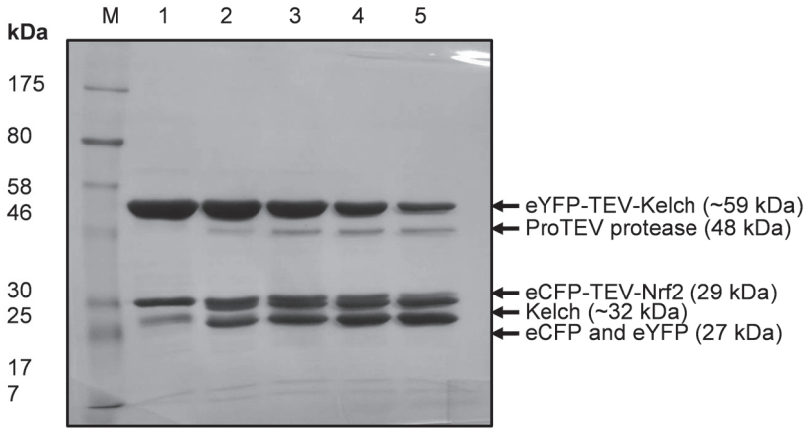

Figure 3.17: The eCFP-TEV-Nrf2 and eYFP-TEV-Kelch proteins were incubated with increasing amounts of ProTEV protease and analysed on a 10% SDS-PAGE gel. Lane M: marker 7 – 175 kDa as labelled, lane 1: the fusion proteins before addition of ProTEV protease, lane 2 - 5: the fusion proteins with increasing amounts of ProTEV protease (2.5, 5.0, 7.5 and 10 units). Presented is a gradual decrease of eCFP-TEV-Nrf2 (29 kDa) and eYFP-TEV-Kelch (~ 59 kDa) proteins and a simultaneous increase of the protein degradation products Kelch (~ 32 kDa), eCFP and eYFP (27 kDa) and the ProTEV protease (48 kDa).

3.2.7 eYFP-TEV-Kelch protein stability

In order to investigate whether the observed smaller protein size of eYFP-TEV-Kelch was due to instability of the protein, a series of experiments was conducted to evaluate factors that could affect its protein stability. An initial experiment was performed to compare the degree of eYFP-TEV-Kelch protein degradation of

de novo purified (batch 1) protein with protein that was purified a month earlier (batch 2) and stored at 4°C. The protein samples were separated by electrophoresis and subsequently analysed by SDS-PAGE. In the process, more of batch 1 protein was loaded compared to proteins from batch 2. As shown in Figure 3.18, both protein samples demonstrate some degree of protein degradation. The batch 2 protein sample in lane 1 shows three distinctive Coomassie stained bands of almost similar density (~ 59 kDa, ~ 32 kDa, and 27 kDa), whereas the batch 1 protein in lane 2 shows a predominant expression of one band (~ 59 kDa). To verify the identity of the protein bands, the eYFP-TEV-Kelch protein samples were subjected to immunoblotting using either anti-Kelch or anti-GFP antibodies. The representative Kelch immunoblot (Figure 3.17 B) shows immunoreactive bands corresponding to the molecular weights of eYFP-TEV-Kelch (~ 59 kDa) and its degradation product Kelch (~ 32 kDa). In the representative GFP immunoblot (Figure 3.17 C), immunoreactive bands were observed at the predicted molecular weight for eYFP-TEV-Kelch (~ 59 kDa) and its degradation product eYFP (27 kDa). The presence of the Kelch and eYFP degradation products following proteolysis was most prominent in the batch 2 protein sample as presented in lane 1 of Figure 3.18.

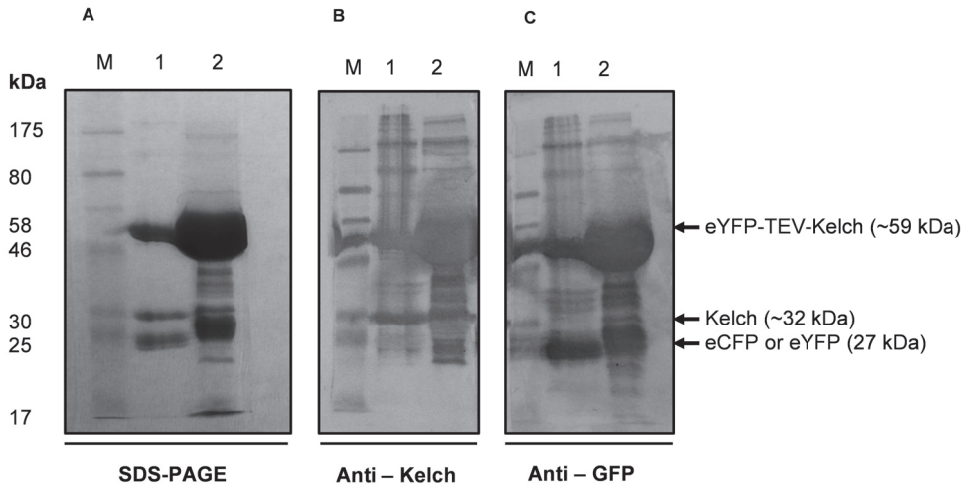

Figure 3.18: Demonstration of the protein stability of batch 1 and batch 2 eYFP-TEV-Kelch. The protein samples were analysed on a 10% SDS-PAGE gel (A) and subjected to western blotting using anti-Kelch (B) or anti-GFP (C) antibodies. Lane M: marker 7 – 175 kDa as labelled, lane 1: the batch 2 protein and lane 2: the batch 1 protein. The eYFP-TEV-Kelch protein degradation products Kelch (~ 32 kDa) (A and B) and eCFP and eYFP (27 kDa) (A and C) are more prominent in lane 1 than in lane 2.

Next, the effectiveness of Halt protease inhibitor cocktail on maintaining the protein stability of eYFP-TEV-Kelch was investigated over a time course of 7 days (Section 2.11). Increasing amounts of Halt protease inhibitor cocktail (0.0x, 0.5x, 1.0x and 10x concentrated) were added to the protein samples. The protein samples were subsequently stored in the dark at 4°C, RT, or 37°C and subjected to SDS-PAGE after 0, 3, 5 or 7 days (Figure 3.19).

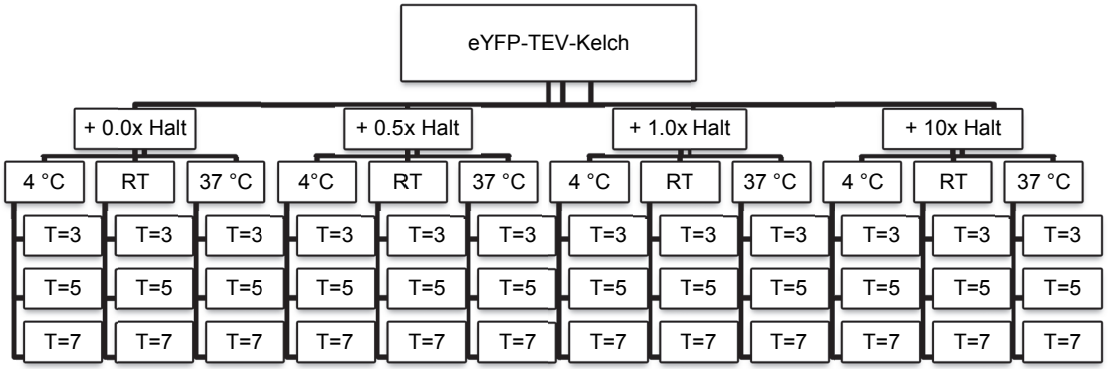

Figure 3.19. Schematic overview of prepared eYFP-TEV-Kelch protein samples and time-points. The eYFP-TEV-Kelch protein samples were prepared with increasing amounts of Halt protease inhibitor cocktail (0.0x, 0.5x, 1.0x or 10x concentrated) and stored in the dark at 4°C, RT, or 37°C. Samples were taken after 3 days (T = 3), 5 days (T = 5) and 7 days (T = 7).

Proteolytic cleavage of the eYFP-TEV-Kelch protein progressively increased over time irrespective of the protease inhibitor (compare Figure 3.20 A with Figure 3.20 D). Further proteolysis is evident when storage conditions reach temperatures above 4°C (compare with RT and 37 °C in Figure 3.20). Yet, addition of increasing concentrations of Halt protease inhibitor cocktail to the protein samples resulted in suppression of the degradation process (compare lane 1 with lane 4 in Figure 3.20). Subsequent eYFP-TEV-Kelch protein purification was performed with the addition of 1.0x concentrated Halt protease inhibitor cocktail to the purification buffer. Proteins were stored away from light sources at 4°C.

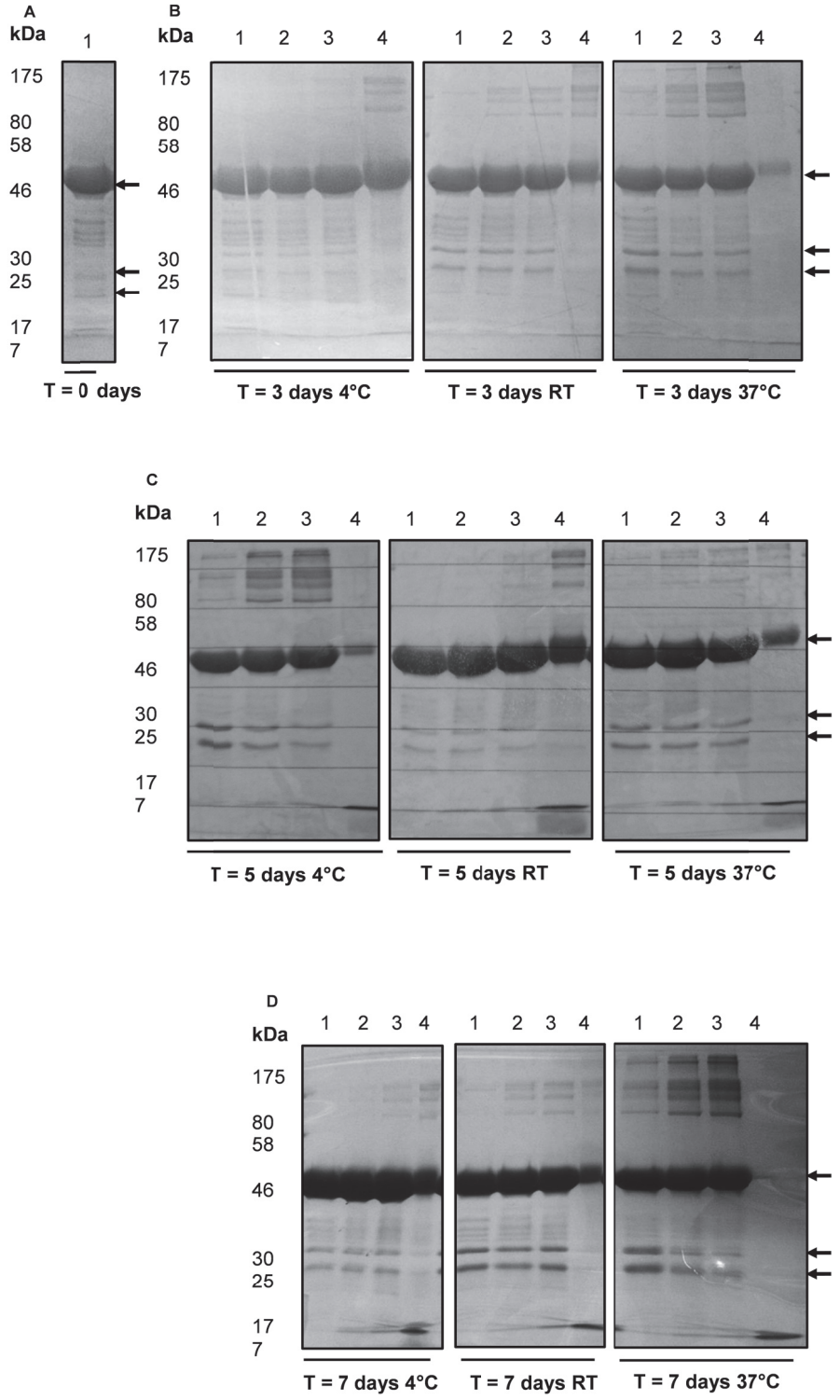

Figure 3.20: SDS-PAGE analysis of factors influencing the protein stability of eYFP-TEV-Kelch. Lane 1 shows the eYFP-TEV-Kelch protein without Halt protease inhibitor and lane 2 – 4 represents the fusion protein with 0.5x, 1.0x or 10x concentrated Halt protease inhibitor. Protein samples were stored at 4°C, RT or 37°C and taken after 0 days (A), 3 days (B), 5 days (C), or 7 days (D). The arrows indicate from top to bottom: eYFP-TEV-Kelch (~ 59 kDa), Kelch (~ 32 kDa) and eYFP (27 kDa).

3.2.8 Effect of DMSO co-solvent and an Nrf2 derived peptide inhibitor on FRET between eYFP-TEV-Kelch and eCFP-TEV-Nrf2

DMSO is often used as a co-solvent for small molecules and peptides. To examine the effect of DMSO on the emission spectra, a range of increasing concentrations (0.1, 0.5, 1.0, 5.0 and 10% DMSO) was added to reaction mixtures of eYFP-TEV-Kelch and eCFP-TEV-Nrf2 in buffer. Emission spectra of the protein mixtures were recorded upon excitation at 425 nm. Increasing DMSO concentrations were found to decrease the overall fluorescence intensity of the emission spectra of both fusion proteins (Figure 3.21). This outcome limited the use of DMSO to a concentration of 0.1% v/v.

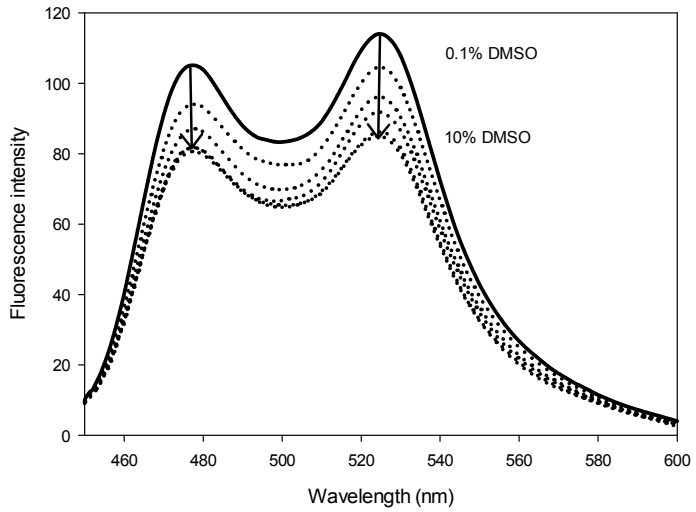

Figure 3.21: The effect of DMSO on the emission spectra of 0.11 µM eCFP-TEV-Nrf2 and 0.30 µM eYFP-TEV-Kelch. The solid line represents the emission spectrum of the fusion protein pair before addition of DMSO and the dotted lines reflect the emission spectra in the presence of 0.1, 0.5, 1.0, 5.0 and 10% DMSO. The arrows indicate the decrease of both donor and acceptor emission following addition increasing concentrations of DMSO. The shown emission spectra are the mean specific emissions from duplicate readings in a representative experiment.

A known Nrf2-derived peptide inhibitor (Ph-DPETGEL-OH, IC_{50} ~ 0.20 µM obtained through a fluorescence polarisation assay [170]) was tested to confirm that the observed energy transfer between the interacting FRET pair could be inhibited.

Reaction mixtures of eYFP-TEV-Kelch and eCFP-TEV-Nrf2 were prepared in buffer with or without 10 µM of the inhibitor (in 0.1% DMSO final concentration). Control reactions containing either the Nrf2 donor or the Kelch acceptor conjugates were supplemented with the inhibitor and were prepared in parallel. Figure 3.22A shows that excitation of the donor at 425 nm results in donor emission at 475 nm and acceptor emission at 527 nm, suggesting FRET. Addition of the inhibitor to the protein mixture resulted in a simultaneous increase in donor emission and decrease in acceptor emission (Figure 3.22 B). This observation suggests that energy transfer can be halted by a suitable (peptide) inhibitor.

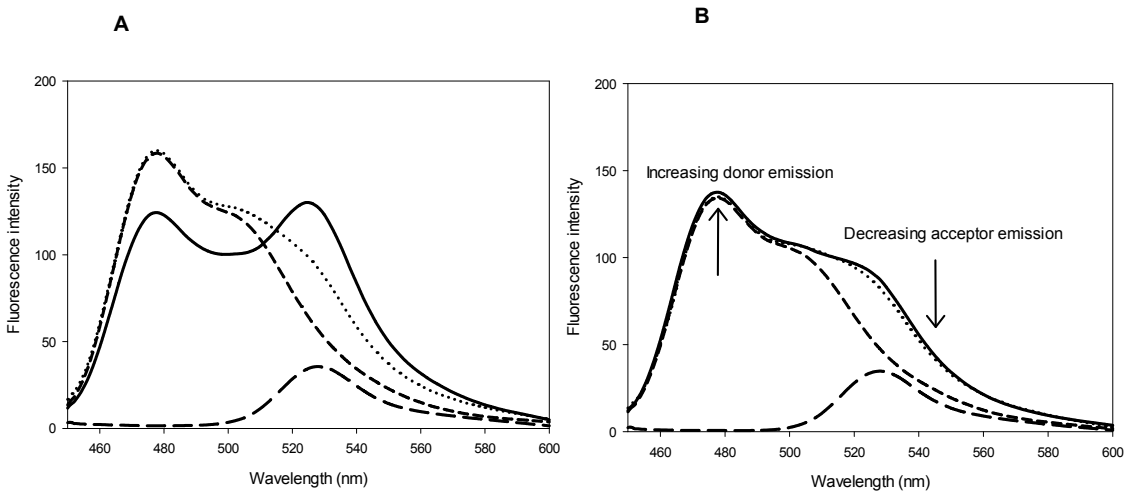

Figure 3.22: Emission spectra of 0.11 µM eCFP-TEV-Nrf2 and 0.30 µM eYFP-TEV-Kelch in the absence (A) and presence (B) of 10 µM of an unlabelled Nrf2-derived peptide inhibitor. Shown are the emission spectra of the donor (**- - -**) and acceptor (**– – –**) the sum of both emission spectra (·····) and the emission spectrum of the FRET pair (──). The arrows indicate the increase in donor emission and coinciding decrease in acceptor emission in the presence of the inhibitor. The shown emission spectra are the mean specific emissions from duplicate readings in representative experiments.

3.2.9 FRET assay adaptation to a multi-well plate format

Following the development of the FRET assay using the fluorescence spectrometer, the assay was adapted to a multi-well plate format. It was hypothesised that the adaption to a micro-plate format would result in a reduction of the assay's sensitivity due to the smaller volumes. Consequently, preliminary experiments were performed

with 10 times more protein than in the original assay (3.0 μM and 1.1 μM versus 0.30 μM and 0.11 μM, acceptor and donor proteins respectively). The recorded FRET, measured immediately after mixing the fusion proteins, was found to be relatively stable over a 24 h period (Figure 3.23). During the optimisation phase, protein volumes < 10 % of the total well volume were found to negatively impact the reproducibility and accuracy of the assay. Additionally, the use of a multi-channel pipette enhanced the assays reproducibility.

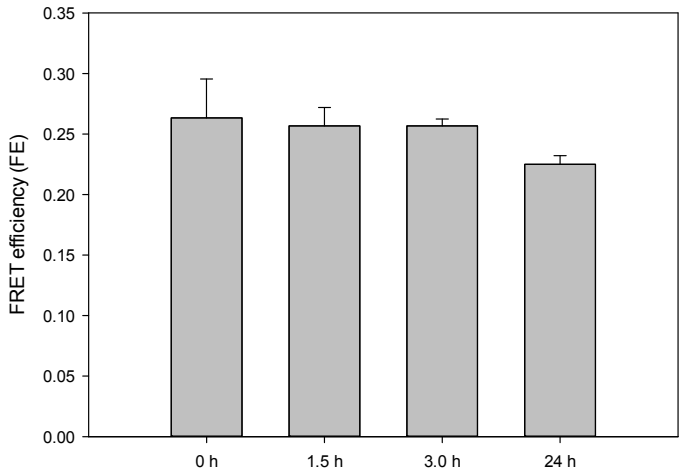

Figure 3.23: FRET efficiency of 1.1 μM eCFP-TEV-Nrf2 and 3.0 μM eYFP-TEV-Kelch after 0, 1.5, 3.0 and 24 h in a multi-well plate format. The error bars represent the standard deviation of n = 3 independent experiments.

To verify the hypothesis that adaption of the FRET assay to a multi-well plate format would reduce its sensitivity, the concentration of the fluorescent fusion proteins was lowered to 0.30 μM eYFP-TEV-Kelch and 0.11 μM eCFP-TEV-Nrf2 (previously optimised concentrations described in Section 3.2.4). Initial experiments showed that lowering the protein concentrations resulted in increased sensitivity. Subsequently, a titration experiment was performed to determine the optimal protein ratio for energy transfer between the fluorescent fusion proteins. A fixed concentration of eCFP-TEV-Nrf2 (0.11 μM) was titrated into varying concentrations of eYFP-TEV-Kelch (0.01 – 0.50 μM). The titration was performed with a lower eYFP-TEV-Kelch starting concentration than in the original format (0.01 vs. 0.05 μM) in order to explore the sensitivity of this assay.

The lower eYFP-TEV-Kelch maximum concentration (0.50 vs. 0.80 µM in the original format) was chosen since, signal saturation started in the original assay at concentrations above 0.30 µM eYFP-TEV-Kelch to 0.11 µM eCFP-TEV-Nrf2. FRET efficiencies were calculated upon excitation of the protein mixture at 430 nm and subsequent emission at 480 and 530 nm (dual emission filters). The data were fitted by non-linear regression using an equation for ligand binding, one site saturation + non-specific and are presented in Figure 3.24.The efficiency of energy transfer between the interacting FRET pairs was optimal using 0.30 µM and 0.11 µM acceptor and donor species respectively (B_{max} = 0.28 FE, K_d = 0.08 µM). These results are consistent with earlier findings (Section 3.2.4). Subsequent multi-well plate assays were performed with an acceptor and donor ratio (0.20 µM and 0.11 µM), which achieved ~ 80% of the maximal FE. This ratio was chosen so that in a competition assay format a small displacement of Nrf2 peptide from the Keap1 Kelch binding site results in a relative large change in FE.

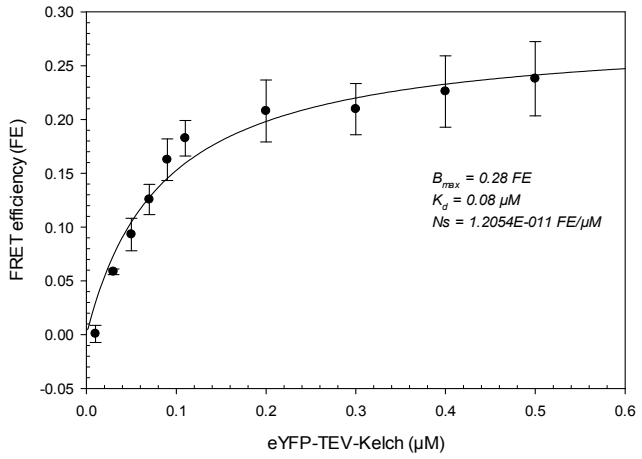

Figure 3.24: FRET efficiency of 0.11 µM eCFP-TEV-Nrf2 titrated with increasing concentrations of eYFP-TEV-Kelch (0.01, 0.03, 0.05, 0.07, 0.09, 0.11, 0.20, 0.30, 0.40 and 0.50 µM) in a multi-well plate format. Binding curves were fitted by non-linear regression: ligand binding, one site saturation + non-specific. The error bars represent the standard deviation of n = 3 independent assays.

3.2.10 Demonstration of the specificity of the Keap1-Nrf2 PPI in a multi-well plate format

X-ray crystallography studies of Keap1 Kelch and Nrf2 derived peptide complexes have shown that ^{77}DxETGE^{82} residues E79 and E82 are essential for the protein-protein interaction; the side chains form salt bridges with R380, R415 and R483 in the Kelch domain [46]. Residue T80 forms both inter-and intramolecular interactions [46-47]. In certain human cancers these Nrf2 residues are mutated to E79Q, E82D and T80K. ITC experiments demonstrated that the ETGE point mutations compromised Keap1 recognition, resulting in abnormal cellular accumulation of Nrf2 [55]. The biologically relevant Nrf2 mutations were used to verify the specificity of the interaction between the eYFP-TEV-Kelch and eCFP-TEV-Nrf2 proteins. The wild-type pET28c-eCFP-TEV-Nrf2 plasmid construct was used as a template to generate proteins containing the three Nrf2 point mutations; eCFP-TEV-Nrf2-E79Q, eCFP-TEV-Nrf2-E82D and eCFP-TEV-Nrf2-T80K (Table 3.1) (details in Section 2.3.2). Titration experiments were performed in which increasing concentrations of eYFP-TEV-Kelch (0.01 – 0.50 μM) were added to a fixed concentration of the mutant eCFP-TEV-Nrf2 proteins (0.11 μM). All three mutant proteins demonstrated a reduced binding affinity for the Keap1 Kelch domain compared to the wild-type eCFP-TEV-Nrf2 protein (Figure 3.25 and Table 3.1).

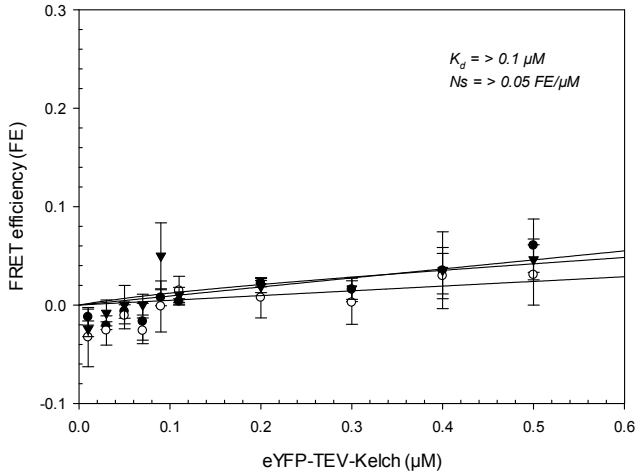

Figure 3.25: FRET efficiency of 0.11 µM eCFP-TEV-Nrf2-E79Q (●), eCFP-TEV-Nrf2-T80K (○) or eCFP-TEV-Nrf2-E82D (▼) titrated with increasing concentrations of eYFP-TEV-Kelch (0.01, 0.03, 0.05, 0.07, 0.09, 0.11, 0.20, 0.30, 0.40 and 0.50 µM) in a multi-well plate format. Binding curves were fitted by non-linear regression: ligand binding, one site saturation + non-specific. The error bars represent the standard deviation of n = 3 independent assays.

Table 3.1: Dissociation constants and Bmax values for eCFP-TEV-Nrf2 fusion proteins.

Protein	Sequence	K_d ± SE (µM)	B_{max} (FE)
eCFP-WT	eCFP-AFFAQLQLDEETGEFL	0.08 ± 0.02	0.28
eCFP-E79Q	eCFP-AFFAQLQLDE<u>Q</u>TGEFL	>0.1	-[a]
eCFP-T80K	eCFP-AFFAQLQLDEE<u>K</u>GEFL	>0.1	-[a]
eCFP-E82D	eCFP-AFFAQLQLDEETG<u>D</u>FL	>0.1	-[a]

Notes: a. Not determined.

3.2.11 Competition assay in a multi-well plate format

To verify whether the newly developed FRET multi-well plate assay could be used to evaluate compounds that competitively inhibit the Keap1-Nrf2 PPI, unconjugated versions of the Nrf2-derived 16-mer peptide sequences in Table 1 were tested. Upon addition of increasing concentrations of the Nrf2-derived 16-mer peptides (0.001 – 100 µM) to the eCFP-TEV-Nrf2 and eYFP-TEV-Kelch protein mixture (0.11 µM and 0.20 µM respectively), the change in FRET efficiency was used to determine IC_{50} values (Figure 3.26 and Table 3.2). The wild-type Nrf2 peptide

presented a dose-dependent reduction in energy transfer, whereas the three mutant Nrf2 peptides failed to disrupt the Keap1-Nrf2 PPI.

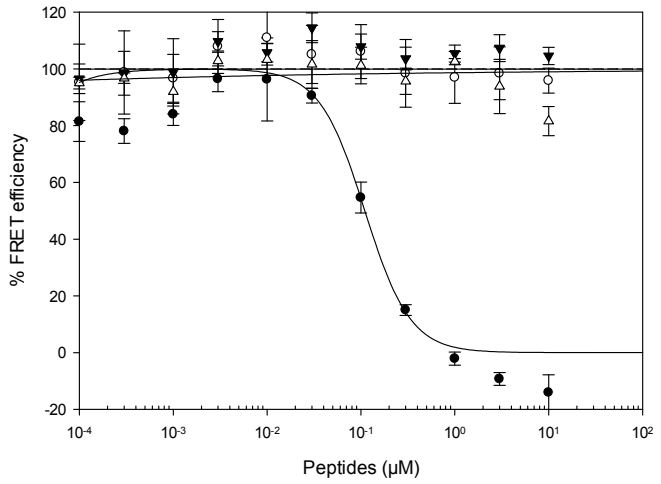

Figure 3.26: Competitive inhibition of FRET between 0.11 μM eCFP-TEV-Nrf2 and 0.20 μM eYFP-TEV-Kelch by increasing concentrations (0.001 – 100 μM) of unlabelled Nrf2-derived 16-mer peptides (●: WT,○: E79Q, ▼: T80K and △: E82D). The data were fitted to a standard four-parameter logistic function. The error bars represent the standard deviation of n = 3 independent assays.

Table 3.2: IC_{50} values for Nrf2-derived 16-mer peptides for the interaction between eCFP-TEV-Nrf2 and eYFP-TEV-Kelch.

Peptide	Sequence	IC_{50} (μM)
WT	AFFAQLQLDEETGEFL	0.11
E79Q	AFFAQLQLDE<u>Q</u>TGEFL	-[a]
T80K	AFFAQLQLDEE<u>K</u>GEFL	-[a]
E82D	AFFAQLQLDEETG<u>D</u>FL	-[a]

Notes: a. Not determined.

The suitability of the developed FRET assay for high throughput screening (HTS) was evaluated by calculation of the Z′ value [143]:

$$Z' = 1 - \frac{3SD_{maxFRET} - 3SD_{minFRET}}{maxFRET_{480nm} - minFRET_{480nm}}$$

Here, the minFRET480nm is the minimal fluorescence intensity observed in the absence of any inhibitor and maxFRET480nm is the maximal fluorescence intensity observed in the presence of an inhibitor, and SD is the standard deviation of the fluorescence emissions at 480 nm.

A Z′ value of > 0.5 is usually considered to be suitable for HTS. Competition experiments with 100 µM of an unlabelled peptide (St-DPETGEL, IC_{50} ~ 0.12 µM [142]) were performed to verify the assay performance based on the maximal and minimal fluorescence intensity at 480 nm (Figure 3.27) [170] (details in Section 2.17.11). Here, the Z′ value was calculated as 0.63 ±0.07, which indicated that the assay was highly suitable for HTS usage.

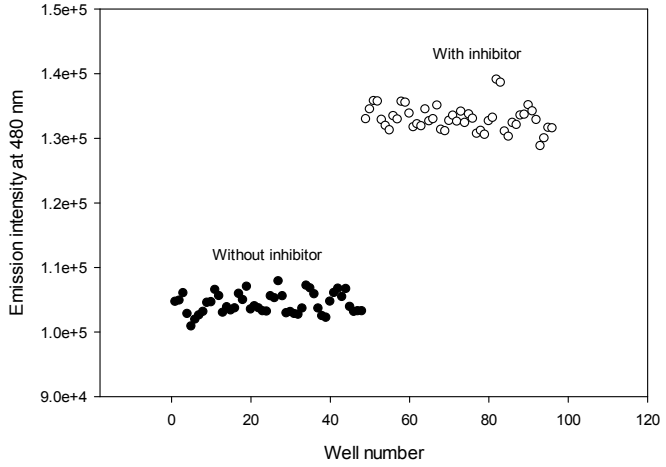

Figure 3.27: Well-to-well variation of FRET between 0.11 µM eCFP-TEV-Nrf2 and 0.20 µM eYFP-TEV-Kelch in the absence (wells 1 – 48) and presence (wells 49 – 96) of 100 µM of an unlabelled Nrf2-derived inhibitor (St-DPETGEL [170]). The mean and standard deviation of the minimal and maximal emission intensities at 480 nm was used to calculate Z′ (Section 2.17.11). The data are from a representative experiment.

3.3 Discussion

Direct disruption of the Keap1-Nrf2 interaction is an emerging approach to increase Nrf2 activity and to stimulate *ARE* driven gene expression. In this respect, a high-throughput steady-state homogeneous FRET assay was devised to examine the binding affinity of a range of potential inhibitors of the Keap1-Nrf2 PPI. FRET was demonstrated between a 16-mer Nrf2 derived peptide conjugated to an eCFP fluorophore and the Keap1 Kelch domain conjugated to an eYFP fluorophore.

The ability to calculate the absolute concentration of the eCFP and eYFP fusion proteins using their molar extinction coefficient and UV absorption enhances the accuracy of the FRET assay [140]. Moreover, the spectral properties of eCFP and eYFP make them a fluorescent protein pair that is well-suited for FRET [157]. This has been demonstrated with the eCFP-TEV-eYFP protein construct that contained both fluorophores, separated by a TEV recognition site (3.8 nm separation between both fluorophores). FRET was observed in a mixture containing only the eCFP and eYFP fusion protein, but was lost following the addition of functional TEV protease (Figures 3.9 and 3.10). This observation suggests that FRET can only occur when the donor, eCFP, and the acceptor, eYFP, are in close proximity. To verify whether FRET can serve as a molecular ruler for determining distances within 10 nm, TEV protease was added to a mixture containing the fusion proteins eCFP-TEV-Nrf2 and eYFP-TEV-Kelch. The addition of TEV protease to the protein mixture revealed the cleavage of the two fusion proteins. However, this resulted only in a decrease in acceptor emission and no change in donor emission (Figure 3.16). The outcome could have been affected by precipitate formation that was observed upon incubation of the protein reaction mixture with TEV protease. This precipitation might have interfered with fluorescence readings by reflecting the excitation and emission light into the detector, which could result in to fluorescence bleed-through. Repetition of the experiment would be desirable to confirm the use of FRET as a spectroscopic ruler in this context.

Conjugation of the eCFP and eYFP fluorophores to proteins of interest increases the fusion proteins stability [171-172]. However, SDS-PAGE and western blot analysis revealed that eYFP-TEV-Kelch presents itself as a smaller size protein band

(~ 54 kDa) than predicted (59 kDa) (Section 3.2.6). Moreover, in an experiment where TEV protease was added to the fusion protein, the Kelch degradation product appeared as a ~ 29 kDa protein on the SDS-PAGE gel instead of its predicted size of 32 kDa (Section 3.2.6). The altered electrophoretic migration might be affected by the amino acid composition of the protein, which can influence the SDS binding affinity and therefore the mobility of the protein [173]. Proteolytic cleavage may also have been a factor affecting the apparent molecular weight of the protein. Hence, the degree of degradation of *de novo* purified eYFP-TEV-Kelch protein was compared to a protein sample that was purified a month earlier and stored at 4°C. Results indicated a more prominent presence of smaller products in the older protein sample, indicating degradation. However, more *de novo* protein sample was loaded compared to the older protein sample, which made direct comparison difficult. Additional experiments showed that eYFP-TEV-Kelch degradation products started to appear when the protein was stored at temperatures above 4°C or for prolonged periods of time (up to 7 days) (Section 3.2.7). Supplementation of the protein storage buffer with a protease inhibitor cocktail did retard the proteolytic process. Nevertheless, mass-spectrometry analysis would be desirable here to verify the extent of protein degradation. Overall, these observations demonstrate the factors that can affect protein stability and therefore the robustness of the assay.

When the donor fusion protein concentration was fixed, increasing FRET was recorded with increasing amounts of the acceptor fusion protein, until optimum FE and SE values were recorded with 0.11 µM eCFP-TEV-Nrf2 and 0.30 µM eYFP-TEV-Kelch (Figure 3.13). Comparable binding affinities were determined when a curve fit for ligand binding was applied to both datasets: K_d ~ 0.08 µM and K_d ~ 0.05 µM for FE and SE datasets respectively. However, the contribution from non-specific binding was most prominent for the calculated SE values (non-specific slope values: 3.17 SE/µM vs.1.41 x 10^{-11} FE/µM). This could be due to background acceptor fluorescence that results from acceptor excitation with light that was used to excite the donor. This crosstalk or bleed-through can generate false positives and may affect the accuracy of the FRET measurement when using sensitised emission. This overlap of absorption spectra is not relevant when observing donor emission, which is used to calculate FE.

In additional titration experiments, the concentration of eYFP-TEV-Kelch was fixed (0.11 µM) and the amount of eCFP-TEV-Nrf2 was varied (0.05 – 0.80 µM). Based on previous outcomes, the hypothesis was that concentrations up to 0.11 µM eCFP-TEV-Nrf2 would increase the FRET signal. FRET was expected to plateau upon the addition of > 0.11 µM of the donor protein. However, an overall decrease of the FE and SE values was observed upon addition of increasing concentrations of eCFP-TEV-Nrf2 to eYFP-TEV-Kelch. The results were inconclusive and may warrant further investigation.

To account for non-specific interactions, eCFP-TEV-Nrf2 was titrated with increasing amounts of unconjugated eYFP. This resulted in a linear increase in acceptor emission at 527 nm. The slope of the curve (110.97 e.u/µM) was comparable to the slope value obtained by direct excitation of increasing concentrations of eYFP-TEV-Kelch (118.23 e.u/µM). This suggests that the determined FRET between the fusion proteins was indeed due to the interaction between Keap1 Kelch and the 16-mer Nrf2 derived peptide and that the non-specific component of the interaction is negligible. Figure 3.14 shows that eCFP-TEV-Nrf2 titration with unconjugated eYFP results in relative unaltered FE and SE values over the concentration range. Nevertheless, the titration with eYFP was only performed once and should be repeated in the multi-well plate format.

The effect of ionic strength was investigated by varying salt concentrations in the buffer. A decrease in FRET efficiency was evident upon increasing NaCl concentrations (up to 150 mM NaCl). This result was consistent with our hypothesis that the high ionic strength of the buffer may negatively impact the electrostatic component of the Keap1-Nrf2 PPI and matches with results from our previously described FP assay [143]. Maintaining buffer conditions at 20 mM Tris-HCl pH 7.4 (without added NaCl) was considered to be of high importance.

The specificity of the PPI was validated by comparing the FRET signal of the original fusion protein pair with eCFP conjugated constructs containing Nrf2 mutations found in cancerous human tissue and cell lines. The Nrf2 mutations, E79Q, ET80K and E82D, where previously shown to exhibit a low Keap1 binding

affinity [55]. FRET studies with eCFP conjugated versions of the mutant Nrf2 derived peptides confirmed this observation (Section 3.2.10). The competition aspect of the assay was verified with unconjugated versions of both the wild-type and mutant 16-mer Nrf2 derived peptides. Only the wild-type Nrf2 peptide was able to perturb the PPI in a dose-dependent manner and restore the eCFP fluorescence emission. The obtained data provides an insight into structure-activity relationships and can aid in the design of potential inhibitors of the Keap1-Nrf2 PPI.

The adaption of the FRET method to a multi-well plate format generated a robust and reproducible assay. Titration experiments with the fusion proteins resulted in identical binding affinities in both assay formats (K_d = 0.08 µM). The accuracy of the assay was improved in the multi-well plate format by using the same protein stock solution for the whole plate and by pipetting protein volumes of at least 10% of the total well volume with a multichannel pipette. Evidence of this improved accuracy can be found by comparing SD values from Figure 3.13 with Figure 3.23; error bars are substantially smaller in the optimised multi-well plate format.

The FRET method described here is distinct from other techniques that have been applied previously to examine the PPI [52, 135, 143, 151]. Although the use of ITC is cost-effective and doesn't require labelling, FRET is higher-throughput and has higher sensitivity [164-165, 174] Therefore, the required sample amounts are usually lower than for ITC. One of the main advantages of the SPR technique is the ability to monitor protein binding in real-time [130]. However, unlike FRET, it requires sample immobilisation that can affect the conformation and/or activity of a protein [161]. Both FP and FRET are fluorescence-based methods that are sensitive, homogeneous and adaptable to a high-throughput format. FP requires complex polarizing optics, whereas FRET can be measured using simple excitation and emission filters, which can be applied to less sophisticated plate readers [162, 175]. Conjugation of the proteins of interest to fluorophores, makes the FRET assay more robust and time-stable than FP assays. Since both methods can be affected by fluorescence interference from inhibitors, further confirmation may be required. Subsequent screening of hit compounds with cell-based assays can identify biological active inhibitors. In this respect, a variation on the FRET technique was recently applied to the Keap1-Nrf2 PPI in single cells [176]. In this study a FRET-based methodology was combined with multi-photon fluorescence lifetime imaging microscopy (FLIM).

The FRET assay described here is a sensitive method that can be applied to quantify protein-protein binding and to screen Nrf2 derived peptides for the competitive inhibition of the interaction between Keap1 and Nrf2. Moreover, the assay has been applied to identify the inhibition potential of small molecules (Section 3.2.11). A future possibility is to adapt the developed FRET assay to a time-resolved (TR) FRET assay format. TR-FRET uses a long-lifetime donor fluorophore and a short-lifetime acceptor fluorophore combined with pulsed-laser excitation and time-resolved detection. The time delay can be very effective in reducing background fluorescence that originates from direct excitation of the acceptor [177].

3.4 Summary

In summary the major findings reported in this chapter are:

- The fusion proteins eCFP-TEV-eYFP, eCFP-TEV-Nrf2 wild type and mutants, eYFP-TEV-Kelch and eYFP were successfully expressed and purified.
- FRET was shown to occur when the eCFP and eYFP fluorophores were in close proximity of each other (< 10 nm) using the eCFP-TEV-eYFP protein construct. Energy transfer was halted following the addition of functional TEV protease, which increased the distance between the fluorophores (> 10 nm).
- FRET was demonstrated between eCFP-TEV-Nrf2 and eYFP-TEV-Kelch and was optimal using a protein ratio of 1:3 respectively. The observed FRET between the fusion proteins was found to be due to the interaction between Keap1 Kelch and the 16-mer Nrf2 derived peptide and not a result of non-specific interactions between the fluorescent tags (Figure 3.27).
- FRET between eCFP-TEV-Nrf2 and eYFP-TEV-Kelch was found to be favoured in a buffer environment with low ionic strength.
- Determining FRET by quantifying the decrease in donor emission is a direct measure of FRET efficiency and minimises the risk of spectral bleed-through in the eCFP fluorescence emission channel.
- The binding affinities of various eCFP-TEV-Nrf2 fusion proteins were determined following titration experiments with eYFP-TEV-Kelch. The developed assay was found to be sufficiently sensitive to detect changes in binding affinity due to single amino acid substitutions in the Nrf2-derived peptide.
- FRET observed between eCFP-TEV-Nrf2 and eYFP-TEV-Kelch was competitively inhibited by unlabelled Nrf2-derived peptides, which resulted in a restored eCFP fluorescence emission.
- The developed FRET assay was successfully adapted to a multi-well plate format that maintained sensitivity and was found suitable for high throughput screening of potential inhibitors of the Keap1-Nrf2 interaction.

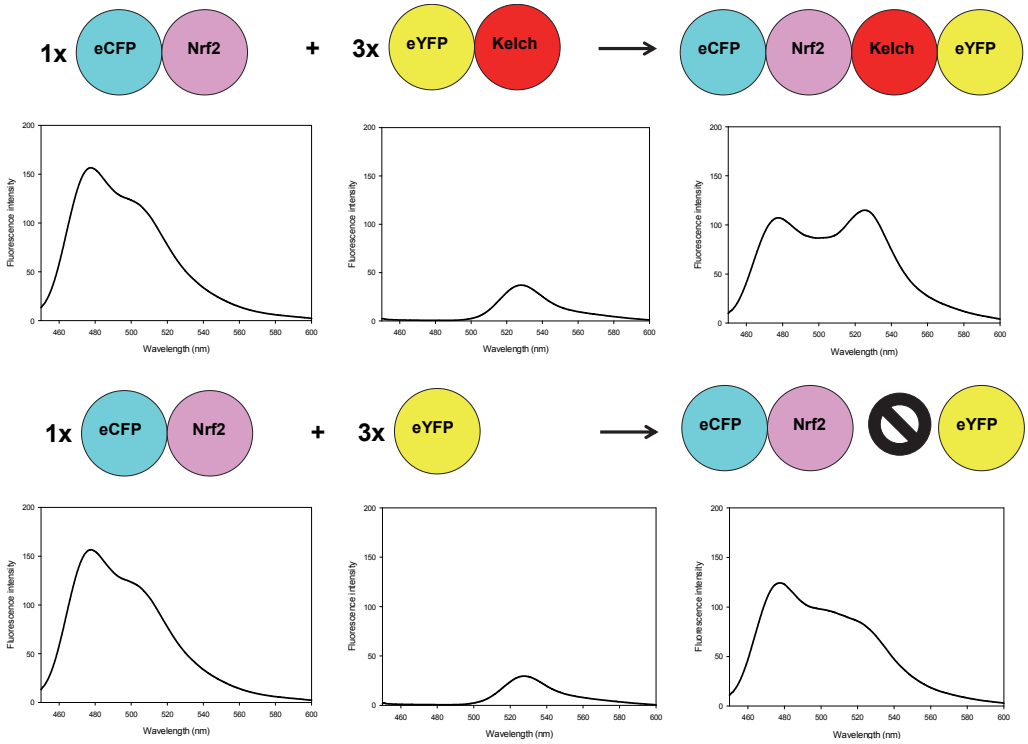

Figure 3.27: Schematic representation and corresponding emission spectra of the specific binding between eCFP-TEV-Nrf2 and eYFP-TEV-Kelch in a 1:3 ratio respectively. No interaction is observed between eCFP-TEV-Nrf2 and unconjugated eYFP.

4 Development of an Nrf2 intracellular staining method for flow cytometry

4.1 Introduction

Chemoprevention by Nrf2 activation, induces the expression of downstream *ARE* regulated detoxifying proteins and enzymes. In this respect, various classes of small molecules and peptides have been reported to induce nuclear Nrf2 accumulation [52, 98]. The Nrf2 induction potential of these molecules can be verified by determining the amount of up-regulated Nrf2 protein in cells. Typically, western blotting or ELISAs have been used for this purpose [178-179]. Flow cytometry is an evolving technique that has been employed in multi-parametric analysis of various cellular characteristics. An important aspect of this versatile technique is its ability to monitor protein levels in single cells using intracellular staining techniques [180-181].

The aim of this chapter is to develop an Nrf2 intracellular staining method for flow cytometry. This method can be used to detect and quantify constitutive and inducible Nrf2 protein levels in different cell lines using various Nrf2 inducer compounds.

The basis of modern flow cytometry was laid by Moldavan (~ 1930) and Crosland-Taylor (1953). Moldavan designed a capillary tube device to count individual cells and Crosland-Taylor developed this technique further by applying the principles of hydrodynamic focusing to align the cells within a fluid stream [182]. This stream is created by a sheath flow, which is maintained at a constant pressure to ensure cells pass through a focused laser beam (interrogation point) one-by-one (Figure 4.1).

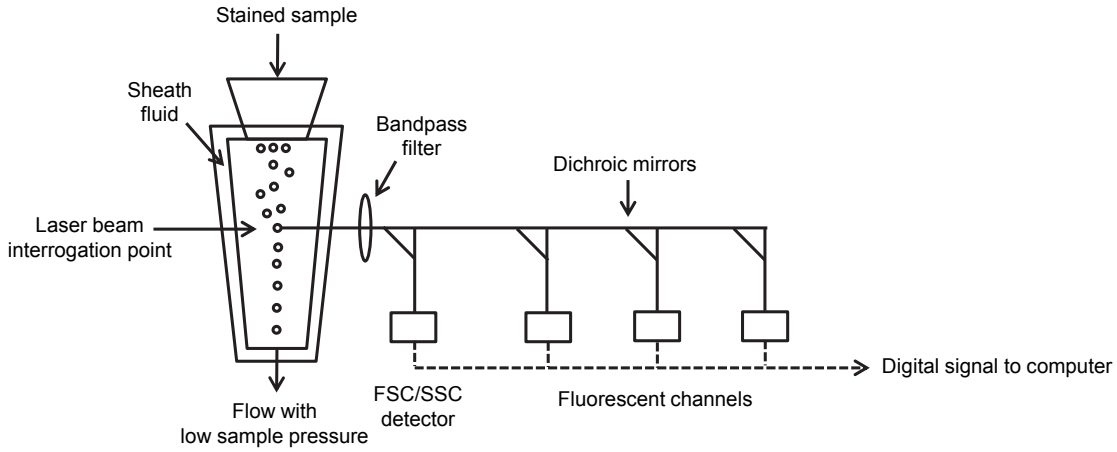

Figure 4.1: Schematic of the flow cytometry principle. Individual (stained) cells are hydrodynamic focused with sheath fluid before they intersect a laser beam. Signals are passed through bandpass filters and collected by optical detectors including a forward scatter detector (FSC), a side scatter detector (SSC) and diverse fluorescent emission detectors. The signals are converted to a digital form and send to a computer system.

The sheath pressure should be lower than the cell sample pressure. When a low pressure is applied to the sample, the sample flow path is narrowed and a drag is created that focuses the cells, allowing them to be analysed one-by-one (hydrodynamic focusing). Increasing the sample pressure widens the flow path and reduces the focus of cells. Therefore, the sample pressure and sample concentration should be kept constant. As cells pass the interrogation point, they scatter the light (by reflection and diffraction) in different angles relative to the interrogation point. Light that is scattered at low angles in a forward direction (forward scattered light or FSC) is used to measure cell size. The light scattered at high angles in a sideward direction (side scattered light or SSC) is affected by the shape (cell and nucleus) and optical homogeneity or granularity of a cell. As fluorescently labelled cells flow through the laser beam, the fluorescent probes are excited to a higher energy state. The fluorescence emission is also measured from light that is emitted at high angles. The scattered light and fluorescent signals are collected by an optical detection system, where the signals are split by dichroic mirrors and filters, which direct each signal to the correct detector (Figure 4.1) [183]. Photomultiplier tubes or PMTs are responsible for the amplification of the fluorescence signal, which is dependent on the voltage applied to each PMT [184].

The fluorescence emission intensity is then converted to a digital signal and is presented as a mean, median or mode of the entire intensity range.

Flow cytometry allows the detection of proteins expressed on cell membranes (surface staining) or inside cells (intracellular staining) [185]. In comparison with cell surface labelling, intracellular staining requires fixation and permeabilisation of the cells to allow antibodies to pass the cell membranes. This is then followed by either a direct or indirect staining approach. In direct staining, cells are incubated with a fluorophore conjugated primary antibody. Since there is only one antibody incubation step, there is a minimal risk of non-specific binding. However, fluorophore conjugated versions of specific primary antibodies are often not available, unless produced in-house. In indirect staining, cells are incubated with an unconjugated primary antibody and a fluorophore conjugated secondary antibody.

In order to interpret the data there is need for control samples. Unstained controls are important to verify the extent of cellular background staining. Isotype controls are unconjugated versions of the secondary antibody and are used as a control to account for non-specific staining from the primary antibody [186]. The level of non-specific staining from the secondary antibody is estimated by cells stained only with the fluorophore conjugated secondary antibody. Furthermore, biological comparison controls are needed to distinguish between positive and negative signals [186]. Cells stimulated with a known protein inducer compound can be used as a positive biological control sample. The level of protein induction upon stimulation can be best determined by using unstimulated cell samples, which serve as negative biological controls.

Western blotting is one of the most frequently used methods to detect and quantify specific proteins in a sample of tissue homogenate or cell lysate. This technique uses electrophoresis to separate proteins, which are subsequently transferred to a membrane and incubated with antibodies specific to the protein of interest (Section 2.16). Chemiluminescence is a commonly used method to visualise the target protein on the membrane [187]. In this case the added secondary antibody is conjugated to horseradish peroxidase (HRP). The membrane bound HRP-

conjugated antibody converts chemiluminescent substrates (peroxide and an enhanced luminol solution) into light that can be detected by a sensitive camera. Protein levels are then determined with densitometry, using a housekeeping gene (e.g. β-actin) as a loading control. Quantifying the expression of proteins using western blotting has several benefits over other methods: it allows for the determination of the size and molecular weight of the target protein and is indicative of the specificity of the primary antibody [188]. Since the signal is amplified enzymatically, proteins expressed at very low levels can be visualised [189]. Although some level of optimisation is required, western blotting is a relatively straight-forward method. Nevertheless, there are some important disadvantages to be considered. Western blotting involves multiple steps, which are rather time-consuming and can take up to two days: sample preparation, SDS-PAGE, protein transfer, blocking of non-specific sites, primary and secondary antibody incubation, multiple washing steps and development of the blot. In addition, western blotting requires large numbers of cells [190-191]. The technique doesn't allow for the separation of cells based on their responsiveness and obtains an average value for the protein expressed in a whole cell population (population analysis) [189]. Consequently, repetition experiments can acquire different datasets and limit the statistical significance. One of the important aspects of flow cytometry is its ability to measure events in individual cells (single-cell analysis). This makes protein quantification using this method more informative and reliable [192].

Over the years flow cytometry has become a widely used and applied technique in both the research laboratory and the clinic. Analysis of e.g. red blood cells, leucocytes and platelets are an important part of routine flow cytometry in the clinic. Cell surface staining allows for the detection and quantification of specific immune cell subsets and has been applied to immunophenotyping (e.g. CD4+ T cell blood counts in HIV patients) and cancer diagnostics (e.g. CD20+ B cell malignancies) [193]. The development of intracellular cytokine staining permits the simultaneous detection of multiple cytokines in one single cell sample [194]. Other applications involve cell cycle and DNA analysis. The use of flow cytometry for (nuclear) protein quantification presents another interesting application. The combination of these flow cytometry techniques can provide valuable information regarding various disease stages.

Although some developed protocols for nuclear protein staining have recently been published [195-197], there is no standard procedure for staining intracellular (nuclear) antigens using flow cytometry and each protocol has to be tailored to the specific (nuclear) protein under study. Nuclear antigens require different fixation and permeabilizing treatments to cytoplasmic antigens. To date, no such protocol has been designed for the detection and quantification of Nrf2. In this study, cells are treated with a known Nrf2 inducer compound before they are fixed and permeabilised (Figure 4.2). Subsequently, an indirect staining approach is used, which includes the incubation of cells with an unconjugated anti-Nrf2 primary antibody followed by a fluorophore conjugated secondary antibody. Since the induction of Nrf2 was expected to result in the accumulation of the transcription factor in the nucleus, the intracellular staining method was adapted to label the Nrf2 protein in both whole cells and isolated nuclei. The level of Nrf2 protein expressed is determined by calculation of the median fluorescence intensity (MFI) for each protein-antibody complex. This chapter describes the development of a working intracellular staining assay protocol and the optimisation of the signal-to-noise ratio.

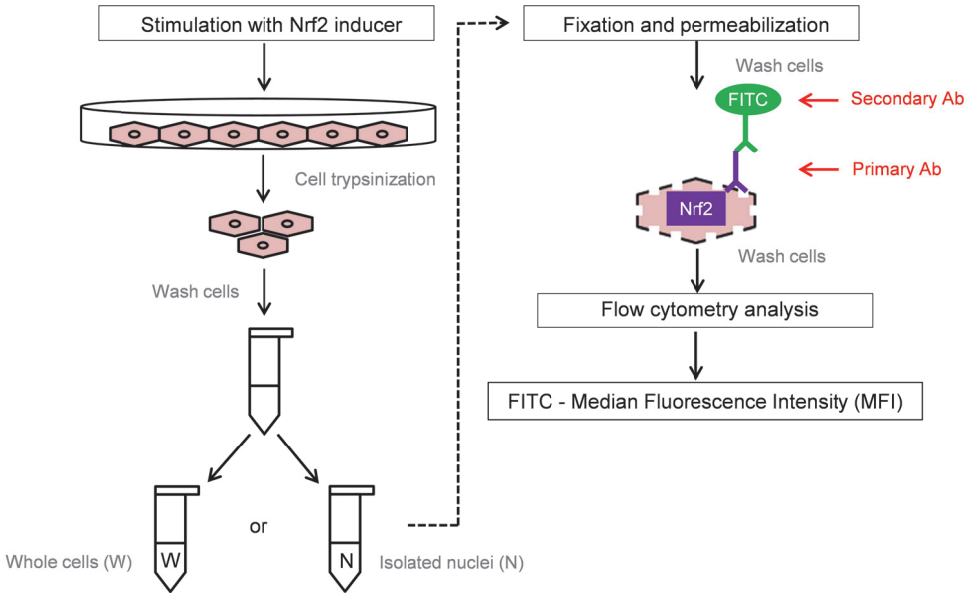

Figure 4.2: Overview of the optimised intracellular Nrf2 staining method. Following stimulation of cells with an Nrf2 inducer compound, cells are trypsinised and washed. Whole cells or isolated nuclei are subsequently fixed and permeabilised. Next, cell samples are stained with an unconjugated anti-Nrf2 primary antibody and a FITC fluorophore conjugated secondary antibody. After a washing step, cells are ready for flow cytometry analysis, where the FITC median fluorescence intensity (MFI) is calculated for each protein-antibody complex.

4.2 Results: set-up of a standard protocol

The paragraphs below describe the different aspects that were considered whilst setting up a standard protocol for the intracellular staining of Nrf2.

4.2.1 Stimulation conditions for Nrf2 induction

To evaluate the ability of flow cytometry to determine Nrf2 protein levels inside cells, stimulation conditions that triggered up-regulation of the transcription factor had to be determined. Literature suggests that the murine hepatoma cell line Hepa1c1c7 is highly responsive to Nrf2 inducer compounds [198]. Hence, this cell line was selected for the initial evaluation of this method. Sulforaphane is a natural product isolated from cruciferous vegetables and a known Nrf2 inducer [68]. This compound up-regulates Nrf2 by covalently modifying cysteine residues in the Keap1 protein, impeding ubiquitination of Nrf2 [40]. Sulforaphane has demonstrated the ability to activate the phase II enzyme NQO1 in Hepa1c1c7 cells [199]. Moreover, western blotting experiments showed induced Nrf2 expression in Hepa1c1c7 cells stimulated with 10 µM sulforaphane for 1 h (Figure 4.6). Hence, cells that received this treatment were used as positive biological comparison controls (also referred to as 'stimulated sample') in the following flow cytometry experiments.

4.2.2 Instrument settings

One of the important steps for the development of a protocol for intracellular staining is setting the PMT voltages (i.e. instrument gain) on the flow cytometer (MACSQuant Analyzer, Miltenyi Biotec). Here, the PMT voltages were set using an unstained cell sample. The FSC and SSC voltages were adjusted until the cells appeared in the middle of the two-dimensional dot-plot (150V FSC, 300V SSC) (Figure 4.3 A). The FITC voltage was set such that the unstained cells appeared in the 1st log decade of the fluorescence histogram (300V FITC). This voltage was used to measure stained cell samples. Figure 4.3 B shows the position of the unstained sample in relation to the isotype control (unconjugated anti-rabbit IgG), the secondary antibody only control (anti-rabbit IgG-FITC conjugated antibody), the

unstimulated sample and the sulforaphane stimulated sample (since control spectra overlap, individual controls are not visible). Since the full range of samples was visible on the logarithmic scale, no adjustments had to be made.

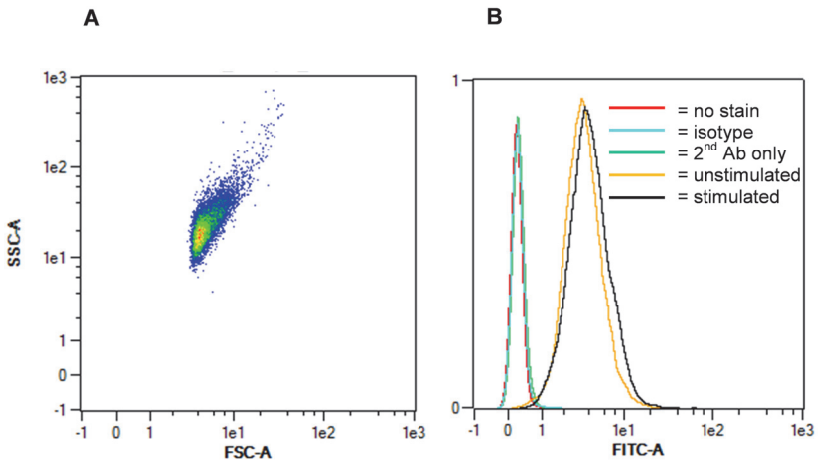

Figure 4.3: Optimisation of instrument settings. (A) Unstained control cells shown in a FSC/SSC dot-plot with optimised voltages: 150V FSC, 300V SSC. (B) Unstained control, isotype control, secondary antibody only control, unstimulated and stimulated sample displayed in a FITC histogram with optimised voltages: 300V.

Cells were stained with the nuclear DAPI stain to verify the amount of debris present in the sample. Figure 4.4 shows a predominant positive staining for DAPI, which implies that there is a minimal amount of debris present. As noise levels were low, the FSC threshold on the flow cytometer didn't need to be adjusted and was set to zero [200].

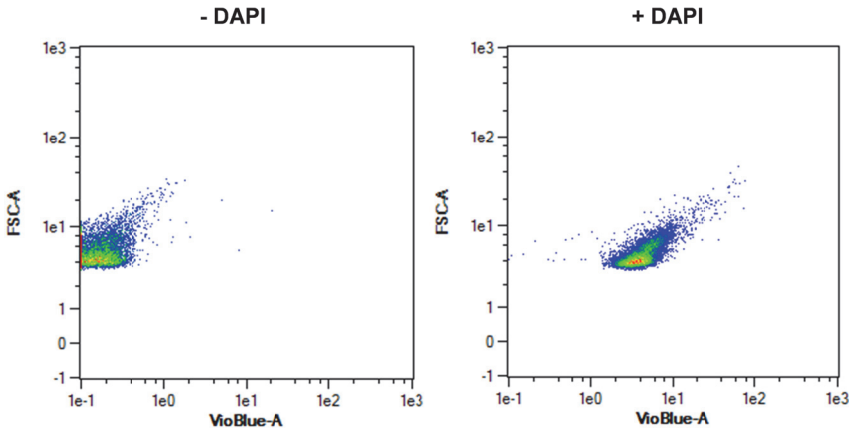

Figure 4.4: FSC/SSC plots of cells that were either unstained (-DAPI) or stained (+DAPI) with DAPI. Shown are representative examples.

The instrument was set to measure 10,000 events/sample, which is the lowest measured number of events per sample as recommended by the flow cytometer manufacturer Miltenyi Biotec.

The fluorescence intensity can be displayed as mean, median or mode. Data generated with flow cytometry often have skewed distributions. The median is the middle value when the data is arranged in numerical order, hence the median is least affected by outliers and gives the best representation of the data [197, 201]. Therefore, the median fluorescence intensity (MFI) was chosen as the output for analysis of the data. The MFI values were normalised to control cell samples that were only stained with the fluorophore conjugated secondary antibody control. This control was used as an internal staining control to account for non-specific fluorescence in each sample. The obtained normalised MFI (nMFI) values allowed the comparison of data from different experiments [202]. Fold changes were calculated by dividing the nMFI of stimulated samples by the nMFI of unstimulated samples.

4.2.3 Fixing and permeabilisation conditions

Prior to intracellular staining, cells need to be fixed and permeabilised. Cells are fixed to maintain and stabilise the cellular structure before the cell membranes are permeabilised to allow antibodies to access. Formaldehyde is a commonly used fixative that cross-links proteins [203]. Formaldehyde prevents cell clumping and maintains cellular scatter properties when used before a permeabilisation reagent [188]. Permeabilisation of the cells with organic solvents such as methanol precipitate and denature proteins, which provides access to nuclear antigens [189]. Hence, the combination of formaldehyde and methanol was expected to suit the intracellular staining of the nuclear transcription factor Nrf2. Initially, cells were fixed with 1.5% formaldehyde and permeabilised with ice-cold methanol, which were the conditions adopted from [188]. Methanol permeabilised cells were found to be stable to storage for up to a week at - 80 °C without substantial loss of staining efficiency.

4.2.4 Antibody selection

Since no fluorescent labelled primary anti-Nrf2 antibody was available, an indirect staining approach was adopted. The rabbit polyclonal anti-Nrf2 H300 (SantaCruz) antibody was used as an unconjugated primary antibody for initial flow cytometry experiments since Nrf2 expression could be demonstrated with western blotting using this antibody (Figure 4.6 A). The goat anti-rabbit IgG-FITC conjugated antibody (SantaCruz) was selected as a fluorophore conjugated secondary antibody. The FITC fluorochrome was chosen as there is a wide range of FITC labelled antibodies available. Both antibodies were titrated at a dilution range of 1:25 – 1:500 using sulforaphane stimulated cell samples (Figure 4.5). The data were best separated into positive (sulforaphane stimulated) and negative signals (unstained) with a minimal use of antibodies using dilutions of 1:100 for the polyclonal primary antibody and 1:500 for the FITC conjugated secondary antibody. Certain antibody combinations resulted in deformity of the FITC fluorescence peaks, which could be due to aggregation of the antibody-protein complexes. The isotype control antibody, unconjugated anti-rabbit IgG (SantaCruz), was matched with the FITC conjugated secondary antibody and used at the same optimised dilution (1:500) (not shown).

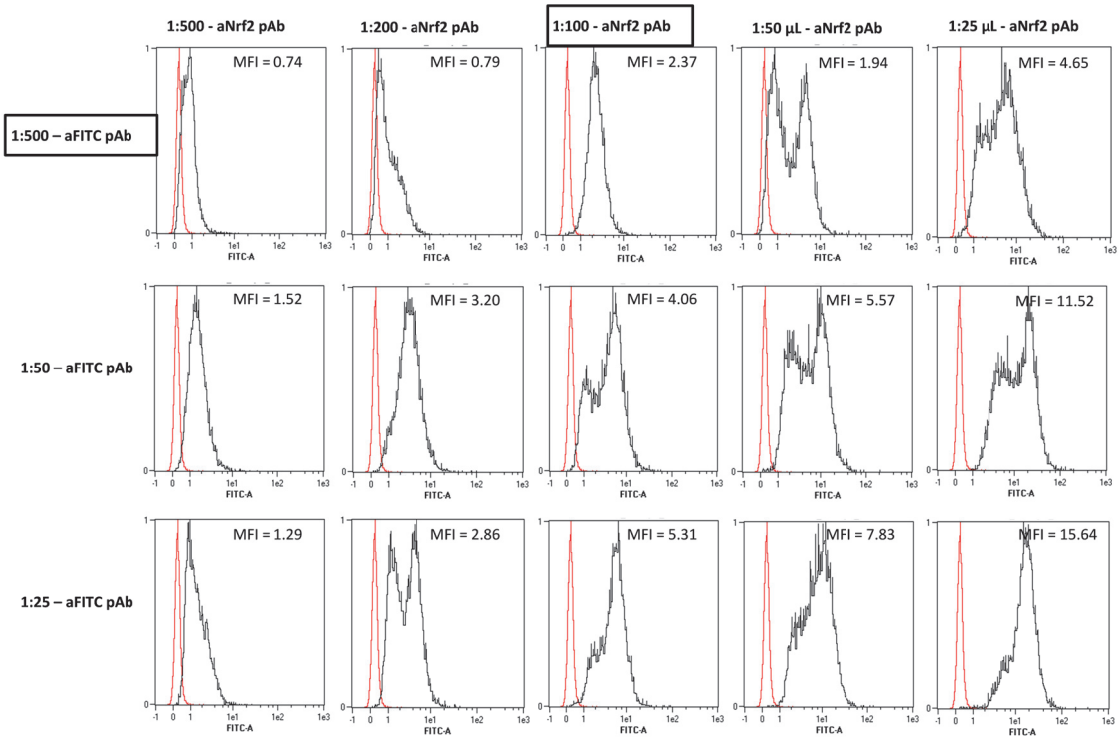

Figure 4.5: Titration of anti-Nrf2 polyclonal antibody (aNrf2 pAb) and anti-FITC polyclonal antibody (aFITC pAb) at a dilution range of 1:25 – 1:500. Unstained samples (negative) are shown in red and stained samples (positive) are displayed in black. FITC MFI values are shown for each antibody combination and the optimal antibody combination is marked with a border.

4.2.5 Troubleshooting of the standard protocol

During the development of the standard protocol for intracellular staining of Nrf2, several problems were identified and resolved. A relative high cell loss was observed in initial experiments. This problem was addressed by reducing the number of washing steps and by adjusting the centrifuge speed and time. The buffer system was optimised with the aim of reducing the irregularity of the FITC fluorescence peaks. Cells were initially washed and incubated in PBS. A final concentration of 2 mM EDTA and 0.5% BSA was added to the buffer to prevent cellular and/or antibody-protein complex aggregation. In addition, BSA helped to prevent the ‘sticking’ of the cells to the micro-centrifuge tubes.

Formaldehyde was added to the buffer to ensure fixation of the cells throughout the procedure. However, the cross-linking nature of formaldehyde induced FITC fluorescence background staining [204]. The final standard protocol that was developed is described in Table 4.1.

Table 4.1: Standard protocol developed for the intracellular staining of Nrf2 using flow cytometry.

Step	Description
1	Stimulate cells with Nrf2 inducer compound
2	Trypsinise cells
3	Pellet cells
4	Resuspend cells in PBS
5	Fix cells cells in 1.5% formaldehyde for 10 min at RT
6	Pellet cells
7	Permeabilise cells in ice-cold methanol for 30 min on ice
8	Wash cells in buffer
9	Block cells in buffer for 10 min at RT
10	Stain cells with 1:100 anti-Nrf2 H300 primary pAb overnight at 4°C
11	Wash cells in buffer
12	Stain cells with 1:500 anti-rabbit IgG FITC conjugated secondary pAb for 1 hour at RT
13	Wash cells in buffer
14	Analyse samples on flow cytometer

4.2.6 Standard protocol

The protocol was applied to stain Nrf2 in unstimulated and sulforaphane stimulated Hepa1c1c7 cells. Flow cytometry analysis showed no visible staining difference between stimulated and unstimulated samples (FD or fold difference ~ 1.2) (Figure 4.6 B). Western blotting analysis was carried out to verify the antibody specificity of the polyclonal anti-Nrf2 primary antibody. Results revealed the presence of multiple non-specific protein bands (Figure 4.6 A).

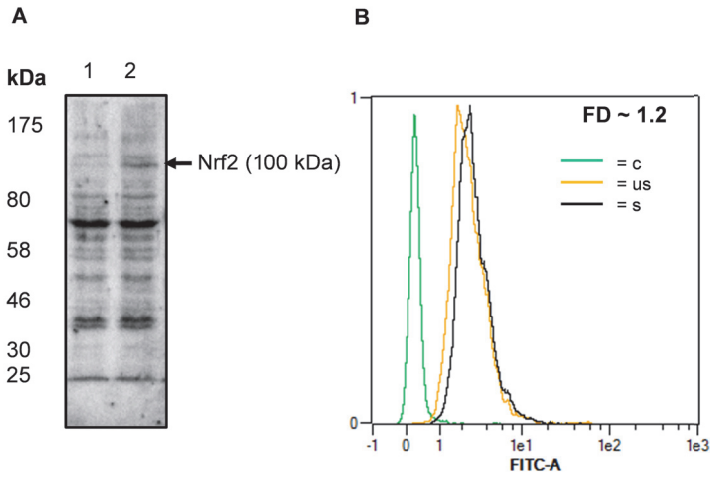

Figure 4.6: Western blotting (A) and flow cytometry analysis (B) of unstimulated (1 or us) and stimulated (2 or s) whole cell samples stained with an anti-Nrf2 polyclonal antibody and an anti-FITC polyclonal antibody. An internal staining control (c) has been used in the flow cytometry analysis. FD = fold difference or fold change. Representative examples are shown.

4.3 Results: optimisation of the standard protocol

The following section describes the optimisation of the standard protocol to enhance the fold change between stimulated and unstimulated samples.

Nrf2 staining of isolated nuclei

The nuclear localisation of the transcription factor was verified by adapting the protocol to stain Nrf2 in isolated nuclei. The nuclei were isolated using a nuclear extraction kit (NE-PER, Thermo Scientific) by lysis of the outer cell membrane to release cytoplasmic proteins and subsequent centrifugation to pellet the nuclei [205] (the same kit was used to lyse the nuclear membrane for SDS-PAGE and western blotting analysis). Following resuspension of the nuclei in PBS, the nuclear integrity was verified by staining an aliquot with trypan blue. Stained nuclei appear round and blue, whole cells remain unstained and cell debris appears as irregular shaped blue particles (Figure 4.7).

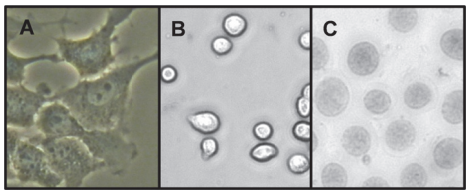

Figure 4.7: Representative phase-contrast images of Hepa1c1c7 cells growing in a tissue culture flask (A), detached whole cell preparation (B) and isolated nuclei preparation (C) stained with trypan blue (objective 20x). Representative examples are shown.

Initially, a high loss of nuclei was observed during the procedure as the pelleted nuclei were less adhesive to the micro-centrifuge tube than pelleted whole cell samples. In addition, the isolated nuclei were found to aggregate in solution more than whole cells. This was confirmed by the flow cytometry analysis which revealed a broadening of the population towards an increased FSC and SSC (compare Figure 4.8 with Figure 4.3 A). These problems were addressed by starting with a minimum of 3 – 4 x 10^6 cells/sample and by resuspending the isolated nuclei through a 21G needle before analysis.

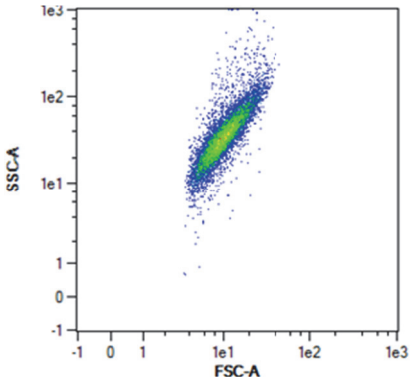

Figure 4.8: FSC/SSC plot of an isolated nuclei sample. A representative example is shown.

Finally, nuclei were stained in the same manner as whole cells according to the standard protocol (Table 4.1). Flow cytometry analysis showed a small improvement in fold difference compared to whole cell samples (FD ~ 1.2 for whole cells versus FD ~ 1.4 for nuclei) (Figure 4.9 B). The corresponding western blot presented a similar small reduction in amount of non-specific protein bands (Figure 4.9 A).

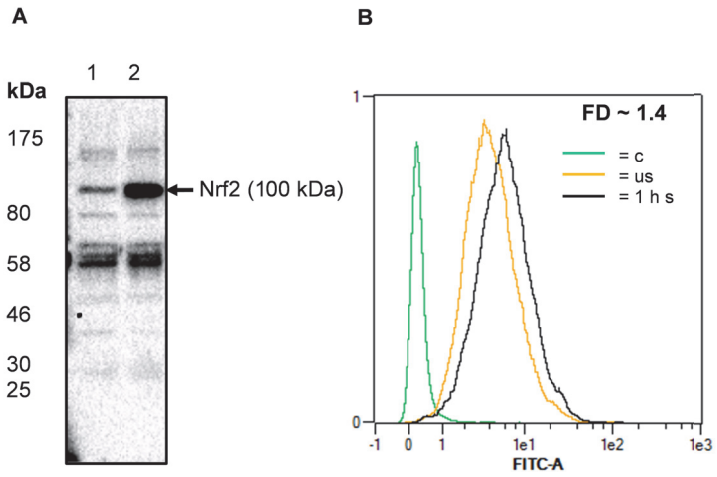

Figure 4.9: Western blotting (A) and flow cytometry analysis (B) of unstimulated (1 or us) and stimulated (2 or s) isolated nuclei samples stained with an anti-Nrf2 polyclonal antibody and an anti-FITC polyclonal antibody. An internal staining control (c) has been used in the flow cytometry analysis. FD = fold difference or fold change. Representative examples are shown.

Monoclonal versus polyclonal primary antibody

The association between antibody specificity and fluorescence signal separation was examined by Nrf2 staining with a monoclonal primary anti-Nrf2 antibody. The rabbit monoclonal anti-Nrf2 D1Z9C-XP (Cell Signalling) was tested as an unconjugated primary antibody in the following flow cytometry experiments. The monoclonal primary antibody was titrated together with the FITC conjugated secondary antibody to find the optimal antibody dilutions (Figure 4.10). From a dilution range of 1:200 – 1:1000, the optimal dilution for the monoclonal primary antibody was found to be 1:1000 and 1:200 for the FITC conjugated secondary antibody.

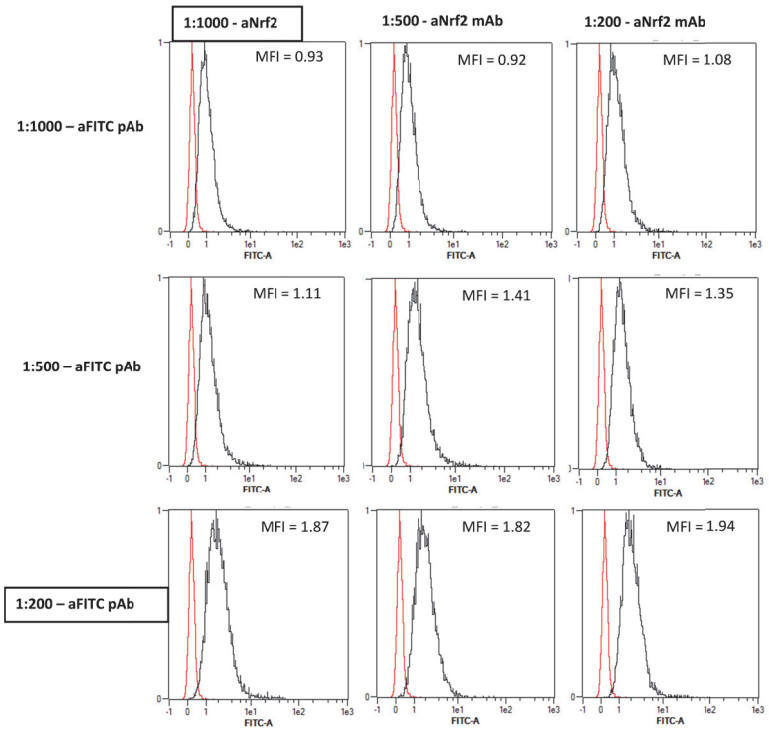

Figure 4.10: Titration of anti-Nrf2 monoclonal antibody (aNrf2 mAb) and anti-FITC polyclonal antibody (aFITC pAb) at a dilution range of 1:200 – 1:1000. Unstained samples (negative) are shown in red and stained samples (positive) are displayed in black. FITC MFI values are shown for each antibody combination and the optimal antibody combination is marked with a border.

Next, the antibodies were used to stain Nrf2 in whole cell and isolated nuclei samples. The fold change between stimulated and unstimulated samples was considerably improved after changing the polyclonal anti-Nrf2 primary antibody for a monoclonal variant: FD ~ 1.2 for polyclonal versus FD ~ 3.4 for monoclonal for whole cell samples and FD ~ 1.4 for polyclonal versus FD ~ 7.7 for monoclonal for nuclei samples (Figure 4.11 B & D respectively). Moreover, western blotting analysis showed enhanced antibody specificity (Figure 4.11 A & C).

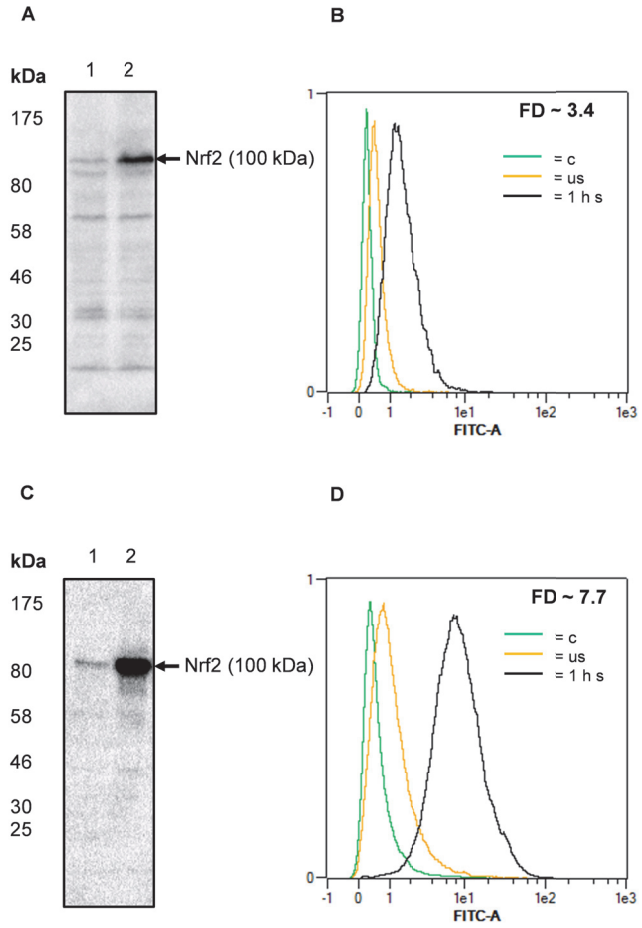

Figure 4.11: Western blotting (A&C) and flow cytometry analysis (B&D) of unstimulated (1 or us) and stimulated (2 or s) whole cells (A & B) and isolated nuclei samples (C & D) stained with an anti-Nrf2 monoclonal antibody and anti-FITC polyclonal antibody. An internal staining control (c) has been used in the flow cytometry analysis. FD = fold difference or fold change. Representative examples are shown.

Antibody incubation time

Initially, samples were incubated overnight with the primary anti-Nrf2 antibody to ensure optimal staining. This incubation time was reduced to 1 h to explore the effect on the staining efficiency. Only a small reduction in fold change was evident (FD ~ 3.4 for overnight incubation versus FD ~ 2.7 for 1 h incubation for whole cells and FD ~ 7.7 for overnight incubation versus FD ~ 7.0 for 1 h incubation for nuclei) and suggests procedure times can be shortened by decreasing the primary antibody incubation time (Table 4.2).

FITC versus PerCP conjugated secondary antibody

Since we found that formaldehyde fixation increased the FITC auto-fluorescence signal (Section 4.2.5), a second fluorophore conjugated secondary antibody was tested. PerCP fluoresces in the red region of the spectrum and is not affected by formaldehyde fixation [204]. However, changing the FITC conjugated secondary antibody to a PerCP conjugated secondary antibody resulted in a substantial reduction in fold change: FD ~ 3.4 for FITC versus FD ~ 2.0 for PerCP for whole cell samples and FD ~ 7.7 for FITC versus FD ~ 2.6 for PerCP for nuclei samples (Table 4.2).

Staining volume

Antibody staining was originally carried out in a final volume of 500 µL. To decrease the amount of antibody needed, the final volume was reduced to 100 µL. However, this resulted in a decreased fold change: FD ~ 3.4 for 500 µL versus FD ~ 2.3 for 100 µL for whole cell sample and FD ~ 7.7 for 500 µL versus FD ~ 4.6 for 100 µL for nuclei samples (Table 4.2).

Formaldehyde fixation

To test whether staining efficiency was affected by the percentage of formaldehyde, cells were fixed with 1.5% or 0.5% formaldehyde. The fold change was slightly reduced when cells were fixed with 0.5% formaldehyde: FD ~ 3.4 for 1.5% versus FD ~ 3.1 for 0.5% for whole cell samples and FD ~ 7.7 for 1.5% versus FD ~ 7.5 for 0.5% for nuclei samples (Table 4.2).

Other

The buffer conditions of the Foxp3 staining buffer set (Miltenyi Biotec) are specifically designed for the intracellular staining of the Foxp3 transcription factor. To verify whether such optimised conditions for a transcription factor could enhance the staining of the Nrf2 transcription factor, the buffer set was compared with the original fixation (1.5% formaldehyde) and permeabilisation (ice-cold methanol)

conditions. Similar results were found for both methods (FD ~ 3.0 for whole cells) (Table 4.2).

Table 4.2: Overview of conditions tested to optimise the standard intracellular Nrf2 staining protocol. Shown are fold changes from representative experiments. Abbreviations used in the table: whole cells (W), nuclei (N), primary antibody (1st Ab), secondary antibody (2nd Ab), polyclonal antibody (pAb), monoclonal antibody (mAb), overnight (o/n) and formaldehyde (FA).

Condition	W or N	1st Ab	2nd Ab	Incubation time	Staining volume	FA fixation	Fold change
1	W	Nrf2 pAb	FITC pAb	o/n	500 µL	1.5 %	1.2
2	N	Nrf2 pAb	FITC pAb	o/n	500 µL	1.5 %	1.4
3	W	Nrf2 mAb	FITC pAb	o/n	500 µL	1.5 %	3.4
4	N	Nrf2 mAb	FITC pAb	o/n	500 µL	1.5 %	7.7
5	W	Nrf2 mAb	FITC pAb	1 h	500 µL	1.5 %	2.7
6	N	Nrf2 mAb	FITC pAb	1 h	500 µL	1.5 %	7.0
7	W	Nrf2 mAb	PerCP pAb	o/n	500 µL	1.5 %	2.0
8	N	Nrf2 mAb	PerCP pAb	o/n	500 µL	1.5 %	2.6
9	W	Nrf2 mAb	PerCP pAb	1 h	500 µL	1.5 %	2.0
10	N	Nrf2 mAb	PerCP pAb	1 h	500 µL	1.5 %	3.0
11	W	Nrf2 mAb	FITC pAb	o/n	100 µL	1.5 %	2.3
12	N	Nrf2 mAb	FITC pAb	o/n	100 µL	1.5 %	4.6
13	W	Nrf2 mAb	FITC pAb	o/n	500 µL	0.5 %	3.1
14	N	Nrf2 mAb	FITC pAb	o/n	500 µL	0.5 %	7.5
15	W	Nrf2 mAb	FITC pAb	o/n	100 µL	0.5 %	1.4
16	N	Nrf2 mAb	FITC pAb	o/n	100 µL	0.5 %	4.2
17	W	Nrf2 mAb	FITC pAb	o/n	500 µL	Foxp3 BS	3.0

4.4 Results: application of the intracellular Nrf2 staining assay

Following on from the evaluation of various conditions for their ability to affect staining efficiency, improvements were found when changing the primary anti-Nrf2 antibody from a polyclonal to a monoclonal variant and by applying the procedure to isolated nuclei. As a result, the staining steps in the standard protocol (Table 4.1) were adapted accordingly and protocol steps were included for isolation of the nuclei. The adapted standard protocol is described in Table 4.3 and was applied to the following flow cytometry experiments.

Table 4.3: Adapted standard protocol for the intracellular staining of Nrf2. Protocol steps describing the staining procedure were adapted from the standard protocol and indicated with *. Protocol steps that were added for the isolation of nuclei are indicated with **.

Step	Description
1	Stimulate cells with Nrf2 inducer compound
2	Trypsinise cells
3	Wash cells in buffer
4	Pellet cells
****5**	Resuspend cells in 100 µL/1x10^6 CER I (NE-PER kit, Thermo Scientific) and incubate for 10 min on ice
****6**	Add 5.5 µL/1x10^6 CER II (NE-PER kit, Thermo Scientific) and incubate for 1 min on ice
****7**	Pellet nuclei
8	Resuspend nuclei in PBS (check nuclear integrity by trypan blue staining)
9	Fix cells cells in 1.5% formaldehyde for 10 min at RT
10	Pellet cells
11	Permeabilise cells in ice-cold methanol for 30 min on ice
12	Wash cells in buffer
13	Block cells in buffer for 10 min at RT
***14**	Stain cells with 1:1000 anti-Nrf2 D1Z9C-XP primary mAb overnight at 4°C
15	Wash cells in buffer
***16**	Stain cells with 1:200 anti-rabbit IgG FITC conjugated secondary pAb for 1 hour at RT
17	Wash cells in buffer
18	Analyse samples on flow cytometer

To verify whether this protocol could be used to quantify Nrf2 protein levels, Hepa1c1c7 cells were stimulated with 10 µM sulforaphane for 1, 3, 6 and 24 h. Next, nuclei were isolated, fixed, permeabilised and stained according to the adapted standard protocol (see above). Although the protocol can also be applied to whole cells, an overall higher signal-to-noise ratio was achieved using nuclei. In parallel, similar sulforaphane stimulated nuclei were lysed and subjected to SDS-PAGE and western blotting. Similar qualitative results were observed for flow cytometry and western blotting analysis (Figure 4.12 A & B).

Next, fold changes were calculated for both methods before the values were normalised to the maximal stimulated sample (i.e. 100% = 1 h 10 µM sulforaphane stimulation). Quantitative comparison of both techniques revealed a difference in absolute fold changes (Figure 4.12 C). However, normalised changes showed a similar trend for Nrf2 induction levels over time (Figure 4.12 D).

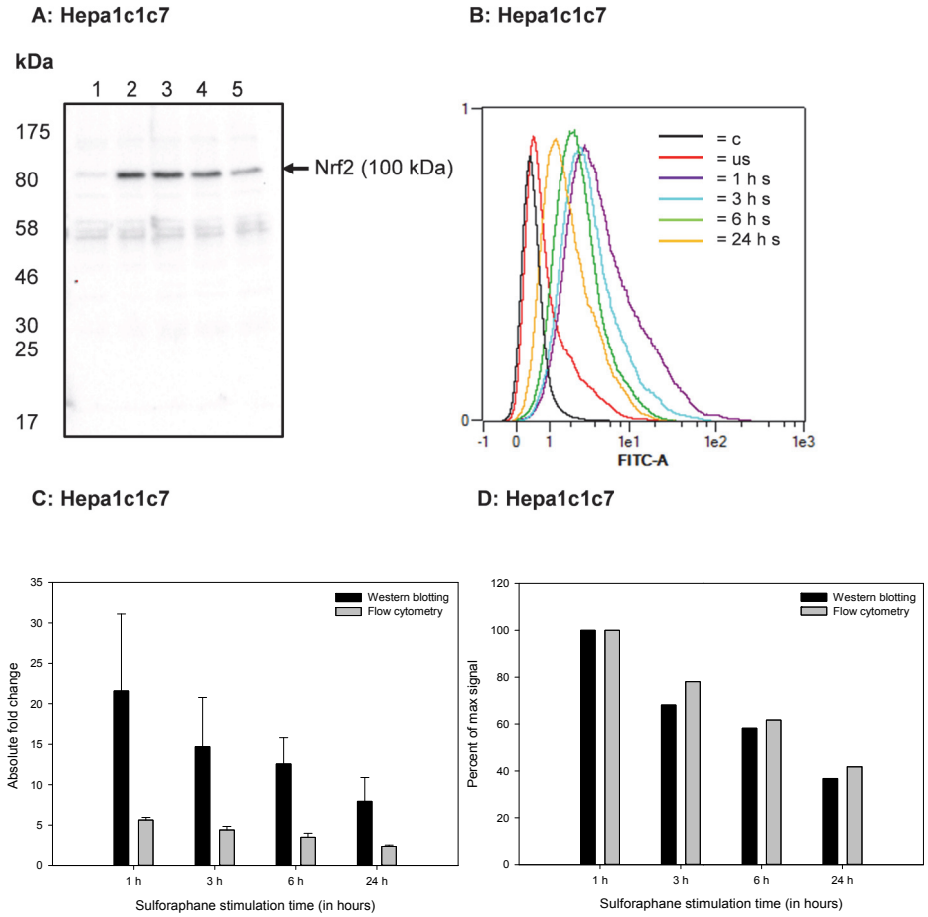

Figure 4.12: Hepa1c1c7 cells were unstimulated (us) or stimulated (s) with 10 µM sulforaphane for 1, 3, 6 and 24 h and subjected to western blotting (A) or flow cytometry analysis (B). An internal staining control (c) has been used in the flow cytometry analysis. Absolute fold changes were calculated using relative protein band intensities for western blotting and FITC-MFI for flow cytometry (C). The error bars represent the standard deviation of n = 3 independent experiments. The fold changes were normalised for the maximally induced sample (here, 1 h stimulation is 100% induction) (D).

To examine whether this intracellular staining method could be used with other cell lines, human HeLa and MCF-7 cells were also stimulated with sulforaphane. Again, western blots of both HeLa and MCF-7 nuclei samples showed a similar response rate to the flow cytometry histograms (compare Figure 4.13 A & C with Figure 4.13 B&D). Figure 4.14 shows the absolute fold changes that were calculated from the flow cytometry data to represent the Nrf2 induction levels in both cell lines. The intracellular Nrf2 staining method was also applied to study the Nrf2 induction potential of other small molecules (Section 6.2.3 and 7.5.4).

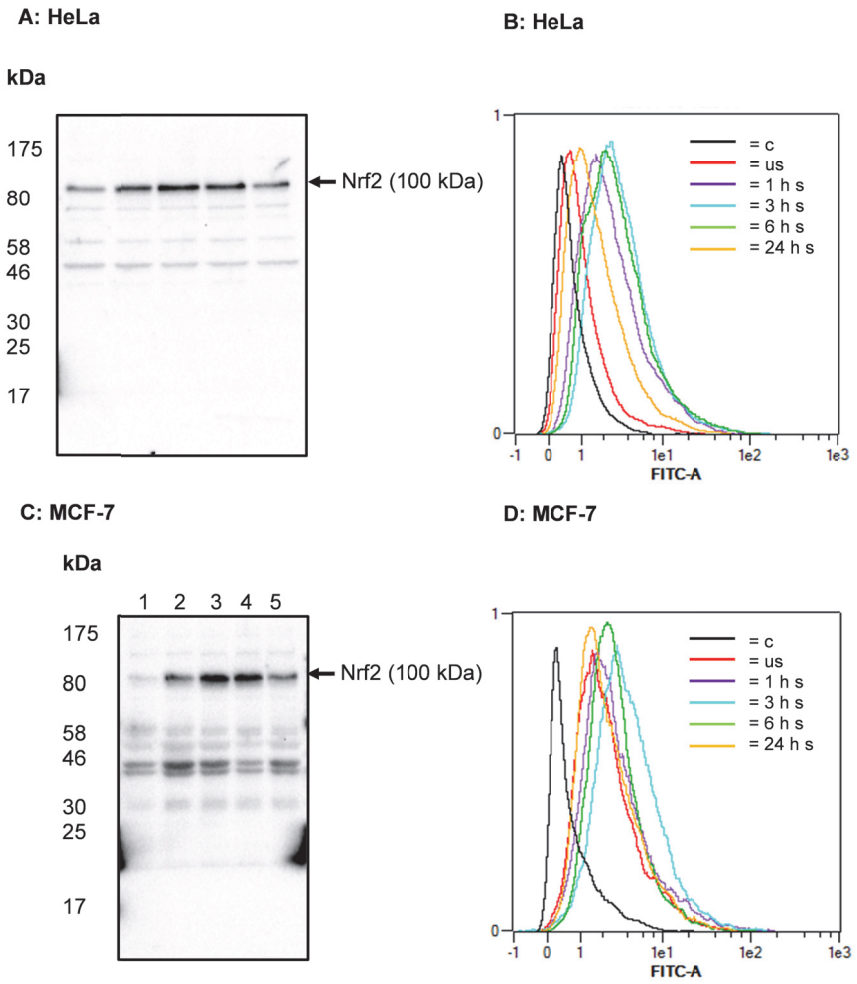

Figure 4.13: HeLa (A & B) and MCF-7 (C & D) cells were unstimulated (us) or stimulated (s) with 10 µM sulforaphane for 1, 3, 6 and 24 h and subjected to western blotting (A & C) or flow cytometry analysis (B & D). An internal staining control (c) has been used in the flow cytometry analysis.

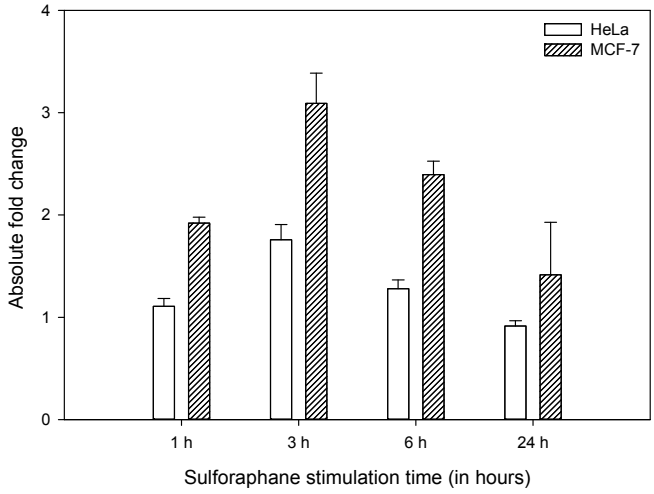

Figure 4.14: Absolute fold changes calculated for flow cytometry analysis of HeLa and MCF-7 cells. The cells were unstimulated or stimulated with 10 µM sulforaphane for 1, 3, 6 and 24 h. The error bars represent the standard deviation of n = 3 independent experiments.

4.5 Discussion

Described here is the development of a flow cytometry method, which presents a novel approach to quantitatively study the expression of the transcription factor Nrf2 in cells. This cell-based assay was shown to detect and quantify Nrf2 induction levels upon cellular stimulation with known Nrf2 inducer molecules. This procedure can be used to stain Nrf2 in whole cells or in nuclei, which enables the confirmation of nuclear localisation. Isolation of intact nuclei via biochemical fractionation was simplified by using a nuclear extraction kit (NE-PER, Thermo Scientific). This kit provides a more efficient approach towards nuclear isolation than existing techniques [196, 206-207]. Higher Nrf2 staining levels were observed in nuclei compared to whole cell samples. This might be due to the removal of the cell membrane, which increases the staining efficiency [197].

Since only a minimal amount of debris was present in the samples (Section 4.2.2), cells have not been gated for FSC and SSC. However, to improve reproducibility, gating by these parameters would allow analysis of a cell population homogenous in size and inner complexity (Figure 4.15). This presents an area for future work.

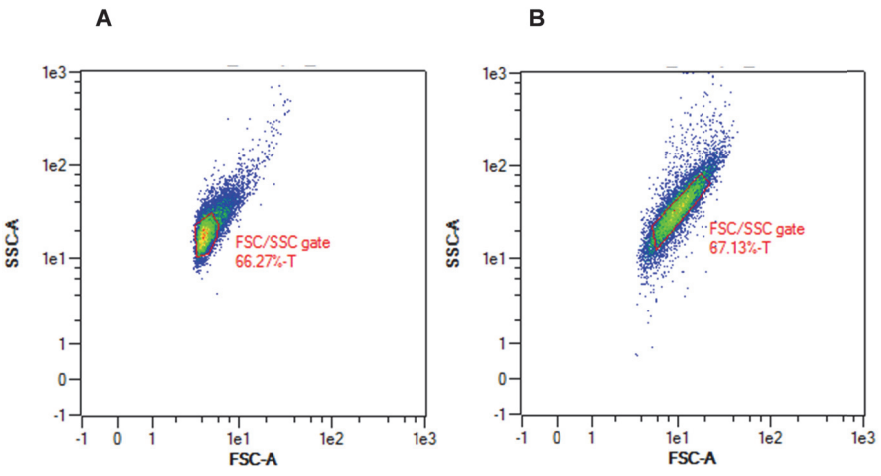

Figure 4.15: Representative examples of FSC/SSC gated whole cells (A) and nuclei (B). The percentages reflect the amount of cells present in the gated populations.

A range of conditions was examined to develop a protocol and to ensure optimal staining levels. An important aspect of the assay development is the selection of antibodies. Here, a monoclonal primary anti-Nrf2 antibody was found to stain more efficiently than a polyclonal anti-Nrf2 antibody. Primary antibody incubation times were optimal overnight, but may be shortened to 1 h with minimal signal loss to speed-up the processing time. Western blotting analysis revealed the presence of more non-specific protein bands when using the polyclonal antibody compared to the monoclonal antibody. This finding suggests that background staining compromised the staining efficiency. In this respect, western blotting was indicative of staining efficiency and served as a supportive tool to verify antibody specificity. The monoclonal anti-Nrf2 antibody was raised against a synthetic linear peptide and thus required protein denaturation to reveal the epitope. The monoclonal antibody recognition of Nrf2 may have benefited from the chosen fixation and permeabilisation conditions. Formaldehyde stabilises antigens by forming a matrix of static proteins thereby preventing further cell signaling [188]. Methanol dehydrates and permeabilises cells, which can cause protein denaturation and may enable enhanced antibody access to nuclear antigens [189, 191]. However, these conditions might have impaired polyclonal antibody recognition of Nrf2. Antibody-antigen binding can also be affected by charge; hence recognition of charged epitopes is dependent on the overall charge of the antibody.

To further optimise staining levels and to decrease formaldehyde induced auto-fluorescence, the fluorophore conjugated to the secondary antibody was changed from a FITC label (emission at 519 nm) to a PerCP label (emission at 675 nm). The observed decrease in staining efficiency might have been affected by the larger size of the PerCP fluorophore (35 kDa) compared to the FITC fluorophore (389 Da). The large PerCP protein may have reduced the uptake of the antibody conjugate into cells and blocked specific antigen binding sites due to steric hindrance [8, 9]. Staining efficiency may benefit from using a different fluorophore that emits light in the red spectrum, but is of a similar size to FITC (e.g. Cy5).

In an attempt to reduce the amount of antibody needed, the staining volume was reduced to 100 µL. However, experiments showed that this resulted in a decreased staining efficiency. An increased volume of 500 µL was needed to ensure optimal antibody-protein contact.

Results have shown that the developed method can generate both qualitative and quantitative data on Nrf2 protein expression levels. Intermediate protein level changes were apparent by both techniques (compare Figure 4.12 A with Figure 4.12 B) and normalised fold changes correlated closely when comparing flow cytometry to western blotting analysis (Figure 4.12 D). However, absolute fold changes and error bars differed between both methods (Figure 4.12 C). Since western blotting uses population analysis to provide one data point, identically stained protein bands may arise from a diverse response rate among a cell population [189]. This may present a risk of under or over estimation of the protein expression. Moreover, the outcome of identical western blotting experiments may differ, which might explain the larger error bars observed. Flow cytometry benefits from its ability to measure protein levels in single cells, which may result in improved reproducibility of the fold changes observed. Furthermore, this technique doesn't employ enzymatic signal amplification hence no saturation can occur [197]. The flow cytometry protocol can be completed in one day whereas two days are needed for western blotting. Although protein quantification with flow cytometry has multiple advantages to western blotting, it remains crucial to verify the specificity of the antibodies using qualitative western blotting [189]. Furthermore, the choice of primary antibody was found to be the key to successful intracellular Nrf2 staining.

The developed intracellular staining method allows for the detection and quantification of constitutive and inducible Nrf2 protein levels in various cell lines. The assay was shown to work in the mouse Hepa1c1c7 and human HeLa and MCF-7 cell lines, but can be adapted for use in other cell lines. A different Nrf2 response profile was observed among the cell lines after stimulation with sulforaphane. This differential effect could be attributed to the cell line's origin (i.e. murine versus human). In addition, a higher Nrf2 induction level was detected in MCF-7 cells compared to HeLa cells. These observations can provide valuable information regarding Nrf2 levels in different species and tissues.

The indirect staining approach used here offers the option of prior evaluation of unconjugated primary antibodies via western blotting. Other potential benefits include: detection of the protein of interest with diverse fluorophores and detection of multiple proteins in one single sample (multi-parameter analysis) [197]. Multi-parameter analysis is a powerful option to study (inducible) expression levels of a

range of proteins involved in the Keap1-Nrf2 pathway. The developed assay has already been used to study the Nrf2 induction potential of various small molecules. Future work may include screening those compounds for their ability to induce both Nrf2 and downstream phase II enzyme (e.g. NQO1 or HO-1) expression levels in multiple cell lines using different fluorescent labelled secondary antibodies. Induction potentials can be studied over a wide dose-range thereby generating IC_{50} values. In addition, pathway specificity of novel Nrf2 inducers may be explored by examining the expression levels of related transcription factors and their target products (e.g. AhR and CYP1A1).

In various cancerous tissues mutations occur in the coding region of Keap1 and/or Nrf2, resulting in constitutive induction and accumulation of Nrf2 [55, 208]. As a result, malignant cells become insensitive to anti-cancer treatments. The developed flow cytometry assay could be used to examine the potency of Nrf2 inhibitors and Nrf2 siRNA, which may enhance chemotherapeutic sensitivity. The effectiveness of these methods may be tested in different (cancerous) cell lines and tissues.

4.6 Summary

In summary, the major findings in this chapter are:

- Nrf2 protein induction levels can be detected and quantified reliably using this flow cytometry method.
- Antibody specificity is essential for optimal intracellular Nrf2 staining efficiency: a monoclonal anti-Nrf2 antibody presented a larger fold change than a polyclonal anti-Nrf2 antibody.
- Western blotting provides a supportive qualitative tool: i.e. verification of the molecular weight of the protein of interest and antibody specificity.
- There appears to be a negative association between the extent of background staining detected by western blotting and intracellular Nrf2 staining efficiency.
- The developed intracellular Nrf2 staining method can be applied to both whole cells and isolated nuclei.
- Application of this method to isolated nuclei resulted in a higher staining efficiency.
- The developed intracellular Nrf2 staining approach can be applied to study the effect of diverse Nrf2 inducer molecules in various cell lines.
- The indirect staining approach offers the option for multi-parameter analysis: the induction of other related proteins can be measured in the same sample (e.g. phase II enzymes NQO1 and HO-1).

5 Reference Nrf2 inducer: sulforaphane

5.1 Introduction

The isothiocyanate, sulforaphane, is one of the first and most extensively studied natural Nrf2 inducers. In the Prochaska NQO1 induction assay [65], sulforaphane doubled the NQO1 enzymatic activity at a concentration range of 0.4 – 0.8 µM in Hepa1c1c7 cells [209]. Moreover, sulforaphane has been shown to up-regulate other phase II enzymes including, heme oxygenase 1 (HO-1), glutamate cysteine synthetase, glutamate peroxidase (GSH), glutathione reductase, glutathione *S*-transferase (GST), epoxide hydrolase, ferritin, thioredoxin and thioredoxin reductase and UDP-glucuronosyltransferase 1A in either cells or *in vivo* [69]. The induction of phase II enzymes by sulforaphane was shown to be dependent on the presence of Nrf2 in Nrf2 knock-out studies [69]. Several studies in mice revealed that sulforaphane inhibited the development of tumours upon exposure to various carcinogens, but this protective effect was abolished in Nrf2 knock-out mice [69, 73]. Sulforaphane was also shown to affect the expression and activity of phase I enzymes from the cytochrome P450 family. In some studies sulforaphane inhibited the activity of and/or downregulated certain CYP enzymes, such as CYP1A1, 1A2, 2B1/2, 2E1 and 3A4 in hepatocytes, whereas in others the isothiocyanate increased the expression of CYP1A1, 1A2, 2B1/2, 2C11 and 3A1 in rat lung tissue [69]. Evidence has emerged from preclinical studies that sulforaphane induces the up-regulation of Nrf2 target genes differently depending on the cell or tissue type [72]. This could be due to e.g. differences in sulforaphane metabolism, direct or indirect exposure via digestion or systemically and nucleotide polymorphisms in downstream target genes [72]. In addition, sulforaphane is found to have a cytoprotective effect at lower doses whereas higher doses are associated with apoptosis, anti-angiogenesis, anti-histone deacetylase activity and metastasis inhibition in cancer cells [72]. The effects at higher doses were shown to target specifically cancerous cells, while normal cells were unaffected [210]. This effect has been partly attributed to the increased inhibitory effect of sulforaphane on the activity of histone deacetylase (HDAC) proteins in cancer cells versus normal cells, resulting in an increase in apoptosis and cell cycle arrest [210]. In diverse types of cancer, the p53 tumour suppressor gene is mutated. Sulforaphane was found to offset the effects of a mutated p53, which suggest its beneficial effect is not restricted to non-mutated/normal cells [211].

These findings are of great clinical importance and advocate sulforaphane as both a preventive and therapeutic agent.

The aim of this chapter is to characterise sulforaphane as a benchmark for the screening and evaluation of direct and indirect Nrf2 inducer molecules.

5.2 Results

5.2.1 NQO1 assay

The cell-based NQO1 assay has been used as an initial screening tool to compare putative Nrf2 inducer molecules with the reference compound sulforaphane. Preliminary experiments showed that Hepa1c1c7 cells need to be exposed to sulforaphane for at least 24 h before NQO1 enzyme activity can be detected. Hence, Hepa1c1c7 and BpRc1 cells were stimulated with sulforaphane for 24 and 48 h before cells were lysed and an enzyme reaction mixture containing glucose-6-phosphate (G6P), glucose-6-phosphate (G6P) dehydrogenase and NADP was added. This reaction generates NADPH that is used by NQO1 to transfer electrons to menadione. Following a colourimetric reaction, to reduce menadione to menodiol, which consecutively reduces MTT (3-(4,5-dimethylthiazol-2-yl)-2,5-diphenyltetrazolium bromide) to a formazan, NQO1 induction levels were determined (Figure 1.14). The compounds concentration that caused a doubling of NQO1 activity relative to the control was used to quantify and rank their ability to up-regulate NQO1 (CD value or concentration that causes a two-fold increase in activity relative to the control).

As mitochondria contain numerous redox enzymes that are able to reduce MTT, prior studies were conducted to confirm the specificity of the reaction. Prochaska *et al.* [65] found that the reduction of MTT is accelerated following the reduction of menadione by NQO1 compared to the direct reduction of MTT by NQO1. The requirement of menadione to reduce MTT more efficiently was verified by comparing the reaction with and without menadione. As hypothesised, the addition of menadione resulted in a significant increase in amount of reduced MTT in sulforaphane stimulated cells. The specificity of the assay for the NQO1-dependent reduction of MTT was further examined by incubating sulforaphane stimulated cells with dicoumarol, a competitive NQO1 inhibitor [212], before adding the enzyme reaction mixture. This resulted in a dose dependent inhibition of MTT reduction.

The NOQ1 dose-response curves for sulforaphane in both the Hepa1c1c7 and BpRc1 cell lines are shown in Figure 5.2 A and B respectively. CD values obtained after 24 h of sulforaphane stimulation were ~ 0.4 µM and ~ 0.6 µM for Hepa1c1c7 and BpRc1 cells respectively. After 48 h sulforaphane stimulation CD values of ~ 0.2 µM and ~ 0.4 µM were obtained for the Hepa1c1c7 and BpRc1 cells respectively. Although CD values were reduced after a longer stimulation time, 24 h of stimulation was sufficient to observe an increase in NQO1 activity and to obtain a CD value. Moreover, increasing the stimulation time to 48 h compromises the time efficiency of the assay. As a result of extended assay time, fewer experiments per week can be executed. Hence, in the following experiments cells were stimulated with compounds for 24 h to measure their NQO1 induction potential.

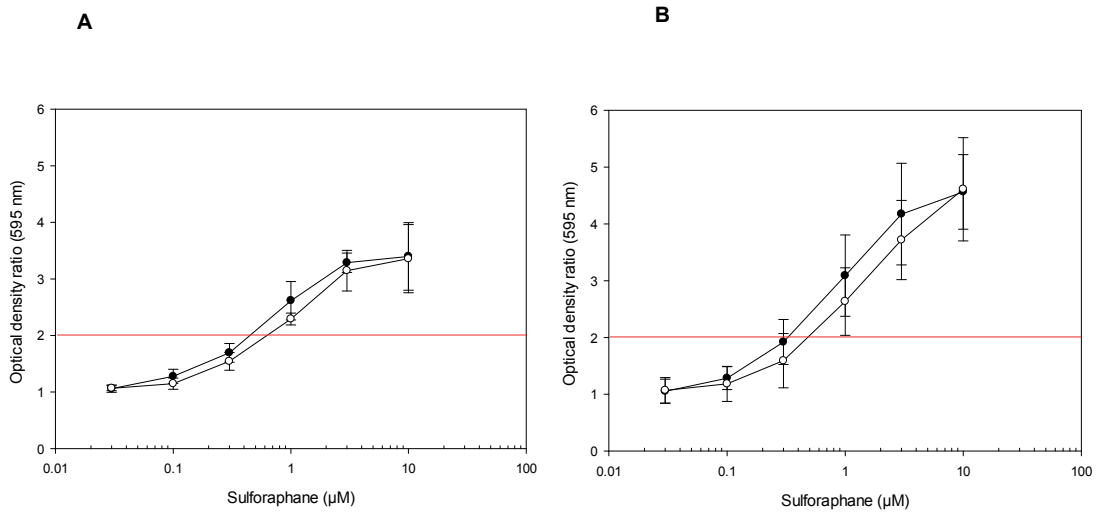

Figure 5.2: Dose response curves for the NQO1 assays of sulforaphane in Hepa1c1c7 (●) and BpRc1 (○) cells after 24 h (A) and 48 h (B) stimulation. The red line indicates a doubling of NQO1 activity (CD value). The error bars represent the standard deviation of n = 3 independent experiments.

5.2.2 SRB cytotoxicity assay

The sulforhodamine B (SRB) colourimetric assay has been widely used for toxicity screening of drugs and compounds. The method is based on the ability of the protein dye SRB to bind to the basic amino acid residues of trichloroacetic acid (TCA) fixed cells under mildly acidic conditions [213]. The UV absorbance of the bound SRB recorded after a washing step is proportional to the cell number and cellular total protein content measured over a cellular confluency range from 1 – 200% [214]. The SRB assay was carried out to verify the cytotoxicity of sulforaphane at concentrations up to 100 µM (in 0.1% DMSO final concentration) after 24 and 48 h of stimulation of Hepa1c1c7, BpRc1 and HeLa cells (Figure 5.3 A, B and C respectively). The mouse hepatoma cell lines were selected for cytotoxicity screening as they were used to determine whether sulforaphane was able to up-regulate Nrf2 and downstream phase II enzymes. To compare cytotoxicity levels with a different tissue and species, the human HeLa cell line was used. Sulforaphane did not affect cell viability in either of the cell lines at concentrations up to 10 µM after 24 and 48 h. However, a concentration of 30 µM reduced cell viability by 10 – 20% and a concentration of 100 µM decreased cell viability by 80 – 100 % in the mouse hepatoma cell lines. Sulforaphane was less cytotoxic in the HeLa cell line; 30% and 50% reduction in cell viability was observed at a concentration of 100 µM after 24 and 48 h respectively. Figure 5.3 C shows an overlay of the NQO1 induction potency and SRB determined cytotoxicity for sulforaphane treated Hepa1c1c7 cells. As a maximum NQO1 induction level was observed at 10 µM of sulforaphane without compromising the cell viability, all subsequent experiments were performed at this concentration.

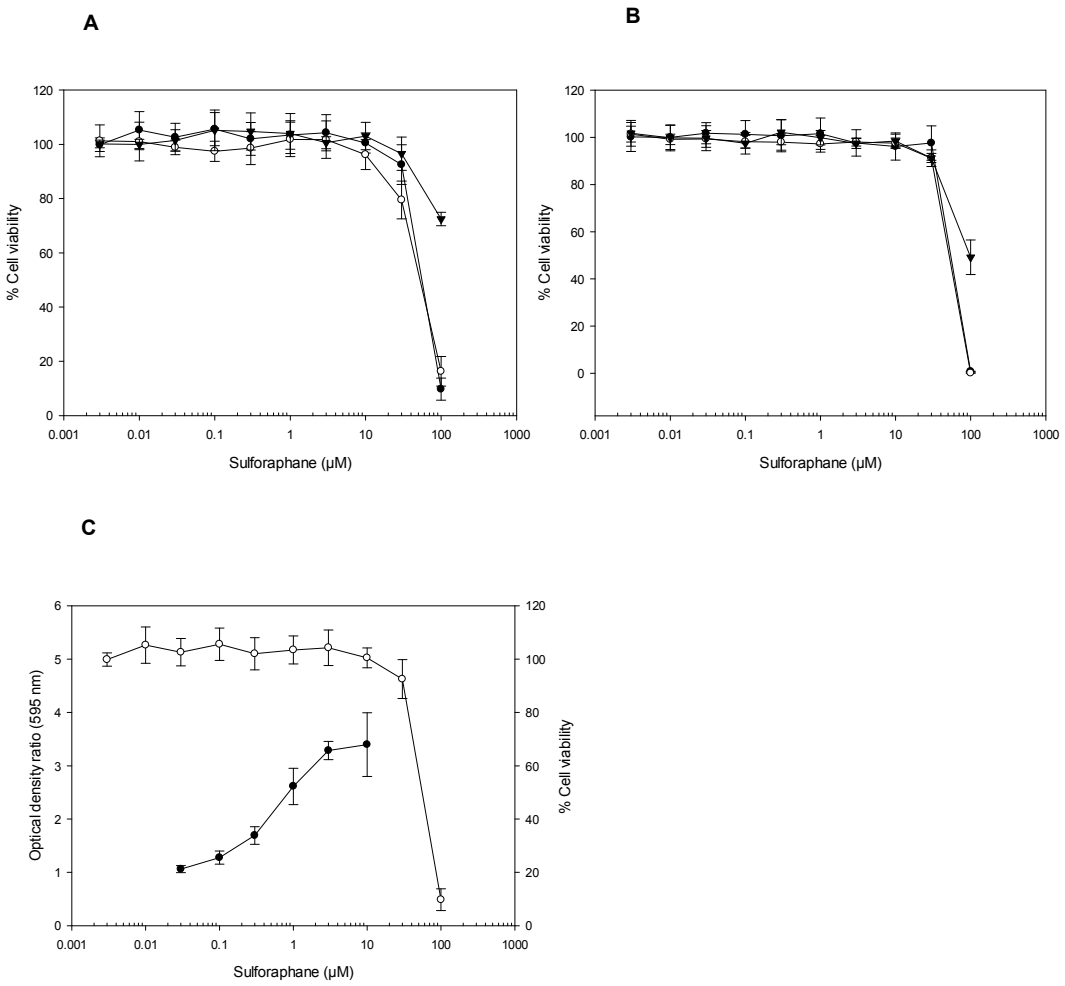

Figure 5.3: Dose response curves for the SRB assays of sulforaphane in Hepa1c1c7 (●), BpRc1 (○) and HeLa cells (▼) after 24 h (A) and 48 h (B) stimulation. Cell viability is calculated as a percentage of cells treated with vehicle only (0.1% DMSO). Error bars are based on n = 4 replicates in a representative experiment. Graph C shows an overlay of the NQO1 induction potency (●) (Figure 5.2 A) and SRB determined cytotoxicity (○) (Figure 5.3 A) of sulforaphane in Hepa1c1c7 cells after 24 h stimulation.

5.2.3 Western Blotting

Western blot experiments were carried out to demonstrate induction of nuclear Nrf2 and the downstream cytoplasmic phase II enzymes HO-1 and NQO1 in Hepa1c1c7 and BpRc1 cells following stimulation at a fixed concentration of 10 μM sulforaphane over a 24 h period. Cell samples were taken after 1, 3, 6 and 24 h of compound exposure and separated into cytoplasmic and nuclear protein fractions. The resulting cell samples were analysed by immunoblotting using either rabbit polyclonal anti-Nrf2 H300, rabbit polyclonal anti-HO-1 H-105 or mouse monoclonal anti-NQO1 antibodies (all SantaCruz). Figure 5.4 A, 5.5 A and Figure 5.6 show an increase in nuclear Nrf2 protein levels in both cell lines that is time dependent with the highest induction level observed after 1 h; the fold induction was ~ 20 in Hepa1c1c7 cells and ~ 15-fold in BpRc1 cells. During the time course stimulation studies, sulforaphane also induced the expression of the phase II enzymes HO-1 and NQO1 (Figures 5.4 - 5.5 C and D respectively and Figure 5.6). Cytoplasmic protein fractions from Hepa1c1c7 and BpRc1 cells showed a peak HO-1 induction after 6 h (fold induction ~ 7 in Hepa1c1c7 cells and a fold induction ~ 6 in BpRc1 cells), though up-regulation of NQO1 was only detected after 24 h. NQO1 protein induction levels were similar in both cell lines.

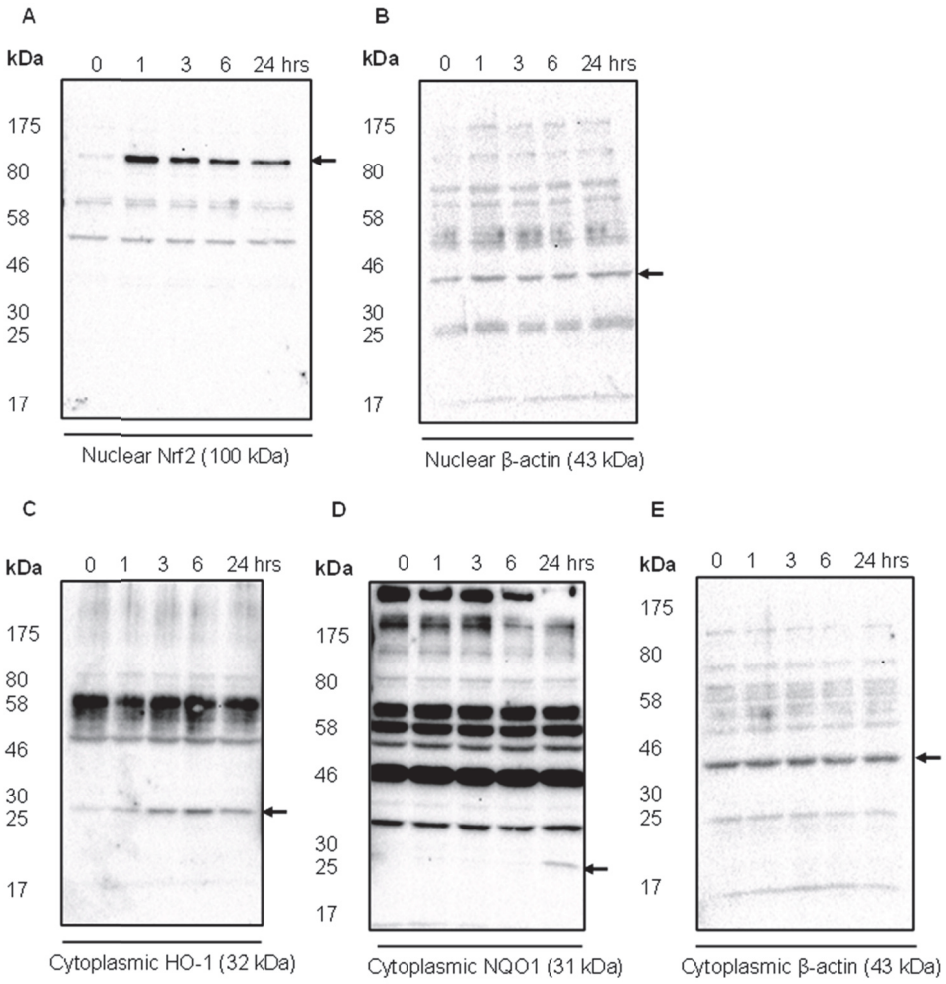

Figure 5.4: Western blot analysis of nuclear Nrf2 accumulation (A) and its downstream targets phase II enzymes HO-1 (C) and NQO1 (D) in Hepa1c1c7 cells after treatment with 10 μM of sulforaphane over a 24 h time period. ß-actin was used as a loading control (B and E). Representative blots are shown.

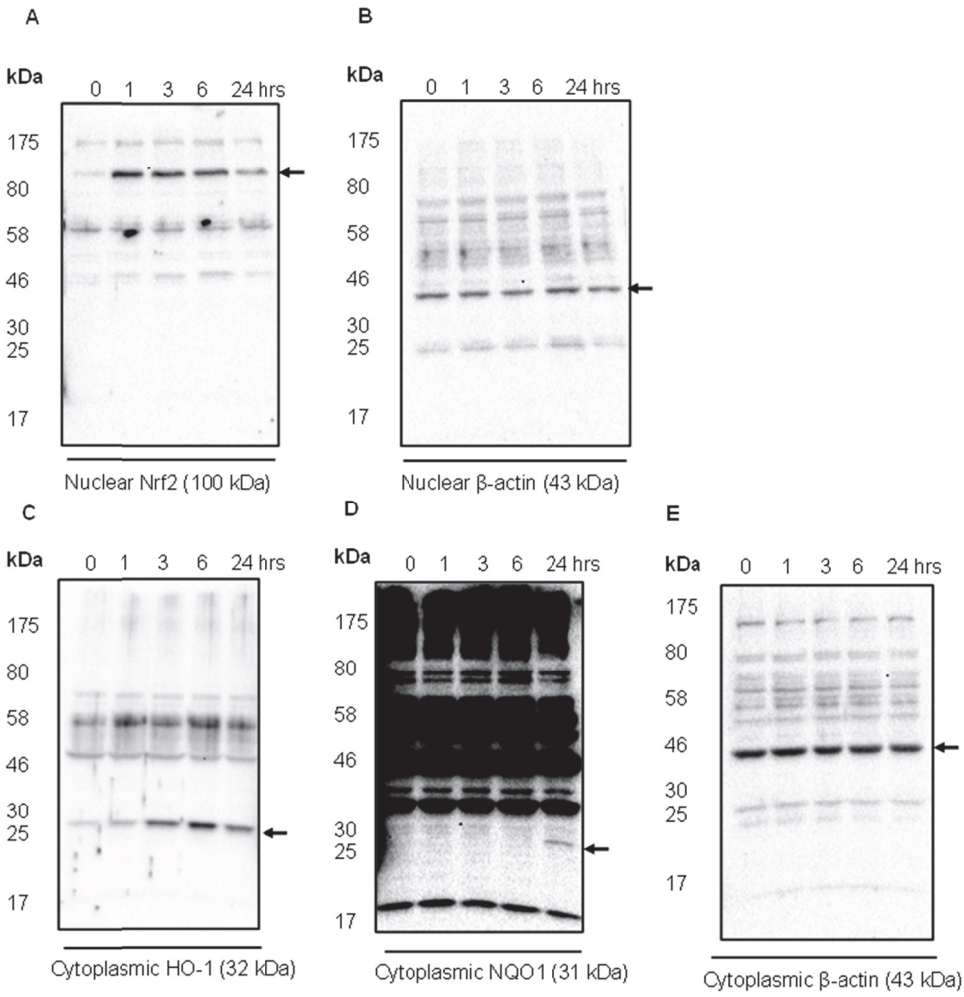

Figure 5.5: Western blot analysis of nuclear Nrf2 accumulation (A) and its downstream targets phase II enzymes HO-1 (C) and NQO1 (D) in BpRc1 cells after treatment with 10 µM of sulforaphane over a 24 h time period. ß-actin was used as a loading control (B and E). Representative blots are shown.

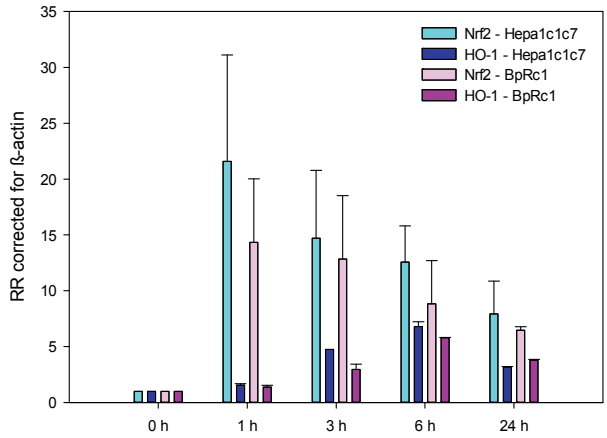

Figure 5.6: Quantitative western blot results of Nrf2 and HO-1 up-regulation in sulforaphane treated Hepa1c1c7 (light and dark blue bars respectively) and BpRc1 cells (light and dark purple bars respectively). Protein induction levels were expressed as relative ratio's (RR) with ß-actin as a loading control. A RR ratio of 1 corresponds to no protein induction. The error bars represent the standard deviation of n = 2 independent experiments.

5.2.4 Intracellular Nrf2 staining – flow cytometry

The up-regulation of nuclear Nrf2 as a result of treating Hepa1c1c7 cells with sulforaphane was quantified by the flow cytometry method developed to determine intracellular Nrf2 staining. The results are discussed in Chapter 3. In summary, flow cytometry revealed a comparable trend to western blotting for Nrf2 up-regulation over time, but a difference in absolute fold changes. A different time course Nrf2 induction pattern was observed in the human cell lines HeLa and MCF-7 compared to the murine hepatoma cell line: a peak Nrf2 protein induction after 3 h versus a maximum Nrf2 induction after 1 h of sulforaphane treatment respectively.

5.2.5 Pathway evaluation

In this section, various methods have been used to verify the possibility that sulforaphane up-regulates phase II enzymes via mechanisms other than the Keap1-Nrf2 pathway.

ARNT-AhR

Two small molecule direct inducers failed to induce the phase II enzyme NQO1 in the ARNT-deficient BpRc1 cell line (Sections 7.3.2 and 7.5.1). This prompted the examination of the involvement of the AhR pathway in upregulation of NQO1 by these compounds (Sections 7.3.5 and 7.5.5). Sulforaphane was used as a reference compound for these studies and was subjected to identical examination. Previous results demonstrated that sulforaphane was able to induce nuclear accumulation of Nrf2 in both Hepa1c1c7 and BpRc1 cells (Section 5.2.3). Moreover, the induction level of NQO1 and HO-1 enzymes was similar in both cell lines after stimulation with sulforaphane (Section 5.2.3). This suggests that up-regulation of phase II enzymes by sulforaphane is likely to be largely independent of the AhR pathway. To verify these findings, western blot analysis was performed of nuclear AhR and cytoplasmic CYP1A1 expression in sulforaphane treated Hepa1c1c7 cells (Figure 5.8 A and B respectively and Figure 5.9). The cells were stimulated with 10 µM sulforaphane over a 24 h time period with nuclear and cytoplasmic protein samples taken at 1, 3, 6 and 24 h. As a positive control, cells were stimulated with the AhR ligand benzo(*a*)pyrene (BaP). An SRB assay was performed to examine the cytotoxicity of BaP at concentrations up to 10 µM in Hepa1c1c7 cells after 24 h of exposure (Figure 5.7). BaP did not affect cell viability at concentrations up to 3 µM, but decreased cell viability at concentrations of 10 µM by 10 – 20 %. Hence, the following experiments were performed at a concentration of 3 µM BaP.

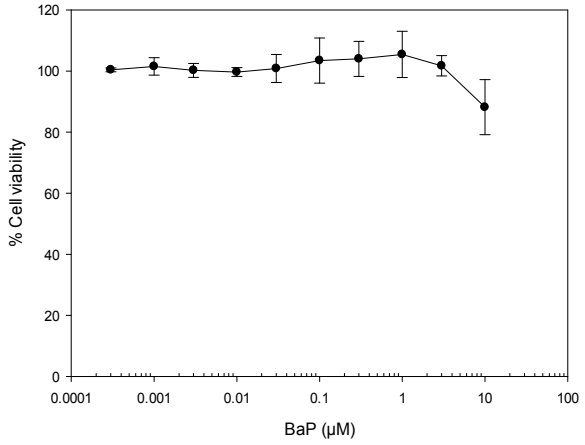

Figure 5.7: Dose response curve for the SRB assays of BaP in Hepa1c1c7 cells after 24 h stimulation. Cell viability is calculated as a percentage of cells treated with vehicle only. Error bars are based on n = 4 replicates in a representative experiment.

Cytoplasmic protein samples of BaP stimulated cells were taken at the same time intervals as sulforaphane treated cells and used for the detection of CYP1A1 (Figure 5.8 C). Sulforaphane treatment resulted in a minor decrease in AhR nuclear accumulation after 1 – 3 h that returned to baseline levels after 3 – 24 h (Figure 5.8 A). Moreover, an up-regulation of the expression of phase I enzyme CYP1A1 was detected after 6 h and continued to increase up to 24 h (fold induction ~ 1.5) (Figure 5.8 B and Figure 5.9). Cells treated with BaP showed an increase in CYP1A1 protein after 3 h and a maximal induction after 6 h (Figure 5.8 C).

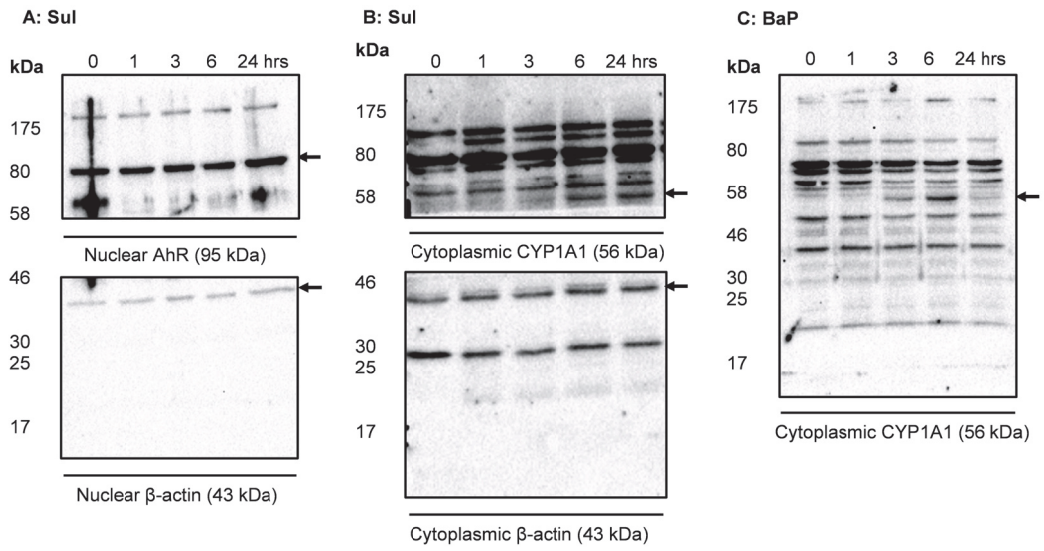

Figure 5.8: Western blot analysis of nuclear AhR accumulation and its downstream target phase I enzyme CYP1A1 in Hepa1c1c7 cells after treatment with 10 µM of sulforaphane (A and B respectively) or 3 µM BaP (C) over a 24 h time period. Representative blots are shown.

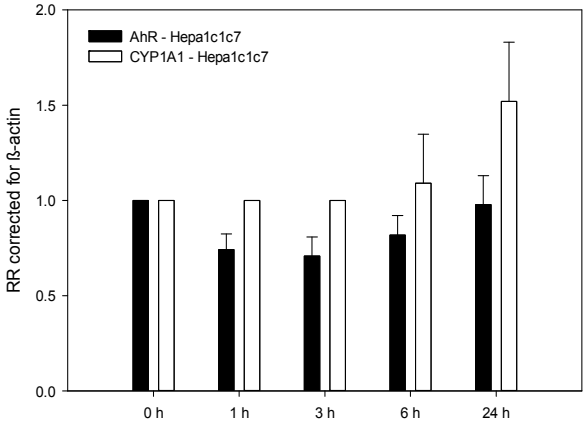

Figure 5.9: Quantitative western blot results of AhR and CYP1A1 up-regulation in 10 µM sulforaphane treated Hepa1c1c7 cells (black and white bars repetitively). Protein induction levels were expressed as relative ratio's (RR) with ß-actin as a loading control. A RR ratio of 1 corresponds to no protein induction. The error bars represent the standard deviation of n = 2 independent experiments.

Next, a CYP1A1 enzyme activity assay (P450 Glo Assay, Promega) was performed to validate the western blot results. This luminescence cellular assay measures the amount of luciferin-derived (CYP1A1 specific) substrate converted by CYP1A1 enzyme activity. In the presence of a luciferin detection reagent (Promega), the liberated luciferin derivative generates an amount of light that is directly proportional to the CYP1A1 enzymatic activity. Hepa1c1c7 cells were stimulated with 10 µM sulforaphane (S) for 6 and 24 h (detectable CYP1A1 enzyme on western blot) before the luciferin substrate was added. Cells stimulated with 3 µM BaP were used as a positive control (P) and the negative control (C) cells were stimulated only with the vehicle DMSO. Since some cell loss was expected as a result of assay handling, the amount of luminescence detected (RLU luciferin) was corrected for cell viability using the SRB assay (detail in Section 2.23) (Figure 5.10 A). Following the measurement of luminescence in the cell culture medium, which is representative of CYP1A1 activity, the cells were fixed in 10% TCA and stained with SRB. The percentage cell viability was calculated and used to correct the luminescence values on an individual well basis. Fold changes for sulforaphane and BaP versus the vehicle control were calculated and displayed in Figure 5.10 B. The positive control BaP shows to have a profound effect on CYP1A1 induction (fold induction ~ 42 after 6 h and ~ 51 after 24 h).

However, a representative western blot (Figure 5.8 C) shows that a peak induction is visible after 6 h. Sulforaphane demonstrates an increase in CYP1A1 activity after 6 h (fold induction ~ 2.4) and 24 h (fold induction ~ 3.8), which is similar to western blotting results (Figure 5.8 B). Nevertheless, fold changes are minor compared to BaP.

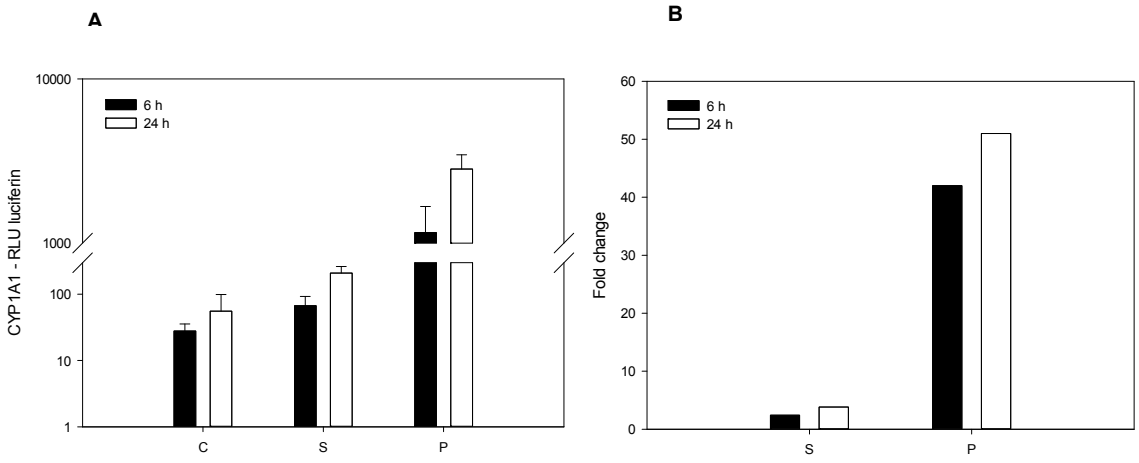

Figure 5.10: CYP1A1 induction measured using the P450 Glo Assay (Promega) following exposure of Hepa1c1c7 cells to vehicle control (C), 10 µM sulforaphane (S) or 3 µM BaP (P). (A): the quantity of luciferin (RLU) detected is proportional to the extent of CYP1A1 enzyme activity. The error bars represent the standard deviation of n = 8 replicates in a representative experiment. (B): fold changes of sulforaphane and BaP versus vehicle control.

ROS production

Reactive oxygen species (ROS) can activate the Keap1-Nrf2 pathway by modification of cysteine residues in Keap1. As a result of the conformational change in Keap1, the ubiquitination process is blocked and Nrf2 is stabilised [215]. This process allows *de novo* produced Nrf2 to translocate to the nucleus where it induces the up-regulation of phase II enzymes [216]. To evaluate whether novel Nrf2 inducers induce the expression of Nrf2 and downstream target genes via the production of ROS, sulforaphane was used as a negative control in a flow cytometry based method for detecting cellular ROS. However, it has been suggested that sulforaphane is able to induce ROS production in certain cell lines, including the human bronchial epithelial BEAS-2B cell line [217]. Hepa1c1c7 cells were stimulated

for 1 h with 10 µM of sulforaphane before the cells were incubated with CellROX Deep Red reagent (Life Technologies). The reagent contains a fluorogenic probe that is non-fluorescent when in a reduced state and fluoresces following oxidation by ROS (excitation/emission maxima at 644/665 nm). The fluorescent signals from the CellROX Deep Red dye are localised in the cytoplasm. The oxidant menadione is known to induce ROS production and was used as a positive control [218]. The negative controls included cells stimulated with vehicle only: DMSO (C1) for sulforaphane (S) and acetonitrile (C2) for menadione (M, positive control). Cells that received no treatment were used as an assay blank. Figure 5.11 shows the measured median fluorescence intensity (MFI) that corresponds to the relative amount of ROS produced. Whilst the positive control, menadione, successfully induced ROS production, no increase is observed after stimulation of Hepa1c1c7 cells with sulforaphane.

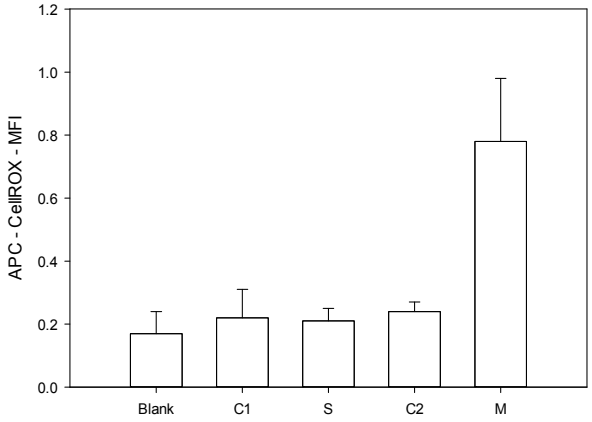

Figure 5.11: ROS production measured using the CellROX Deep Red dye after exposure of Hepa1c1c7 cells to 10 µM sulforaphane (S) or 50 µM menadione (M) for 1 h. As controls, cells were exposed to the sulforaphane vehicle, DMSO (C1) and the menadione vehicle, acetonitrile (C2). The amount of fluorescence (APC MFI) detected is proportional to the extent of ROS production. The error bars represent the standard deviation of n = 3 independent experiments.

5.3 Discussion

The reference compound sulforaphane is one of the most extensively studied (indirect) Nrf2 inducers and hence was evaluated for its biological activity.

Sulforaphane was found to decrease cell viability at concentrations higher than 10 µM in mouse hepatoma cell lines after 24 and 48 h. This is consistent with the literature [219]. Lower cytotoxicity levels were found in the human HeLa cell line. An increased level of cytotoxicity may be found in hepatocytes compared to other tissue derived cell lines as they are the primary target for metabolizing drugs [220]. Future experiments should include the assessment of the long-term toxicity of sulforaphane on diverse cell lines. Hepa1c1c7 cells demonstrated after 24 h of exposure to sulforaphane a doubling of NQO1 activity at a concentration of ~ 0.4 µM, which is in agreement with the literature [209]. This finding was confirmed by time-dependent western blot experiments, which demonstrated detectable NQO1 protein levels after 24 h of exposure to the phytochemical. Evidence emerged that sulforaphane is able to up-regulate other phase II enzymes such as glutamate cysteine synthetase, glutathione peroxidase, glutathione reductase, ferritin, GST, thioredoxin and thioredoxin reductase, UDP-glucuronosyltransferase 1A and HO-1 [69]. Indeed, sulforaphane up-regulated HO-1 in Hepa1c1c7 cells after only 1 h and continued to induce expression of the protein up to 6 h. To verify whether sulforaphane induced the phase II enzymes via the Keap1-Nrf2 pathway, Nrf2 nuclear accumulation was studied using western blotting and flow cytometry techniques. Induction of the transcription factor was maximal after as early as 1 h. Sulforaphane demonstrated to induce phase II enzyme NQO1 in the ARNT-deficient BpRc1 cell line with a similar induction potential as in Hepa1c1c7 cells. Moreover, western blot analysis showed up-regulation of NQO1, HO-1 and Nrf2 nuclear accumulation in BpRc1 cells. The time course and level of protein induction was analogous to the Hepa1c1c7 cell line. In the BpRc1 cell line, the AhR transcription factor is unable to accumulate in the nucleus, hence these results are not suggestive of AhR pathway involvement. Nevertheless, CYP1A1 protein and enzyme activity (using western blot analysis and the P450 Glo Assay respectively) was weakly induced in Hepa1c1c7 cells after 6 – 24 h of stimulation with sulforaphane. Western blot analysis indicated that AhR nuclear accumulation was slightly inhibited in Hepa1c1c7 cells after 1 – 3 h of exposure to sulforaphane, but

this inhibition reversed after 3 – 24 h (Section 5.2.5). These results suggest that the inhibitory effect may be transient up to 3 h. After this time, sulforaphane induces AhR nuclear accumulation and the transcription of AhR downstream target CYP1A1 to some extent. Sulforaphane may up-regulate Nrf2 by intracellular ROS production; however, no evidence of this was found here. This suggests that phase II enzyme up-regulation is a result of the transcriptional activation of Nrf2 gene expression in response to sulforaphane. However, some studies have proposed that sulforaphane has an effect on the AhR pathway and its downstream target, the phase I bioactivating enzyme CYP1A1 [69, 219]. These studies suggested that sulforaphane up-regulates CYP1A1 mRNA, protein and catalytic activity in Hepa1c1c7 cells, which may be mediated through direct or indirect effects on the AhR pathway. Anwar-Mohamed *et al.* [219] found that CYP1A1 mRNA levels increased up to 6 h after compound exposure. Furthermore, they revealed that sulforaphane induced the AhR/ARNT/XRE complex formation in the cytosol [219]. A recent study [221] suggested that sulforaphane is a poor agonist for the AhR as the compound modestly elevated CYP1A1 mRNA levels in rat liver. Moreover, the same study demonstrated that the isothiocyanate was able to displace bound BaP from the AhR and reduced BaP induced CYP1A1 activity [221]. The gene promotors of Nrf2, AhR and NQO1 possess both ARE and XRE, which could result in potential pathway cross-talk between Nrf2 and AhR [104, 102]. Shin *et al.* [106] suggest that Nrf2 partially regulates the expression of AhR and its downstream targets, i.e. CYP1A1, through interaction of Nrf2 with ARE in the promoter region of the AhR gene. The observed induction of AhR nuclear accumulation by sulforaphane could be a result of this proposed mechanism or alternatively, the isothiocyanate may be a weak AhR ligand. Nevertheless, the induction of CYP1A1 enzyme activity by sulforaphane is relative small compared to the high enzyme activity detected with the AhR ligand, BaP. Although a dissimilar time course was evident, western blotting analysis of the CYP1A1 protein showed similar intensity protein bands after cellular exposure to either sulforaphane or BaP. The inability of the western blotting technique to reveal the difference in CYP1A1 protein levels following cellular exposure to compounds with dissimilar potency is likely due to the population analysis approach this method uses to acquire data-points (Chapter 4). This highlights the importance of an additional assay to quantify protein induction levels.

The observations discussed illustrate the rationale behind the selection of sulforaphane as a reference tool compound. Although, the isothiocyanate is a

potent inducer of Nrf2 and downstream target enzymes, i.e. HO-1 and NQO1, there is some indication of involvement of other pathways (i.e. ARNT-AhR). Hence, the biological evaluation of novel Nrf2 inducer molecules should include verification of their Keap1-Nrf2 pathway specificity.

6 Indirect Nrf2 inducers: Cyclohexadienone analogues

6.1 Introduction

A common feature of indirect Nrf2 inducers is their thiol reactivity. Michael acceptors react readily with sulfhydryl groups of cysteine residues via a conjugate addition (Michael-type) reaction and represent an important class of indirect Nrf2 inducer compounds [222]. Michael acceptors are olefins or acetylic groups conjugated to electron-withdrawing groups including aldehydes, ketones, esters and nitro groups [52]. They are thought to induce Nrf2 activity by reacting with key cysteine residues (e.g. C273 and C288) in the Keap1 intervening region domain [62]. At low concentrations Michael acceptors react with cysteine residues in Keap1, but at high concentrations they are capable of reacting indiscriminately; an effect that is associated with cytotoxicity [86, 223]. However, evidence has emerged that the reaction between Michael acceptors and thiols can be reversible (via a retro-Michael-type reaction) [224], which may contribute to lowering the toxicity of these compounds in some cases (Figure 6.1).

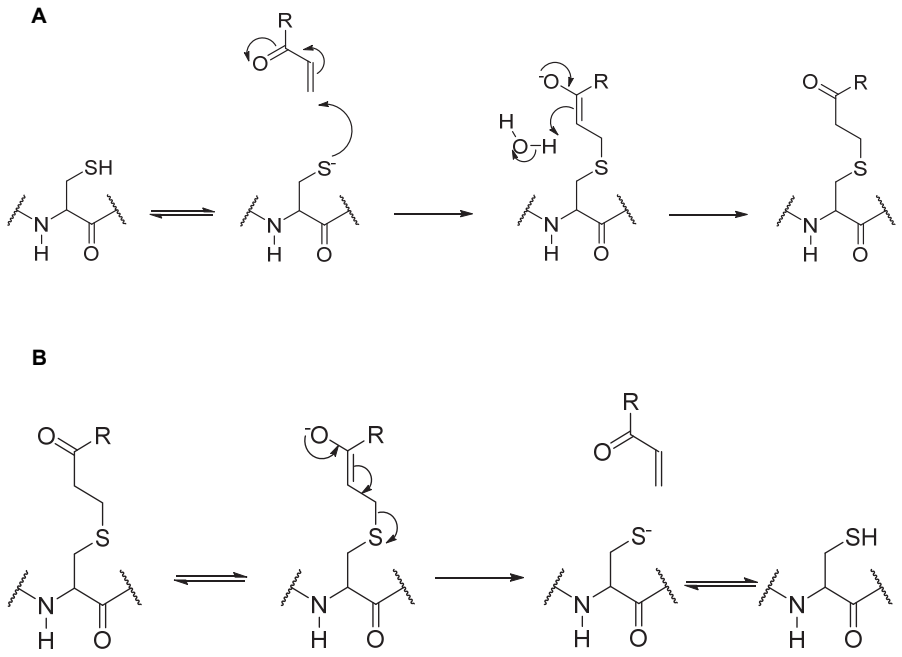

Figure 6.1: Forward Michael-type reaction of a thiol with an a,b-unsaturated carbonyl compound (A) and reverse (retro) Michael-type reaction of an adduct to yield a thiol and an a,b-unsaturated carbonyl compound (B).

The indirect Nrf2 inducers described in this chapter are a group of cyclohexadienone analogues that contain Michael acceptors [62]. The core *p*-quinol (4-hydroxycyclohexadienone) structure (Figure 6.2) was elaborated to study the effect of various substituents on the ability of the compounds to induce Nrf2 activity and to develop a structure-activity relationship (SAR).

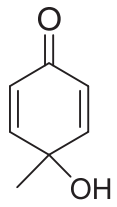

Figure 6.2: The core *p*-quinol structure.

Some phytochemicals that are found in fruit and vegetables carry Michael acceptor functionality and can exhibit relatively low cytotoxicity levels. In an attempt to find potent Nrf2 inducer molecules associated with low cytotoxicity, phytochemicals and analogues that contain the *p*-quinol core structure were synthesised. Structural changes to the two 4-position substituents of the core structure were introduced in order to explore their effects on compound activity (Figure 6.2). Furthermore, the reactivity of the Michael acceptor groups was adjusted by adding various electron-withdrawing groups to the 2-position of the cyclohexadienone ring in order to evaluate the effects on compound reactivity and biological activity. The expected additive or synergistic effect of molecules containing two electron-withdrawing groups has previously been demonstrated with related structures and suggests that reaction with two closely located cysteine residues in Keap1 may contribute to their activity [35] [52]. The cyclohexadienone analogues (n = 71) were subdivided into five distinct groups based on their chemical structures. The structures of the five groups and the corresponding substituents are described in Tables 6.1 – 6.5. All compounds contain at least one Michael acceptor group. The compounds in Table 6.1 with an R_3 substituent contain two electron-withdrawing groups, which potentially increases their reactivity towards cysteine residues. All structures were screened for their ability to activate the Keap1-Nrf2 pathway via induction of the downstream target enzyme NQO1. Several promising indirect Nrf2 inducers were assessed further using western blotting and flow cytometry (assay development described in Chapter 4) to confirm Nrf2 and phase II enzyme activation.

The aim of this chapter is to screen a group of cyclohexadienone analogues for their ability to indirectly induce Nrf2 target genes and to further characterise the most promising molecules.

6.2 Results – Evaluation of cyclohexadienone analogues

6.2.1 NQO1 assay

First, the compounds were screened at a fixed dose concentration of 1 μM for their ability to up-regulate the downstream Nrf2 product NQO1 in Hepa1c1c7 cells, which allowed the ranking of molecules based on their induction potencies [65]. A fixed concentration of 1 μM was chosen as cytotoxicity was expected at higher concentrations. Cytotoxicity levels were determined on the basis of the dose that caused a decline in NQO1 enzyme activity [67]. Compounds that demonstrated promising activity were further evaluated by determining their therapeutic index (TI), which is the ratio between the dose above which NQO1 enzymatic activity declines and the dose that doubles NQO1 enzymatic activity:

$$TI = \frac{\text{Toxicity concentration (μM)}}{\text{CD value (μM)}}$$

In addition, dose-response experiments were performed for the most promising molecules.

Screening of compounds

The compounds in Table 6.1 showed promising NQO1 induction potential (CD ~ 0.5 – 10 μM) with varying cytotoxicity (1 - ≥ 30 μM) (Table 6.1). The *p*-acetoxy substituted compound **6.2** (Figure 6.3) was one of the initial compounds based around the *p*-quinol core structure, which was active (CD ~ 1 μM), showed moderate cytotoxicity (≥ 10 μM) and resulted in a TI value of ~ 10. Several compounds were synthesised to explore the structure activity relationships in relation to this simple core structure. Generally, extending the alkyl chain in the 4-position and replacing the 4-acetoxy group with a hydroxyl (e.g. **6.3**, **6.4**, **6.5**) did not improve activity or significantly change the toxicity of the compounds.

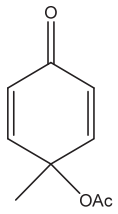

Figure 6.3: The structure of compound **6.2**.

The 4-phenyl-substituted compound **6.29** (Figure 6.4 A) was relatively potent (CD ~ 1 μM), but showed cytotoxicity at concentrations > 1 μM (TI ~ 1). Replacing the 4-hydroxyl group with a methoxy substituent, **6.31** (Figure 6.4 B), resulted in lower potency (CD ~ 2 μM) and cytotoxicity (≥ 30 μM), and a higher TI of 15. This suggests that the phenyl group is a good substituent at the 4-position of the core quinol structure with scope for further improvement of the structure.

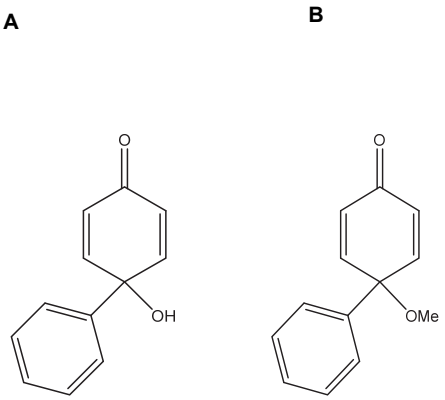

Figure 6.4: The structure of compounds **6.29** (A) and **6.31** (B).

The favourable effect on activity of an additional electron-withdrawing group at the 2-position of the core cyclohexadienone structure was shown previously with compound **6.35** (Figure 6.5 C): CD value of 0.15 μM [225]. This structure is a monocyclic derivative of the highly potent Nrf2-inducing compound CDDO. In the assays conducted here it demonstrated here a comparable NQO1 induction potency: CD value of 0.5 μM (TI ~ 20). The effect of alternative electron withdrawing groups was evaluated via the related compounds **6.33** and **6.34** (Figure 6.5 A and B) they demonstrated a decreased activity compared to **6.35** (**6.33** CD ~ 1.2 μM;

6.34 CD ~ 2 µM), but they were less cytotoxic (≥ 30 µM versus ≥ 10 µM), resulting in a higher TIs (TI ~ 25 for **6.33**).

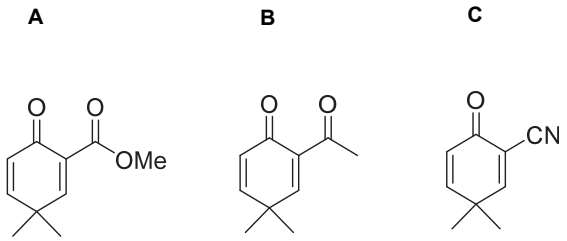

Figure 6.5: Structure of compounds **6.33** (A), **6.34** (B) and **6.35** (C).

Combining the addition of an acetyl electron-withdrawing group at the 2-position of the *p*-quinol structure with the *p*-phenyl substituent resulted in the active compound **6.46** (Figure 6.6; CD ~ 1.5 µM), which demonstrated relative low cytotoxicity levels (≥ 30 µM) (TI ~ 20).

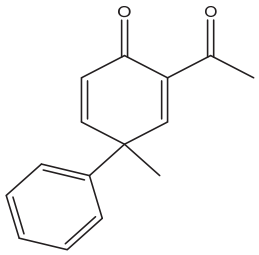

Figure 6.6: The structure of compound **6.46**.

Introducing an electron-withdrawing group to the 3- or 4-position of the phenyl ring resulted in further improvement of the potency: i.e. the 4-cyanophenyl substituent, **6.48** (Figure 6.7 A) and the 3-chlorophenyl substituent, **6.49** (Figure 6.7 B) (CD values of 1.7 µM and 1 µM respectively). This resulted in TI values of 5.9 for **6.48** and 10 for **6.49**. The 4-*tert*-butylphenyl substituent **6.54** (Figure 6.7 C) was the least active compound in this range (no CD value could be determined). Additional compounds that were synthesised and evaluated are shown in Table 6.1.

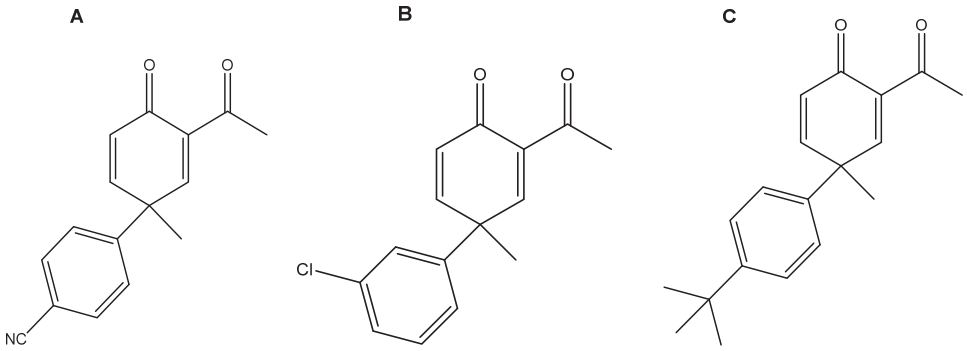

Figure 6.7: The structures of compounds **6.48** (A), **6.49** (B) and **6.54** (C).

Table 6.1: NQO1 (in the Hepa1c1c7 cell line) results for group 1 of the cyclohexadienone analogues.

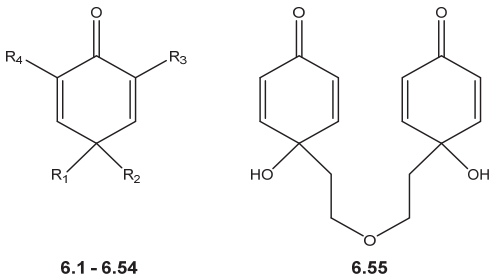

6.1 - 6.54 **6.55**

Cpds	R_1	R_2	R_3	R_4	NQO1[a]	NQO1 CD (μM)	Toxicity NQO1 (μM)
6.1	Me	OOH	H	H	1.9	1.5	≥ 3.0
6.2	Me	OAc	H	H	2.0	1.0	≥ 10.0
6.3	Et	OH	H	H	1.6	3.0	≥ 3.0
6.4	iPr	OH	H	H	1.0	10	> 10
6.5	C≡CH	OH	H	H	1.7	3.0	≥ 3.0
6.6	$CH_2CH_2CO_2Et$	OH	H	H	1.6	3.0	≥ 3.0
6.7	CH_2CO_2Me	OH	H	H	2.0	1.0	≥1.0
6.8	CH_2CO_2Me	OH	Cl	Cl	2.0	1.0	≥ 3.0
6.9	CH_2CO_2Me	OAc	H	H	1.8	1.5	≥ 10.0
6.10	CH_2CO_2Me	OCO_2Me	H	H	2.0	1.0	≥ 3.0
6.11	CH_2CO_2Et	OH	H	H	1.8	3.0	≥ 3.0
6.12	CH_2CO_2Et	OH	F	H	1.5	-[b]	≥ 3.0
6.13	CH_2CO_2Et	OH	Cl	Cl	1.7	-[b]	≥ 1.0
6.14	CH_2CO_2Et	OH	Br	Br	1.8	-[b]	≥ 3.0
6.15	$CH_2CH_2CH_2CO_2H$	OH	H	H	1.9	3.0	≥ 3.0
6.16	$CH_2CH_2CH_2CO_2Et$	OH	H	H	1.3	-[b]	≥ 3.0
6.17	CH_2CH_2OAc	OH	H	H	1.8	1.5	≥ 10
6.18	R_1-$CH_2CH_2CO_2$-R_2		H	H	1.5	-[b]	≥ 3.0
6.19	CH_2CH_2OH	OMe	H	H	1.3	-[b]	-[b]
6.20	CH_2CH_2O (glucopyranos-1β-yl)	OMe	H	H	1.0	-[b]	-[b]
6.21	Me	NHAc	H	H	1.0	10	> 10
6.22	Et	NHAc	H	H	1.1	-[b]	-[b]

Cpds	R_1	R_2	R_3	R_4	NQO1[a]	NQO1 CD (μM)	Toxicity NQO1 (μM)
6.23	iPr	NHAc	H	H	1.1	-[b]	-[b]
6.24	CH_2CO_2Me	NHAc	H	H	1.1	-[b]	-[b]
6.25	CH_2CO_2Et	NHAc	H	H	1.5	-[b]	-[b]
6.26	$CH_2CH_2CO_2Et$	NHAc	H	H	1.2	-[b]	-[b]
6.27	CH_3	F	H	H	1.4	-[b]	-[b]
6.28	CH_2CO_2Et	F	H	H	1.3	-[b]	≥ 3.0
6.29	C_6H_5	OH	H	H	2.0	1.0	≥ 1.0
6.30	4-methoxyphenyl	OH	H	H	2.3	0.6	≥ 3.0
6.31	C_6H_5	OMe	H	H	1.6	2.0	≥ 30.0
6.32	C_6H_5	OCH_2CH_2OH	H	H	1.2	10	≥ 30.0
6.33	Me	Me	CO_2Me	H	1.9	1.2	≥ 30.0
6.34	Me	Me	COMe	H	1.6	2.0	≥ 30.0
6.35	Me	Me	CN	H	2.3	0.5	≥ 10
6.36	Et	Me	CO_2Me	H	1.2	-[b]	-[b]
6.37	Et	Me	COMe	H	1.4	-[b]	-[b]
6.38	Pr	Me	CO_2Me	H	1.2	-[b]	-[b]
6.39	Pr	Me	COMe	H	1.4	-[b]	-[b]
6.40	R_1-$[CH_2]_5$-R_2		CO_2Me	H	1.3	-[b]	-[b]
6.41	R_1-$[CH_2]_5$-R_2		COMe	H	1.6	4.0	≥ 30.0
6.42	C_6H_5	C_6H_5	CO_2Me	H	1.1	-[b]	-[b]
6.43	C_6H_5	C_6H_5	COMe	H	1.3	-[b]	-[b]
6.44	C_6H_5	Me	H	H	1.0	10	> 100
6.45	C_6H_5	Me	CO_2Me	H	1.4	-[b]	-[b]
6.46	C_6H_5	Me	COMe	H	1.7	1.5	≥ 30.0
6.47	4-chlorophenyl	Me	COMe	H	1.7	1.5	≥ 10.0
6.48	4-cyanophenyl	Me	COMe	H	2.0	1.7	≥ 10.0
6.49	3-chlorophenyl	Me	COMe	H	2.1	1.0	≥ 10.0
6.50	3,4-dichlorophenyl	Me	COMe	H	1.5	1.5	≥ 10.0
6.51	4-methoxyphenyl	Me	COMe	H	1.4	2.5	≥ 30.0
6.52	4-methylphenyl	Me	COMe	H	1.4	3.5	≥ 30.0
6.53	4-isopropylphenyl	Me	COMe	H	1.1	5.0	≥ 30.0
6.54	4-*tert*-butylphenyl	Me	COMe	H	1.0	-[b]	≥ 10.0
6.55	-	-	-	-	0.9	-[b]	≥ 10.0

Notes: a. Fold induction at 1 μM; b. Not determined.Compounds (Cpds).

The structures in Table 6.2 and 6.3 ranged from inactive to weakly active without a doubling of NQO1 activity at the tested concentration range.

The compounds in group 2a-c represent derivatives of the natural plant product rengyolone. The structures in group 2a and b contain one single Michael acceptor, whereas the structure in group 2c contains two Michael acceptor groups. However, none of the molecules were particularly active in the NQO1 assay.

Table 6.2a: NQO1 (in the Hepa1c1c7 cell line) results for group 2a-c of the cyclohexadienone analogues.

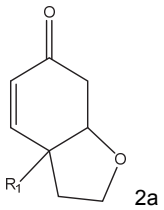

2a

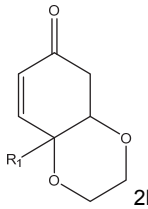

2b

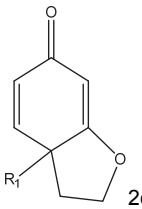

2c

Cpds	Group 2a-c	R1	NQO1[a]	NQO1 CD (μM)	Toxicity NQO1 (μM)
6.56	2a	MeO	1.4	-[b]	-[b]
6.57	2a	OH	1.0	-[b]	> 10
6.58	2b	MeO	1.4	-[b]	-[b]
6.59	2b	C_6H_5	1.3	-[b]	-[b]
6.60	2c	OH	0.9	-[b]	≥ 30.0

Notes: a. Fold induction at 1 μM; b. Not determined. Compounds (Cpds).

The compounds in group 3 are related to the benzylidenemalononitriles, which were found to induce the phase II enzyme HO-1; a property that was associated with the reactivity of the Michael acceptor [62]. However, none of the related structures in Table 6.3 were able to double NQO1 activity at the test concentration of 1 μM.

Table 6.3: NQO1 (in the Hepa1c1c7 cell line) results for group 3 of the cyclohexadienone analogues.

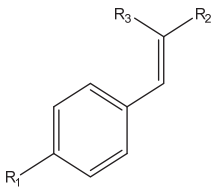

Cpds	R1	R2	R3	NQO1[a]	NQO1 CD (μM)	Toxicity NQO1 (μM)
6.61	OMe	CN	CN	1.0	-[b]	> 100
6.62	Cl	CN	CN	1.0	-[b]	≥ 30.0
6.63	CN	CN	CN	1.0	-[b]	≥ 30.0
6.64	OMe	$CONH_2$	CN	1.0	-[b]	> 100
6.65	NO_2	CN	CN	1.0	-[b]	> 100
6.66	Cl	$CONH_2$	CN	1.0	-[b]	> 100
6.67	CN	$CONH_2$	CN	1.0	-[b]	> 100
6.68	NO_2	$CONH_2$	CN	1.0	-[b]	> 100
6.69	H	CN	CN	1.1	-[b]	> 100
6.70	CN	CONMe2	CN	1.0	-[b]	> 100
6.71	NO_2	CONMe2	CN	1.0	-[b]	> 100

Notes: a. Fold induction at 1 μM; b. Not determined. Compounds (Cpds).

Compound selection for further characterisation

Although compounds **6.33** and **6.46** presented interesting therapeutic index values, they were not chosen for further characterisation in this study but warrant further investigation in the future.

Compounds **6.48**, **6.49** and **6.54** from group 1, carried an additional electron-withdrawing group at the R_3-position of the cyclohexadienone, but different substituents at the 4-position of the R_1-phenyl substituent (**6.48** -Cl, **6.49**–CN and **6.54** *t*-Bu) and presented dissimilar activity in the NQO1 assay. Therefore, they were selected for further characterisation. As the compounds contain reactive Michael acceptor groups, they were thought to induce NQO1 enzyme activity via the Keap1-Nrf2 pathway. Nevertheless, the compounds may have the potential to be ligands for the AhR as the structures contain aryl moieties. Hence, the NQO1 induction activity of compounds **6.48**, **6.49** and **6.54** was additionally examined in the ARNT-defective BpRc1 cell line. Dose response profiles were generated in both Hepa1c1c7 and BpRc1 cell lines (Figure 6.8 A and B). All structures were able to up-regulate NQO1 in both the Hepa1c1c7 and the ARNT-defective BpRc1 cell line with comparable induction potencies.

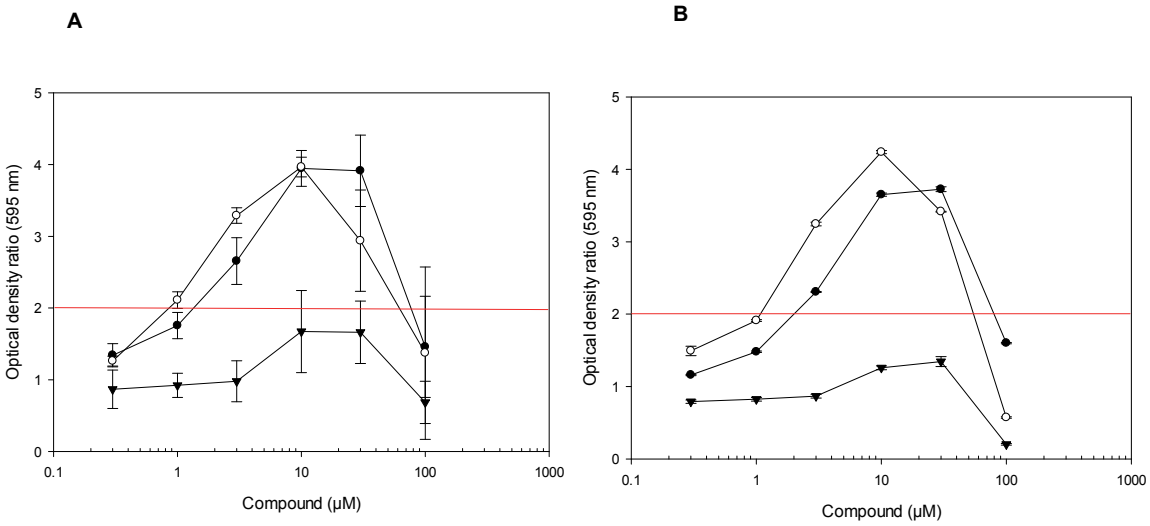

Figure 6.8: Dose response curves for the NQO1 assays of compounds **6.48**(●), **6.49** (○) and **6.54** (▼) in Hepa1c1c7 (A) and BpRc1 (B) cells after 24 h stimulation. The error bars represent the standard deviation of (A) n = 3 independent experiments and (B) n = 4 replicates in a representative experiment.

6.2.2 Western Blotting

The most active compound **6.49** and the less active structure **6.54** were further evaluated for their effect on Nrf2 nuclear accumulation in Hepa1c1c7 cells. Since **6.49** and **6.54** demonstrated no cytotoxicity up to a concentration of 10 µM in the NQO1 assay, Hepa1c1c7 cells were stimulated with 10 µM of compound for 1, 3, 6 and 24 h. Probing the nuclear protein fraction with an anti-Nrf2 antibody revealed the time-dependent induction of Nrf2 with a maximal effect after 3 h with **6.49** (Figure 6.9). The effect from **6.54** on Nrf2 induction was reduced overall compared to **6.49** with an induction peak after 3 - 6 h (Figure 6.9).

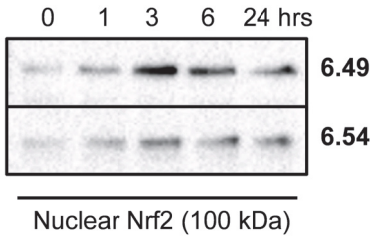

Figure 6.9: Western blot analysis of nuclear Nrf2 accumulation in Hepa1c1c7 cells after treatment with 10 µM of **6.49** or 10 µM **6.54** over a 24 hour time period. Representative blots are shown.

6.2.3 Intracellular Nrf2 staining – flow cytometry

The ability of **6.49** and **6.54** to induce Nrf2 nuclear activity in Hepa1c1c7 cells was quantified with the developed intracellular Nrf2 staining assay (Chapter 4). Hepa1c1c7 cells were stimulated with 10 µM of **6.49** or **6.54** over a period of 24 h, nuclei were isolated, fixed, permeabilised and stained with a primary unconjugated anti-Nrf2 antibody and FITC-conjugated secondary antibody. Figure 6.10 A and B shows the flow cytometry histograms and Figure 6.10 C demonstrates the calculated absolute fold changes. A comparable Nrf2 induction pattern can be observed from the western blots (Figure 6.9) and flow cytometry data (Figure 6.10); the absolute fold changes reveal a maximal Nrf2 protein induction after 1 - 3 h with **6.49** whereas the highest level of induction was reached after 3 - 6 h with **6.54**.

Although the Nrf2 western blot with **6.54** showed a reduced protein expression level compared to **6.49**, the absolute fold changes obtained by flow cytometry demonstrate quantitative evidence.

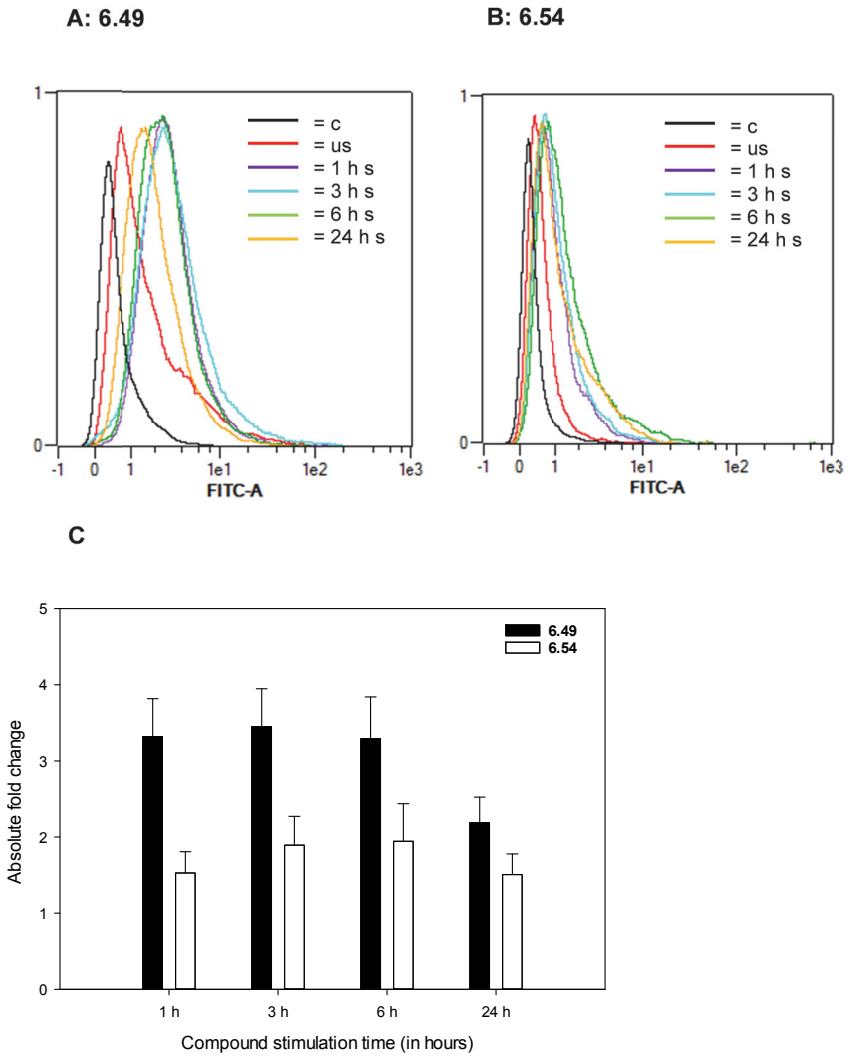

Figure 6.10: Hepa1c1c7 cells were unstimulated (us) or stimulated (s) with 10 µM **6.49** (A) or 10 µM **6.54** (B) for 1, 3, 6 and 24 h and subjected to flow cytometry analysis. An internal staining control (c) was analysed in parallel. Absolute fold changes of Nrf2 induction were calculated for each compound (C). The error bars represent the standard deviation of n = 3 independent experiments.

6.3 Discussion

An important class of indirect inducers are compounds that contain Michael acceptors. Michael acceptors are reactive towards sulfhydryl groups and are thought to interact with key cysteine residues in Keap1, thereby causing conformational changes and as a result induce the Keap1-Nrf2 pathway. The indirect Nrf2 inducers described here are quinol-derived (cyclohexadienone) analogues containing Michael acceptor group(s).

Various structures were screened for their ability to up-regulate the downstream Nrf2 target enzyme, NQO1. The compounds showed a wide range of NQO1 induction potential and cytotoxicity in Hepa1c1c7 cells. Although, the most active compounds up-regulate NQO1 at relatively low concentrations (CD ~ 0.5 – 1.0 μM), they also demonstrate cytotoxicity at higher concentrations (≥ 10 μM). This is likely to be due to the compounds interacting with thiols (with a low pKa) other than those in Keap1 at higher concentrations. The most promising molecules were structures containing two Michael acceptor groups. This observation is in agreement with the hypothesis that the addition of an extra Michael acceptor group increases the structures reactivity towards thiol groups [35 52]. Moreover, NMR studies [62] confirmed the reversibility of the compounds reaction with thiol groups [224], which may contribute to lower cytotoxicity levels. Three representative compounds containing two Michael acceptors (two active; **6.48** and **6.49** and one moderately active; **6.54**) were further evaluated. A differential NQO1 induction pattern was observed for the three compounds in both Hepa1c1c7 and BpRc1 cells. The cell lines showed matching dose response profiles, which supports the proposition that the compounds up-regulate the NQO1 enzyme through the Keap1-Nrf2 pathway and is not suggestive of AhR pathway involvement. Moreover, exposure of Hepa1c1c7 cells to compounds **6.49** or **6.54** demonstrated Nrf2 nuclear accumulation using both western blotting and flow cytometry techniques. The quantitative difference in Nrf2 up-regulation between **6.49** and **6.54** was best demonstrated using the flow cytometry assay; the moderately active NQO1 inducer **6.54** demonstrated a reduced Nrf2 protein expression compared to the more active NQO1 inducer **6.49**. These matching data suggests that the colourimetric NQO1 assay is a good initial screening tool for ranking the indirect Nrf2 inducers. Although both sulforaphane and the cyclohexadienone analogues are believed to induce Nrf2 via reactivity

towards thiol residues in Keap1, the cyclohexadienone analogues show a different time-dependent Nrf2 induction to sulforaphane; Nrf2 showed a peak induction after 1-3 h with **6.49** and after 3-6 h with **6.54** in Hepa1c1c7 cells, whereas cellular exposure to sulforaphane resulted in a maximal nuclear accumulation of Nrf2 after only 1 hour.

The cyclohexadienone analogues are a group that includes members with strong Nrf2-inducing capabilities. In particular, structures containing two Michael acceptor groups and additional electron-withdrawing substituents showed an increased potency towards the up-regulation of NQO1. Further optimisation of the lead structure **6.49** should be targeted at maximizing potency and reducing overall cytotoxicity levels. Although induction of NQO1 enzyme activity in the ARNT deficient BpRc1 cell line is not suggestive of AhR involvement, additional future work on Keap1-Nrf2 pathway specificity would be desirable.

7 Direct Nrf2 inducers: peptides and small molecules

7.1 Introduction

NMR, crystallography, mutagenesis and isothermal calorimetry studies have provided structural insight into the Keap1 – Nrf2 PPI [30]. The Nrf2 Neh2 domain (K_D = 5 – 9 nM) binds to the Keap1 Kelch domain using both a low affinity motif ^{29}DLG^{31} (K_D = 1000 nM) and a high affinity motif ^{79}ETGE^{82} (K_D = 5 nM) (hinge and latch, two binding-sites mechanism) [47]. Both motifs interact with the Keap1 Kelch domain electrostatically via salt bridges between negatively charged Asp and Glu residues in Nrf2 and positively charged Arg residues in the Kelch domain. Figure 7.1 shows the five binding sub-pockets of the Keap1 Kelch domain (P1 - P5) with an Nrf2-ETGE peptide bound. Both P1 and P2 are positively charged and bind the peptide via electrostatic interactions (residues E79 and E82 from Nrf2 respectively). P3 is polar (interacts with the Nrf2-ETGE peptide backbone) and the sub-pockets P4 and P5 are hydrophobic (interacts with residues L76, E78 and F83 from Nrf2). This structural information can be used to design highly specific inhibitors of the Keap1-Nrf2 PPI and offers an alternative strategy to thiol reactive compounds and their associated off-target effects for up-regulation of Nrf2 and downstream phase II enzymes.

The aim of this chapter is to screen a group of Nrf2 derived peptides and small molecules for their ability to directly disrupt the Keap1-Nrf2 PPI and to further characterise the most promising molecules.

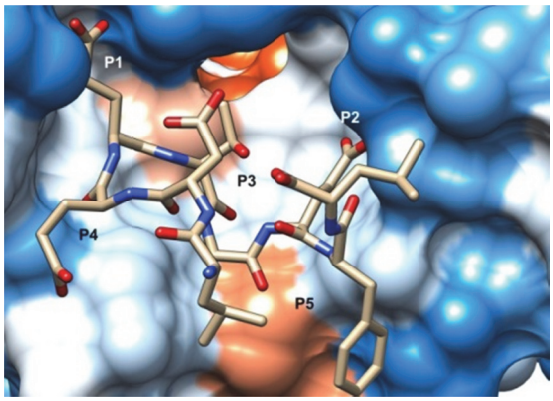

Figure 7.1: Surface representation of the crystal structure of Keap1-Kelch bound to an Nrf2 – ETGE peptide (PDB code: 1X2R). The Kelch binding sub-pockets are indicated as P1 – P5. The surface of Keap1 was coloured as hydrophobicity; blue is hydrophilic, white is neutral and red is hydrophobic.

7.1.1 Peptides

A study from 2006 demonstrated that a 16-mer Nrf2 derived peptide can bind to the Keap1 Kelch domain with high affinity (K_D = 20 nM) when the central ^{77}DEETGE^{82} motif is conserved [46]. Moreover, Chen *et al.* [226] synthesised several ETGE containing Nrf2 peptides and found that the minimal Keap1 binding sequence was a 9-mer Nrf2 peptide ^{76}LDEETGEFL^{84} (K_D = 352 nM). A range of 7-mer Nrf2 derived synthetic peptides based on the high-affinity ETGE motif were previously designed in our research group and evaluated for their ability to disrupt the Keap1-Nrf2 PPI using a fluorescence polarisation (FP) assay [143, 170]. Peptides derived from the binding sequences of sequestosome-1 (p62) (residues 347 - 353), which was found to interact with Keap1, were also synthesised. A series of peptide conjugates were also synthesised to improve cell permeability, i.e. peptides were coupled at their N-terminus to the C_{18} fatty acid stearic acid to promote cellular penetration. In order to quantify the binding activity of the peptides, a previously developed competitive FP assay was applied that utilised an FITC labelled 7-mer Nrf2 peptide (FITC-β-DEETGEF-OH) as the fluorescent probe and Keap1 Kelch domain as the target protein [143]. FP results revealed that peptides based on the Keap1 binding sequences of both Nrf2 and sequestosome-1 presented the highest binding affinity to Keap1 [143]. In this chapter, several of these 7-mer Nrf2 derived peptides were evaluated further. A FRET based competition assay was developed to screen direct inhibitors of the Keap1-Nrf2 PPI (Chapter 3) and was used as an additional *in vitro* tool to verify the inhibition potential of the peptides. Their ability to penetrate the cell membrane and to induce the Nrf2 downstream target NQO1 was examined in the colourimetric cell-based NQO1 assay in Hepa1c1c7 cells. A promising Nrf2 derived peptide that was able to induce NQO1 enzyme activity was conjugated to a FITC fluorophore to examine cellular uptake and localisation.

7.1.2 Small molecules

The use of non-reactive small molecules to inhibit the Keap1-Nrf2 PPI presents a novel approach to directly induce Nrf2 activity. Structural data enabled the design of specific inhibitor molecules that demonstrate high affinity. Most of these structures are designed to mimic the Nrf2 high affinity ETGE peptide motif in order to compete with Nrf2 for Keap1 binding sites. The use of small molecules for inhibiting PPIs presents certain advantages over peptides i.e. oral bioavailability and improved stability [129]. An example is described by Hu *et al.* [119], who performed high-throughput screening of the MLPCN library of 337,116 compounds using an FP-based assay. They found eight promising molecules that were evaluated further. The 'Hit 1' compound was the most active inhibitor of the Keap1-Nrf2 PPI and demonstrated an IC_{50} value of 3 μM and a K_D value of 1.9 μM (Figure 7.2).

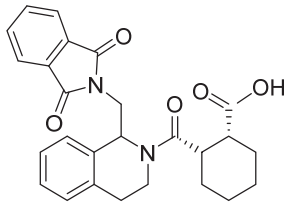

Hit 1

Figure 7.2: Small molecule inhibitor of the Keap1-Nrf2 PPI as described by Hu *et al.* [119].

In this chapter, various other putative small molecule inhibitor groups were evaluated. The *in vitro* FRET assay developed in Chapter 3 was used to screen the molecules inhibitory properties. Cellular techniques, i.e. a cellular NQO1 screening assay, western blotting and flow cytometry, were employed to explore the molecules ability to induce Nrf2 and its downstream target enzymes. Finally, the pathway specificity of potent Nrf2 inducers was examined using various cell based methods.

Initially, a group of previous identified compounds, **7A1** – **7A10** [115, 119, 227-228], were studied. Marcotte *et al.* [227] developed the bis-sulphonamide derivative 'compound 16', a potent inhibitor of the Keap1-Nrf2 PPI (Figure 7.3 A).

A close analogue of 'compound 16', **7A4**, was further evaluated in our group (Figure 7.3 B). Moreover, Jiang *et al.* [129] used 'compound 16' as a scaffold to design a series of more potent analogues, including 'compound 2' [129] (Figure 7.3 C). Our group designed a close analog series of 7B compounds related to 'compound 2' [129]. The compound **7B1** represents 'compound 2'. In addition, a group of 7C compounds were synthesised by our group based upon a 1,4-diaryl-1,2,3-triazole scaffold. The small molecules were screened for their ability to disrupt the Keap1-Nrf2 PPI and up-regulate the phase II enzyme NQO1. Promising structures were characterised further.

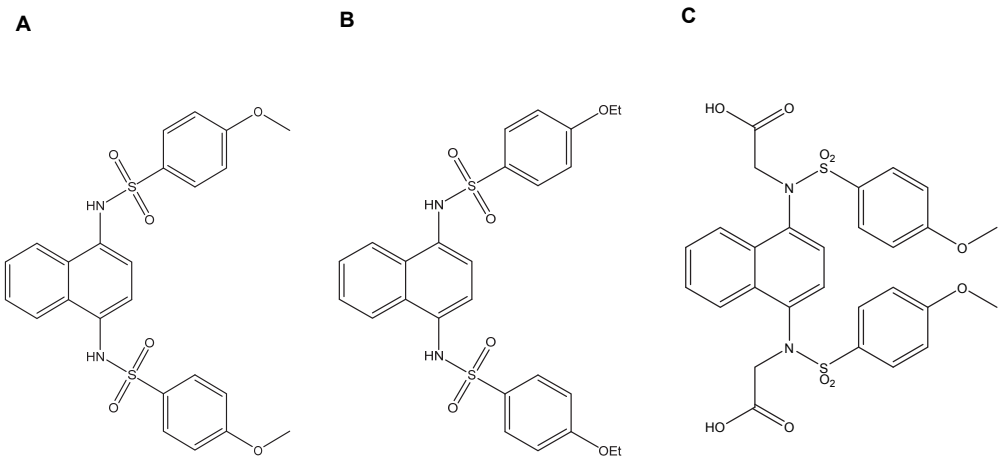

Figure 7.3: Chemical structures of A: 'compound 16', a small molecule inhibitor of the Keap1-Nrf2 PPI as described by Marcotte *et al.* [227], B: **7A4**, a close analogue of 'compound 16' and C: the 'compound 2'/**7B1** small molecule inhibitor of the Keap1-Nrf2 PPI as described by Jiang *et al.* [129].

7A compounds

The 7A compounds present a range of putative Keap1-Nrf2 PPI inhibitors with distinct (chemical) properties. A library of 47,000 compounds (Microsource, Prestwick, and Chembridge Libraries) were screened with a luciferase reporter gene assay by Wu *et al.* [115]. Compounds **7A1**, **7A3** and **7A6** were amongst the top 4 molecules with the lowest EC_{50} values for Nrf2-ARE activation (EC_{50} = 0.9 µM, EC_{50} = 1.0 µM and EC_{50} = 0.9 µM respectively). Marcotte *et al.* [227] screened 267,551 compounds from the Evotec Lead Discovery library and an additional 1,911

compounds derived from virtual screening using a homogenous confocal fluorescence anisotropy assay. 'Compound 16' (Figure 7.3 A), a close analogue of **7A4**, was one of the highly potent inhibitors of the Keap1-Nrf2 PPI (IC_{50} = 2.7 μM) and is part of the benzenesulfonamide subclass of compounds [227]. 'Compound 16' was also shown to be active in an Nrf2 specific ARE-driven luciferase cell-based assay in a dose-dependent manner [227]. Moreover, the compound induced the expression of Nrf2 protein and the phase II enzyme NQO1 in a DLD1-ARE reporter stable cell line; protein levels were decreased by siRNA Nrf2 gene knockdown [227]. Mass-spectrometry analysis indicated that 'compound 16' was not cysteine reactive [227]. Analysis of the co-crystallisation structure of 'compound 16' with the Keap1 Kelch domain revealed that the second ring of the naphthalene binds in the P3 sub-pocket of the Kelch domain (Figure 7.4) [227]. The two methoxy substituted benzene rings, connected by the sulfonamide moieties, bind in the P4 and P5 sub-pockets via non-covalent interactions with aromatic residues (π-stacking) that surround the sub-pockets [227]. Compound **7A4**, a close analogue of 'compound 16', was used for subsequent biological evaluation (Figure 7.3 B). Compounds **7A2**, **7A5** and **7A7-9** were all derived from the PubChem Bioassay database: AID 588683 [228]. They were also shown to be potent disrupters of the Keap1-Nrf2 PPI in an FP based assay.

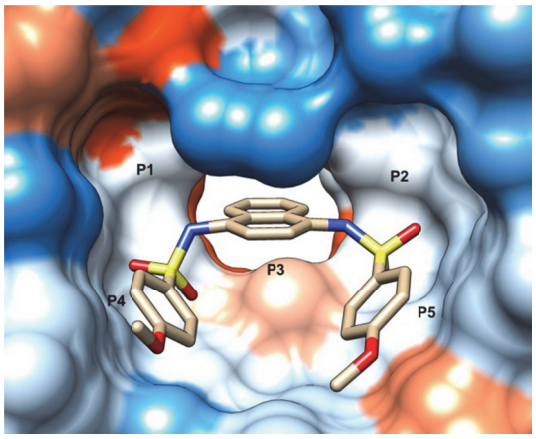

Figure 7.4: Surface representation of the crystal structure of Keap1-Kelch bound to 'compound 16' (PDB code: 4IQK). The Kelch binding sub-pockets are indicated as P1 – P5. The surface of Keap1 was coloured as hydrophobicity; blue is hydrophilic, white is neutral and red is hydrophobic.

7B compounds

The crystal structure of 'compound 16' with the Keap1 Kelch domain [227] formed the basis for the ligand design as described by Jiang *et al.* [129]. The 'compound 16' analogue that was developed, 'compound 2'/**7B1**, contains two additional acetic acid side chains, linked to the sulfonamide nitrogen of the 'compound 16' scaffold (Figure 7.3 C) [129].

It is proposed that the two additional carboxylate groups interact electrostatically with the P1 and P2 sub-pockets of Keap1 [129]. Moreover, docking studies revealed that the compound binds in all five sub-pockets of Keap1 (Figure 7.5) [129].

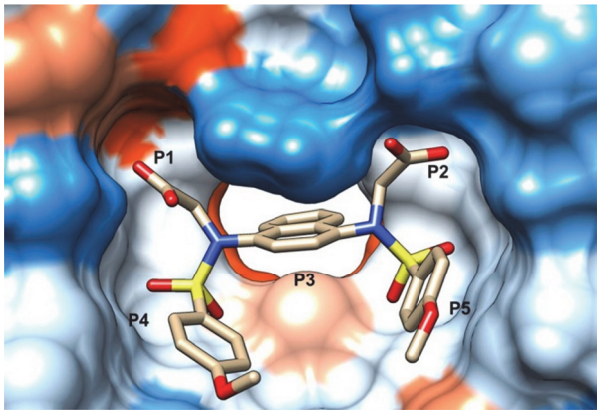

Figure 7.5: Surface representation of the crystal structure of Keap1-Kelch bound to the 'compound 2'/**7B1**. The Kelch binding sub-pockets are indicated as P1 – P5. The surface of Keap1 was coloured as hydrophobicity; blue is hydrophilic, white is neutral and red is hydrophobic.

Further characterisation of the potent Keap1-Nrf2 PPI inhibitor showed an IC_{50} of 28.6 nM and a K_D of 3.59 nM in an FP based assay [129]. The compound demonstrated concentration dependent activity in an Nrf2 ARE-luciferase reporter assay [129]. In addition, 'compound 2'/**7B1** induced the expression of Nrf2 regulated genes, including glutamate-cysteine ligase (GCLM), NQO1 and HO-1 in HCT116 cells using qRT-PCR [129]. A series of 7B compounds that were derived from the structure of 'compound 2'/**7B1** were developed by our group. They were separated into two series. The structures in group 1 contain a naphthalene ring system and various replacements for the two carboxylic acid groups of 'compound 2'/**7B1** to

improve binding potency and cell penetration. They are thought to occupy the same space in the Keap1 binding pocket as 'compound 2'/**7B1** [129]. The structures in group 2 contain substituents that should mimic the naphthalene rings and are predicted to bind in a similar manner to 'compound 2'/**7B1** and the structures in group 1. Moreover, docking studies suggest that these compounds bind deeper in the Keap1 binding pocket than the compounds containing a naphthalene ring system. Previously obtained FP results by our group showed promising inhibitory properties of the developed 7B compound series.

7C compounds

An *in silico* fragment-based approach was used to dock ~ 178,000 compounds (a subset of the ZINC virtual screening database) into the Keap1 Kelch binding pocket where the Nrf2 ETGE motif binds. From this docking study, 360 promising molecules were selected for further evaluation. Figure 7.6 shows three core scaffolds (A: oxotetrahydrothiazole, B: 1, 2, 4-triazole and C: 1, 2, 3-triazole) that were identified for development by structural modification and introduction of various functional groups, i.e. carboxylic acid, carboxamide and nitro groups (R, R'). These groups function as hydrogen bond acceptors that can form salt bridges or hydrogen bonding interactions with the Keap1 Kelch domain, hence mimicking the binding of the high-affinity Nrf2-ETGE motif. Scaffolds A and B were derived from structures that frequently appeared as potent Keap1-Nrf2 PPI inhibitors in the virtual screen (submitted and in the press [229]), whereas scaffold C was designed to mimic the distance between the two carboxylic acid groups of the Nrf2 – ETGE motif.

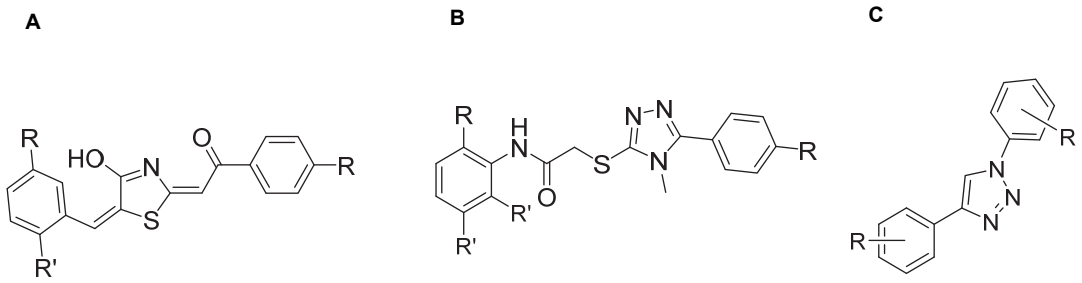

Figure 7.6: Core scaffolds used for the development of small molecule inhibitors of the Keap1-Nrf2 PPI. A: oxotetrahydrothiazole, B: 1, 2, 4-triazole and C: 1, 2, 3-triazole.

The oxotetrahydrothiazole derivatives presented high levels of fluorescence interference in FP assays performed by our group [143], hence they were not evaluated further. Although the 1,2,4-triazoles derivatives were not very active in the FP based assay, their ability to induce phase II enzymes was examined in a cellular NQO1 induction assay. The 1,2,3-triazoles derivatives showed the most promising results in the FP based assay and were subjected to further examination in various cellular assays.

7.2 Results – Evaluation of peptides (7P)

7.2.1 FRET assay

The Keap1-Nrf2 PPI inhibition potential of several of 7-mer Nrf2-derived peptides was examined using a FRET competition assay (assay development described in Chapter 3). Increasing concentrations of the Nrf2 derived peptides (0.001 – 100 μM) were added to a mixture of the eCFP-TEV-Nrf2 and eYFP-TEV-Kelch proteins (0.11 μM and 0.20 μM respectively) and IC_{50} values were determined using the reduction in FRET efficiency. Figure 7.7 shows the dose-dependent competitive inhibition of FRET between eCFP-TEV-Nrf2 and eYFP-TEV-Kelch proteins and Table 7.1 shows the corresponding IC_{50} values. The IC_{50} values obtained using the FP assay were included as a comparison. The 7-mer **7P1** peptide is a truncated version of the 16-mer Nrf2 WT peptide (Section 3.2.11) and showed a 30-fold higher IC_{50} value (3.34 μM vs. 0.11 μM). Peptides **7P2**, **7P3** and **7P4** contain a hybrid binding sequence derived from both Nrf2 and sequestosome-1. They all contained an E78P substitution, which improved activity considerably. Substitution of the *N*-terminal acetyl for a stearic acid increased inhibition potencies of peptides **7P5** and **7P4** (the stearic acid versions of **7P1** and **7P3** respectively). The peptide **7P6** is a scrambled version of peptide **7P5** and showed a marked reduction in inhibition of the Keap1-Nrf2 PPI indicating the importance and specificity of the correct peptide sequence. The IC_{50} values obtained from the FRET and FP assay show a comparable trend.

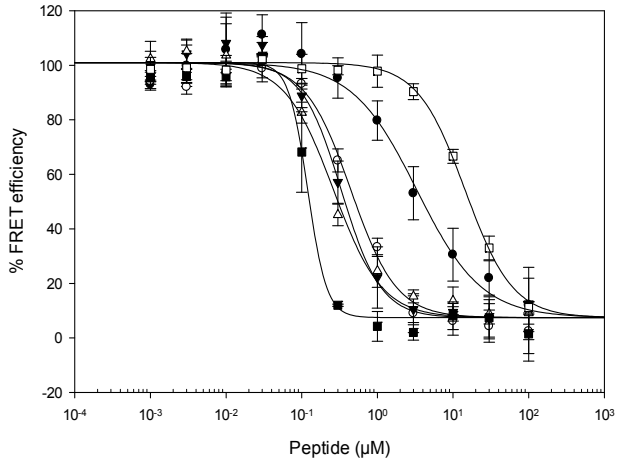

Figure 7.7: Competitive inhibition of FRET between 0.11 μM eCFP-TEV-Nrf2 and 0.20 μM eYFP-TEV-Kelch by increasing concentrations (0.001 – 100 μM) of unlabelled Nrf2-derived peptides (●: **7P1**, ○: **7P5**, ▼: **7P2**, △: **7P3**, ■: **7P4** and □: **7P6**). The data were fitted to a standard four-parameter logistic function. The error bars represent the standard deviation of n = 3 independent assays. Adapted from [142].

Table 7.1: FRET and FP assay results for the 7P peptide range.

Peptides	Sequence	FRET IC_{50} ± SE (μM)	FP IC_{50} ± SE (μM)
7P1	Ac-DEETGEF-OH	3.34 ± 0.44	5.39 ± 0.58
7P2	Ac-DPETGEF-OH	0.33 ± 0.03	0.25 ± 0.04
7P3	Bz-DPETGEL-OH	0.26 ± 0.03	0.16 ± 0.02
7P4	St-DPETGEL-OH	0.12 ± 0.01	0.02 ± 0.003
7P5	St-DEETGEF-OH	0.45 ± 0.05	0.18 ± 0.04
7P6	St-DEGEETF-OH	14.5 ± 1.60	11.8 ± 2.67

Notes: FP assays performed by Rowena Hancock, UCL School of Pharmacy

7.2.2 NQO1 assay

Several 7-mer Nrf2 derived peptides were examined for their ability to induce NQO1 expression in Hepa1c1c7 cells (Table 7.2). Included are the IC_{50} values from the FP assay. Figure 7.8 shows the peptides that were able to induce NQO1 enzyme activity.

Table 7.2: NQO1 (in the Hepa1c1c7 cell line) results for the 7P peptide range.

Peptides	Sequence	FP IC_{50} ± SE (μM)	NQO1[a]	NQO1 CD (μM)	Toxicity NQO1 (μM)
7P1	Ac-DEETGEF-OH	5.39 ± 0.58	1.0	-[b]	> 100
7P7	Ac-DPETGEL-OH	0.12 ± 0.01	1.0	-[b]	> 100
7P4	St-DPETGEL-OH	0.02 ± 0.003	1.0	100	> 100
7P3	Bz-DPETGEL-OH	0.16 ± 0.02	1.0	-[b]	> 100
7P8	Ac-DPGEETL-OH	-[b]	1.0	-[b]	> 100
7P9	St-DPGEETL-OH	73.91 ± 38.57	1.0	-[b]	> 100
7P10	St-NPETGEL-NH_2	3.71 ± 1.14	1.0	-[b]	> 100
7P11	St-NPETGEL-OH	0.27 ± 0.03	1.0	100	> 100
7P5	St-DEETGEF-OH	0.18 ± 0.04	1.2	20	> 100
7P6	St-DEGEETF-OH	11.8 ± 2.67	1.0	40	> 100

Notes: FP assays performed by Rowena Hancock, UCL School of Pharmacy; a. Fold induction at 10 μM; b. Not determined.

The FP data obtained previously (Table 7.1) [143] and the FRET [142] data show that peptide **7P1**, containing the original Nrf2 sequence, was a good inhibitor of the Keap1-Nrf2 PPI. Peptides **7P7** and **7P3** are proline-substituted versions of peptide **7P1** and dramatically improved the inhibition potential in the FP and FRET assay [143] [170] [142]. The peptide **7P8** is a scrambled version of peptide **7P1** and demonstrated to be inactive in the FP assay [170]. None of the above mentioned peptides demonstrated up-regulation of NQO1 gene expression in the cellular NQO1 assay. The introduction of a stearic acid group to the peptides **7P5** (version of **7P1**) and **7P4** (version of **7P3**) increased the inhibition potential in the FP and FRET assay [170] [142]. Both these peptides showed NQO1 induction potencies (CD ~ 20 and 100 μM respectively) (Figure 7.8). Scrambled stearic acid conjugates **7P9** and **7P6** showed increased inhibition of the Keap1-Nrf2 PPI compared to their native sequences (**7P8** and **'**peptide 17' [170] respectively) in the FP and FRET assay [170, 142]. No increase in NQO1 activity was found with peptide **7P9**, but a CD value of 40 μM was obtained with the **7P6** peptide (Figure 7.8). Reduction of the negative charge by introducing the substitution of D76N reduced the activity of peptides **7P10** and **7P11** in the FP assay [170], but peptide **7P11** maintained cellular activity in the NQO1 assay that was comparable to peptide **7P4** (both CD ~ 100 μM) (Figure 7.8).

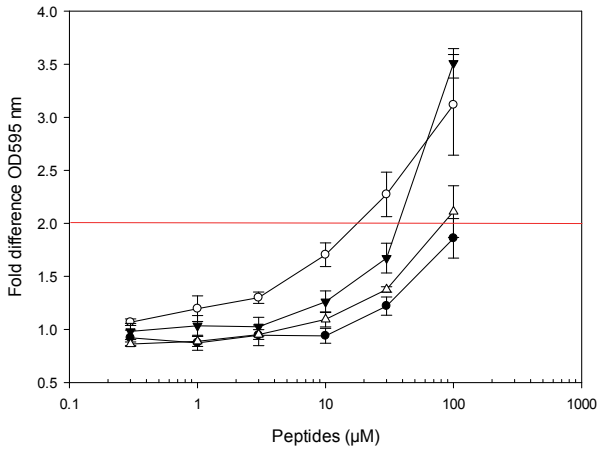

Figure 7.8: Dose response curves for the NQO1 assays of compounds **7P4** (●), **7P5** (○) and **7P6** (▼) **7P11** (∆) in Hepa1c1c7 after 24 h stimulation. The error bars represent the standard deviation of n = 3 independent experiments.

7.2.3 Cellular uptake

Several stearic-acid conjugated Nrf2-derived peptides were shown to have promising cellular activity in the colourimetric cell-based NQO1 assay. To study their cellular uptake, the peptide **7P11** was modified to incorporate an FITC fluorophore conjugated to the side chain of a lysine residue introduced at the N-terminus of the peptide sequence; this resulted in peptide **7P12** (Table 7.3). Flow cytometry was used to quantify the cellular uptake of the peptide and confocal microscopy facilitated mapping of the intracellular distribution of **7P12**. TAT is a well-known cell-penetrating peptide (CPP) that is derived from the HIV viral protein [230]. TAT was conjugated to FITC and used as a positive control peptide in both flow cytometry and confocal analysis (AnaSpec) (Table 7.3). CPPs are short peptide sequences (< 30 amino acids) that are mostly positively charged [231]. They are thought to interact electrostatically with the plasma membrane then enter the cell by a process of endocytosis [232]. The FITC labelled 7-mer peptide **7P13** (Table 7.3) was designed to match the high-affinity ETGE motif to be used in previous FP assays [101]. The **7P13** peptide (which lacks a conjugated fatty acid) was used as a negative control to account for background FITC fluorescence in flow cytometry analysis.

Table 7.3: Sequences of peptides studied. The LC in the TAT peptide sequence represents a long chain that prevents FITC from degradation.

Peptides	Sequence
7P12	St-K-(FITC)-NPETGEL-OH
7P13	FITC-β-DEETGEF-OH
TAT	FITC - LC - 47YGRKKRRQRRR57

To measure cellular uptake of the peptides, Hepa1c1c7 cells were incubated with a final concentration of 1 µM peptide at 37 °C for 5, 10, 30, 60 and 120 min before removing surface-bound peptide with trypsin. Cells were subsequently washed with PBS before the internalisation process was measured using flow cytometry. Figure 7.9 shows the cellular uptake of the peptides by plotting FITC - median fluorescence intensity (MFI) vs. time. The data were fitted by non-linear regression using an equation for ligand binding:

$$\text{Ligand binding} = \frac{B_{max} * \text{abs}(x)}{K_d + \text{abs}(x)} + Ns * x$$

Where B_{max} represents the FITC – MFI, the K_d represents the time in min, abs is the absorbance and Ns is the slope of the non-specific binding line:

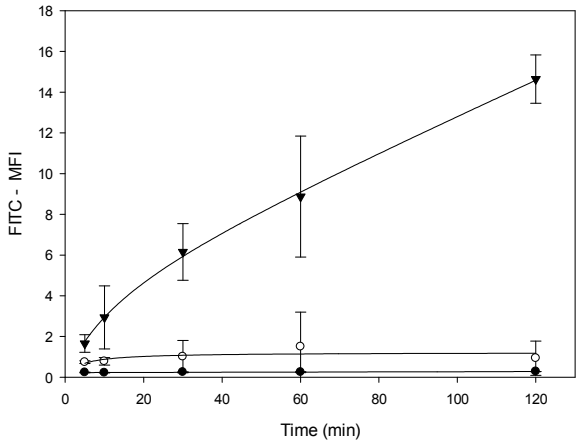

Figure 7.9: Kinetics of cellular uptake of **7P13** (●), **TAT** (○) and **7P12** (▼) peptides in Hepa1c1c7 cells over time (up to 120 min).

The FITC fluorescence signal for the **7P12** peptide increased rapidly after only 5 min and continued to increase after 120 min without having reached a plateau, which demonstrates a progressively increasing cell entry over time. Although low FITC background signals were observed with the negative control **7P13** peptide, no significant cellular uptake was detected with the positive control FITC-TAT peptide.

The cellular distribution of the FITC conjugated **7P12** and TAT peptides were examined in both living and fixed Hepa1c1c7 cells. Hepa1c1c7 cells were incubated with a final concentration of either 10 µM FITC - **7P12** or 1 µM FITC-TAT peptide at 37°C for 1 h. Fixed cells (2% PFA) were stained with CellMask (Life Technologies), a cellmembrane dye, before they were mounted on glass slides using mounting medium containing the fluorescent dye DAPI that stains nuclei. Living cells were washed with PBS before staining the cells with the nuclear Hoechst 33342 dye and the cell membrane with CellMask dye. The Hoechst 33342 dye was used for living cells since DAPI is less efficient at penetrating the cell membrane of living cells. Commonly used cell membrane markers include fluorophore conjugated lectins. These markers depend on cell-specific surface sugars for staining, which may result in inconsistencies. The CellMask stain consists of an amphipathic probe that enables anchoring of the dye in the plasma membrane. Moreover, its staining efficiency is not dependent on a specific cell type. A predominant cytoplasmic distribution of the **7P12** peptide was observed in both living and fixed cells (Figure 7.10 A and B respectively), although to a lesser extent in living cells. In contrast, the TAT peptide could not be detected in living cells (Figure 7.10 A), but was present in both the cytoplasm and the nucleus in fixed cells (7.10 C). The **7P12** peptide was visible as small intense green vesicles inside the cells, whereas the TAT peptide showed a more even distribution.

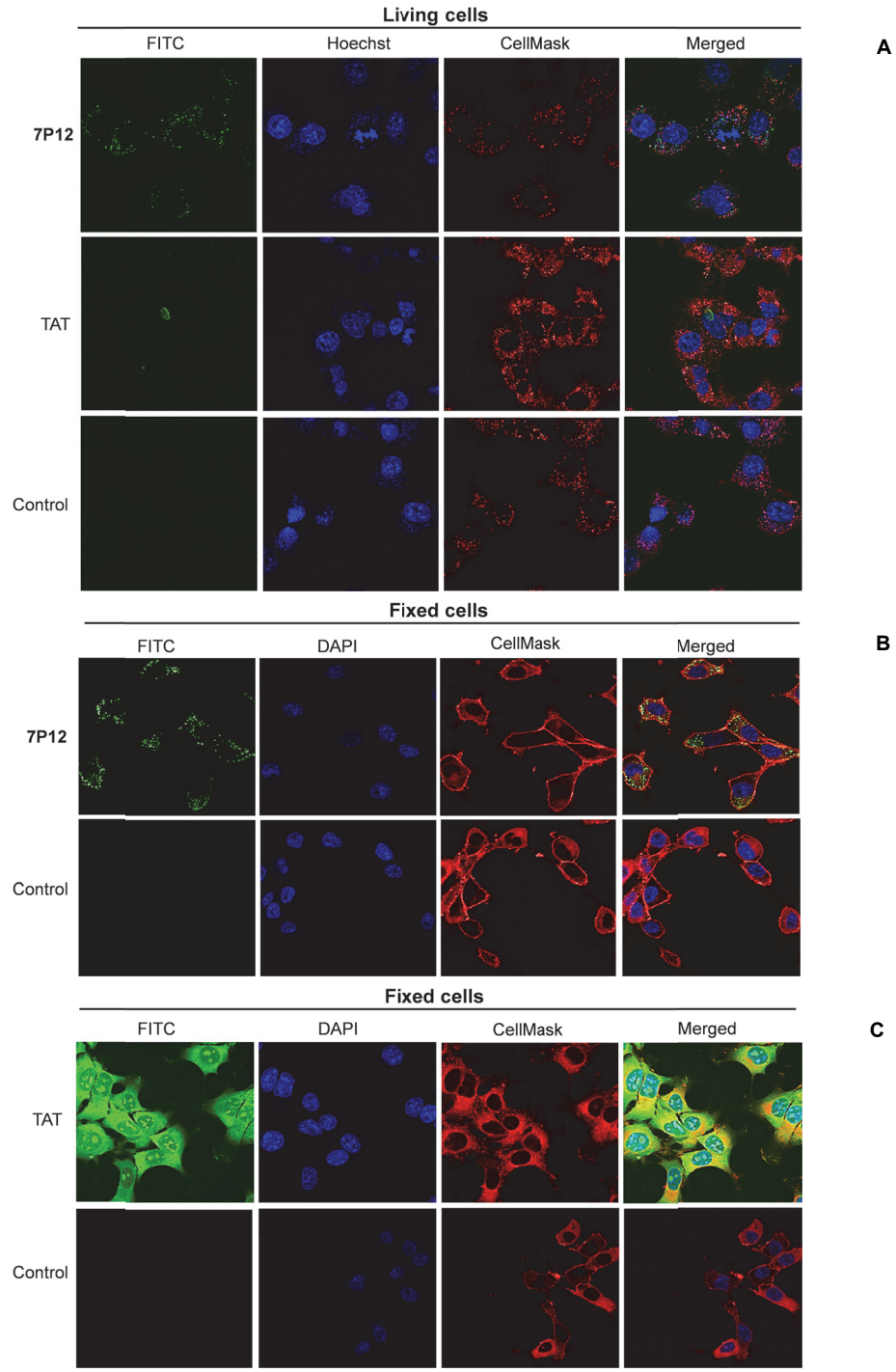

Figure 7.10: Intracellular distribution of FITC labelled **7P12** and TAT peptides examined by confocal microscopy (Zeiss LSM 710) using a 63x oil immersion objective. Hepa1c1c7 cells were incubated at 37°C for 1 h with either 10 µM **7P12** (A & B) or 1 µM TAT FITC (A & C) labelled peptides and were imaged as living (A) or fixed cells (B & C). Control cells were not incubated with peptide and were imaged with identical instrument settings. Nuclei were stained with Hoechst (living cells) or DAPI (fixed cells) and cell membranes were stained with CellMask (Life Technologies).

7.3 Results – Evaluation of small molecules (7A)

7.3.1 FRET assay

Screening of compounds

A FRET competition assay was employed to evaluate the ability of the different 7A compounds (Figure 7.11) to inhibit the Keap1-Nrf2 PPI. The inhibition potential was determined by measuring the decrease in FRET efficiency at a fixed dose concentration of 25 μM. A second read-out counter assay was performed in the absence of both eCFP-TEV-Nrf2 and eYFP-TEV-Kelch proteins to determine any potential auto-fluorescence properties of the compounds. Table 7.4 shows the fixed dose (25 μM) inhibition of the Keap1-Nrf2 PPI by 7A compounds using the FRET assay. FRET inhibition percentages were corrected for potential fluorescence interference by subtracting the compounds fluorescence emission values upon excitation in the absence of the fluorescent proteins. As a comparison, uncorrected percentages of inhibition at concentrations of 10 μM and 100 μM that were obtained using an FP assay are also included in the table.

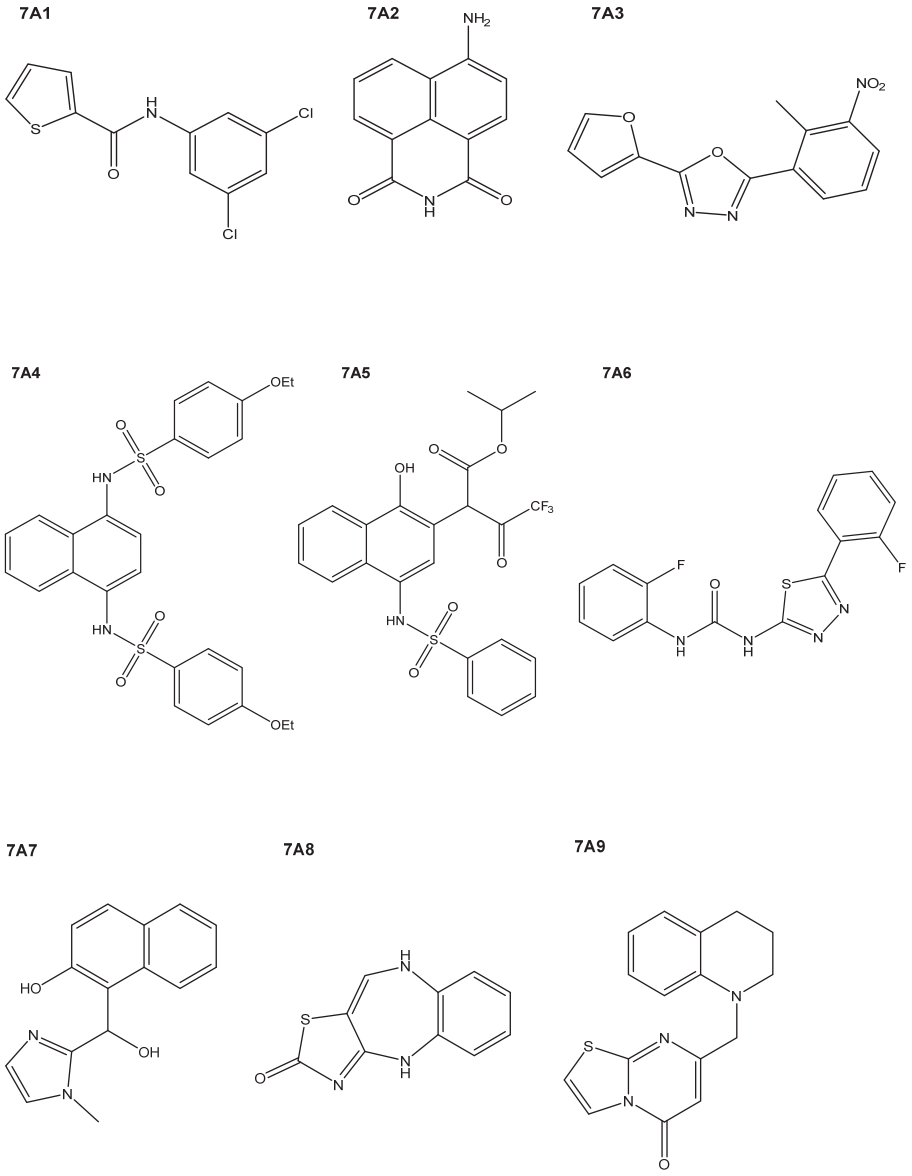

Figure 7.11: Chemical structures of the 7A compounds 1 – 9.

Table 7.4: FRET and FP assay results for the 7A compound range.

Cpds	FRET[a]	FP[b1]	FP[b2]
7A1	12.7	13	9.0
7A2	0.3*	110*	110*
7A3	3.2	0.9	-32.9
7A4	76.2	-116.6*	110.3*
7A5	58.4	51.1	51.3
7A6	8.4	1.0*	-45.7*
7A7	18.4	28.9	13.5
7A8	0.3*	102.2*	102.2*
7A9	-27.5*	1.0	42.3

Notes: FP assays performed by Adrian Fowkes, UCL School of Pharmacy; a. Auto-fluorescence corrected percentage inhibition at 25 µM; b1 Percentage inhibition at 10 µM; b2. Percentage inhibition at 100 µM; *large amounts of observed auto-fluorescence. Compounds (Cpds).

Compound selection for further characterisation

The most promising inhibition potential in the FRET experiments was observed with compounds **7A4** and **7A5**, which were selected for further evaluation in dose-response experiments. The obtained dose-response profiles revealed that **7A4** binds with an apparent IC_{50} of 2.84 µM and **7A5** with an apparent IC_{50} of 12.20 µM (Figure 7.12).

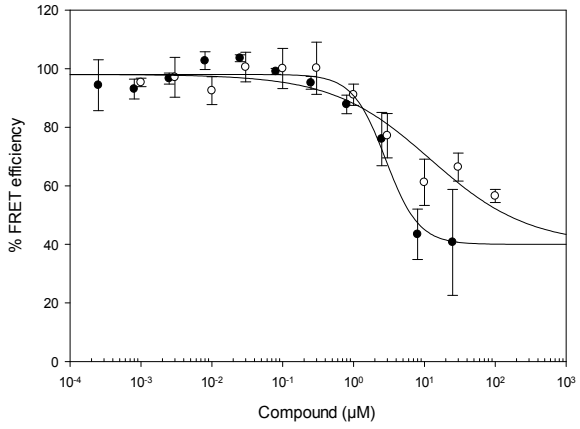

Figure 7.12: Competitive inhibition of FRET between 0.11 µM eCFP-TEV-Nrf2 and 0.20 µM eYFP-TEV-Kelch by increasing concentrations (0.001 – 100 µM) of ●: **7A4** and ○: **7A5**. IC_{50} values of 2.84 µM and 12.20 µM were obtained for **7A4** and **7A5** respectively. The data were fitted to a standard four-parameter logistic function. The error bars represent the standard deviation of n = 3 independent assays.

7.3.2 NQO1 assay

Screening of compounds

To verify whether the Keap1-Nrf2 PPI inhibition potential of the various 7A compounds is accompanied by an up-regulation of the NQO1 enzyme in Hepa1c1c7 cells, the compounds were screened at a fixed dose concentration of 25 µM. The fold induction at this concentration is displayed in Figure 7.13 and Table 7.5. The majority of the compounds were able to up-regulate NQO1 in cells at a concentration of 25 µM (fold induction > 1.0), except for **7A2**, **7A5** and **7A7** (fold induction ≤ 1.0).

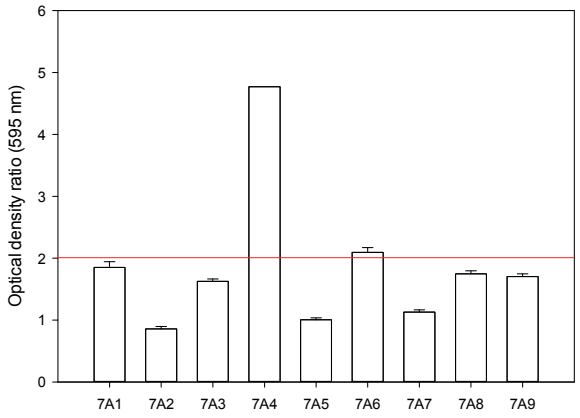

Figure 7.13: NQO1 induction in Hepa1c1c7 cells after 24 h of stimulation with **7A1-9** at a fixed concentration of 25 µM. The red line indicates a doubling of NQO1 activity (CD value). Error bars are based on n = 4 replicates in a representative experiment.

Table 7.5: NQO1 enzymatic activity induction by the 7A compounds in the Hepa1c1c7 cell line.

Cpds	NQO1[a]	NQO1 CD (µM)	Toxicity NQO1 (µM)
7A1	1.9	-[b]	≥ 30
7A2	0.9	-[b]	-[b]
7A3	1.6	-[b]	> 100
7A4	4.8	8	> 25
7A5	1.0	-[b]	-[b]
7A6	2.1	0.8	> 25
7A7	1.1	-[b]	-[b]
7A8	1.7	30	> 100
7A9	1.7	30	> 100

Notes: a. Fold induction at 25 µM; b Not determined. Compounds (Cpds).

Compound selection for further characterisation

To examine the active compounds further, dose-response curves were created for **7A1**, **7A3**, **7A4**, **7A6**, **7A8** and **7A9** in both Hepa1c1c7 and ARNT-defective BpRc1 cell lines (Figure 7.14). **7A4** and **7A6** were the most potent NQO1 inducer compounds in the Hepa1c1c7 cell line; **7A4**: CD ~ 8 μM and max fold induction ~ 5.0 at 25 μM, **7A6**: CD ~ 0.8 μM and max fold induction ~ 2.6 μM at 25 μM. Only **7A4** was able to slightly increase NQO1 activity in the BpRc1 cell line and was selected for further characterisation.

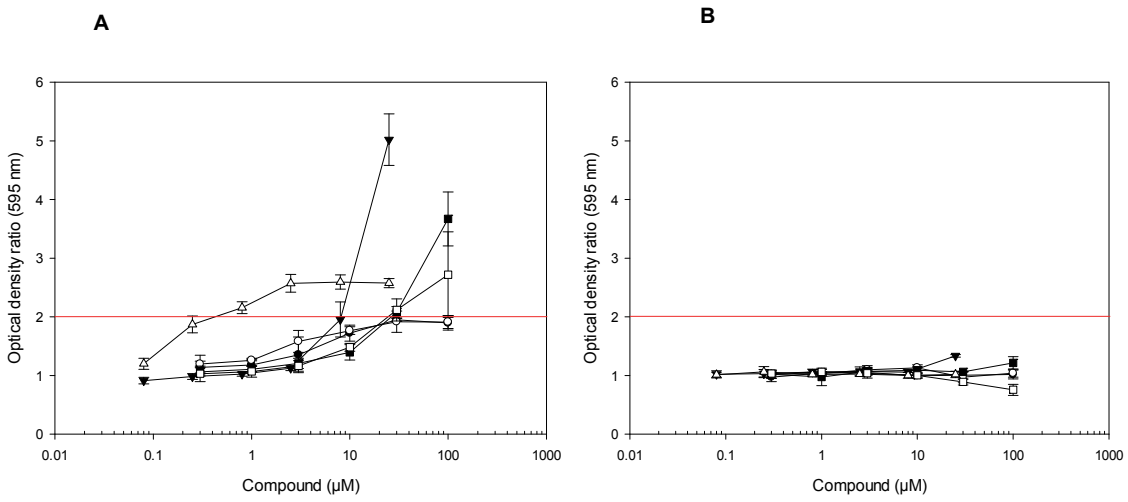

Figure 7.14: Dose response curves for the NQO1 assays of compounds **7A1** (●), **7A3** (○), **7A4** (▼), **7A6** (△), **7A8** (■) and **7A9** (□) in Hepa1c1c7 (A) and BpRc1 (B) cells after 24 h stimulation. The red line indicates a doubling of NQO1 activity (CD value). The error bars represent the standard deviation of n = 3 independent experiments.

7.3.3 SRB assay

The **7A4** compound appeared not to be toxic at concentrations up to 25 μM in the cellular NQO1 assay as the NQO1 enzyme activity didn't show a decline at this dose. An SRB assay was performed to verify the cytotoxicity of **7A4** at concentrations up to 250 μM (in 1% DMSO final concentration) after 24 and 48 h of stimulation of Hepa1c1c7, BpRc1 and HeLa cells (Figure 7.15 A and B respectively). In agreement with the NQO1 assay results, **7A4** was not cytotoxic in either of the cell lines at concentrations up to 25 μM after 24 and 48 h.

Though, cell viability was reduced by ~ 50 - 60% at a concentration of ~ 80 µM and decreased by ~ 60 - 70% at a concentration of 250 µM in the mouse hepatoma cell lines after 24 h. The cytotoxic effect of **7A4** in HeLa cells was reduced compared to the other two cell lines (~ 10% decrease of cell viability at 250 µM after 48 h). As cell viability started to reduce at concentrations > 25 µM, a **7A4** dose of 25 µM was used in all following experiments.

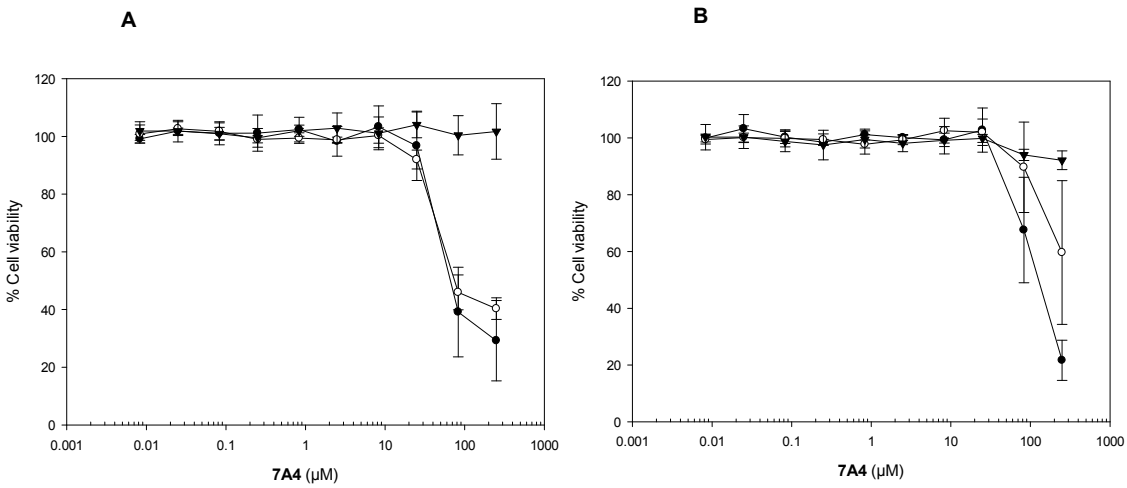

Figure 7.15: Dose response curves for the SRB assays of **7A4** in Hepa1c1c7 (●), BpRc1 (○) and HeLa cells (▼) after 24 h (A) and 48 h (B) stimulation. Cell viability is calculated as a percentage of cells treated with vehicle only. Error bars are based on n = 4 replicates in a representative experiment.

7.3.4 Western blotting

To examine whether the **7A4** compound is able to activate nuclear Nrf2 accumulation and the up-regulation of downstream target enzymes HO-1 and NQO1 in Hepa1c1c7 and BpRc1 cells, protein levels were measured by Western blot analysis. Following treatment of the cells with 25 µM **7A4**, samples were taken after 1, 3, 6 and 24 h of exposure and divided into cytoplasmic and nuclear protein fractions. A maximal induction of nuclear Nrf2 was observed after 1 h in Hepa1c1c7 cells (fold induction ~ 5), but only a weak induction was promoted in BpRc1 cells (fold induction < 2) (Figure 7.16 A, C and E). Expression of NQO1 by **7A4** was only detected after 24 h in the Hepa1c1c7 cell line (Figure 7.16 B and D). A time dependent induction of HO-1 was also observed with a peak induction after 6 h (fold induction ~ 5) in Hepa1c1c7 cells (Figure 7.16 B and E). HO-1 protein levels were only slightly induced in the BpRc1 cell line with a maximal increase detected after 3 h (fold induction < 2) (Figure 7.16 D and E).

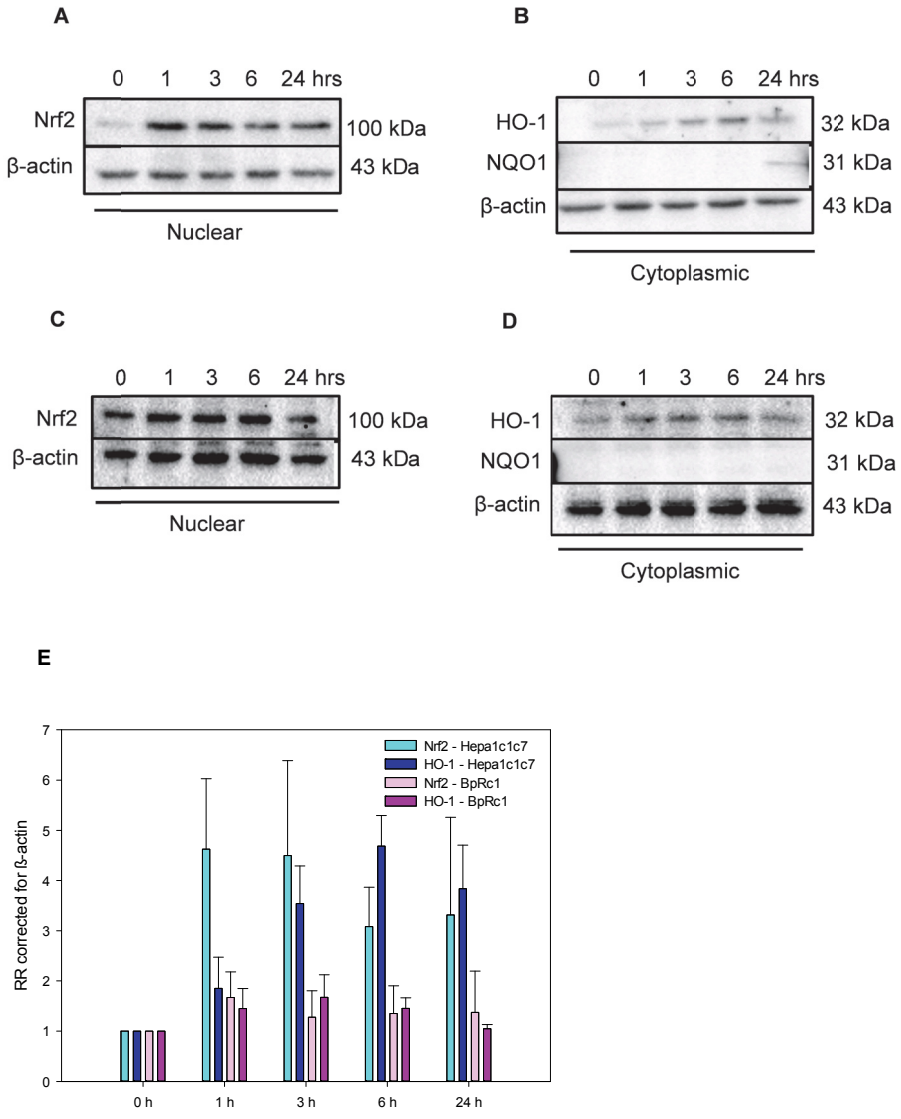

Figure 7.16: A - D: Western blot analysis of nuclear Nrf2 accumulation and its downstream targets phase II enzymes HO-1 and NQO1 in Hepa1c1c7 cells (A and B respectively) and BpRc1 cells (C and D respectively) after treatment with 25 µM of **7A4** over a 24 h time period. ß-actin was used as a loading control. Representative blots are shown. E: Quantitative western blot results of Nrf2 and HO-1 up-regulation in **7A4** treated Hepa1c1c7 (light and dark blue bars respectively) and BpRc1 cells (light and dark purple bars respectively). Protein induction levels were expressed as relative ratio's (RR) with ß-actin as a loading control. A RR ratio of 1 corresponds to no protein induction. The error bars represent the standard deviation of n = 2 independent experiments.

7.3.5 Pathway evaluation

ARNT-AhR

The inability of **7A4** to significantly up-regulate NQO1 (and Nrf2 and HO-1) in the ARNT-deficient BpRc1 cell line is suggestive of the involvement of other pathways (i.e. ARNT-AhR) in the induction of this phase II enzyme. As a result, **7A4** treated Hepa1c1c7 cells were examined by western blot analysis for the expression of nuclear AhR and cytoplasmic CYP1A1 proteins. The cells were stimulated with 25 μM **7A4** over a 24 h time period with nuclear and cytoplasmic protein samples taken at 0, 1, 3, 6 and 24 h time intervals. Following **7A4** exposure, Hepa1c1c7 cells demonstrated an increase in AhR nuclear accumulation, which peaked after 1 h (fold induction ~ 4.5) (Figure 7.17 A and C). After 6 h, CYP1A1 expression was observed (fold induction ~ 2.5) that had decreased by 24 h (Figure 7.17 B and C).

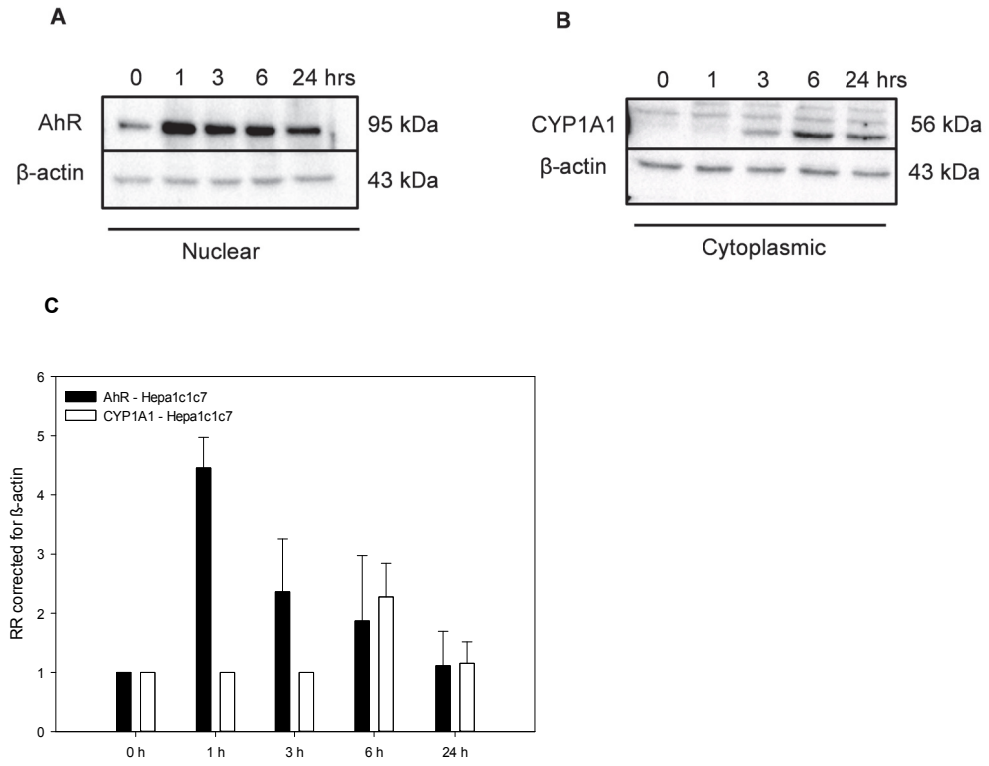

Figure 7.17 A and B: Western blot analysis of nuclear AhR accumulation and its downstream target phase I enzyme CYP1A1 in Hepa1c1c7 cells after treatment with 25 µM of **7A4** (A and B respectively) over a 24 h time period. Representative blots are shown. Figure C: Quantitative western blot results of AhR and CYP1A1 up-regulation in **7A4** treated Hepa1c1c7 cells (black and white bars repetitively). Protein induction levels were expressed as relative ratio's (RR) with ß-actin as a loading control. A RR ratio of 1 corresponds to no protein induction. The error bars represent the standard deviation of n = 2 independent experiments.

A luciferase CYP1A1 enzyme activity assay was carried out to validate the detected CYP1A1 protein induction by **7A4**. Figure 7.18 A shows the luminescence detected following 6 and 24 h treatment of Hepa1c1c7 cells with 25 µM of the **7A4** compound. The amount of observed luminescence is proportional to the amount of CYP1A1 enzyme present. Figure 7.18 B illustrates the calculated fold changes of the different treatments versus the control (vehicle DMSO). The previously described luminescence values for the controls: cells treated with vehicle only (C) and cells treated with 3 µM BaP (P), were included in the graphs for comparison purposes. The absolute luminescence values after 6 and 24 h of exposure to **7A4** were identical. However, the calculated fold-changes demonstrated a higher

CYP1A1 induction value after 6 h (fold induction ~ 3.9) compared to 24 h and (fold induction ~ 1.9). These results confirm western blot observations. Though, the fold-changes detected with the AhR ligand BaP (fold induction ~ 42 after 6 h and ~ 51 after 24 h) are substantially higher than with **7A4**.

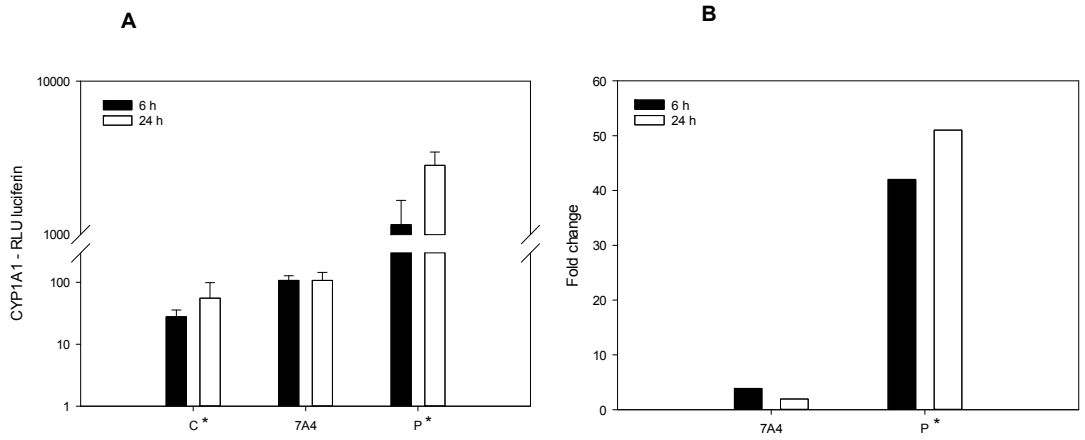

Figure 7.18: CYP1A1 induction measured using the P450 Glo Assay (Promega) following exposure of Hepa1c1c7 cells to vehicle (C), 25 µM **7A4** or 3 µM BaP (P). (A): the quantity of luciferin (RLU) detected is proportional to the extent of CYP1A1 enzyme activity. The error bars represent the standard deviation of n = 8 replicates in a representative experiment. (B): fold changes of **7A4** and BaP versus vehicle control. Data indicated with an * are previously shown data in Section 5.2.5.

ROS production

A flow cytometry based ROS assay was employed to examine whether ROS production occurs in Hepa1c1c7 cells following exposure to **7A4**, which possibly contributes to the nuclear accumulation of Nrf2 and up-regulation of the phase II enzymes HO-1 and NQO1. Cells were treated with 25 µM of **7A4** for 1 h and subsequently stained with CellROX Deep Red reagent (Life Technologies). The fluorescence detected from the CellROX (MFI) probe is proportional to the ROS concentration and is shown in Figure 7.19. The previous described fluorescence values for the blank and negative controls: DMSO (C1) and acetonitrile (C2) and positive control: menadione (M), are included in the graph. As can be observed from Figure 7.19, cellular treatment with **7A4** did not result in an induction of ROS production.

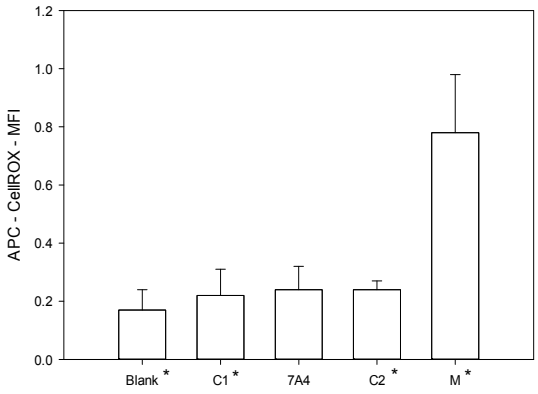

Figure 7.19: ROS production measured using the CellROX Deep Red dye after exposure of Hepa1c1c7 cells) to 25 µM **7A4** or 50 µM menadione (M) for 1 h. As controls, cells were exposed to the **7A4** vehicle, DMSO (C1) and the menadione vehicle, acetonitrile (C2). The amount of fluorescence (APC MFI) detected is proportional to the extent of ROS production. The error bars represent the standard deviation of n = 3 independent experiments. Data indicated with an * are previously shown data in Section 5.2.5.

7.4 Results – Evaluation of small molecules (7B)

7.4.1 NQO1 assay

Screening of compounds

Initially, the 7B structures (n = 14) were examined in an *in vitro* FP assay [101] to evaluate their Keap1-Nrf2 PPI inhibition potencies (performed by Nikolaos Georgakopoulos, UCL School of Pharmacy). Subsequently, the NQO1 induction potency was tested in a cellular NQO1 assay in which Hepa1c1c7 cells were exposed to a fixed dose concentration of 10 μM of each compound. In the fixed dose screen three compounds from group 1 (Table 7.6); **7B1**, **7B8** and **7B9**, and three compounds from group 2 (Table 7.7); **7B11**, **7B13** and **7B14**, were found to up-regulate NQO1 enzyme activity.

Compound selection for further characterisation

As the active molecules from group 2 were poorly soluble, dose response profiles were only created for the compounds from group 1 (Figure 7.20). FP results obtained by our group revealed that **7B1**, **7B8** and **7B9** were potent inhibitors of the Keap1-Nrf2 PPI; IC_{50} = 59 nM, IC_{50} = 143 nM and IC_{50} = 76 nM respectively. The compound **7B1** represents 'compound 2' as developed by Jiang *et al.* [129]. In the cellular NQO1 assay, **7B1** was shown to double the NQO1 induction at a concentration of 4 μM with no detected cytotoxicity up to 10 μM. Compound **7B9** contains two tetrazole substituents in place of the carboxylic acids, and the **7B8** compound contains an amide substituent in place of one of the carboxylate groups. These groups have a lower acidity and higher lipophilicity compared to the carboxylic acid-substituted **7B1**, which should reduce the structure's negative charge at physiological pH and may improve cellular penetration properties. However, **7B9** and **7B8** only showed moderate activity in the NQO1 assay (fold induction ~ 1.8 at 10 μM). Compounds **7B11**, **7B13** and **7B14** were slightly less potent in the FP assay; IC_{50} = 575 nM, IC_{50} = 815 nM and IC_{50} = 677 nM. Nevertheless, NQO1 results suggest that they largely retain their cellular potency; a fold induction of 1.7 for **7B11** and a fold induction of ~ 1.9 for **7B13** and **7B14** were observed at the test concentration of 10 μM.

Table 7.6: NQO1 (in the Hepa1c1c7 cell line) and FP results for group 1 of the 7B compound range.

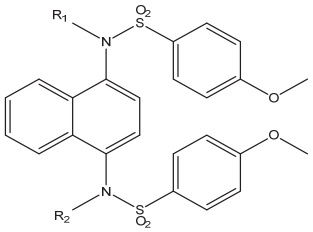

Cpds	R1	R2	FP IC_{50} ± SE (μM)	NQO1[a]	NQO1 CD (μM)	Toxicity NQO1 (μM)
7B1	CH_2CO_2H	CH_2CO_2H	0.059 ± 0.006	2.9	4.0	> 10
7B2	CH_2CO_2Et	CH_2CO_2H	-[b]	1.1	-[b]	> 10
7B3	CH_2CO_2Et	CH_2CO_2Et	-[b]	0.9	-[b]	≥ 10
7B4	CH_2CO_2Et	CH_2CO_2tBu	-[b]	0.8	-[b]	≥ 10
7B5	CH_2CO_2Et	CH_2CONH_2	-[b]	1.2	-[b]	> 10
7B6	CH_2CO_2Et	CH_2CN	-[b]	0.6	-[b]	≥ 10
7B7	CH_2CO_2H	CH_2CN	-[b]	0.8	-[b]	≥ 10
7B8	CH_2CONH_2	CH_2CO_2H	0.143 ± 0.018	1.8	-[b]	> 10
7B9	CH_2CN_4H	CH_2CN_4H	0.076 ± 0.003	1.8	-[b]	> 10

Notes: FP assays performed by Nikolaos Georgakopoulos, UCL School of Pharmacy; a. Fold induction at 10 μM; b. Not determined. Compounds (Cpds).

Table 7.7: NQO1 (in the Hepa1c1c7 cell line) and FP results for group 2 of the 7B compound range.

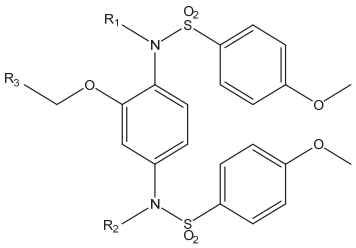

Cpds	R1	R2	R3	FP IC_{50} ± SE (μM)	NQO1[a]	NQO1 CD (μM)	Toxicity NQO1 (μM)
7B10	CH_2CO_2Et	CH_2CO_2Et	C_6H_5	-[b]	1.0	-[b]	-[b]
7B11	CH_2CO_2H	CH_2CO_2H	C_6H_5	0.575 ± 0.072	1.7	-[b]	-[b]
7B12	CH_2CO_2Et	CH_2CO_2Et	Me	-[b]	0.9	-[b]	≥ 10
7B13	CH_2CO_2H	CH_2CO_2H	Me	0.815 ± 0.06	1.9	-[b]	-[b]
7B14	CH_2CO_2H	CH_2CO_2H	Pr	0.677 ± 0.059	1.95	-[b]	-[b]

Notes: FP assays performed by Nikolaos Georgakopoulos, UCL School of Pharmacy; a. Fold induction at 10 μM; b. Not determined. Compounds (Cpds).

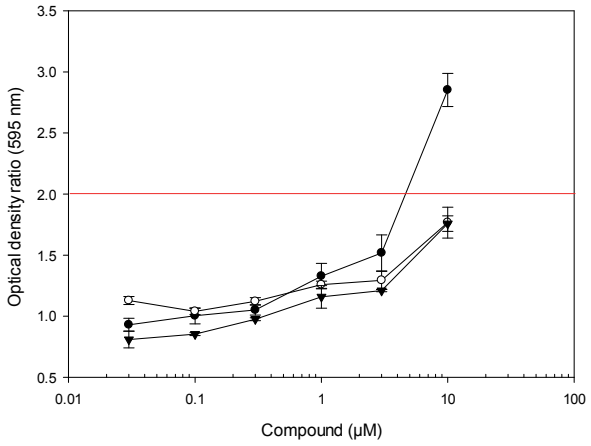

Figure 7.20: Dose response curves for the NQO1 assays of compounds **7B1** (●), **7B8** (▼) and **7B9** (○) in Hepa1c1c7 after 24 h stimulation. The red line indicates a doubling of NQO1 activity (CD value). The error bars represent the standard deviation of n = 4 replicates in a representative experiment.

7.5 Results – Evaluation of small molecules (7C)

7.5.1 NQO1 assay

First, 7C compounds were screened *in vitro* using an FP assay [101] to examine their ability to disrupt the Keap1-Nrf2 PPI (performed by Helene Bertrand and Adrian Fowkes, UCL School of Pharmacy). Next, the structures were subjected to a cellular screen in which their induction capabilities for the Nrf2 dependent NQO1 enzyme were evaluated. Initially, the compounds were tested at a fixed concentration of 10 μM. Dose response profiles were created for compounds that demonstrated a good NQO1 induction potency. Tables 7.8 – 7.24 list the tested compounds and their corresponding FP and NQO1 results.

Screening of compounds

The first group to be screened in the NQO1 assay were the 1,2,4-triazole derivatives (n = 7) (Table 7.8). These compounds were poor inhibitors of the Keap1-Nrf2 PPI in the FP assay and were not able to up-regulate the NQO1 enzyme.

Table 7.8: NQO1 (in the Hepa1c1c7 cell line) and FP results for the 1,2,4 – triazole derivatives.

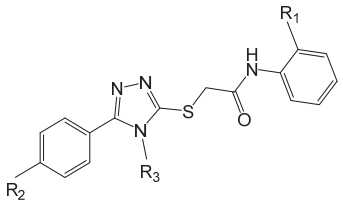

Cpds	R1	R2	R3	R4	FP[a]	NQO1[b]	NQO1 CD (μM)	Toxicity NQO1 (μM)
7C1	NO_2	NO_2	CH_3	C	14.6	1.0	-[c]	> 10
7C2	CO_2H	NO_2	CH_3	C	13.4	1.0	-[c]	-[c]
7C3	NO_2	CO_2H	CH_3	C	14.9	1.0	-[c]	-[c]
7C4	NO_2	NO_2	C_6H_5	C	12.7	1.0	-[c]	-[c]
7C5	CO_2H	NO_2	C_6H_5	C	10.5	1.0	-[c]	-[c]
7C6	NO_2	H	H	S	6.3	1.0	-[c]	> 10
7C7	CO_2H	H	H	S	9.6	1.0	-[c]	-[c]

Notes: FP assays performed by Helene Bertrand, UCL School of Pharmacy; a. Percentage inhibition at 100 μM; b. Fold induction at 10 μM; c. Not determined. Compounds (Cpds).

Subsequently, a first library of 1,2,3-triazole derivatives (n = 36) was studied, which was synthesised from a series of ethynyl- and azido-benzene intermediates with nitro, carboxylic acid or carboxamide functional groups (Table 7.9, group 1.1). This library presented a diverse range in activity in both the FP and NQO1 assay. The most promising activities were observed with molecules containing an R1/R2 – NO_2 and R3/R4 – NO_2 or R1/R2 – NO_2 and R3/R4 – $CONH_2$ or R1/R2 – $CONH_2$ and R3/R4 – NO_2 groups. However, some carboxamide substituents demonstrated fluorescence interference in the FP assay. Several structures containing carboxyl substituents were active in the FP assay, but not in the NQO1 assay possibly due to their negative charge at physiological pH and thus poor cell-penetrating capabilities.

Table 7.9: NQO1 (in the Hepa1c1c7 cell line) and FP results for group 1.1 of the 1,2,3-triazole derivatives.

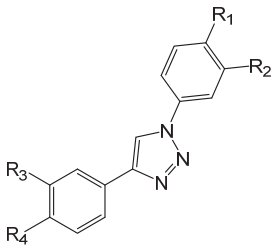

Cpds	R1/R2	R3/R4	FP[a]	FP IC_{50} (μM)	NQO1[b]	NQO1 CD (μM)	Toxicity NQO1 (μM)
7C8	R1 - NO_2	R4 - NO_2	72.6	8.7	1.0	-[c]	-[c]
7C9	R2 - NO_2	R4 - NO_2	46.5	-[c]	1.8	-[c]	-[c]
7C10	R1 - NO_2	R3 - NO_2	74.8	8.8	3.4	0.2	> 10
7C11	R2 - NO_2	R3 - NO_2	81	11.5	2.3	~ 10	> 10
7C12	R1 - CO_2H	R4 - NO_2	81.3	50.1	1.0	-[c]	-[c]
7C13	R2 - CO_2H	R4 - NO_2	61	-[c]	0.7	-[c]	≥ 10
7C14	R1 - CO_2H	R3 - NO_2	39.4	-[c]	1.0	-[c]	-[c]
7C15	R2 - CO_2H	R3 - NO_2	80.1	-[c]	0.8	-[c]	≥ 10
7C16	R1 - NO_2	R4 - CO_2H	83.8	16.7	0.9	-[c]	≥ 10
7C17	R2 - NO_2	R4 - CO_2H	87.5	21.1	1.1	-[c]	-[c]
7C18	R1 - NO_2	R3 - CO_2H	82.3	62.7	1.1	-[c]	-[c]
7C19	R2 - NO_2	R3 - CO_2H	63.8	-[c]	0.8	-[c]	≥ 10
7C20	R1 - $CONH_2$	R4 - NO_2	46.1	-[c]	1.1	-[c]	-[c]
7C21	R2 - $CONH_2$	R4 - NO_2	62.2	-[c]	1.0	-[c]	-[c]
7C22	R1 - $CONH_2$	R3 - NO_2	64.5	-[c]	2.1	10	> 10
7C23	R2 - $CONH_2$	R3 - NO_2	65.3	-[c]	2.1	7.7	≥ 30
7C24	R1 - NO_2	R4 - $CONH_2$	-23.3	-[c]	1.0	-[c]	-[c]
7C25	R2 - NO_2	R4 - $CONH_2$	2.34	-[c]	1.3	-[c]	-[c]
7C26	R1 - NO_2	R3 - $CONH_2$	48	-[c]	1.1	-[c]	-[c]
7C27	R2 - NO_2	R3 - $CONH_2$	32	-[c]	2.1	10	≥10
7C28	R1 - $CONH_2$	R4 - CO_2H	76.5	182.4	1.0	-[c]	-[c]
7C29	R1 - $CONH_2$	R3 - CO_2H	87.9	16	1.0	-[c]	-[c]
7C30	R1 - $CONH_2$	R4 - $CONH_2$	-159.1	-[c]	1.0	-[c]	-[c]
7C31	R2 - $CONH_2$	R3 - CO_2H	96.3	45.6	1.0	-[c]	-[c]
7C32	R2 - $CONH_2$	R4 - $CONH_2$	43.7	-[c]	1.0	-[c]	-[c]
7C33	R2 - $CONH_2$	R4 - CO_2H	15.4	-[c]	1.0	-[c]	-[c]
7C34	R1 - $CONH_2$	R3 - $CONH_2$	-44.7	-[c]	1.0	-[c]	-[c]
7C35	R2 - $CONH_2$	R3 - $CONH_2$	53.3	-[c]	1.0	-[c]	-[c]
7C36	R1 - CO_2H	R4 - CO_2H	77.3	23.6	1.0	-[c]	-[c]
7C37	R1 - CO_2H	R4 - $CONH_2$	-20.4	-[c]	1.0	-[c]	-[c]
7C38	R1 - CO_2H	R3 - CO_2H	92.8	50	1.0	-[c]	-[c]
7C39	R1 - CO_2H	R3 - $CONH_2$	70.7	14.6	1.0	-[c]	-[c]
7C40	R2 - CO_2H	R4 - CO_2H	89.6	49.1	1.0	-[c]	-[c]
7C41	R2 - CO_2H	R4 - $CONH_2$	-23.4	-[c]	1.0	-[c]	-[c]
7C42	R2 - CO_2H	R3 - CO_2H	82.3	51	1.0	-[c]	-[c]
7C43	R2 - CO_2H	R3 - $CONH_2$	78.6	18.6	1.0	-[c]	-[c]

Notes: FP assays performed by Helene Bertrand, UCL School of Pharmacy; a. Percentage inhibition at 100 μM; b. Fold induction at 10 μM; c. Not determined. Compounds (Cpds).

The second library containing 16 compounds (Table 7.10, group 1.2) was designed based on these findings; the R3 NO_2 group was fixed and the R1 and R2 groups were varied (Table 7.9, group 1.1). Most compounds were active in both assays, apart from the fluorine substituted **7C52** and cyano substituted **7C57** that were less active in the FP assay. The iodine containing compound **7C55** was one of the most potent compounds in this series, demonstrating a low IC_{50} value in the FP assay and a CD value of 0.6 μM in the NQO1 assay.

Table 7.10: NQO1 (in the Hepa1c1c7 cell line) and FP results for group 1.2 of the 1,2,3-triazole derivatives.

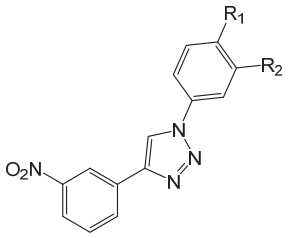

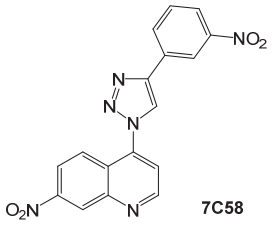

7C58

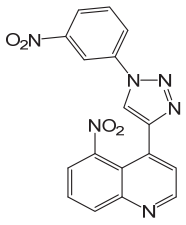

7C59

Cpds	R1/R2/R3	FP[a]	FP IC_{50} (μM)	NQO1[b]	NQO1 CD (μM)	Toxicity NQO1 (μM)
7C44	H	66.9	20.6	2.0	10	> 10
7C45	R2 – CH_3	68.9	10	2.2	1.3	> 10
7C46	R2 – tBu	69.8	37.8	1.9	-[c]	-[c]
7C47	R2 – OCH_3	68.2	15	2.6	4.7	> 100
7C48	R2 – OCH_2CH_3	69.3	11.3	2.5	-[c]	-[c]
7C49	R1/2 -OCH_2O-	67.2	15	2.2	-[c]	-[c]
7C50	R2 – SCH_3	77.7	38.5	3.0	-[c]	-[c]
7C51	R2 – $N[CH_3]_2$	65.4	12.7	2.9	2.0	≥ 10
7C52	R2 – F	42.6	-[c]	2.3	-[c]	-[c]
7C53	R2 – Cl	60.4	8.8	2.5	0.8	> 10
7C54	R2 - Br	68.2	24.5	2.9	1.2	> 100
7C55	R2 – I	67.2	7.1	4.0	0.6	> 10
7C56	R2 – CF_3	66.9	22.6	2.5	-[c]	-[c]
7C57	R2 – CN	36.8	-[c]	2.0	10	> 10
7C58		16.5	-[c]	1.8	-[c]	-[c]
7C59		-16.5	-[c]	1.7	-[c]	-[c]

Notes: FP assays performed by Helene Bertrand, UCL School of Pharmacy; a. Percentage inhibition at 100 μM; b. Fold induction at 10 μM; c. Not determined. Compounds (Cpds).

A small third library of compounds with a tetrazole substituent (n = 8) at the R3 position was developed as an alternative to the carboxylic acid or nitro group in that position, which previous showed promising activity in the FP assay but not in the cellular assay (Table 7.12, group 1.3b). It was hypothesised that the less acidic and more lipophilic tetrazole groups would favour cell penetration. The synthesis of the

tetrazole compounds was performed from a cyano group; hence this series of compounds with a cyano group at the R3 position (n = 5) were also tested (Table 7.11 group 1.3a). However, neither of the two compound groups exhibited an improvement in cellular activity.

Table 7.11: NQO1 (in the Hepa1c1c7 cell line) and FP results for group 1.3a of the 1,2,3-triazole derivatives.

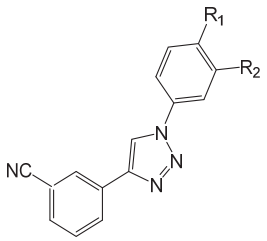

Cpds	R1/R2	FP[a]	FP IC_{50} (μM)	NQO1[b]	NQO1 CD (μM)	Toxicity NQO1 (μM)
7C60	R2 – OCH_2CH_3	24.5	-[c]	1.3	-[c]	-[c]
7C61	R2 – Cl	19.9	-[c]	2.0	10	≥ 10
7C62	R2 – I	21.9	-[c]	1.5	-[c]	-[c]
7C63	R1 - CO_2H	52.8	1.6	1.0	-[c]	-[c]
7C64	R2 – CN	58.8	46.2	1.9	-[c]	-[c]

Notes: FP assays performed by Helene Bertrand, UCL School of Pharmacy; a. Percentage inhibition at 100 μM; b. Fold induction at 10 μM; c. Not determined. Compounds (Cpds).

Table 7.12: NQO1 (in the Hepa1c1c7 cell line) and FP results for group 1.3b of the 1,2,3-triazole derivatives.

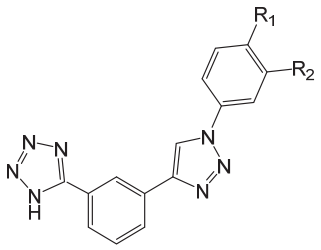

Cpds	R1/R2	FP[a]	FP IC_{50} (μM)	NQO1[b]	NQO1 CD (μM)	Toxicity NQO1 (μM)
7C65	R2 – CH_3	30.4	-[c]	0.9	-[c]	-[c]
7C66	R2 – OCH_2CH_3	39.6	-[c]	1.3	-[c]	-[c]
7C67	R2 – Cl	40.7	-[c]	1.2	-[c]	-[c]
7C68	R2 – I	51.5	-[c]	0.4	-[c]	≥ 10
7C69	R2 - NO_2	71.1	51.4	1.8	-[c]	-[c]
7C70	R1 - CO_2H	70	63.7	1.0	-[c]	-[c]
7C71	R2 – CHN_4	13.7	-[c]	0.8	-[c]	≥ 10
7C72	R1 - *	74.2	15.8	1.0	-[c]	-[c]

Notes: FP assays performed by Helene Bertrand, UCL School of Pharmacy; a. Percentage inhibition at 100 μM; b. Fold induction at 10 μM; c. Not determined; * R1/R3 – CO2CH2CH2-(N-morpholine). Compounds (Cpds).

The structures in Table 7.13 contain an additional R5 group compared to the structures described in Table 7.9. Compounds **7C77**, **7C78** and **7C79** have a similar core structure but differ from each other by their R5 group; **7C78** and **7C79** contain a $CH{=}CHCH_2OCH_3$ and a $C{\equiv}CCH_2OH$ R5 group respectively, whereas **7C77** has an iodide at this position. Their cellular activity appears to be related to the size of their R5 group; **7C77** displays a CD value of 0.9 μM, whereas **7C79** and **7C78** demonstrate CD values of 4 μM and 40 μM respectively. Moreover, FP results reveal a high level of inhibition at 10 μM for **7C77**, but **7C78** caused fluorescence interference in the assay. It is possible that the bulky R5 groups of **7C79** and **7C78** may cause stearic hindrance in the Keap1 binding pocket and decrease the inhibition potential of the compounds. The sulphonamide/sulphone-containing compounds **7C81**-**7C85** generally showed reasonable inhibitory activity in the fixed dose FP assay, but did not induce NQO1 activity at the lower test concentration.

Table 7.13: NQO1 (in the Hepa1c1c7 cell line) and FP results for group 1.4 of the 1,2,3-triazole derivatives.

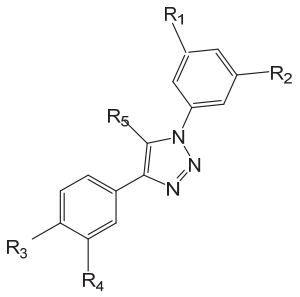

Cpds	R1	R2	R3	R4	R5	FP[a]	NQO1[b]	NQO1[c]	NQO1 CD (μM)	Tox. NQO1 (μM)
7C73	NO_2	H	H	*	H	22	-[d]	3.2	1.5	> 10
7C74	Br	H	NO_2	CH_2OH	H	43.1	-[d]	1.0	-[d]	-[d]
7C75	Br	CH_2OH	NO_2	H	H	40	1.4	2.2	10	> 100
7C76	CN	H	NO_2	H	I	62.1	1.1	-[d]	-[d]	-[d]
7C77	CN	H	H	NO_2	I	97[a1]	2.1	2.2	0.9	> 10
7C78	CN	H	H	NO_2	**	[a2]	1.1	1.6	40	> 100
7C79	CN	H	H	NO_2	***	-[d]	1.5	2.7	4.0	> 10
7C80	CN	H	H	*	H	24.2	1.0	-[d]	-[d]	≥ 3.0
7C81	CN	H	H	SO_2NH_2	H	52.0	-[d]	1.0	-[d]	-[d]
7C82	SO_2NH_2	H	H	SO_2NH_2	H	52	1.0	1.0	-[d]	-[d]
7C83	SO_2NH_2	H	H	CO_2H	H	-[d]	-[d]	1.0	-[d]	-[d]
7C84	SO_2NH_2	H	H	CN	H	54.6	-[d]	1.0	-[d]	-[d]
7C85	SO_2CH_3	H	H	CN	H	50.3	-[d]	1.1	-[d]	-[d]

Notes: FP assays performed by Adrian Fowkes, UCL School of Pharmacy; a. Percentage inhibition at 100 μM; a[1]. Percentage inhibition at 10 μM; a[2].fluorescence interference; b. Fold induction at 1 μM; c. Fold induction at 10 μM; d. Not determined; *$CO_2CH_2CH_2$ N-morpholino. ** $CH=CHCH_2OCH_3$ *** $C\equiv CCH_2OH$. Compounds (Cpds).

The structures in Table 7.14 are dimers of the core structure in Table 7.10. Although, these compounds showed promising inhibition potencies in the FP assay, none of them were active in cell-based assays.

Table 7.14: NQO1 (in the Hepa1c1c7 cell line) and FP results for group 1.5 of the 1,2,3-triazole derivatives.

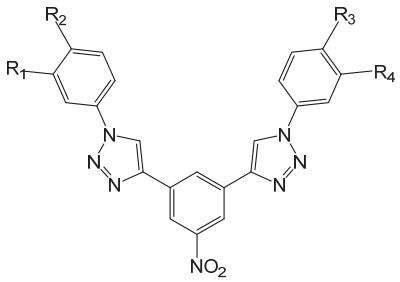

Cpds	R1+R4	R2+R3	FP[a]	NQO1[b]	NQO1[c]	NQO1 CD (μM)	Toxicity NQO1 (μM)
7C86	OCH_3	H	66	1.0	-[d]	-[d]	-[d]
7C87	I	H	69	1.0	-[d]	-[d]	-[d]
7C88	CO_2H	H	74	1.0	-[d]	-[d]	-[d]
7C89	$CONH_2$	H	70	1.0	-[d]	-[d]	-[d]
7C90	H	$CONH_2$	66	1.0	-[d]	-[d]	-[d]

Notes: FP assays performed by Adrian Fowkes, UCL School of Pharmacy; a. Percentage inhibition at 100 μM; b. Fold induction at 1 μM; c. Fold induction at 10 μM; d. Not determined. Compounds (Cpds).

Group 2 (n = 20) contains a range of 1,2,3-triazole derived structures that incorporate a spacer between the triazole and one of the phenyl rings (Table 7.15 – 7.19, group 2.1 – 2.5). Compounds **7C91** and **7C92**, **7C93** and **7C94** have a methylene spacer at the 1-position of the triazole, whereas the compounds in Table 7.17 – 7.19 incorporate a spacer unit at the triazole 4-position. These molecules were designed to evaluate the positioning of the functional groups that form hydrogen bonds with amino acid residues in the binding pocket of the Keap1 protein. Although some compounds showed moderate potency in either or both FP and NQO1 assays, the overall activity was not improved from the structures in group 1.2.

Table 7.15: NQO1 (in the Hepa1c1c7 cell line) and FP results for group 2.1 of the 1,2,3-triazole derivatives.

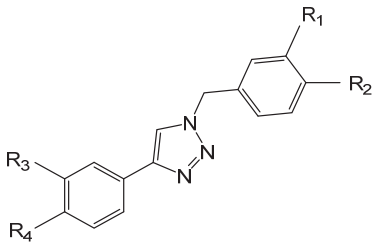

Cpds	R1/R2	R3/R4	FP[a]	NQO1[b]	NQO1 CD (μM)	Toxicity NQO1 (μM)
7C91	R1 - NO_2	R3 - NO_2	47.2	1.0	-[c]	-[c]

Notes: FP assays performed by Helene Bertrand, UCL School of Pharmacy; a. Percentage inhibition at 100 μM; b. Fold induction at 10 μM; c. Not determined. Compounds (Cpds).

Table 7.16: NQO1 (in the Hepa1c1c7 cell line) and FP results for group 2.2 of the 1,2,3-triazole derivatives.

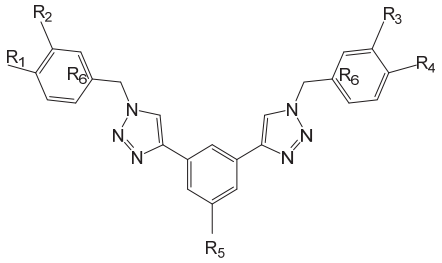

Cpds	R1+R4	R2+R3	R5	R6	FP[a]	NQO1[b]	NQO1[c]	NQO1 CD (μM)	Toxicity NQO1 (μM)
7C92	H	NO_2	NO_2	C	69	1.0	-[d]	-[d]	-[d]
7C93	H	SO_2	CO_2H	N	77.6	1.0	1.1	-[d]	-[d]
7C94	H	SO_2	$CO_2CH_2O_2CCH_3$	N	-[d]	1.0	1.0	-[d]	-[d]

Notes: FP assays performed by Adrian Fowkes, UCL School of Pharmacy; a. Percentage inhibition at 100 μM; b. Fold induction at 1 μM; c. Fold induction at 10 μM; d. Not determined. Compounds (Cpds).

Table 7.17: NQO1 (in the Hepa1c1c7 cell line) and FP results for group 2.3 of the 1,2,3-triazole derivatives.

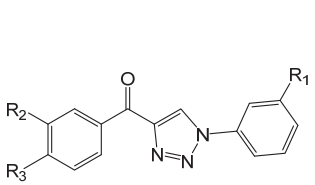

1

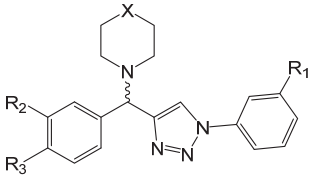

2

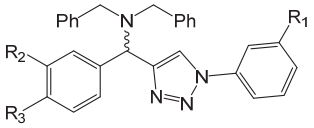

3

Cpds	Structure type	R1	R2/R3	FP[a]	FP IC_{50} (μM)	NQO1[b]	NQO1[c]	NQO1 CD (μM)	Toxicity NQO1 (μM)
7C95	1	NO_2	R2 - NO_2	40.3	-[c]	-[d]	2.2	1.0	> 3.0
7C96	1	NO_2	R2 - CO_2H	74.8	8.1	-[d]	1.0	-[d]	-[d]
7C97	1	CO_2H	R2 - CO_2H	78.8	9.6	-[d]	1.0	-[d]	-[d]
7C98	1	$CONH_2$	R2 - CO_2Me	10.0	-[c]	-[d]	1.2	-[d]	-[d]
7C99	1	CN	R2 - CO_2Me	-5.9	-[c]	-[d]	1.1	-[d]	-[d]
7C100	1	NO_2	R2 - CO_2Me	-51.3	-[c]	-[d]	2	10	> 10
7C101	2 (X = CH_2)	CO_2H	H						
7C102	2 (X = CH_2)	NO_2	R2 - NO_2	-0.2	-[c]	-[d]	1.8	-[d]	-[d]
7C103	2 (X = CH_2)	NO_2	R3 - Cl	-21.4	-[c]	-[d]	1.7	-[d]	-[d]
7C104	2 (X =S)	NO_2	R3 - CH_3O	54.4	11.1	1.0	1.3	-[d]	-[d]
7C105	3	NO_2	H	-9.8	-[c]	-[d]	1.0	-[d]	-[d]

Notes: FP assays performed by Helene Bertrand, UCL School of Pharmacy; a. Percentage inhibition at 100 μM; b. Fold induction at 1 μM; c. Fold induction at 10 μM; d. Not determined. Compounds (Cpds).

Table 7.18: NQO1 (in the Hepa1c1c7 cell line) and FP results for group 2.4 of the 1,2,3-triazole derivatives.

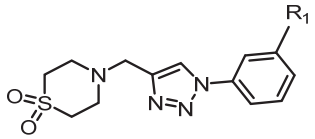

Cpds	R1	FP[a]	FP IC_{50} (μM)	NQO1[b]	NQO1[c]	NQO1 CD (μM)	Toxicity NQO1 (μM)
7C106	CO_2H	56.9	1.34	1.0	-[d]	-[d]	-[d]
7C107	$CO_2CH_2O_2CCH_3$	-[d]	-[d]	1.0	1.0	-[d]	-[d]
7C108	NO_2	62.3	10	1.0	1.0	-[d]	-[d]

Notes: FP assays performed by Adrian Fowkes, UCL School of Pharmacy; a. Percentage inhibition at 100 μM; b. Fold induction at 1 μM; c. Fold induction at 10 μM; d. Not determined. Compounds (Cpds).

Table 7.19: NQO1 (in the Hepa1c1c7 cell line) and FP results for group 2.5 of the 1,2,3-triazole derivatives.

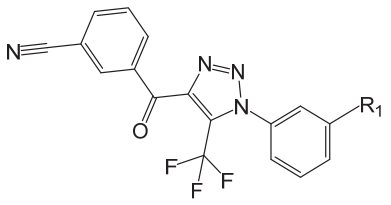

Cpds	R1	FP[a]	NQO1[b]	NQO1[c]	NQO1 CD (μM)	Toxicity NQO1 (μM)
7C109	NO_2	a1	-[d]	1.0	-[d]	-[d]
7C110	SO_2Me	16.6	-[d]	1.0	-[d]	-[d]

Notes: FP assays performed by Adrian Fowkes, UCL School of Pharmacy; a. Percentage inhibition at 100 μM; a1. Fluorescence interference; b. Fold induction at 1 μM; c. Fold induction at 10 μM; d. Not determined. Compounds (Cpds).

The structures in group 3 (n = 12) contain an imidazole heterocycle, which was not particularly active in either FP or NQO1 assays (Table 7.20 – 7.23, group 3.1 – 3.4). An exception to the poor activity is demonstrated by compound **7C116**, which showed negative values in the FP assay (possibly due to fluorescence interference), but was highly potent in the NQO1 assay, CD ~ 0.6 μM.

Table 7.20: NQO1 (in the Hepa1c1c7 cell line) and FP results for group 3.1 of the 1,2,3-triazole derivatives.

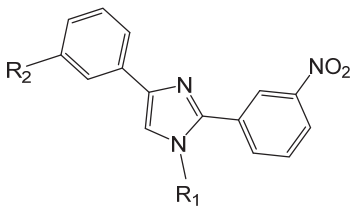

Cpds	R1	R2	FP[a]	NQO1[b]	NQO1 CD (μM)	Toxicity NQO1 (μM)
7C111	H	NO_2	8.6	1.9	-[c]	-[c]
7C112	CH_3	NO_2	19.7	2.2	10	> 10
7C113	C_6H_5	NO_2	-14.1	2.0	10	> 10
7C114	H	CO_2Me	18.4	1.5	-[c]	-[c]
7C115	CH_3	CO_2Me	8.5	1.0	-[c]	-[c]

Notes: FP assays performed by Helene Bertrand, UCL School of Pharmacy; a. Percentage inhibition at 100 μM; b. Fold induction at 10 μM; c. Not determined. Compounds (Cpds).

Table 7.21: NQO1 (in the Hepa1c1c7 cell line) and FP results for group 3.2 of the 1,2,3-triazole derivatives.

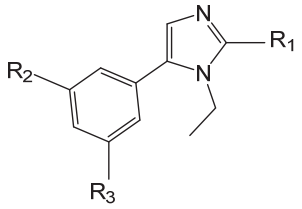

Cpds	R1	R2/R3	FP[a]	NQO1[b]	NQO1 CD (μM)	Toxicity NQO1 (μM)
7C116	$C_6H_5NO_2$	R2 - NO_2	-53.1	2.4	0.6	≥ 10
7C117	H	R3 - NO_2	8.6	1.2	-[c]	-[c]

Notes: FP assays performed by Helene Bertrand, UCL School of Pharmacy; a. Percentage inhibition at 100 μM; b. Fold induction at 10 μM; c. Not determined. Compounds (Cpds).

Table 7.22: NQO1 (in the Hepa1c1c7 cell line) and FP results for group 3.3 of the 1,2,3-triazole derivatives.

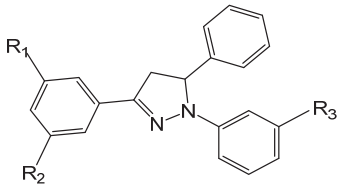

Cpds	R1/R2	R3	FP[a]	NQO1[b]	NQO1[c]	NQO1 CD (μM)	Toxicity NQO1 (μM)
7C118	R1 - Cl	NO_2	a1	-[d]	1.0	-[d]	-[d]
7C119	R1 - Cl	Cl	a1	1.1	-[d]	-[d]	-[d]
7C120	R1 - CN	NO_2	a1	-[d]	1.2	-[d]	-[d]

Notes: FP assays performed by Adrian Fowkes, UCL School of Pharmacy; a. Percentage inhibition at 100 μM; a1. Fluorescence interference; b. Fold induction at 1 μM; c. Fold induction at 10 μM; d. Not determined Compounds (Cpds).

Table 7.23: NQO1 (in the Hepa1c1c7 cell line) and FP results for group 3.4 of the 1,2,3 – triazole derivatives.

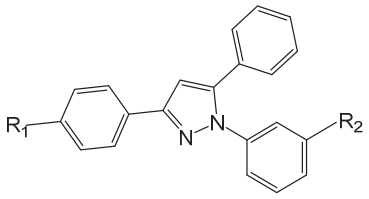

Cpds	R1	R2	FP[a]	NQO1[b]	NQO1 CD (µM)	Toxicity NQO1 (µM)
7C121	Cl	NO_2	a1	1.2	- [c]	- [c]
7C122	NO_2	Cl	a1	1.0	- [c]	- [c]

Notes: FP assays performed by Adrian Fowkes, UCL School of Pharmacy; a. Percentage inhibition at 100 µM; a1. Fluorescence interference; b. Fold induction at 10 µM; c. Not determined. Compounds (Cpds).

The quinolone-based structures in group 4 (n = 8) (Table 7.24) showed generally a large amount of fluorescence interference in the FP assay, but revealed high potency in the NQO1 assay. However, the compounds are structurally similar to AhR ligands [233] and tyrosine kinase inhibitors [234]. Hence, it may be unlikely that the molecules induced the NQO1 enzyme via the Keap1-Nrf2 pathway.

Table 7.24: NQO1 (in the Hepa1c1c7 cell line) and FP results for group 4 of the 1,2,3-triazole derivatives.

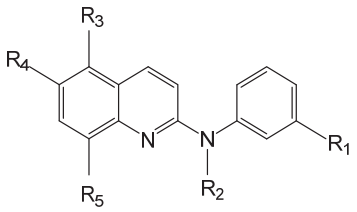

Cpds	R1	R2	R3/R4/R5	FP[a]	NQO1[b]	NQO1 CD (µM)	Toxicity NQO1 (µM)
7C123	NO_2	H	R5 - NO_2	-0.7	1.0	-[c]	-[c]
7C124	NO_2	H	R3 - NO_2	11.2	3.9	0.3	> 100
7C125	NO_2	H	R4 - NO_2	100.2	3.5	1.0	> 10
7C126	NO_2	C_2H_5O	R5 – NO_2	5.2	1.5	- [c]	- [c]
7C127	NO_2	C_2H_5O	R3 – NO_2	5.0	3.5	1.0	> 100
7C128	NO_2	C_2H_5O	R4 – NO_2	0.6	3.6	-[c]	-[c]
7C129	CO_2Me	H	R3 - NO_2	-26.6	3.8	-[c]	-[c]
7C130	CO_2H	H	R4 - NO_2	-10.1	1.9	- [c]	- [c]

Notes: FP assays performed by Helene Bertrand, UCL School of Pharmacy; a. Percentage inhibition at 100 µM; b. Fold induction at 10 µM; c. Not determined. Compounds (Cpds).

Compound selection for further characterisation

Four compounds from group 1.1 and 1.2 demonstrating different activity in the FP and NQO1 assays were selected for further evaluation (Figure 7.21 A). **7C33** showed only a low inhibition in the FP assay (~ 15% inhibition at 100 μM) and no NQO1 induction in the cellular assay. **7C46** was able to displace the fluorescent Nrf2 peptide with an IC_{50} of 37.8 μM and revealed a slight NQO1 induction (fold change ~ 1.9 at 10 μM). **7C45** demonstrated an improved IC_{50} of 10 μM in the FP assay and a moderate activity in the NQO1 assay (CD ~ 1.3 μM). **7C55** was the most promising molecule; presenting an IC_{50} of 7.1 μM in the FP assay and a doubling of NQO1 activity at 0.6 μM. Dose response profiles were created in both Hepa1c1c7 and BpRc1 cells for the two most potent compounds **7C45** and **7C55** (Figure 7.21 B and C respectively). Neither of the two structures was able to up-regulate the NQO1 enzyme in the ARNT-deficient BpRc1 cell line.

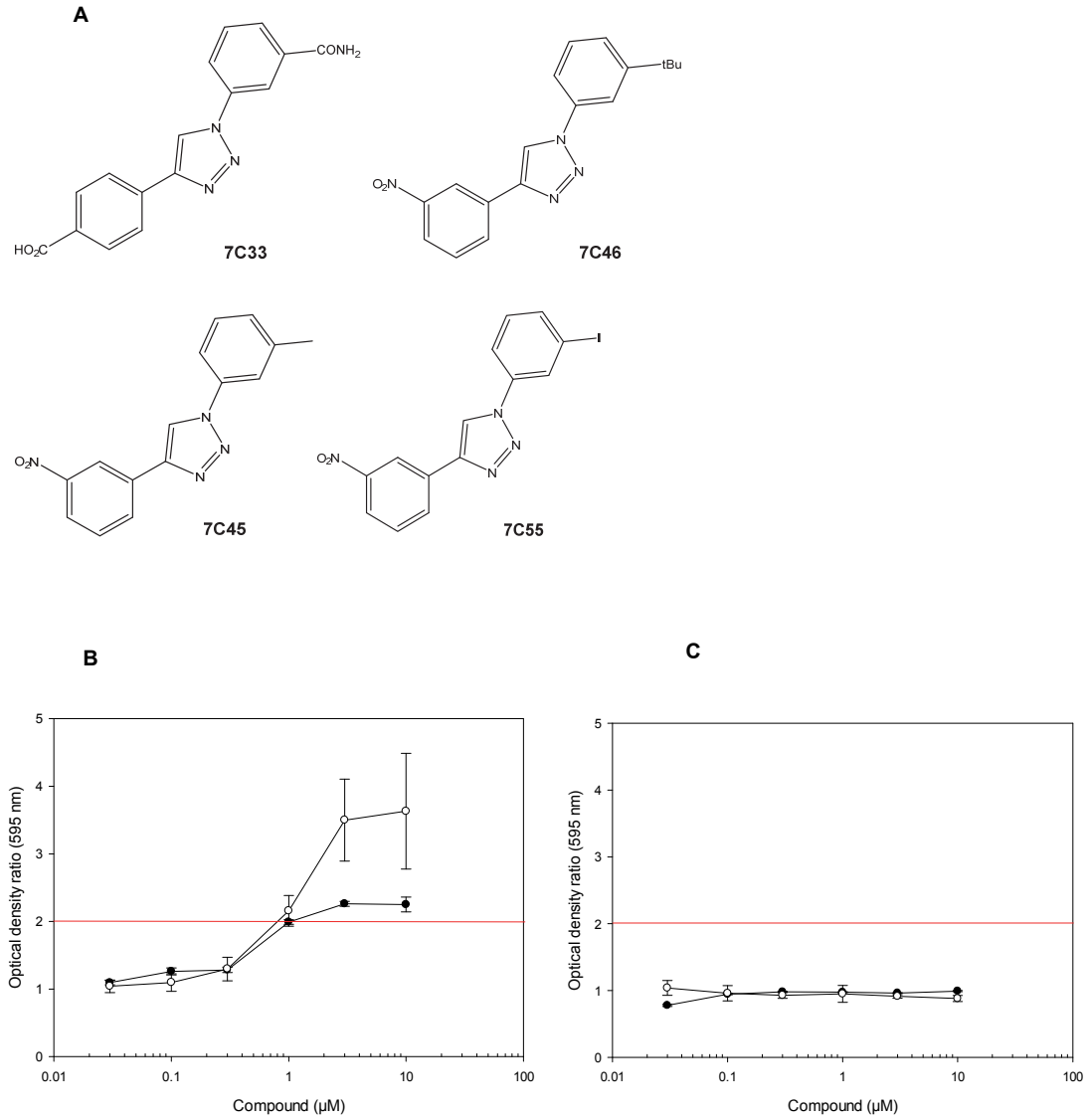

Figure 7.21: Chemical structures of compounds **7C33**, **7C46**, **7C45** and **7C55** (A) and dose response curves for the NQO1 assays of compounds **7C45** (●) and **7C55** (○) in Hepa1c1c7 (B) and BpRc1 (C) after 24 h stimulation. The red line indicates a doubling of NQO1 activity (CD value). The error bars represent the standard deviation of n = 3 independent experiments.

7.5.2 SRB assay

No decrease in NQO1 induction was observed at concentrations up to 10 μM of the **7C55** compound in the cell-based NQO1 induction assay, which therefore indicates no cytotoxicity. Hepa1c1c7, BpRc1 and HeLa cells were exposed for 24 and 48 h to **7C55** at concentrations up to 250 μM (in 1% DMSO final concentration) to evaluate potential cytotoxicity in an SRB assay. No cytotoxicity was detected up to 250 μM after 24 and 48 h in either of the cell lines (Figure 7.22 A and B respectively). For consistency purposes, all subsequent experiments with **7C55** were carried out at a concentration of 10 μM.

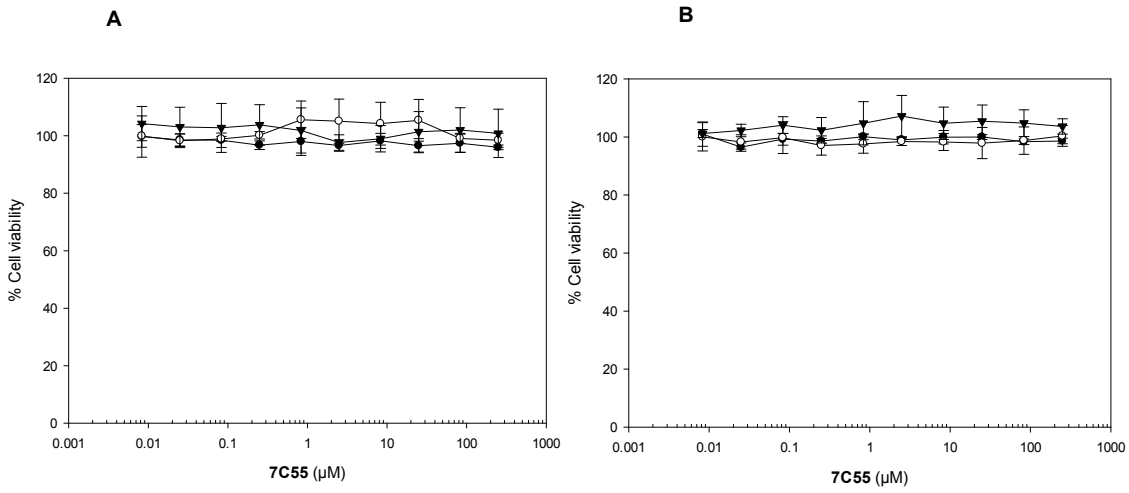

Figure 7.22: Dose response curves for the SRB assays of **7C55** in Hepa1c1c7 (●), BpRc1 (○) and HeLa cells (▼) after 24 h (A) and 48 h (B) stimulation. Cell viability is calculated as a percentage of cells treated with vehicle only. Error bars are based on n = 4 replicates in a representative experiment.

7.5.3 Western blotting

Western blot analysis was used to verify whether **7C55** can activate the nuclear accumulation of Nrf2 and expression of Nrf2 regulated proteins HO-1 and NQO1 in Hepa1c1c7 and BpRc1 cells. Cells were exposed to 10 μM **7C55** over 24 h before samples were extracted after 1, 3, 6 and 24 h and separated into cytoplasmic and nuclear protein fractions. Treatment with **7C55** resulted in an increase of Nrf2 accumulation in Hepa1c1c7 cells that was time dependent; the protein induction was maximal between 3 – 6 h (fold induction ~ 3 and 5 respectively) (Figure 7.23 A and E). However, Nrf2 induction in BpRc1 cells was barely detected (fold induction < 1.5) (Figure 7.23 C and E). Up-regulation of the expression of downstream target protein HO-1 was also promoted by **7C55**; showing a peak HO-1 induction after 6 h in Hepa1c1c7 cells (fold induction ~ 9) (Figure 7.23 B and E), but a reduced maximum induction after 3 h in BpRc1 cells (fold induction ~ 2) (Figure 7.23 D and E). Induction of the other phase II enzyme, NQO1, was only observed after 24 h in Hepa1c1c7 cells, but was undetectable in BpRc1 cells (Figure 7.23 B and D respectively).

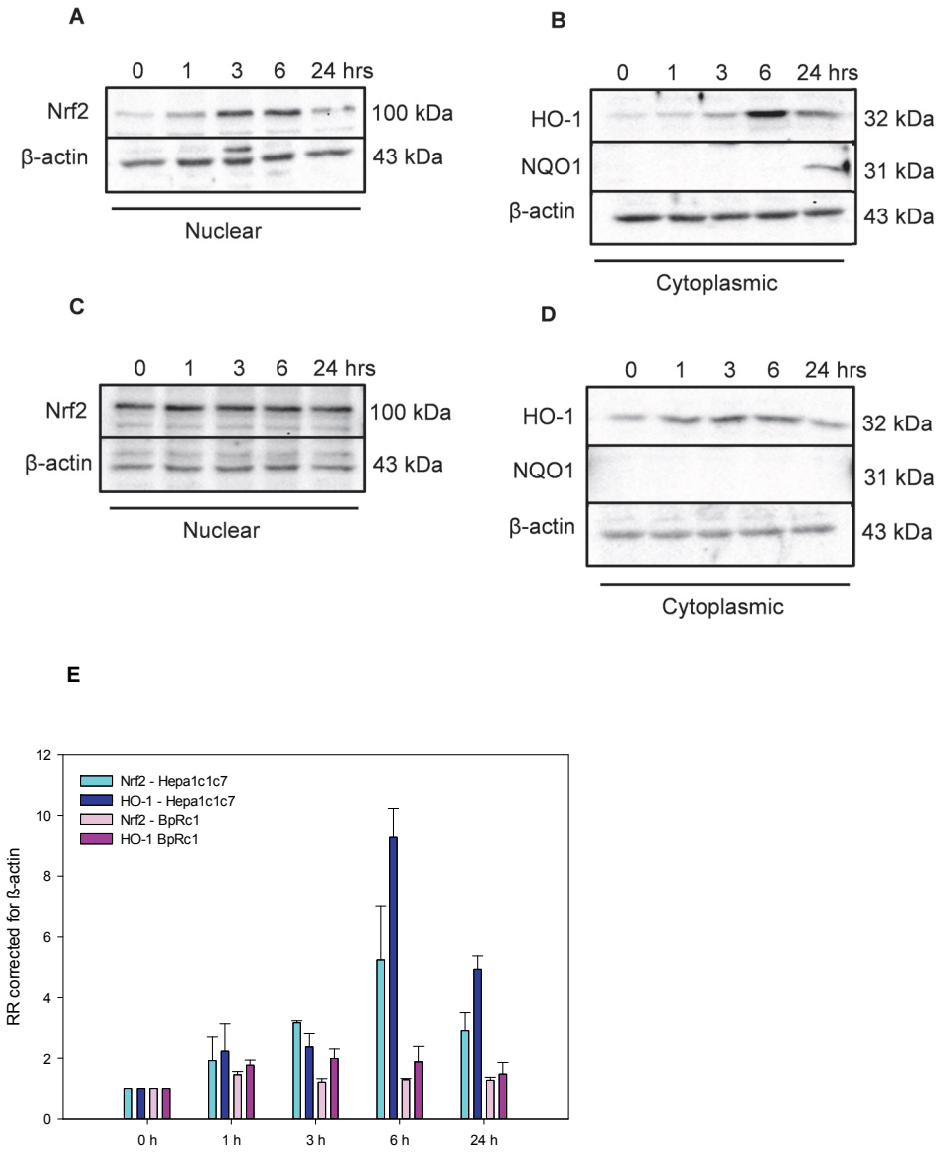

Figure 7.23: A - D: Western blot analysis of nuclear Nrf2 accumulation and its downstream targets phase II enzymes HO-1 and NQO1 in Hepa1c1c7 cells (A and B respectively) and BpRc1 cells (C and D respectively) after treatment with 10 µM of **7C55** over a 24 h time period. ß-actin was used as a loading control. Representative blots are shown. E: Quantitative western blot results of Nrf2 and HO-1 up-regulation in **7C55** treated Hepa1c1c7 (light and dark blue bars respectively) and BpRc1 cells (light and dark purple bars respectively). Protein induction levels were expressed as relative ratio's (RR) with ß-actin as a loading control. A RR ratio of 1 corresponds to no protein induction. The error bars represent the standard deviation of n = 2 independent experiments.

The Nrf2 induction potential of three other 7C compounds (in group 1) in Hepa1c1c7 cells was verified in additional western blot experiments. Previously obtained cellular NQO1 induction results indicated that compared to **7C55** (fold induction at 10 µM ~ 4), **7C45** showed a moderate potency (fold induction at 10 µM ~ 2.2), **7C46** demonstrated to be weakly active (fold induction at 10 µM ~ 1.9) and **7C33** was not active at all (fold induction at 10 µM ~ 1.0). Western blotting analysis of cells exposed to **7C45** revealed a similar Nrf2 induction pattern to **7C55**, but a slight overall reduced effect. Cells treated with **7C46** presented a similar time-dependent trend, but a further reduced effect compared to **7C45**. No Nrf2 up-regulation was detected in cells stimulated with **7C33** (Figure 7.24).

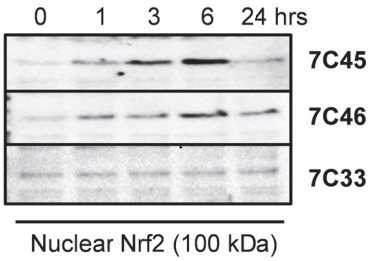

Figure 7.24: Western blot analysis of nuclear Nrf2 accumulation in Hepa1c1c7 cells over a 24 h time period after treatment with 10 µM of **7C45**, 10 µM of **7C46** or 10 µM **7C33**. Representative blots are shown.

7.5.4 Intracellular Nrf2 staining – flow cytometry

The flow cytometry-based assay developed in Chapter 3 was employed to quantify the extent of Nrf2 induction in **7C55** treated Hepa1c1c7 cells. Cells were exposed to the inactive compound **7C33** as a comparison. Following stimulation of Hepa1c1c7 cells with 10 µM **7C55** or **7C33** during 24 h, nuclei were isolated, fixed and stained with a primary unconjugated anti-Nrf2 antibody and FITC conjugated secondary antibody. The flow cytometry histograms are shown in Figure 7.25 A for **7C55** and in Figure 7.25 B for **7C33** with the absolute fold changes described in Figure 7.25 C. The time dependent trend in Nrf2 induction for **7C55** is analogous to earlier described western blotting results (Figure 7.23 A and E); a peak induction was detected after 3 – 6 h (fold induction ~ 2 and 3 respectively).

Similarly, no up-regulation of Nrf2 is present after cellular treatment with **7C33**. However, the absolute fold changes were overall reduced compared to the quantitative western blotting results (compare Figure 7.25 C with Figure 7.23 E).

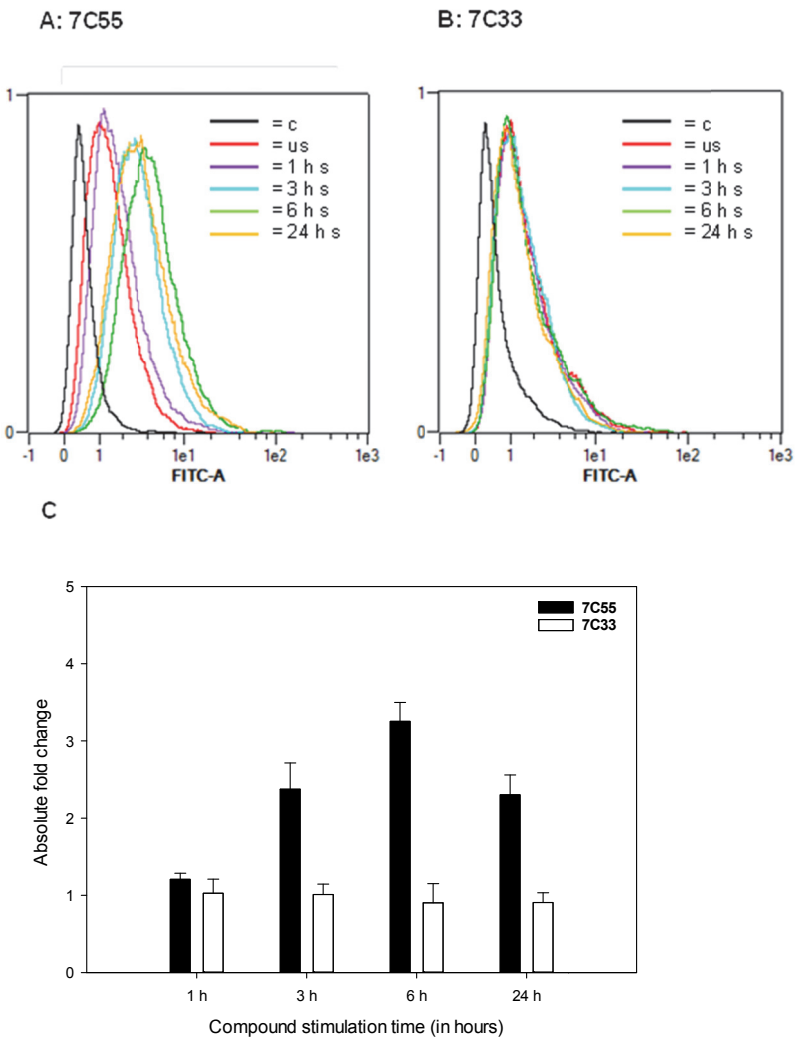

Figure 7.25: Hepa1c1c7 cells were unstimulated (us) or stimulated (s) with 10 µM **7C55** (A) or 10 µM **7C33** (B) for 1, 3, 6 and 24 h and subjected to flow cytometry analysis. An internal staining control (c) was analysed in parallel. Absolute fold changes of Nrf2 induction were calculated for each compound (C). The error bars represent the standard deviation of n = 3 independent experiments.

7.5.5 Pathway evaluation

ARNT – AhR

Cellular NQO1 induction assays and western blotting experiments indicated that **7C55** was not able to induce NQO1 in the ARNT-deficient BpRc1 cell line (Figure 7.21 C and Figure 7.23 D respectively). Moreover, no significant nuclear accumulation of Nrf2 was observed in BpRc1 cells following **7C55** treatment (Figure 7.23 C). To verify whether the ARNT-AhR pathway is involved in the up-regulation of NQO1 in Hepa1c1c7 cells, western blot experiments were performed to examine the expression of nuclear AhR and cytoplasmic CYP1A1 proteins. Hepa1c1c7 cells were exposed to 10 µM **7C55** and cytoplasmic and nuclear samples were obtained over a time period of 24 h. Up to 1 h, **7C55** treatment resulted in an induction of nuclear AhR (fold induction ~ 1.7) that returned to baseline levels after 1 – 24 h (Figure 7.26 A and C). An induction of CYP1A1 protein was visible after 6 h (fold induction ~ 2.0) that decreased between 6 – 24 h (Figure 7.26 B and C).

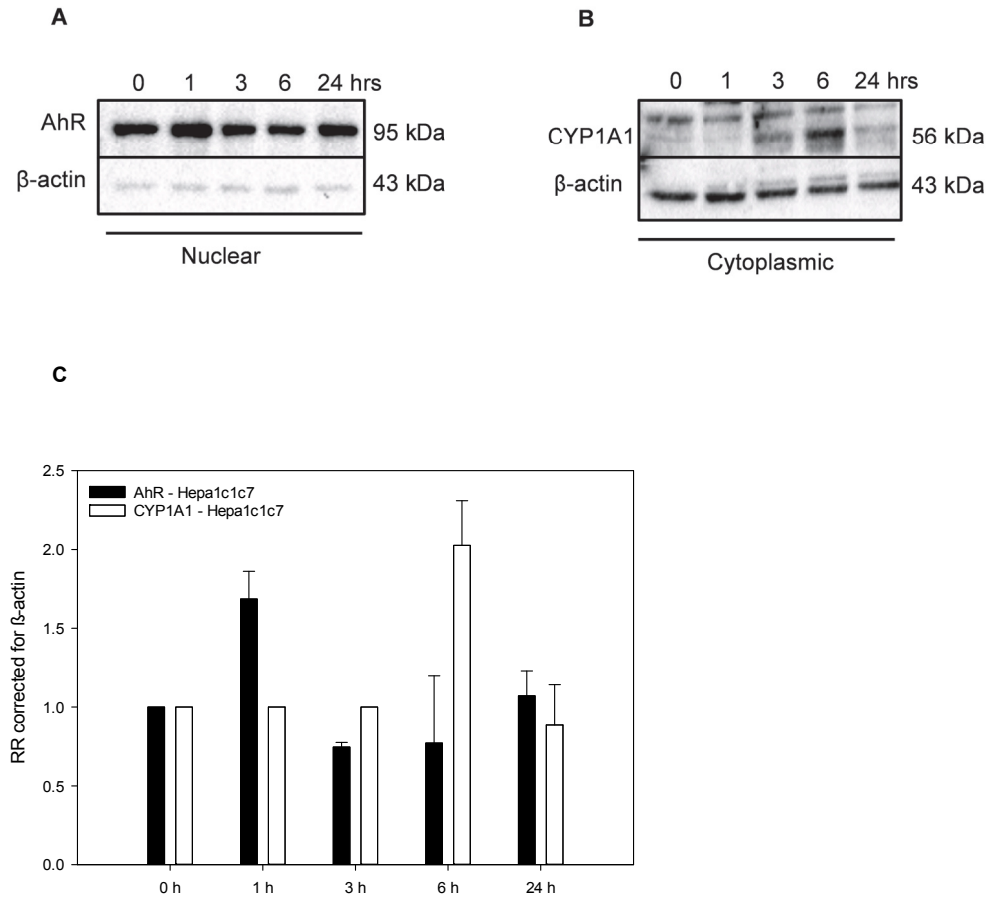

Figure 7.26 A and B: Western blot analysis of nuclear AhR accumulation and its downstream target phase I enzyme CYP1A1 in Hepa1c1c7 cells after treatment with 10 µM of **7C55** (A and B respectively) over a 24 h time period. Representative blots are shown. Figure C: Quantitative western blot results of AhR and CYP1A1 up-regulation in **7C55** treated Hepa1c1c7 cells (black and white bars repetitively). Protein induction levels were expressed as relative ratio's (RR) with ß-actin as a loading control. A RR ratio of 1 corresponds to no protein induction. The error bars represent the standard deviation of n = 2 independent experiments.

The induction of the CYP1A1 enzyme detected by western blotting was further assessed by a luciferase CYP1A1 enzyme activity assay. Following 6 and 24 h of cellular exposure to 10 µM of **7C55**, the amount of converted luciferin CYP1A1-specific substrate was measured by detection of produced luminescence (Figure 7.27 A). Subsequently, absolute luminescence values were converted into fold changes compared to the control (Figure 7.27 B). Previously reported data for the controls (Section 5.2.5): cells treated with vehicle only (C) and cells treated with 3 µM BaP (P), were also displayed in Figure 7.27 to provide context for the test compound. After 6 and 24 h of **7C55** stimulation, Hepa1c1c7 cells show a small increase in CYP1A1 activity (fold induction ~ 1.4 and ~ 1.6 respectively). This finding is not in complete agreement with earlier described western blotting results, which showed a peak induction after 6 h (fold induction ~ 2.0).

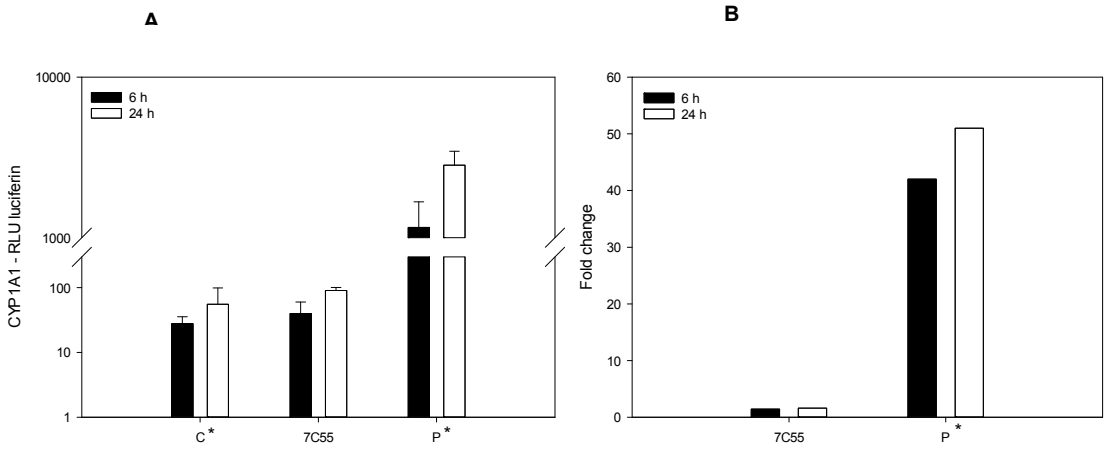

Figure 7.27: CYP1A1 induction measured using the P450 Glo Assay (Promega) following exposure of Hepa1c1c7 cells to vehicle (C), 10 µM **7C55** or 3 µM BaP (P). (A): the quantity of luciferin (RLU) detected is proportional to the extent of CYP1A1 enzyme activity. The error bars represent the standard deviation of n = 8 replicates in a representative experiment. (B): fold changes of **7C55** and BaP versus vehicle control. Data indicated with an * are previously shown data in Section 5.2.5.

ROS

To verify whether ROS is produced after exposure of Hepa1c1c7 cells to **7C55**, a flow cytometry based assay was performed. ROS production may promote the nuclear translocation of Nrf2 by reacting with thiol groups of Keap1. After treatment of Hepa1c1c7 cells with 10 µM **7C55** for 1 h, cells were stained with CellROX Deep Red reagent (Life Technologies) and fluorescence was measured on a flow cytometer (Figure 7.28). The results of the blank and previously described controls were also shown in Figure 7.28: negative controls DMSO (C1) and acetonitrile (C2) and positive control: menadione (M). No ROS production was evident after cellular exposure to **7C55**.

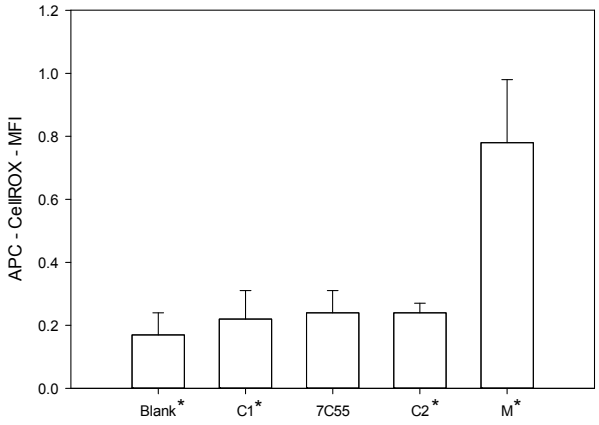

Figure 7.28: ROS production measured using the CellROX Deep Red dye after exposure of Hepa1c1c7 cells to 10 µM **7C55** or 50 µM menadione (M) for 1 h. As controls, cells were exposed to the **7C55** vehicle, DMSO (C1) and the menadione vehicle, acetonitrile (C2). The amount of fluorescence (APC MFI) detected is proportional to the extent of ROS production. The error bars represent the standard deviation of n = 3 independent experiments. Data indicated with an * are previously shown data in Section 5.2.5.

7.6 Discussion

7.6.1 Peptides

Although there are some disadvantages associated with the use of peptides as drugs, such as rapid degradation and poor cell permeability, they are highly suited to inhibit protein-protein interactions [235]. Moreover, peptides are highly specific and are straightforward to synthesise and modify, which is especially useful in the earlier stages of drug development. In this respect, peptidomimetics are powerful tools to enhance the pharmacological properties of peptides and present a development route for highly active Nrf2 peptide-derived inducer molecules [235].

Previous synthesised 7-mer peptides and derivatives were designed to include or mimic the high affinity ETGE interaction. Initial FP results [143] suggested that the minimal binding motif is ^{77}DEETGEF^{83} (**7P1**) (IC_{50} ~ 5.39 μM), but that the inhibition potential of the peptide structure was improved by introducing an E78P substitution. This substitution is derived from the binding sequence of Keap1 interactor, sequestosome-1. The original sequestosome-1 binding sequence demonstrated moderate inhibition potency in the FP assay (IC_{50} ~ 34.4 μM) [143], but modifying the peptide structure to become more ETGE-like (**7P2**) improved the activity drastically (IC_{50} ~ 0.25 μM) [143]. Both peptides **7P1** and **7P2** exhibited matching inhibition potencies in the FRET assay that was developed in Chapter 3 (IC_{50} ~ 3.34 μM and IC_{50} ~ 0.33 μM respectively). However, they were not found to be active in a cell-based NQO1 assay. The modification of the peptide structure with an N-terminal stearic acid group (peptides **7P4** and **7P5**) improved not only cellular penetration properties as demonstrated in the NQO1 assay, but also enhanced binding affinities in both FP [170] and FRET assays. Scrambled versions of the peptide (peptides **7P8**, **7P9** and **7P6**) were not active in any of the assays and demonstrated the importance of the ETGE motif for binding. However, scrambled stearic acid conjugates (i.e. peptides **7P8** and **7P6**) appeared to have a non-specific advantageous effect on binding, which should be further explored. The designed peptides have an overall net negative charge at physiological pH. This is an unfavourable physical property for cell penetration as the plasma membrane is a non-polar environment. In an attempt to reduce this charge, a D76N substitution was introduced, resulting in peptides **7P10** and **7P11**.

This charge reduction was detrimental for the binding properties of the peptide as the D76 residue is essential for maintaining the peptide secondary structure (a β-turn-like structure) when bound to Keap1. However, induction of NQO1 activity in the cell-based assay was similar for both **7P4** and **7P11**. Although the overall net charge of peptide **7P11** remained negative, the peptide has improved cell penetrating properties and was therefore conjugated to a FITC fluorophore to study its uptake in cells. The FITC conjugated peptide **7P12** (10 μM) showed a time-dependent cell penetration in Hepa1c1c7 cells measured up to 2 h using flow cytometry analysis. Moreover, a cytoplasmic distribution in both living and fixed cells was observed after 1 h of cellular incubation with 10 μM **7P12**. Only a minimal amount of the peptide co-localised with the CellMask cell membrane marker, suggesting that the peptide does not associate strongly with the cell membrane. The peptides may form micelles or vesicles within the cell (visible as small, intensely green areas), which is enabled by the conjugated stearic acid group. Nevertheless, this hypothesis needs to be verified in further experiments. The TAT peptide is a widely used CPP; hence an FITC conjugated version was used as a positive control in the cellular uptake study. The TAT peptide has a positive net charge at physiological pH and is thought to bind to the highly negative charged plasma membrane and enter the cell via endocytosis, within the cell the TAT peptide accumulates within the nucleus in the vicinity of the negatively charged DNA. The FITC conjugated TAT peptide (1 μM) demonstrated a cytoplasmic and nuclear distribution in fixed cells, but no cellular uptake was detected in living cells (flow and confocal analysis). Some studies have suggested that the TAT peptide has to reach a certain threshold concentration to translocate to the cytoplasm and nucleus via endocytosis [236] [237]. The concentration used here, 1 μM, might be too low, which is surprising considering the cellular distribution in fixed cells at the same concentration. However, the fixation process causes disruption of the membrane and may facilitate influx of the peptide. Future work may include studying the peptide uptake and distribution in different cell types.

Recently, a series of TAT-conjugated ETGE peptides has been reported to induce the expression of Nrf2 and its downstream target gene HO-1 in THP-1 cells in a similar concentration range to those required for peptides **7P4**, **7P5** and **7P11** to induce NQO1 up-regulation in Hepa1c1c7 cells [238]. These and our findings suggest that peptides and peptide conjugates may contribute to finding potent inducers of Nrf2 activity via inhibition of the Keap1-Nrf2 PPI.

In particular, stearic acid conjugated peptides showed promising cell penetrating capabilities in both an NQO1 induction assay and cellular uptake studies.

7.6.2 Small molecules

Similar to peptidomimetic compounds, small molecule inhibitors of protein-protein interactions bind target sites in a highly specific and non-covalent manner and generally possess better cellular penetrating properties than peptides. Moreover, identification of small molecule inhibitors benefited from the ability to screen large compound libraries using *in silico* methods, without the need for synthesizing every molecule [239].

A selection of different small molecule inhibitors (7A range) was tested to examine their ability to disrupt the Keap1-Nrf2 PPI and up-regulate Nrf2 and its downstream target genes. These small molecules were previously identified from a wide range of compound libraries. Initial screening using an *in vitro* FP and FRET screening and a cellular NQO1 assay was performed to establish the biological activity profiles of the molecules. Compound **7A4** possessed the best pharmacological properties of the series; the compound inhibited the PPI with an IC_{50} of 2.84 μM obtained with the FRET assay, which is similar to a previously found IC_{50} of 2.7 μM with close analogue 'compound 16' [227] using a confocal fluorescence anisotropy assay. However, **7A4** showed a significant amount of fluorescence interference in the FP assay. This could be due to specific spectral overlap with the FITC fluorophore used in the FP assay. The fluorescence properties of the eCFP and eYFP conjugated proteins used in the FRET assay may have less potential for fluorescence overlap or interference in this assay system. **7A4** demonstrated a CD value of 8 μM in the cellular NQO1 induction assay in Hepa1c1c7 cells. Further western blotting analysis in this cell line revealed an Nrf2 dependent up-regulation of the phase II enzymes HO-1 and NQO1. **7A4** showed a similar protein induction pattern to the reference compound sulforaphane in Hepa1c1c7 cells; a peak Nrf2, HO-1 and NQO1 induction occurred after 1, 6 and 24 h respectively. Indeed, Marcotte *et al.* [227] found an induction of Nrf2 and NQO1 in a DLD1-ARE reporter cell line upon exposure to close analogue 'compound 16'. The Nrf2 dependency of the NQO1 induction was confirmed by activity in an Nrf2 specific ARE-driven luciferase cell-based assay and

by a detected decrease in NQO1 expression upon Nrf2 gene knockdown [227]. However, **7A4** failed to induce NQO1 expression in the ARNT-defective BpRc1 cell line, which was observed alongside a significant reduced induction of Nrf2 and HO-1 protein levels. This is in contrast to the unaltered induction profile of Nrf2 and phase II enzymes that was observed with sulforaphane. A modest up-regulation of the AhR transcription factor and target enzyme CYP1A1 was found in the Hepa1c1c7 cells after 1 h and 6 h of **7A4** exposure respectively. Sulforaphane did not show a significant nuclear accumulation of the AhR transcription factor, but the CYP1A1 protein and enzyme activity was modestly induced after 24 h. Nevertheless, the CYP1A1 induction with **7A4** or sulforaphane was small compared to enzyme activity levels detected with cellular exposure to AhR ligand BaP. Although the mutant cell line, BpRc1, should only differ from its wild-type cell line, Hepa1c1c7, by a defective ARNT, evidence has emerged that other significant differences exist. Seidel and Denison [110] used the approach of differential display to verify the gene expression in both wild-type and mutant cell lines and found an ARNT-independent modified gene expression between Hepa1c1c7 and BpRc1 cells. In addition, differential growth profiles were observed between wild-type and mutant cells and between two different ARNT deficient mutant cell lines (BpRc1 and c4). More recently, Wang *et al.* [240] re-introduced ARNT into the ARNT deficient c4 cells and subjected the cells to DNA microarray analysis. Twenty-seven genes other than AhR were found to be induced following re-introduction of ARNT and represent target genes for ARNT. These findings suggest that the inability of **7A4** to induce NQO1 in the BpRc1 cell line is not necessarily (only) due to ARNT-AhR dependence, but could also be related to other factors. **7A4** demonstrated no evidence of ROS production upon exposure to Hepa1c1c7 cells. Hence, ROS production is an unlikely factor to have contributed to the up-regulation of phase II enzymes. This is consistent with the direct disruption of the interaction between Keap1 and Nrf2. Moreover, close analogue 'compound 16' was not found to be cysteine reactive [227]. Further characterisation of **7A4** revealed no cytotoxicity up to 25 µM in Hepa1c1c7, BpRc1 and HeLa cells after 24 and 48 h of compound exposure, but cell viability started to decline at higher concentrations. Future experiments should include the assessment of the long-term toxicity of **7A4** on diverse cell lines. Co-crystal structure data obtained by Marcotte *et al.* [227] revealed that 'compound 16' binds in subpockets P3, P4 and P5 of Keap1, but is unable to occupy the highly positive charged P1 and P2 subpockets. The latter Keap1 binding sites are of high importance for the binding of the Nrf2 ETGE motif; the two side

chain carboxylic acids from the residues E79 and E82 mainly interact electrostatically with arginine residues in Keap1.

Jiang *et al.* [129] designed 'compound 2' based on the co-crystal structure of 'compound 16' bound in the Keap1 binding pocket. The two carboxylic acids linked to the nitrogen of the sulfonamide groups, enabled occupancy of the P1 and P2 subpockets. Moreover, Jiang *et al.* [129] found 'compound 2' to inhibit the Keap1-Nrf2 PPI with an improved IC_{50} of 28.6 nM in a FP assay (IC_{50} 2.7 µM for 'compound 16' [227]). Our group developed a compound series based on this ligand design. Compound **7B1** was synthesised and identical in structure to 'compound 2'. The activity of **7B1** was very similar to the quoted activity of 'compound 2', with an FP IC_{50} 59 nM in our assay system. **7B1** was also able to up-regulate the NQO1 enzyme in Hepa1c1c7 cells, demonstrating a higher potency than **7A4** (CD ~ 4 µM versus 8 µM). This is in agreement with earlier reported findings were the compound showed activity in an Nrf2 ARE-luciferase reporter assay and Nrf2-associated gene expression was up-regulated. Although no cytotoxicity tests were performed, **7B1** did not affect cell viability at concentrations up to 10 µM under the conditions of the NQO1 assay in Hepa1c1c7 cells. According to docking studies and FP assays, this compound is suggested to bind with higher affinity and specificity in the Keap1 binding pocket compared to 'compound 16' [227] or **7A4**. However, the added carboxylic acid groups introduce a net negative charge to the compound at physiological pH. This could be detrimental for the cell penetrating properties of the compound. Consequently, 7B compounds were developed containing less acidic side chains, e.g. tetrazole and amide groups. However, these structures did not show an improvement in the cellular NQO1 induction assay. Another strategy involved mimicking the naphthalene ring to improve binding potency, yet FP results showed increased IC_{50} values and the NQO1 induction potency remained similar to naphthalene ring equivalents. Ongoing work is conducted to improve Keap1 binding properties and cellular potency of these promising small molecule inhibitors.

In an attempt to discover other potent small molecule inhibitors of the Keap1-Nrf2 PPI, a docking screen was performed with a fragment library of 178,000 compounds. An FP screen revealed that 1,2,3-triazole derivatives (7C range) demonstrated the most promising results. These structures were based on a 1,4-diaryl-1,2,3-triazole scaffold that was designed to mimic the distance between the glutamate side chains of the Nrf2 – ETGE motif. Additional cellular screening with a

NQO1 induction assay revealed a range of different activities using various functional group substituents. The main findings included: carboxylic acid substituents were good for binding *in vitro*, but less so for cellular potency as negatively charged molecules do not favour cell penetration. Carboxamide and nitro groups showed better NQO1 inducing abilities, but carboxamide substituents caused some fluorescence FP interference. However, generally, compounds containing nitro groups should be avoided in drug development as their metabolism can generate reactive species that may induce cytotoxicity [241]. The introduction of linkers or alterations to the heterocycle of the core structure didn't improve *in vitro* or cellular potency significantly. Quinoline-containing structures were active in cell-based assays, but may not up-regulate NQO1 via disruption of the Keap1-Nrf2 PPI as they share structural similarity with some known AhR ligands, including 9,10-dimethyl-1.2-benzanthracene (DMBA), benzo*(a)*pyrene (BaP) and 3,4,5,3',4'-pentachlorobiphenyl (PCB 126) [242]. These compounds also showed FP interference, which could be due to their large aromatic planar rings. The most promising compound tested was the nitro and iodine substituted compound **7C55**, which was not cytotoxic at concentrations up to 250 µM in Hepa1c1c7, BpRc1 and HeLa cells after 24 and 48 h of compound exposure. Future experiments should include the assessment of the long-term toxicity of **7C55** on diverse cell lines. This small molecule inhibited the Keap1-Nrf2 PPI with an IC_{50} of 7.1 µM in the FP assay and induced the downstream enzyme NQO1 by 4-fold at 10 µM with a CD value of 0.6 µM in Hepa1c1c7 cells. Western blotting analysis confirmed the up-regulation of the NQO1 protein. This induction was observed alongside the expression of other phase II enzyme HO-1 and nuclear accumulation of Nrf2 in Hepa1c1c7 cells. A reduced performance in the FP assay and a decreased NQO1 induction of related compounds **7C33**, **7C45** and **7C46** was consistent with a diminished nuclear accumulation of Nrf2. Flow cytometry analysis quantitatively confirmed the differential expression of Nrf2 upon cellular exposure to **7C55** or the non-active compound **7C33**. Compared to the reference compound sulforaphane, **7C55** showed a later peak induction of Nrf2 (3 - 6 h versus 1 h). However, a similar time dependent up-regulation of HO-1 was observed for both compounds (max induction after 6 h). Nevertheless, **7C55** was not able to induce NQO1 expression in the ARNT-deficient BpRc1 cell line. Similar to **7A4**, Nrf2 and HO-1 protein induction was substantially decreased in this mutant Hepa1c1c7 cell line. In addition, **7C55** showed an induction of AhR after 1 h and CYP1A1 after 6 h, which was also observed with **7A4**. However, the AhR induction was slightly lower compared to **7A4** (fold difference of 1.7 *vs*. 4.5). **7C55** induced the nuclear accumulation of Nrf2 with

delayed kinetics (after 3 – 6 h) compared to the induction of nuclear AhR (after 1 h). This is in agreement with a study by Wang *et al.* [105], who found a similar trend for 2,3,7,8-tetrachlorodibenzo-p-dioxin (TCDD). The relative small induction of AhR and CYP1A1 proteins compared to levels detected with AhR ligand BaP, suggests that a mechanism other than the ARNT-AhR pathway may be responsible for the inability of **7C55** to up-regulate NQO1 in the BpRc1 cell line. Moreover, **7C55** activates the Keap1-Nrf2 pathway in Hepa1c1c7 cells with a dissimilar kinetic profile to sulforaphane and **7A4**. These data indicate that **7C55** may have additional effects on other pathways. Similar to sulforaphane and **7A4**, no ROS production was found upon stimulation of Hepa1c1c7 cells with **7C55**.

Docking studies performed within the research group predict that the 4-(3-nitrophenyl) group of **7C55** bind in the P3 sub-pocket of Keap1 were they form hydrogen bonds and electrostatic interactions with positively charged residues of Keap1 (Figure 7.29 A). The lipophilic iodine group makes contact with the P5 sub-pocket of Keap1 and may promote the cell penetrating properties of the compound. Figure 7.29 B shows both **7C55** and **7B1** docked in Keap1 binding pocket and indicates the overlapping binding sites.

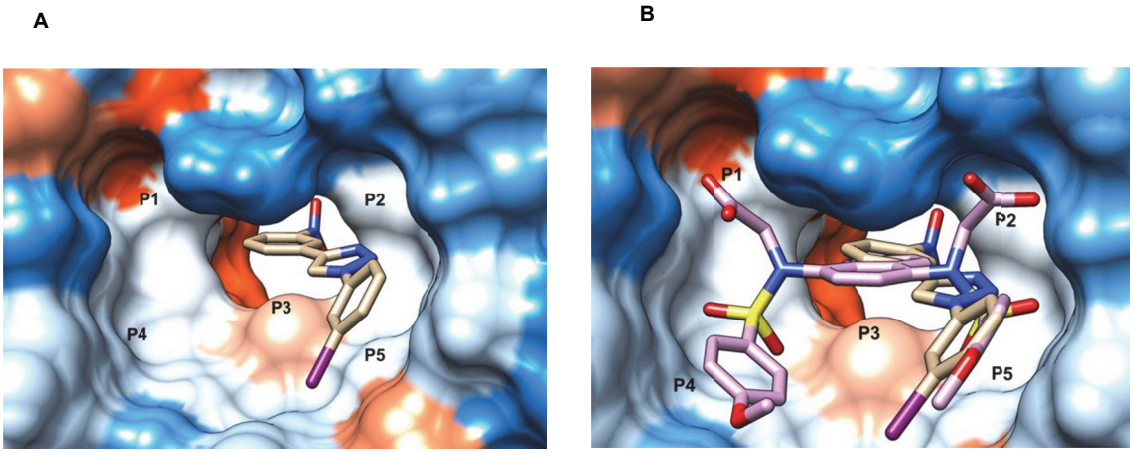

Figure 7.29: Surface representation of the crystal structure of Keap1-Kelch bound to (A): **7C55** and (B) **7C55** and **7B1**. The Kelch binding sub-pockets are indicated as P1 – P5. The surface of Keap1 was coloured as hydrophobicity; blue is hydrophilic, white is neutral and red is hydrophobic.

The group of Albena Dinkova-Kostova developed a FRET-based method combined with multi-photon fluorescence lifetime imaging microscopy (FLIM) (submitted and in the press [229]). The hinge and latch theory describes an open confirmation of the Keap1-Nrf2 complex when Keap1 is only bound by the high affinity motif Nrf2-ETGE and a closed conformation of the complex when Keap1 is bound by both high affinity ETGE and low affinity DLG motifs. The results from Dinkova-Kostova indicate that sulforaphane and other electrophilic inducers cause an accumulation of the closed confirmation, where Nrf2 is not ubiquinated by the covalently modified Keap1 and *de novo* Nrf2 can accumulate in the nucleus. However, **7C55** causes an accumulation of the open complex confirmation and suggests that the small molecule disrupts the interaction of Keap1 with low affinity DLG motif. These observations are supportive of the **7C55**-Keap1 docking studies.

In the process of mitophagy, damaged mitochondria are degraded and recycled by autophagosomes and lysosomes [243]. The expression of P62 or sequestosome-1 is partly regulated by Nrf2 and plays a crucial role in mitophagy by targeting autophagy. A defective mitophagy process is related to cancer and several neurodegenerative diseases. East *et al.* [244] showed that unlike sulforaphane, **7C55** is able to induce mitophagy in MEF cells in an Nrf2 and p62-mediated manner and thus demonstrates potential as a tool compound in mitochondrial quality control. Overall, the **7C55** compound shows promising inhibitory and cellular activity towards the disruption of the Keap1-Nrf2 PPI. Hence, the relative simple chemical structure can be used as a tool compound for further development.

The small molecule inhibitors discussed here present powerful examples of an alternative to thiol-reactive compounds for the induction of Nrf2. However, evaluation of pathway specificity demonstrates the potential involvement of other pathways than Keap-Nrf2 in the up-regulation of phase II enzymes i.e. NQO1. Future work, including Nrf2 and AhR knock-out experiments would be essential to verify the extent of AhR involvement in the induction of NQO1.

8 Miscellaneous Nrf2 inducers

8.1 Introduction

In this chapter, Nrf2 inducer compounds that cannot yet be classified as direct or indirect Nrf2 inducers are discussed. Several of these compounds showed promising activity in a cellular NQO1 enzyme activity assay. However, the exact mode of action for most of the structures described is unknown.

The aim of this chapter is to screen Nrf2 inducers with an unknown mechanism of action for their ability to induce Nrf2 target genes.

8.1.1 8A compounds

These compounds, which were developed by our group [62], were synthetic intermediates for the synthesis of a series of *p*-quinol derivatives via oxidation reactions (described in Chapter 6). They were evaluated as potential Nrf2-inducing agents in order to compare their activity with their oxidised counterparts and because various phenolic compounds have been shown to induce NQO1 activity in previous studies. In some cases bio-oxidation can convert phenols into electrophilic quinones containing Michael acceptor groups e.g. tBHQ (*tert*-butyl-*p*-hydroquinone) [84-85]. Michael acceptors are able to up-regulate phase II enzymes i.e. NQO1 by their reactivity towards thiol residues.

8.1.2 8B compounds

Chalcones are naturally occurring compounds that are biological and synthetic precursors of flavonoids and isoflavonoids; they consist of two phenyl rings linked by a three-carbon α,β-unsaturated carbonyl group (Figure 8.1 A) [245]. This compound group has been shown to exhibit multiple biological properties, including anti-inflammatory, anti-fungal and anti-cancer related activities [52]. Certain chalcones

have been demonstrated to induce Nrf2-dependent cytoprotective enzymes [52]. It has been proposed that this is a result of the thiol reactivity of the α,β-unsaturated carbonyl group (a Michael acceptor). Chalcones and related flavonoid compounds have been reported to act as AhR ligands, suggesting that the mode of Nrf2 induction may be complex and involve Keap1-independent activities [246]. Kumar *et al.* [247] developed chalcone derivatives that were potent Nrf2 activators. Figure 8.1 B shows the structure of the most active Nrf2 inducer, 'compound 2b' [247]. However, the induction of Nrf2 seemed to be independent of changes in redox state or ROS [247]. The 8B compound series, which was designed by our group, is based on these chalcone analogs.

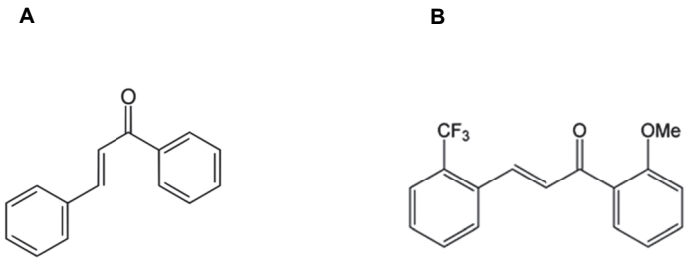

Figure 8.1: Chemical structures of A: chalcone and B: 2-trifluoromethyl-2'-methoxychalone or 'compound 2b' [247].

8.1.3 8C compounds

The skins of red grapes contain the stilbenoid, resveratrol, which is a non-flavonoid polyphenolic compound that is associated with anti-cancer and anti-inflammatory effects. Resveratrol (Figure 8.2 A) has been reported to possess intrinsic antioxidant properties, which are attributed to the phenolic hydroxyl group [248]. Moreover, the antioxidant compound is thought to up-regulate phase II enzymes NQO1, HO-1 and gamma-glutamylcysteine synthetase via inducing the transcriptional activity of Nrf2 [249]. However, resveratrol is found to be relatively unstable and demonstrates a rapid clearance [250]. Mayhoub *et al.* [251] designed derivatives of the *trans*-resveratrol structure in which the stilbene double bond was replaced with a thiadiazole ring and the phenol groups were removed to improve activity towards NQO1 induction and specificity in the inhibition of NF-kB and the phase I enzyme aromatase. The

inhibition of NF-kB may affect the promotion and progression of cancer cells via the induction of apoptosis [251]. Inhibition of the aromatase enzyme, which is responsible for estrogen production, is a well-known strategy in the treatment and prevention of oestrogen receptor-positive breast cancer. Figure 8.2 B shows the 3,5-diaryl-1,2,4 – thiadiazole core scaffold that was used to develop analogues [251]. This structure presents a high level of similarity with the lead compound from the 7C range, **7C55** (Figure 8.2 C). Hence, the 8C compound series was developed by our group based on the 3,5-diaryl-1,2,4 – thiadiazole core structure.

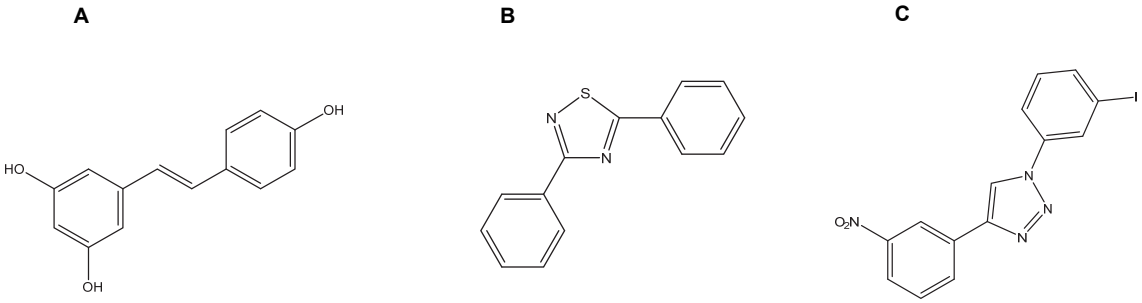

Figure 8.2: Chemical structures of A: *trans*-resveratrol, B: 3,5-diaryl-1,2,4 – thiadiazole core scaffold [251] and C: **7C55**.

8.2 NQO1 results

8.2.1 8A compounds

This group of phenolic compounds (n = 7) exhibited weak NQO1 induction potency in the Hepa1c1c7 cell line; fixed dose studies at a concentration of 1 μM, resulting in a fold induction of < 1.5 for the most potent structures, **8A2** and **8A4** (Table 8.1). No cytotoxicity was observed at this concentration.

Table 8.1: NQO1 (in the Hepa1c1c7 cell line) results for phenolic 8A compounds.

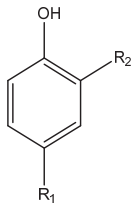

Cpds	R1	R2	NQO1[a]	NQO1 CD (μM)	Toxicity NQO1 (μM)
8A1	CH_2CH_2OAc	H	1.0	-[b]	-[b]
8A2	CH_2CO_2Et	H	< 1.5	-[b]	-[b]
8A3	CH_2CO_2Et	F	1.0	-[b]	-[b]
8A4	$CH_2CH_2CO_2Et$	H	< 1.5	-[b]	-[b]
8A5	CH=CHCOMe	H	1.1	-[b]	-[b]
8A6	$CH_2CH_2CH_2CO_2Et$	H	1.0	-[b]	-[b]
8A7	4-Methoxyphenyl	H	1.0	-[b]	-[b]

Notes: a. Fold induction at 1 μM; b. Not determined. Compounds (Cpds).

8.2.2 8B compounds

The series of compounds (n = 18), which was divided over two groups, was examined for their ability to induce NQO1 enzyme activity in a cellular assay in the Hepa1c1c7 cell line. A fixed dose study at a concentration of 10 μM was performed first before promising structures were examined further in a dose-dependent manner.

The group 1 core structure (Table 8.2) is similar to 'compound 2b' (Figure 8.1 B) as described by Kumar *et al.* [247]. Chloro and trifluoromethyl groups in the R_1 and/or R_2 positions appear to be favourable for NQO1 activity; three structures in group 1, **8B6**, **8B8** and **8B9**, demonstrated a moderate NQO1 induction potency with CD values ranging from 3 – 6 μM and were not cytotoxic up to 10 μM. Compound **8B10** also exhibited the ability to up-regulate NQO1 in the fixed dose study (fold induction ~ 3.5 at 10 μM), but was not examined further.

Table 8.2: NQO1 (in the Hepa1c1c7 cell line) results for group 1 of the 8B compound range.

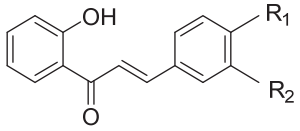

Cpds	R1	R2	NQO1[a]	NQO1 CD (μM)	Toxicity NQO1 (μM)
8B1	H	H	1.9	-[b]	-[b]
8B2	CH_3	H	1.4	-[b]	-[b]
8B3	OMe	H	1.7	-[b]	-[b]
8B4	OMe	OMe	1.8	-[b]	-[b]
8B5	SCH_3	H	1.7	-[b]	-[b]
8B6	H	Cl	2.5	6.0	> 10
8B7	Cl	H	1.2	-[b]	-[b]
8B8	Cl	Cl	2.9	5.0	> 10
8B9	CF_3	H	6.8	3.0	> 10
8B10	Cl	CF_3	3.5	-[b]	-[b]

Notes: a. Fold induction at 10 μM; b. Not determined. Compounds (Cpds).

The compounds in group 2 (Table 8.3) vary in activity; ranging from inactive (**8B14**, fold induction ~ 1.0 at 10 μM) to highly active (**8B17** and **8B18**, CD ~ 0.04 μM). No cytotoxicity was detected up to 10 μM. Again, the Cl and CF_3 groups at the R_1 and/or R_2 position promoted NQO1 induction.

Table 8.3: NQO1 (in the Hepa1c1c7 cell line) results for group 2 of the 8B compound range.

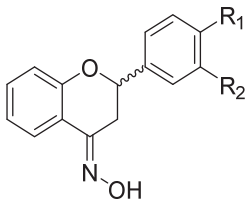

Cpds	R1	R2	NQO1[a]	NQO1 CD (μM)	Toxicity NQO1 (μM)
8B11	H	H	1.3	-[b]	-[b]
8B12	CH_3	H	2.0	-[b]	-[b]
8B13	OMe	H	1.3	-[b]	-[b]
8B14	OMe	OMe	1.0	-[b]	-[b]
8B15	SCH_3	H	2.3	8.0	> 10
8B16	Cl	H	3.0	6.0	> 10
8B17	Cl	Cl	4.2	0.04	> 10
8B18	CF_3	H	3.6	0.04	> 10

Notes: a. Fold induction at 10 μM; b. Not determined. Compounds (Cpds).

Figure 8.3 shows the dose response profiles that were created for the three most active compounds in group 1 (**8B9**) and group 2 (**8B17** and **8B18**).

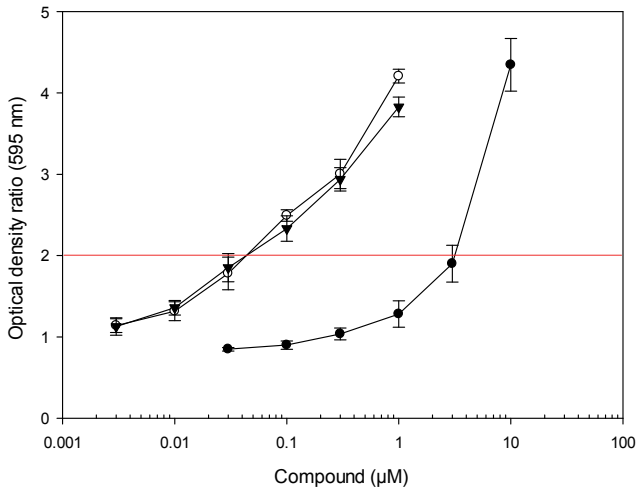

Figure 8.3: Dose response curves for the NQO1 assays of compounds **8B9** (●), **8B17** (○) and **8B18** (▼) in Hepa1c1c7 after 24 h stimulation. The error bars represent the standard deviation of n = 4 replicates in a representative experiment.

8.2.3 8C compounds

The NQO1 induction potential of 8C compounds (n = 9) was studied in Hepa1c1c7 cells. The compounds were subdivided into four separate groups based on their chemical structures. Initially, all compounds were examined at a fixed dose concentration of 10 μM. Several compounds were screened in an *in vitro* FP assay [101] for their ability to interfere with the interaction between Keap1 and Nrf2 (performed by Adrian Fowkes, UCL School of Pharmacy).

The compounds in group 1 (Table 8.4) are thiadiazole derivatives and are based on the structures of **8C1** and **8C3**, which represent compound '3ii' and '3hh' respectively, as described by Mayhoub *et al.* [251] (Figure 8.4 A and B respectively). These structures were found to range from not active (**8C2**, fold induction ~ 1.0 at 10 μM) to highly active (**8C4**, CD ~ 0.2 μM) with varying cytotoxicity levels. Changing the R1 and R2 groups from OMe (**8C1**) to NO_2 (**8C4**) improved the activity considerably (CD ~ 2 μM versus 0.2 μM). Moreover, FP results revealed slight inhibition activity by **8C1** (17.5% inhibition at 100 μM). None of the other compounds were shown to inhibit the Keap1-Nrf2 PPI in the FP assay.

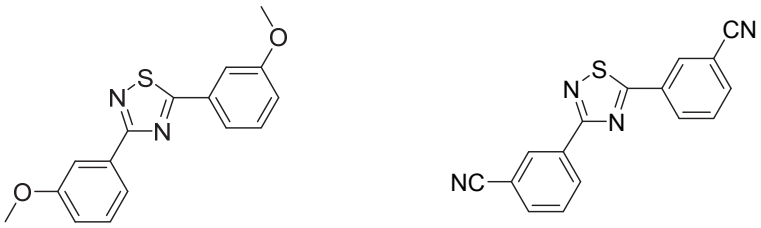

Figure 8.4: Chemical structures of A: **8C1** or 'compound 3ii' and B: **8C3** or 'compound 3hh' [251].

Table 8.4: NQO1 (in the Hepa1c1c7 cell line) results for group 1 of the 8C compound range.

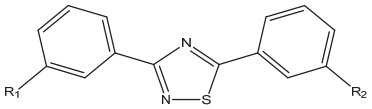

Cpds	R1	R2	FP[a]	NQO1[b]	NQO1 CD (μM)	Toxicity NQO1 (μM)
8C1	OMe	OMe	17.5	2.8	2.0	> 10
8C2	NH_2	CN	- 0.3	1.0	-[c]	-[c]
8C3	CN	CN	[a1]	1.8	-[c]	-[c]
8C4	NO_2	NO_2	- 0.7	3.6	0.2	> 3.0

Notes: FP assays performed by Adrian Fowkes, UCL School of Pharmacy; a. Percentage inhibition at 100 μM; a1. Fluorescence interference b. Fold induction at 10 μM; c. Not determined. Compounds (Cpds).

The two structures in group 2 (Table 8.5) containing a linker group (X) were moderately active with CD values ranging from 3 – 10 μM and no cytotoxicity up to 10 μM. A weak inhibition was observed for **8C6** in the FP assay.

Table 8.5: NQO1 (in the Hepa1c1c7 cell line) results for group 2 of the 8C compound range.

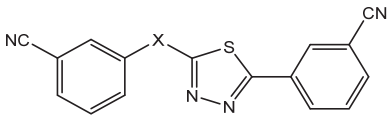

Cpds	X	FP[a]	NQO1[b]	NQO1 CD (μM)	Toxicity NQO1 (μM)
8C5	NH	0.7	2.0	10	> 10
8C6	NMe	8.7	2.3	3.0	> 10

Notes: FP assays performed by Adrian Fowkes, UCL School of Pharmacy; a. Percentage inhibition at 100 μM; b. Fold induction at 10 μM. Compounds (Cpds).

The **8C7** compound (Table 8.6) contains a NH-linker group and an altered heterocycle. This compound was highly active in the cell-based assay (CD ~ 0.6 μM) and showed cytotoxicity at a relative high concentration (≥ 30 μM).

Table 8.6: NQO1 (in the Hepa1c1c7 cell line) results for group 3 of the 8C compound range.

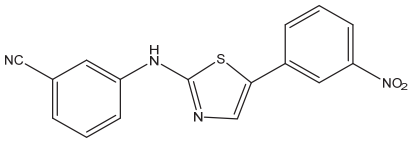

Cpds	NQO1[a]	NQO1 CD (μM)	Toxicity NQO1 (μM)
8C7	2.8	0.6	≥ 30

Notes: a. Fold induction at 10 μM. Compounds (Cpds).

The compounds in group 4 (Table 8.7) are succinimide derivatives and were not active at a fixed dose of 10 μM.

Table 8.7: NQO1 (in the Hepa1c1c7 cell line) results for group 4 of the 8C compound range.

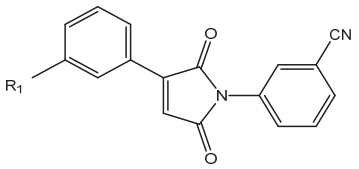

Cpds	R1	NQO1[a]	NQO1 CD (μM)	Toxicity NQO1 (μM)
8C8	CN	1.0	-[b]	-[b]
8C9	NO_2	1.0	-[b]	-[b]

Notes: a. Fold induction at 10 μM; b. Not determined. Compounds (Cpds).

The two most active compounds (**8C4** and **8C7**) (CD < 1.0 μM) and one moderately active compound (**8C5**) are shown in the following dose response graph (Figure 8.5).

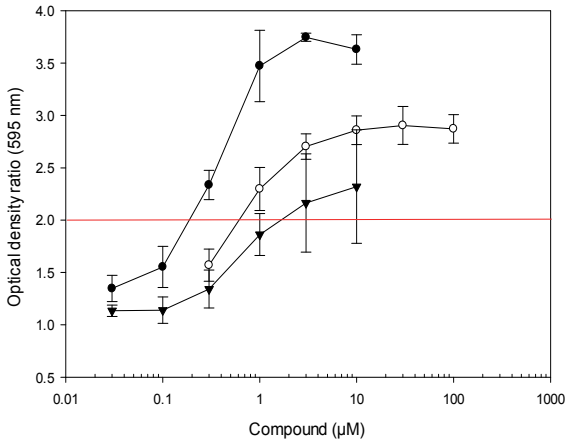

Figure 8.5: Dose response curves for the NQO1 assays of compounds **8C4** (●), **8C7** (○) and **8C5** (▼) in Hepa1c1c7 after 24 h stimulation. The error bars represent the standard deviation of n = 3 independent experiments.

8.3 Discussion

Although the phenolic 8A compounds may exert their NQO1 inducing ability after oxidation similarly to compounds containing Michael acceptors, they only showed modest activity in the cellular NQO1 assay. It is possible that their bio-oxidation might not be as effective as some other potent phenolic compounds such as t-BHQ.

The 8B compounds are chalcone based structures, similar to those developed by Kumar *et al.* [247]. Chloro and trifluoromethyl substituted derivatives of 8B groups 1 and 2 demonstrated promising activity in the cellular NQO1 assay. The NQO1 induction potencies of the group 1 structures were similar to activities found with 'compound 2b'-related structures (Figure 8.1 B) [247]. Moreover, the 8B compounds based on the group 2 core structure were highly active presenting CD values of 0.04 μM for the most potent **8B17** and **8B18** compounds. Group 2 compounds present a level of structural similarity with the 1,2,3-triazole derivatives (7C range group 4) and might be equally able to disrupt the interaction between Keap1 and Nrf2. However, these structures were not active in an FP-based assay. Nevertheless, 8B compounds ability to induce NQO1 activity may also be a result of an interaction with the AhR, as flavonoids and related structures are thought to act as AhR ligands [246]. Consequently, the compounds should additionally be examined in the ARNT-deficient BpRc1 cell line.

As the 8C compounds display structural similarity with the direct Nrf2 inducers described previously in Chapter 7 (7C range group 1), they were expected to be able to disrupt the Keap1-Nrf2 PPI to some extent and in this manner up-regulate the expression of NQO1. However, only weak inhibition potencies were observed in the FP assay; the highest inhibition percentage was observed with **8C1**, 17.5 % at 100 μM. The **8C1** compound demonstrated a similar NQO1 induction potency to that observed by Mayhoub *et al.* [251] (CD ~ 2 μM versus 4 μM). This activity improved considerably by substitution of the OMe groups to NO_2 (**8C4**) groups (CD ~ 0.2 μM). This is in agreement with observed NQO1 potencies for 1,2,3-triazole derivatives containing nitro substituents (group 1.1 7C compounds, Chapter 7). Moreover, the highly active lead compound **7C55** contains one nitro group and inhibited the Keap1-Nrf2 PPI in an FP based assay. However, **8C4** was cytotoxic at

concentration ≥ 3 μM. Compounds containing nitro groups are often associated with cytotoxicity as they can be bio-activated by cytochrome p450 enzymes to generate reactive products [241]. These reactive species can cause carcinogenicity, hepatotoxicity, mutagenicity and bone marrow suppression [241]. Compound **8C2** and **8C3** are structurally similar to the compounds in group 1.3a from the 7C compound range and present similar weak to moderate NQO1 activity in the cellular induction assay. The two 8C structures **8C5**, **8C6** and **8C7** share some level of structural similarity with structures in group 2.3 from the 7C compound range. However, none of the 7C structures were as potent as **8C7** in the NQO1 assay. The core scaffold of this compound has been reported as a component of a FLT3 kinase inhibitor [252]; hence, **8C7** may demonstrate off-target effects. The succinimide derivatives (**8C8** and **8C9**) were not active. As the 8C compounds were not highly active in the FP assay, their exact mode of action warrants further investigation.

9 Final discussion

The focus of this thesis is chemoprevention as an alternative strategy to current cancer treatments. Both natural and synthetic compounds have the potential to be developed into chemopreventive drugs. Here, several biological methods have been specifically optimised or developed to evaluate diverse libraries of small molecules and peptides for their ability to induce cytoprotective mechanisms by manipulating the Keap1-Nrf2 pathway. The main methods utilised included a cellular NQO1 induction assay that was optimised for screening purposes, an *in vitro* fluorescence polarisation (FP) screening assay that was previously developed in our group [143] and western blotting analysis. In addition to these optimised methods, two novel assays were developed: the *in-vitro* steady-state Förster resonance energy transfer (FRET) assay can be used to screen direct inhibitors of the Keap1-Nrf2 complex and the intracellular Nrf2 staining method for flow cytometry enables the quantification of Nrf2 protein levels and supports western blotting analysis.

Potential direct inhibitors of the Keap1-Nrf2 PPI were initially screened using an FP assay [143]. However, complex polarizing optics are necessary for FP based screening. The FRET technique requires only simple excitation and emission filters and is at present successfully applied to study diverse PPIs [140-141]. Here, a steady state FRET assay was developed to quantify protein-protein binding and to screen direct inhibitors of the Keap1-Nrf2 PPI. FRET was observed between the fusion proteins eCFP-TEV-Nrf2 and eYFP-TEV-Kelch due to a specific protein-protein interaction between the Keap1 Kelch domain and a 16-mer Nrf2 derived peptide. Subsequently, binding affinities were determined of both wild-type and (point) mutated Nrf2 derived peptides for the Keap1 Kelch domain. Competition was measured by monitoring the efficiency of energy transfer of the fluorescent labelled FRET pair during the addition of an unlabelled peptide or small molecule. IC_{50} values were determined from the observed reduction in FRET efficiency. Moreover, the FRET assay was adapted to a multi-well plate format and was found suitable for HTS with a Z′ value of 0.63 ±0.07.

During the project, western blotting was used as an approach to determine the level of protein expression. However, in this method one data point (stained protein band) is obtained by generating an average value for the protein expressed in an entire cell population (population analysis). As a consequence, datasets might differ from each other due to a range of responses within (multiple) cell populations. Flow cytometry applies the principle of single-cell analysis, which measures events in individual cells. The determination of protein induction levels using this technique improves the reliability and reproducibility of the obtained data. Here, a flow cytometry based method was developed to detect Nrf2 protein induction levels in both whole cells and isolated nuclei in a quantitative manner to support the more qualitative western blotting analysis. The application of the intracellular Nrf2 staining technique was verified using various Nrf2 inducing compounds in multiple cell lines. A specific primary antibody was found to be essential to ensure efficient staining.

For the biological evaluation of compound libraries, the thiol reactive natural product sulforaphane was shown to be a good reference compound with good Nrf2 and phase II enzyme induction potency in both Hepa1c1c7 and ARNT-deficient BpRc1 cells (NQO1 CD value ~ 0.4 μM and ~ 0.6 μM respectively). Subsequently, a library of quinol (cyclohexadienone) analogues, containing Michael acceptors, were evaluated for their ability to up-regulate the phase II enzyme NQO1. Structures that contained two Michael acceptors were found to be the most active. Especially, a series of optimised *p*-phenyl compounds demonstrated high potency and relatively low cytotoxicity levels (Table 6.1). The most promising structure was **6.49**, a 3-chlorophenyl compound. This molecule was able to up-regulate NQO1 enzyme activity in both Hepa1c1c7 and ARNT-deficient BpRc1 cells (CD values ~ 1 μM), which is indicative of a monofunctional inducer of Nrf2 [107]. Moreover, **6.49** stimulated nuclear Nrf2 accumulation in Hepa1c1c7 cells. Overall, **6.49** has potential to be developed as an effective indirect Nrf2 inducer molecule by reducing its cytotoxicity and by investigating its effect on other (related) pathways.

Direct Nrf2 inducers activate Nrf2 nuclear accumulation in a different way to cysteine reactive compounds. These structures are designed to interfere directly with the Keap1-Nrf2 PPI. In this inducer category several compound libraries have been examined. Peptides based on the high affinity ^{77}DEETGE^{82} sequence from Nrf2 demonstrated promising inhibitory properties.

In particular, peptides containing an E78P substitution, derived from the binding sequence of sequestosome-1, performed well in both FP and FRET competition assays. Although, these peptides were not active in the cell-based NQO1 induction assay, stearic acid (C_{18}) fatty acid conjugation promoted cellular penetration. Conjugation to a FITC fluorophore enabled the observation of peptide uptake and cellular distribution. Peptides and peptide conjugates are useful tools to identify and study the key binding sites in a PPI. Moreover, they can be used to develop small molecules with (enhanced) inhibitory properties.

The 7A series of small molecules is a selection of previously identified compounds with Keap1-Nrf2 PPI specific inhibitory properties. **7A4**, a bis-sulphonamide derivative, was one of the most potent molecules and demonstrated an IC_{50} of 2.84 μM in the developed FRET assay and a CD value of 8 μM in the cellular NQO1 induction assay in Hepa1c1c7 cells. Moreover, Nrf2 and downstream target enzymes HO-1 and NQO1 were up-regulated in a time dependent manner in Hepa1c1c7 cells. However, the induction of these proteins was significantly reduced in the ARNT-deficient BpRc1 cell line. Although a modest induction of the AhR transcription factor and downstream target CYP1A1 enzyme was found, other pathways may be affected by the **7A4** compound. Analysis of the closely related 'compound 16' described by Marcotte *et al.* [227] revealed the interaction of the compound with subpockets P3, P4 and P5 of Keap1 (Figure 7.4). The binding of this structure in the Keap1 subpockets was improved by Jiang *et al.* [129] who developed 'compound 2'. This structure contains two acetic acid side chains conjugated to the sulphonamide nitrogen from 'compound 16' and demonstrated additional interactions with the Keap1 P1 and P2 subpockets. Since the structure appears to make contact with all five subpockets of Keap1, 'compound 2' has the ability to disrupt the Keap1-Nrf2 PPI with high affinity. Studies performed here with the identical compound **7B1**, showed an IC_{50} value of 59 nM in an FP assay and a CD ~ 4 μM for NQO1 induction in Hepa1c1c7 cells. Although, attempts were made to optimise the cell-penetrating properties by reducing the compounds overall acidity and increasing lipophilicity, no successful structural improvements were made thus far.

As part of a docking screen, compound **7C55**, a 1,2,3-triazole derivative, was one of the most promising early molecules. The distance between the glutamate side chains of the Nrf2 high affinity motif ETGE was used to develop the scaffold of this structure. A **7C55** – Keap1 docking study revealed interactions of the compound with the P3 and P5 subpockets of Keap1. This virtual prediction was supported by promising FP results; IC_{50} ~ 7.1 μM and a FRET-FLIM study in which **7C55** was able to disrupt the Keap1-Nrf2 DLG motif interaction (submitted and in the press [229]). In addition, **7C55** was shown to be highly active in the cellular NQO1 induction assay; CD ~ 0.6 μM in Hepa1c1c7 cells. This induction was accompanied by nuclear Nrf2 accumulation and up-regulation of HO-1. Nevertheless, **7C55** was unable to induce the expression of Nrf2 and phase II enzymes in the ARNT-deficient BpRc1 cell line whilst modestly up-regulating the expression of AhR and CYP1A1 in the Hepa1c1c7 cell line. Moreover, **7C55** was found to induce mitophagy in MEF cells [244]. These data demonstrates **7C55**'s wide range of (cellular) activity and potential for further development.

The 8C compounds were of a similar design to **7C55** and evaluated as Keap1-Nrf2 PPI inhibitors. However, FP results demonstrated only low inhibition percentages. Nevertheless, these structures were able to induce the expression of NQO1 via an as yet unknown mechanism. 8B compounds represent a group of chalcone and flavanone derivatives with a very high potency for NQO1 up-regulation (CD values ~ 40 nM). Although these compounds also share some level of structural similarity with **7C55**, they were barely active in the FP assay (data not shown). In future studies, both compound groups should be evaluated in the ARNT-deficient BpRc1 cell line to verify potential cross-talk with the AhR.

Results of the biological evaluation of diverse direct and indirect Nrf2 inducer compounds aid in the future development of drugs targeted at the disruption of the Keap1-Nrf2 pathway. This is of vital importance as inhibitors of the Keap1-Nrf2 PPI may have additional effects on other pathways. In particular, potential AhR-XRE cross-talk may be responsible for cellular activity. For cross-talk activity it is desirable to include assays which generate additional data beyond enzyme induction, to provide a coherent drug discovery approach and to get a better impression of compounds selective behaviour.

10 Future perspectives

The work described in this thesis has developed a number of research themes that warrant further study in the future. Some of these topics and experiments are described in more detail in the sections below.

10.1 *In vitro* steady-state FRET based assay

Future work may be targeted at improvement of the observed FRET between the interacting proteins by using a different fluorescent FRET pair or by altering the position or orientation of the fluorophores. In addition, the binding efficiencies of other Keap1 or Nrf2 interacting proteins may be studied by fusing them to appropriate fluorophores.

The anti-apoptotic protein Bcl2 is reported to interact with the Keap1 – Kelch domain through its BH2 domain [253]. It has been proposed that Bcl2 can escape Keap1 mediated ubiquitination and degradation through oxidative stress or electrophilic compounds that modify key cysteine residues in Keap1 [254]. As a result, apoptosis reduces whilst cell survival increases. To examine whether Bcl2 directly competes with Nrf2 for Keap1 binding sites, preliminary FRET experiments were performed using a 16-mer Bcl2 - BH2 domain peptide. No change in FRET efficiency was observed upon addition of BH2 peptide (100 μM, final concentration) to the eCFP-TEV-Nrf2 and eYFP-TEV-Kelch protein mixture (0.11 μM and 0.20 μM respectively). However, *in vitro*, the BH2 peptide may not fold into a conformation that is recognised by the Keap1 Kelch domain. The Keap1 binding affinity of the Bcl2 protein may be determined by future FRET experiments in which the anti-apoptotic protein is conjugated to an eCFP fluorophore and the Keap1 Kelch protein is fused to an eYFP protein.

10.2 Crystal structure determination eYFP-TEV-Kelch protein

In 2004, Li *et al.* [255] determined the crystal structure of the Kelch domain of human Keap1. Two years later Lo *et al.* [46] published the crystal structure of Keap1-Kelch in complex with a 16-mer Nrf2 based peptide. In this project an eYFP conjugated Kelch protein was expressed and purified for the development of a steady-state FRET based assay to identify inhibitors of the Keap1-Nrf2 PPI. To obtain structural information regarding the eYFP fusion protein binding properties of peptides and small molecules, preliminary experiments were performed to determine the crystal structure for the eYFP-TEV-Kelch protein alone and in complex with an Nrf2 based 7-mer peptide. Following immobilised metal affinity chromatography (IMAC), the fluorophore fusion protein was additionally purified using size exclusion chromatography. Crystallisation screens with diverse conditions were set up using the hanging drop vapour diffusion method. Although the eYFP-TEV-Kelch protein benefits from enhanced protein stability due to fluorophore conjugation, no crystals were obtained. Future determination of the crystal structure of the eYFP conjugated Kelch protein may allow further optimisation of the steady-state FRET based assay by providing information regarding the position and orientation of the fluorophore.

10.3 Nrf2 intracellular staining method for flow cytometry

Further assay improvements may be made by including the fluorescent labelling of other relevant proteins (phase II enzymes) to enable the measurement of multiple parameters in an individual sample and by adapting the assay to a multi-well plate format using suitable instruments and further method development to facilitate HTS screening.

10.4 Compound combination effect

The combined effect (synergism, additive or antagonism) of direct and indirect inducers on the up-regulation of the Nrf2 target gene NQO1 in Hepa1c1c7 cells was examined in preliminary experiments to gain better understanding on the disruption of the interaction between Keap1 and Nrf2 (data not shown). The hypothesis was

that when two compounds target the same site the combined effect may plateau at a particular concentration due to occupation of the binding site by either or both compounds. Alternatively, combining two mechanistically different molecules could result in either an additive or synergistic effect as the target site is dissimilar. However, results were inconclusive and follow-up experiments are needed to observe possible different effects at a wide dose range. This may aid in the development of Nrf2 inducer molecules with multiple mode of actions, hence maximizing potency.

10.5 Gene silencing of AhR and Nrf2

Preliminary gene silencing experiments with short hairpin RNA (shRNA) were performed to examine the effect of AhR and Nrf2 protein knockdown on Nrf2 inducer dependent NQO1 induction (Figure 10.1). Transfection of cells with shRNA enables long-term gene silencing through stable integration of shRNA [256]. Moreover, transfection efficiency can be monitored with a co-expressed reporter gene e.g a fluorophore. Hepa1c1c7 cells were transfected with an AhR or Nrf2-specific shRNA plasmid containing a coding sequence for a Green Fluorescent Protein (GFP) (Figure 10.1). Although flow cytometry analysis demonstrated an increase in GFP fluorescence in transfected cells, western blots using antibodies against AhR and Nrf2 presented no evidence of protein knockdown. Successful protein knockdown experiments could aid in the evaluation of a compound's potential AhR-XRE cross-talk activity.

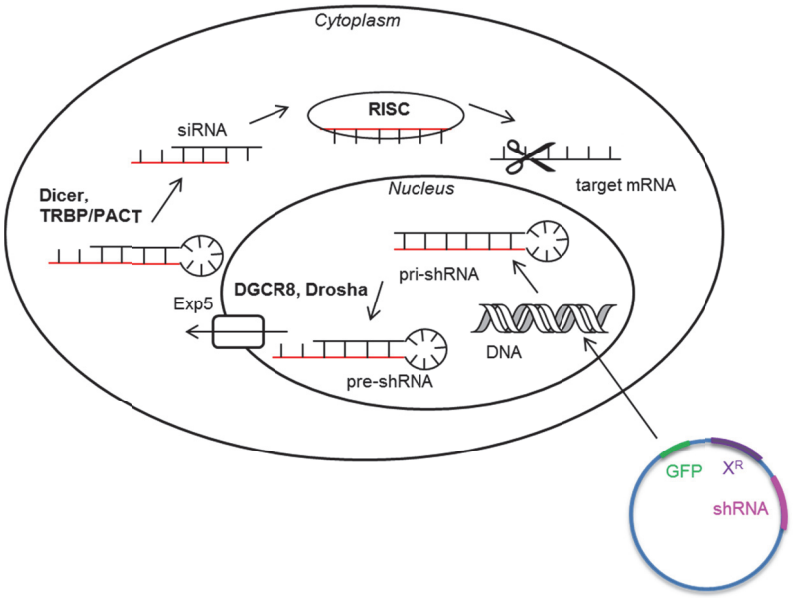

Figure 10.1: Schematic overview of shRNA induced gene silencing, adapted from [256]. Following the transfection of plasmid based short hairpin RNAs (shRNAs) into cells, pri-shRNAs are synthesised in the nucleus. The pri-shRNAs are bound and processed by dsRNA-binding protein DiGeorge syndrome chromosomal region 8 (DGCR8) and RNase III enzyme Drosha, resulting in pre-shRNAs, which are exported to the cytoplasm by Exportin-5 (Exp5). The RNase III enzyme Dicer and binding partners trans-activation response RNA-binding protein (TRBP) or protein activator of PKR (PACT) cleave the pre-shRNAs to remove the hairpin and to create two nucleotides overhang at the 3' end. The generated siRNA is then bound by the RNA-induced silencing complex (RISC). The RISC removes one of the RNA strands and allows the siRNA to target mRNA with a complementary sequence, resulting in their degradation. The shRNA plasmid contains a coding region for the reporter gene GFP, an antibiotic resistance gene (X^R) and the shRNA.

10.6 Transcription factor array

To examine whether the Keap1-Nrf2 pathway is able to activate other transcription factors, preliminary experiments were performed using the transcription factor activation profiling array (Signosis) (data not shown). This method uses biotin-labeled probes that contain consensus sequences of transcription factor DNA binding sites. These probes are incubated with nuclear extracts of cells that are stimulated with Nrf2 inducer compounds. Following the formation of transcription factor-probe complexes, the bound probes are detached and hybridised with complementary sequences of the probes that are pre-coated on a plate.

Streptavidin-HRP is used to detect the bound probes. Although this array would provide important information regarding the activation of other transcription factors upon induction of the Keap1-Nrf2 pathway, the results were inconclusive. Hence, re-evaluation using similar assays is needed.

References

1. http://publications.cancerresearchuk.org/downloads/Product/CS_REPORT_MORTALITY.pdf. (accessed 25 February 2015).
2. http://publications.cancerresearchuk.org/downloads/Product/CS_KF_ALLCANCERS.pdf. (accessed 25 February 2015).
3. http://publications.cancerresearchuk.org/downloads/Product/CS_REPORT_TOP10INCMORT.pdf. (accessed 25 February 2015).
4. Jemal, A., et al., Global cancer statistics. *CA: a cancer journal for clinicians*, **2011**, 61, 69-90.
5. Anand, P., et al., Cancer is a Preventable Disease that Requires Major Lifestyle Changes. *Pharmaceutical Research*, **2008**, 25, 2097-2116.
6. Bray, F., et al., Global cancer transitions according to the Human Development Index (2008-2030): a population-based study. *The Lancet. Oncology*, **2012**, 13, 790-801.
7. Lyman, G. H., Counting the costs of cancer care. *The Lancet. Oncology*, **2013**, 14, 1142-3.
8. http://www.patient.co.uk/health/cancer-a-general-overview. (accessed 25 February 2015).
9. http://www.cancer.org/treatment/treatmentsandsideeffects/treatmenttypes/surgery/surgery-how-is-surgery-used-for-cancer. (accessed 25 February 2015).
10. Chabner, B. A.; Roberts, T. G., Chemotherapy and the war on cancer. *Nat Rev Cancer*, **2005**, 5, 65-72.
11. http://www.cancer.org/treatment/treatmentsandsideeffects/treatmenttypes/chemotherapy/chemotherapyprinciplesanin-depthdiscussionofthetechniquesanditsroleintreatment/chemotherapy-principles-types-of-chemo-drugs. (accessed 25 February 2015).
12. http://www.cancerresearchuk.org/about-cancer/cancers-in-general/treatment/chemotherapy/about/how-chemotherapy-works. (accessed 25 February 2015).
13. Baskar, R., et al., Cancer and radiation therapy: current advances and future directions. *International journal of medical sciences*, **2012**, 9, 193-9.
14. http://www.cancer.gov/researchandfunding/progress/immunotherapy-using-immune-system-to-treat-cancer. (accessed 25 February 2015).
15. Cross, D.; Burmester, J. K., Gene Therapy for Cancer Treatment: Past, Present and Future. *Clinical Medicine and Research*, **2006**, 4, 218-227.
16. Pitot, H. C., The molecular biology of carcinogenesis. *Cancer*, **1993**, 72, 962-70.
17. Weston, A., Harris, C.C. , Multistage Carcinogenesis. In Holland-Frei Cancer Medicine 6th edition, Kufe DW, P. R., Weichselbaum RR, et al., Ed. Hamilton (ON): BC Decker, **2003**.
18. Waris, G.; Ahsan, H., Reactive oxygen species: role in the development of cancer and various chronic conditions. *J Carcinog*, **2006**, 5, 14.
19. Lobo, V., et al., Free radicals, antioxidants and functional foods: Impact on human health. *Pharmacognosy Reviews*, **2010**, 4, 118-126.
20. Waris, G.; Ahsan, H., Reactive oxygen species: role in the development of cancer and various chronic conditions. *Journal of Carcinogenesis*, **2006**, 5, 14-14.

21. Sporn, M. B., et al., Prevention of chemical carcinogenesis by vitamin A and its synthetic analogs (retinoids). *Fed Proc*, **1976**, 35, 1332-8.
22. Wattenberg, L. W., Prevention--therapy--basic science and the resolution of the cancer problem. *Cancer Res*, **1993**, 53, 5890-6.
23. Wattenberg, L. W., Chemoprevention of cancer. *Cancer Res*, **1985**, 45, 1-8.
24. Manson, M. M., et al., Blocking and suppressing mechanisms of chemoprevention by dietary constituents. *Toxicol Lett*, **2000**, 112-113, 499-505.
25. Omiecinski, C. J., et al., Xenobiotic metabolism, disposition, and regulation by receptors: from biochemical phenomenon to predictors of major toxicities. *Toxicological sciences : an official journal of the Society of Toxicology*, **2011**, 120 Suppl 1, S49-75.
26. Jancova, P., et al., Phase II drug metabolizing enzymes. *Biomedical papers of the Medical Faculty of the University Palacky, Olomouc, Czechoslovakia*, **2010**, 154, 103-16.
27. Lee, J. S.; Surh, Y. J., Nrf2 as a novel molecular target for chemoprevention. *Cancer letters*, **2005**, 224, 171-84.
28. Nguyen, T., et al., Transcriptional regulation of the antioxidant response element. Activation by Nrf2 and repression by MafK. *Journal of Biological Chemistry*, **2000**, 275, 15466-15473.
29. Itoh, K., et al., An Nrf2/small Maf heterodimer mediates the induction of phase II detoxifying enzyme genes through antioxidant response elements. *Biochemical and biophysical research communications*, **1997**, 236, 313-22.
30. Itoh, K., et al., Keap1 represses nuclear activation of antioxidant responsive elements by Nrf2 through binding to the amino-terminal Neh2 domain. *Genes & development*, **1999**, 13, 76-86.
31. Katoh, Y., et al., Two domains of Nrf2 cooperatively bind CBP, a CREB binding protein, and synergistically activate transcription. *Genes to cells : devoted to molecular & cellular mechanisms*, **2001**, 6, 857-68.
32. Nioi, P., et al., The carboxy-terminal Neh3 domain of Nrf2 is required for transcriptional activation. *Molecular and cellular biology*, **2005**, 25, 10895-906.
33. McMahon, M., et al., Redox-regulated turnover of Nrf2 is determined by at least two separate protein domains, the redox-sensitive Neh2 degron and the redox-insensitive Neh6 degron. *The Journal of biological chemistry*, **2004**, 279, 31556-67.
34. Chowdhry, S., et al., Nrf2 is controlled by two distinct beta-TrCP recognition motifs in its Neh6 domain, one of which can be modulated by GSK-3 activity. *Oncogene*, **2013**, 32, 3765-81.
35. Baird, L.; Dinkova-Kostova, A. T., The cytoprotective role of the Keap1-Nrf2 pathway. *Arch Toxicol*, **2011**, 85, 241-72.
36. Kobayashi, M., et al., Identification of the interactive interface and phylogenic conservation of the Nrf2-Keap1 system. *Genes to cells : devoted to molecular & cellular mechanisms*, **2002**, 7, 807-20.
37. Zipper, L. M.; Mulcahy, R. T., The Keap1 BTB/POZ dimerization function is required to sequester Nrf2 in cytoplasm. *The Journal of biological chemistry*, **2002**, 277, 36544-52.
38. McMahon, M., et al., Keap1-dependent proteasomal degradation of transcription factor Nrf2 contributes to the negative regulation of antioxidant response element-driven gene expression. *The Journal of biological chemistry*, **2003**, 278, 21592-600.
39. He, X., et al., Arsenic Induces NAD(P)H-quinone Oxidoreductase I by Disrupting the Nrf2·Keap1·Cul3 Complex and Recruiting Nrf2·Maf to the Antioxidant Response Element Enhancer. *Journal of Biological Chemistry*, **2006**, 281, 23620-23631.
40. Dinkova-Kostova, A. T., et al., Direct evidence that sulfhydryl groups of Keap1 are the sensors regulating induction of phase 2 enzymes that protect against

carcinogens and oxidants. *Proceedings of the National Academy of Sciences of the United States of America*, **2002**, 99, 11908-13.
41. Kobayashi, A., et al., Oxidative and electrophilic stresses activate Nrf2 through inhibition of ubiquitination activity of Keap1. *Molecular and cellular biology*, **2006**, 26, 221-9.
42. Niture, S. K., et al., Nrf2 signaling and cell survival. *Toxicology and applied pharmacology*, **2010**, 244, 37-42.
43. Geismann, C., et al., Cytoprotection "gone astray": Nrf2 and its role in cancer. *OncoTargets and therapy*, **2014**, 7, 1497-518.
44. Hayes, J. D.; Dinkova-Kostova, A. T., The Nrf2 regulatory network provides an interface between redox and intermediary metabolism. *Trends in biochemical sciences*, **2014**, 39, 199-218.
45. Tong, K. I., et al., Different electrostatic potentials define ETGE and DLG motifs as hinge and latch in oxidative stress response. *Molecular and cellular biology*, **2007**, 27, 7511-21.
46. Lo, S. C., et al., Structure of the Keap1:Nrf2 interface provides mechanistic insight into Nrf2 signaling. *EMBO J*, **2006**, 25, 3605-17.
47. Tong, K. I., et al., Keap1 recruits Neh2 through binding to ETGE and DLG motifs: characterization of the two-site molecular recognition model. *Molecular and cellular biology*, **2006**, 26, 2887-900.
48. McMahon, M., et al., Dimerization of substrate adaptors can facilitate cullin-mediated ubiquitylation of proteins by a "tethering" mechanism: a two-site interaction model for the Nrf2-Keap1 complex. *The Journal of biological chemistry*, **2006**, 281, 24756-68.
49. Tong Kit, I., et al., Two-site substrate recognition model for the Keap1-Nrf2 system: a hinge and latch mechanism. In Biological chemistry, **2006**, Vol. 387, p 1311.
50. Villeneuve, N. F., et al., USP15 negatively regulates Nrf2 through deubiquitination of Keap1. *Molecular cell*, **2013**, 51, 68-79.
51. Aoki, Y., et al., Accelerated DNA adduct formation in the lung of the Nrf2 knockout mouse exposed to diesel exhaust. *Toxicology and applied pharmacology*, **2001**, 173, 154-60.
52. Magesh, S., et al., Small molecule modulators of Keap1-Nrf2-ARE pathway as potential preventive and therapeutic agents. *Medicinal research reviews*, **2012**, 32, 687-726.
53. Kim, Y. R., et al., Oncogenic NRF2 mutations in squamous cell carcinomas of oesophagus and skin. *J Pathol*, **2010**, 220, 446-51.
54. Padmanabhan, B., et al., Structural basis for defects of Keap1 activity provoked by its point mutations in lung cancer. *Molecular cell*, **2006**, 21, 689-700.
55. Shibata, T., et al., Cancer related mutations in NRF2 impair its recognition by Keap1-Cul3 E3 ligase and promote malignancy. *Proceedings of the National Academy of Sciences of the United States of America*, **2008**, 105, 13568-73.
56. Zhang, P., et al., Loss of Kelch-like ECH-associated protein 1 function in prostate cancer cells causes chemoresistance and radioresistance and promotes tumor growth. *Molecular cancer therapeutics*, **2010**, 9, 336-46.
57. Homma, S., et al., Nrf2 enhances cell proliferation and resistance to anticancer drugs in human lung cancer. *Clin Cancer Res*, **2009**, 15, 3423-32.
58. Singh, A., et al., Expression of ABCG2 (BCRP) is regulated by Nrf2 in cancer cells that confers side population and chemoresistance phenotype. *Molecular cancer therapeutics*, **2010**, 9, 2365-76.
59. Kensler, T. W.; Wakabayashi, N., Nrf2: friend or foe for chemoprevention? *Carcinogenesis*, **2010**, 31, 90-9.
60. Wang, X. J., et al., Nrf2 enhances resistance of cancer cells to chemotherapeutic drugs, the dark side of Nrf2. *Carcinogenesis*, **2008**, 29, 1235-43.

61. Xiang, M., et al., Nrf2: bane or blessing in cancer? *Journal of cancer research and clinical oncology*, **2014**, 140, 1251-9.
62. Jones, G. W. The design, synthesis and evaluation of novel cyclohexadienones as cancer chemopreventive agents. UCL, School of Pharmacy, **2013**.
63. Talalay, P., Mechanisms of induction of enzymes that protect against chemical carcinogenesis. *Advances in enzyme regulation*, **1989**, 28, 237-50.
64. Talalay, P., Chemoprotection against cancer by induction of phase 2 enzymes. *BioFactors (Oxford, England)*, **2000**, 12, 5-11.
65. Prochaska, H. J.; Santamaria, A. B., Direct measurement of NAD(P)H:quinone reductase from cells cultured in microtiter wells: a screening assay for anticarcinogenic enzyme inducers. *Analytical biochemistry*, **1988**, 169, 328-36.
66. Atia, A., et al., A Review of NAD(P)H:Quinone Oxidoreductase 1 (NQO1); A Multifunctional Antioxidant Enzyme. *J App Pharm Sci*, **2014**, 4, 118-122.
67. Prochaska, H. J., et al., Rapid detection of inducers of enzymes that protect against carcinogens. *Proceedings of the National Academy of Sciences of the United States of America*, **1992**, 89, 2394-2398.
68. Zhang, Y., et al., A major inducer of anticarcinogenic protective enzymes from broccoli: isolation and elucidation of structure. *Proceedings of the National Academy of Sciences of the United States of America*, **1992**, 89, 2399-403.
69. Zhang, Y.; Tang, L., Discovery and development of sulforaphane as a cancer chemopreventive phytochemical. *Acta Pharmacol Sin*, **2007**, 28, 1343-1354.
70. Ahn, Y. H., et al., Electrophilic tuning of the chemoprotective natural product sulforaphane. *Proceedings of the National Academy of Sciences of the United States of America*, **2010**, 107, 9590-5.
71. Li, W.; Kong, A. N., Molecular mechanisms of Nrf2-mediated antioxidant response. *Molecular carcinogenesis*, **2009**, 48, 91-104.
72. Houghton, C. A., et al., Sulforaphane: translational research from laboratory bench to clinic. *Nutrition Reviews*, **2013**, 71, 709-726.
73. Jaramillo, M. C.; Zhang, D. D., The emerging role of the Nrf2-Keap1 signaling pathway in cancer. *Genes & development*, **2013**, 27, 2179-91.
74. Bueding, E., et al., The antischistosomal activity of oltipraz. *Research communications in chemical pathology and pharmacology*, **1982**, 37, 293-303.
75. Clapper, M. L., Chemopreventive activity of oltipraz. *Pharmacology & therapeutics*, **1998**, 78, 17-27.
76. Moon, R. C., et al., Chemoprevention of OH-BBN-induced bladder cancer in mice by oltipraz, alone and in combination with 4-HPR and DFMO. *Anticancer research*, **1994**, 14, 5-11.
77. Zhang, Y.; Munday, R., Dithiolethiones for cancer chemoprevention: where do we stand? *Molecular cancer therapeutics*, **2008**, 7, 3470-3479.
78. Miao, W., et al., Oltipraz Is a Bifunctional Inducer Activating Both Phase I and Phase II Drug-Metabolizing Enzymes via the Xenobiotic Responsive Element. *Molecular Pharmacology*, **2003**, 64, 346-354.
79. Yu, R., et al., Butylated Hydroxyanisole and Its Metabolitetert-Butylhydroquinone Differentially Regulate Mitogen-activated Protein Kinases: The role of oxidative stress in the activation of mitogen-activated protein kinases by phenolic antioxidants. *Journal of Biological Chemistry*, **1997**, 272, 28962-28970.
80. Duffy, S., et al., Activation of endogenous antioxidant defenses in neuronal cells prevents free radical-mediated damage. *Journal of neurochemistry*, **1998**, 71, 69-77.
81. Yan, D., et al., Induction of the Nrf2-driven antioxidant response by tert-butylhydroquinone prevents ethanol-induced apoptosis in cranial neural crest cells. *Biochem Pharmacol*, **2010**, 80, 144-9.

82. Murphy, T. H., et al., Enhanced NAD(P)H:quinone reductase activity prevents glutamate toxicity produced by oxidative stress. *Journal of neurochemistry*, **1991**, 56, 990-5.
83. Li, J., et al., Stabilization of Nrf2 by tBHQ confers protection against oxidative stress-induced cell death in human neural stem cells. *Toxicological sciences : an official journal of the Society of Toxicology*, **2005**, 83, 313-28.
84. Hong, F., et al., Specific patterns of electrophile adduction trigger Keap1 ubiquitination and Nrf2 activation. *The Journal of biological chemistry*, **2005**, 280, 31768-75.
85. Dinkova-Kostova, A. T.; Wang, X. J., Induction of the Keap1/Nrf2/ARE pathway by oxidizable diphenols. *Chemico-Biological Interactions*, **2011**, 192, 101-106.
86. Kumar, H., et al., Natural product-derived pharmacological modulators of Nrf2/ARE pathway for chronic diseases. *Natural product reports*, **2014**, 31, 109-39.
87. Gharavi, N., et al., Chemoprotective and carcinogenic effects of tert-butylhydroquinone and its metabolites. *Current drug metabolism*, **2007**, 8, 1-7.
88. Ravanan, P., et al., Growth inhibitory, apoptotic and anti-inflammatory activities displayed by a novel modified triterpenoid, cyano enone of methyl boswellates. *Journal of biosciences*, **2011**, 36, 297-307.
89. Dinkova-Kostova, A. T., et al., Extremely potent triterpenoid inducers of the phase 2 response: correlations of protection against oxidant and inflammatory stress. *Proceedings of the National Academy of Sciences of the United States of America*, **2005**, 102, 4584-9.
90. Klaassen, C. D.; Reisman, S. A., Nrf2 the Rescue: Effects of the Antioxidative/Electrophilic Response on the Liver. *Toxicology and applied pharmacology*, **2010**, 244, 57-65.
91. Thimmulappa, R. K., et al., Preclinical evaluation of targeting the Nrf2 pathway by triterpenoids (CDDO-Im and CDDO-Me) for protection from LPS-induced inflammatory response and reactive oxygen species in human peripheral blood mononuclear cells and neutrophils. *Antioxidants & redox signaling*, **2007**, 9, 1963-70.
92. Wang, Y. Y., et al., Preclinical evidences toward the use of triterpenoid CDDO-Me for solid cancer prevention and treatment. *Molecular cancer*, **2014**, 13, 30.
93. Wang, Y.-Y., et al., Bardoxolone methyl (CDDO-Me) as a therapeutic agent: an update on its pharmacokinetic and pharmacodynamic properties. *Drug Design, Development and Therapy*, **2014**, 8, 2075-2088.
94. Zhao, C. R., et al., Nrf2-ARE signaling pathway and natural products for cancer chemoprevention. *Cancer epidemiology*, **2010**, 34, 523-33.
95. Nguyen, T., et al., The Nrf2-Antioxidant Response Element Signaling Pathway and Its Activation by Oxidative Stress. *Journal of Biological Chemistry*, **2009**, 284, 13291-13295.
96. Chen, A. F.; Kirsner, R. S., Mechanisms of Drug Action: The Potential of Dimethylfumarate for the Treatment of Neoplasms. *J Invest Dermatol*, **2011**, 131, 1181-1181.
97. To, C., et al., Dimethyl fumarate and the oleanane triterpenoids, CDDO-Imidazolide and CDDO-Methyl Ester, both activate the Nrf2 pathway but have opposite effects in the A/J model of lung carcinogenesis. *Carcinogenesis*, **2015**.
98. Zhuang, C., et al., Updated Research and Applications of Small Molecule Inhibitors of Keap1-Nrf2 Protein-Protein Interaction: a Review. *Current medicinal chemistry*, **2014**.
99. Rusten, T. E.; Stenmark, H., p62, an autophagy hero or culprit? *Nat Cell Biol*, **2010**, 12, 207-209.

100. Jain, A., et al., p62/SQSTM1 is a target gene for transcription factor NRF2 and creates a positive feedback loop by inducing antioxidant response element-driven gene transcription. *Journal of Biological Chemistry*, **2010**.
101. Hancock, R. The discovery and evaluation of inhibitors of the Keap1-Nrf2 protein-protein interaction. School of Pharmacy, UCL, **2012**.
102. Han Xiao, F. L., Derek Stewart and Yiguo Zhang, Mechanisms underlying chemopreventive effects of flavonoids via multiple signaling nodes within Nrf2-ARE and AhR-XRE gene regulatory networks. *Current Chemical Biology*, **2013**, 7, 151-176.
103. Kohle, C.; Bock, K. W., Coordinate regulation of Phase I and II xenobiotic metabolisms by the Ah receptor and Nrf2. *Biochem Pharmacol*, **2007**, 73, 1853-62.
104. Hayes, J. D., et al., Cross-talk between transcription factors AhR and Nrf2: lessons for cancer chemoprevention from dioxin. *Toxicological sciences : an official journal of the Society of Toxicology*, **2009**, 111, 199-201.
105. Wang, L., et al., The aryl hydrocarbon receptor interacts with nuclear factor erythroid 2-related factor 2 to mediate induction of NAD(P)H:quinoneoxidoreductase 1 by 2,3,7,8-tetrachlorodibenzo-p-dioxin. *Archives of biochemistry and biophysics*, **2013**, 537, 31-8.
106. Shin, S., et al., NRF2 modulates aryl hydrocarbon receptor signaling: influence on adipogenesis. *Molecular and cellular biology*, **2007**, 27, 7188-97.
107. The AH receptor in Biology and Toxicology. Pohjanvirta, R., Ed. John Wiley & Sons Inc., **2012**, 115-117.
108. Fahey, J. W., et al., The "Prochaska" microtiter plate bioassay for inducers of NQO1. *Methods Enzymol*, **2004**, 382, 243-58.
109. Cancer Chemoprevention, Volume 2: Strategies for Cancer Chemoprevention. Humana Press, **2005**.
110. Seidel, S. D.; Denison, M. S., Differential gene expression in wild-type and arnt-defective mouse hepatoma (Hepa1c1c7) cells. *Toxicological sciences : an official journal of the Society of Toxicology*, **1999**, 52, 217-25.
111. Boerboom, A.-M. J. F., et al., Newly constructed stable reporter cell lines for mechanistic studies on electrophile-responsive element-mediated gene expression reveal a role for flavonoid planarity. *Biochemical Pharmacology*, **2006**, 72, 217-226.
112. Wang, X. J., et al., Generation of a stable antioxidant response element-driven reporter gene cell line and its use to show redox-dependent activation of nrf2 by cancer chemotherapeutic agents. *Cancer Res*, **2006**, 66, 10983-94.
113. Wang, X. J., et al., Identification of retinoic acid as an inhibitor of transcription factor Nrf2 through activation of retinoic acid receptor alpha. *Proceedings of the National Academy of Sciences of the United States of America*, **2007**, 104, 19589-94.
114. Dinkova-Kostova, A. T., et al., An exceptionally potent inducer of cytoprotective enzymes: elucidation of the structural features that determine inducer potency and reactivity with Keap1. *The Journal of biological chemistry*, **2010**, 285, 33747-55.
115. Wu, K. C., et al., Implementation of a high-throughput screen for identifying small molecules to activate the Keap1-Nrf2-ARE pathway. *PloS one*, **2012**, 7, e44686.
116. Smirnova, N. A., et al., Development of Neh2-luciferase reporter and its application for high throughput screening and real-time monitoring of Nrf2 activators. *Chem Biol*, **2011**, 18, 752-65.
117. DiscoveRx, Product Booklet: 93-0821C3. In PathHunter® Keap1-Nrf2 Functional Assay for chemiluminescent detection of activated Nrf2, DiscoveRx: **2011**.
118. Wang L, L. T., Zhang YL, et al., The identification and characterization of non-reactive inhibitor of Keap1-Nrf2 interaction through HTS using a fluorescence

polarization assay. In Probe Reports from the NIH Molecular Libraries Program, National Center for Biotechnology Information **2012**.
119. Hu, L., et al., Discovery of a small-molecule inhibitor and cellular probe of Keap1-Nrf2 protein-protein interaction. *Bioorganic & medicinal chemistry letters*, **2013**, 23, 3039-43.
120. Kwak, M.-K., et al., Enhanced Expression of the Transcription Factor Nrf2 by Cancer Chemopreventive Agents: Role of Antioxidant Response Element-Like Sequences in the nrf2 Promoter. *Molecular and cellular biology*, **2002**, 22, 2883-2892.
121. Chemical, C., Nrf2 Transcription Factor Assay Kit: 600590. Cayman Chemical.
122. Inc., A. M., TransAM Nrf2: 50296 & 50796. Active Motif Inc.: **2014**.
123. Biotechnology, A., Nrf2 colorimetric cell-based ELISA: CB5496. In CytoGlow, Assay Biotechnology.
124. Heid, C. A., et al., Real time quantitative PCR. *Genome research*, **1996**, 6, 986-94.
125. Bustin, S. A.; Mueller, R., Real-time reverse transcription PCR (qRT-PCR) and its potential use in clinical diagnosis. *Clinical science (London, England : 1979)*, **2005**, 109, 365-79.
126. Mahmood, T.; Yang, P.-C., Western Blot: Technique, Theory, and Trouble Shooting. *North American Journal of Medical Sciences*, **2012**, 4, 429-434.
127. Lea, W. A.; Simeonov, A., Fluorescence Polarization Assays in Small Molecule Screening. *Expert opinion on drug discovery*, **2011**, 6, 17-32.
128. Hu, L., et al., Discovery of a small-molecule inhibitor and cellular probe of Keap1-Nrf2 protein-protein interaction. *Bioorganic & medicinal chemistry letters*, **2013**, 23, 3039-43.
129. Jiang, Z. Y., et al., Discovery of potent Keap1-Nrf2 protein-protein interaction inhibitor based on molecular binding determinants analysis. *Journal of medicinal chemistry*, **2014**, 57, 2736-45.
130. Neumann, T., et al., SPR-based fragment screening: Advantages and applications. *Current Topics in Medicinal Chemistry*, **2007**, 7, 1630-1642.
131. John, B. N., et al., Small-Molecule And Peptide Activators Of The Nrf2-Dependent Antioxidant Response Element. In A62. Lung Fibrosis: Fibroblast Biology, American Thoracic Society, **2014**, A2019-A2019.
132. Cino, E. A., et al., Binding of disordered proteins to a protein hub. *Scientific reports*, **2013**, 3, 2305.
133. Fowkes, A., et al., Biochemical assays and biophysical tools for inhibitor identification and validation. In Understanding and Exploiting Protein-Protein Interactions as Drug Targets, Future Science Ltd, **2013**, 104-116.
134. Kask, P., et al., Two-dimensional fluorescence intensity distribution analysis: theory and applications. *Biophysical journal*, **2000**, 78, 1703-13.
135. Marcotte, D., et al., Small molecules inhibit the interaction of Nrf2 and the Keap1 Kelch domain through a non-covalent mechanism. *Bioorganic & medicinal chemistry*, **2013**, 21, 4011-9.
136. Vivoli, M., et al., Determination of Protein-ligand Interactions Using Differential Scanning Fluorimetry. **2014**, e51809.
137. Vollrath, F., et al., Differential Scanning Fluorimetry provides high throughput data on silk protein transitions. *Sci. Rep.*, **2014**, 4.
138. Niesen, F. H., et al., The use of differential scanning fluorimetry to detect ligand interactions that promote protein stability. *Nature protocols*, **2007**, 2, 2212-21.
139. Zhuang, C., et al., Rapid identification of Keap1-Nrf2 small-molecule inhibitors through structure-based virtual screening and hit-based substructure search. *Journal of medicinal chemistry*, **2014**, 57, 1121-6.

140. Martin, S. F., et al., Quantitative analysis of multi-protein interactions using FRET: application to the SUMO pathway. *Protein science : a publication of the Protein Society*, **2008**, 17, 777-84.
141. Stankovic-Valentin, N., et al., An in vitro FRET-based assay for the analysis of SUMO conjugation and isopeptidase cleavage. *Methods in molecular biology (Clifton, N.J.)*, **2009**, 497, 241-51.
142. Schaap, M., et al., Development of a steady-state FRET-based assay to identify inhibitors of the Keap1-Nrf2 protein-protein interaction. *Protein science : a publication of the Protein Society*, **2013**, 22, 1812-9.
143. Hancock, R., et al., Peptide inhibitors of the Keap1-Nrf2 protein-protein interaction. *Free Radic Biol Med*, **2012**, 52, 444-51.
144. http://www.bio.davidson.edu/Courses/Molbio/MolStudents/spring2003/Causey/pET.htmlThe (accessed 1 April 2015).
145. Judelson, H., Primer Guidelines. http://oomyceteworld.net/protocols/primer%20designing2.pdf. (accessed 13 March 2015).
146. PCR Primer Design Guidelines. Biosoft, P., http://www.premierbiosoft.com/tech_notes/PCR_Primer_Design.html. (accessed 13 March 2015).
147. Usage instructions PHUSER primer design. analysis, C. f. b. s., http://www.cbs.dtu.dk/services/PHUSER/instructions.php. (accessed 13 March 2015).
148. Wallace, R. B., et al., Hybridization of synthetic oligodeoxyribonucleotides to phi chi 174 DNA: the effect of single base pair mismatch. *Nucleic Acids Res*, **1979**, 6, 3543-3557.
149. Nkansah, E. In vitro studies of STAT3 dimerisation and DNA binding. UCL School of Pharmacy, **2011**.
150. Bradford, M. M., A rapid and sensitive method for the quantitation of microgram quantities of protein utilizing the principle of protein-dye binding. *Analytical biochemistry*, **1976**, 72, 248-54.
151. Hu, L. Q., et al., Discovery of a small-molecule inhibitor and cellular probe of Keap1-Nrf2 protein-protein interaction. *Bioorganic & medicinal chemistry letters*, **2013**, 23, 3039-3043.
152. T., F. In Transfer mechanisms of electronic excitation., 10th spiers memorial lecture, Discussions of the Faraday Society. , **1959**, 7-17.
153. Jablonski, A., Efficiency of Anti-Stokes Fluorescence in Dyes. *Nature*, **1933**, 131, 839-840.
154. Damjanovich, S., Fluorescence energy transfer (FRET). In Biophysical aspects of transmembrane signalling, Schreck, S., Ed. Springer Science & Business Media, **2006**.
155. Clegg, R. M., Förster resonance energy transfer - FRET what is it, why do it, and how it's done. In Laboratory Techniques in Biochemistry and Molecular Biology, Gadella, T. W. J., Ed. Elsevier B.V., **2009**, Vol. 33, 38.
156. Selvin, P. R., Fluorescence resonance energy transfer. In Methods in Enzymology, Kenneth, S., Ed. Academic Press, **1995**, Vol. 246, 300-334.
157. Pollok, B. A.; Heim, R., Using GFP in FRET-based applications. *Trends in Cell Biology*, **1999**, 9, 57-60.
158. Perez-Jimenez, R., et al., Mechanical unfolding pathways of the enhanced yellow fluorescent protein revealed by single molecule force spectroscopy. *The Journal of biological chemistry*, **2006**, 281, 40010-4.
159. Rizzo, M. A., et al., An improved cyan fluorescent protein variant useful for FRET. *Nature biotechnology*, **2004**, 22, 445-9.

160. Pettersen, E. F., et al., UCSF Chimera--a visualization system for exploratory research and analysis. *Journal of computational chemistry*, **2004**, 25, 1605-12.
161. Chen, Y., et al., Kinetic Analyses of Keap1-Nrf2 Interaction and Determination of the Minimal Nrf2 Peptide Sequence Required for Keap1 Binding Using Surface Plasmon Resonance. *Chemical biology & drug design*, **2011**, 78, 1014-1021.
162. Inoyama, D., et al., Optimization of Fluorescently Labeled Nrf2 Peptide Probes and the Development of a Fluorescence Polarization Assay for the Discovery of Inhibitors of Keap1-Nrf2 Interaction. *Journal of Biomolecular Screening*, **2012**, 17, 435-447.
163. Pierce, M. M., et al., Isothermal titration calorimetry of protein-protein interactions. *Methods*, **1999**, 19, 213-21.
164. Liang, Y., Applications of isothermal titration calorimetry in protein science. *Acta biochimica et biophysica Sinica*, **2008**, 40, 565-76.
165. Zhou, X., et al., A universal method for fishing target proteins from mixtures of biomolecules using isothermal titration calorimetry. *Protein science : a publication of the Protein Society*, **2008**, 17, 1798-804.
166. Ladbury, J. E., et al., Adding calorimetric data to decision making in lead discovery: a hot tip. *Nature reviews. Drug discovery*, **2010**, 9, 23-7.
167. Lea, W. A.; Simeonov, A., Fluorescence polarization assays in small molecule screening. *Expert opinion on drug discovery*, **2011**, 6, 17-32.
168. Guimarães, A. M. R. PhD thesis: screening molecular interactions for drug discovery. UCL, School of Pharmacy, **2013**.
169. Nkansah, E., et al., Observation of unphosphorylated STAT3 core protein binding to target dsDNA by PEMSA and X-ray crystallography. *FEBS letters*, **2013**, 587, 833-9.
170. Hancock, R., et al., Peptide inhibitors of the Keap1-Nrf2 protein-protein interaction with improved binding and cellular activity. *Organic & biomolecular chemistry*, **2013**, 11, 3553-7.
171. Cubitt, A. B., et al., Understanding, improving and using green fluorescent proteins. *Trends in biochemical sciences*, **1995**, 20, 448-55.
172. Tsien, R. Y., The green fluorescent protein. *Annu Rev Biochem*, **1998**, 67, 509-44.
173. Shi, Y., et al., Abnormal SDS-PAGE migration of cytosolic proteins can identify domains and mechanisms that control surfactant binding. *Protein science : a publication of the Protein Society*, **2012**, 21, 1197-209.
174. Jecklin, M. C., et al., Label-free determination of protein-ligand binding constants using mass spectrometry and validation using surface plasmon resonance and isothermal titration calorimetry. *Journal of molecular recognition : JMR*, **2009**, 22, 319-29.
175. Song, Y., et al., Development of FRET assay into quantitative and high-throughput screening technology platforms for protein-protein interactions. *Annals of biomedical engineering*, **2011**, 39, 1224-34.
176. Baird, L., et al., Monitoring Keap1-Nrf2 interactions in single live cells. *Biotechnology advances*, **2014**, 32, 1133-44.
177. Qin QP, P. O., Pettersson K, Time-resolved fluorescence resonance energy transfer assay for point-of-care testing of urinary albumin. *Clinical Chemistry*, **2003**, 49, 1105-1113.
178. Jensen, E. C., The basics of western blotting. *Anatomical record*, **2012**, 295, 369-71.
179. Parnas, D.; Linial, M., Highly sensitive ELISA-based assay for quantifying protein levels in neuronal cultures. *Brain Research Protocols*, **1998**, 2, 333-338.

180. Grupillo, M., et al., An improved intracellular staining protocol for efficient detection of nuclear proteins in YFP-expressing cells. *BioTechniques*, **2011**, 51, 417-20.
181. Pandey, G. S., et al., Detection of intracellular Factor VIII protein in peripheral blood mononuclear cells by flow cytometry. *BioMed research international*, **2013**, 2013, 793502.
182. Macey, M. G., Flow Cytometry: Principles and Applications. Humana Press, **2007**.
183. Cho, S. H., et al., Review Article: Recent advancements in optofluidic flow cytometer. *Biomicrofluidics*, **2010**, 4.
184. Shapiro, H. M., How Flow Cytometers Work. In Practical Flow Cytometry, John Wiley & Sons, Inc., **2005**, 101-223.
185. Brown, M.; Wittwer, C., Flow Cytometry: Principles and Clinical Applications in Hematology. *Clinical Chemistry*, **2000**, 46, 1221-1229.
186. Maecker, H. T.; Trotter, J., Flow cytometry controls, instrument setup, and the determination of positivity. *Cytometry. Part A : the journal of the International Society for Analytical Cytology*, **2006**, 69, 1037-42.
187. Dickinson, J.; Fowler, S., Quantification of Proteins on Western Blots Using ECL. In The Protein Protocols Handbook, Walker, J., Ed. Humana Press, **2002**, 429-437.
188. Krutzik, P. O.; Nolan, G. P., Intracellular phospho-protein staining techniques for flow cytometry: monitoring single cell signaling events. *Cytometry. Part A : the journal of the International Society for Analytical Cytology*, **2003**, 55, 61-70.
189. Krutzik, P. O., et al., Analysis of protein phosphorylation and cellular signaling events by flow cytometry: techniques and clinical applications. *Clinical immunology*, **2004**, 110, 206-21.
190. Doan, L. L., et al., Intranuclear staining of proteins in heterogeneous cell populations and verification of nuclear localization by flow cytometric analysis. *Journal of immunological methods*, **2003**, 279, 193-8.
191. Irena Koutna, P. S., Petra Ondračkova and Lenka Tesarrova, Flow Cytometry Analysis of Intracellular Protein. In Flow Cytometry - Recent Perspectives, Schmid, M. S. I., Ed. InTech, **2012**.
192. Walker, J. M., Flow Cytometric Quantitation of Cellular Proteins. In The Protein Protocols Handbook, Walker, J. M., Ed. Springer Science & Business Media, **2002**.
193. Jaye, D. L., et al., Translational Applications of Flow Cytometry in Clinical Practice. *The Journal of Immunology*, **2012**, 188, 4715-4719.
194. Pala, P., et al., Flow cytometric measurement of intracellular cytokines. *Journal of immunological methods*, **2000**, 243, 107-124.
195. Festuccia, N.; Chambers, I., Quantification of pluripotency transcription factor levels in embryonic stem cells by flow cytometry. *Current protocols in stem cell biology*, **2011**, Chapter 1, Unit 1B.9.
196. Garcia-Garcia, E., et al., A simple and efficient method to detect nuclear factor activation in human neutrophils by flow cytometry. *Journal of visualized experiments : JoVE*, **2013**.
197. Rosner, M., et al., Merging high-quality biochemical fractionation with a refined flow cytometry approach to monitor nucleocytoplasmic protein expression throughout the unperturbed mammalian cell cycle. *Nature protocols*, **2013**, 8, 602-26.
198. Hu, X., et al., Accelerated ovarian failure induced by 4-vinyl cyclohexene diepoxide in Nrf2 null mice. *Molecular and cellular biology*, **2006**, 26, 940-54.
199. Kelloff, G. J., et al., Cancer Chemoprevention: Volume 2: Strategies for Cancer Chemoprevention. Humana Press, **2008**.
200. Biosciences, B. Introduction to Flow Cytometry: A Learning Guide **2000**, p. 26.

201. Van Dam, P. A., Flow Cytometry Data Analysis. Basic Concepts and Statistics. *Journal of Clinical Pathology*, **1993**, 46, 975-975.
202. Chan, L. Y., et al., Normalized median fluorescence: an alternative flow cytometry analysis method for tracking human embryonic stem cell states during differentiation. *Tissue engineering. Part C, Methods*, **2013**, 19, 156-65.
203. Thavarajah, R., et al., Chemical and physical basics of routine formaldehyde fixation. *Journal of Oral and Maxillofacial Pathology : JOMFP*, **2012**, 16, 400-405.
204. Niki, H., et al., A new immunofluorostaining method using red fluorescence of PerCP on formalin-fixed paraffin-embedded tissues. *Journal of immunological methods*, **2004**, 293, 143-51.
205. NE-PER Nuclear and Cytoplasmic Extraction Reagents. http://www.piercenet.com/product/ne-per-nuclear-protein-extraction-kit.
206. Hasbold, J.; Hodgkin, P. D., Flow cytometric cell division tracking using nuclei. *Cytometry*, **2000**, 40, 230-7.
207. Rosner, M.; Hengstschlager, M., Cytoplasmic and nuclear distribution of the protein complexes mTORC1 and mTORC2: rapamycin triggers dephosphorylation and delocalization of the mTORC2 components rictor and sin1. *Human molecular genetics*, **2008**, 17, 2934-48.
208. Hayes, J. D.; McMahon, M., NRF2 and KEAP1 mutations: permanent activation of an adaptive response in cancer. *Trends in biochemical sciences*, **2009**, 34, 176-88.
209. Myzak, M. C.; Dashwood, R. H., Chemoprotection by sulforaphane: keep one eye beyond Keap1. *Cancer letters*, **2006**, 233, 208-18.
210. Clarke, J. D., et al., Differential effects of sulforaphane on histone deacetylases, cell cycle arrest and apoptosis in normal prostate cells versus hyperplastic and cancerous prostate cells. *Molecular nutrition & food research*, **2011**, 55, 999-1009.
211. Fimognari, C., et al., A mutated p53 status did not prevent the induction of apoptosis by sulforaphane, a promising anti-cancer drug. *Investigational new drugs*, **2005**, 23, 195-203.
212. Asher, G., et al., The crystal structure of NAD(P)H quinone oxidoreductase 1 in complex with its potent inhibitor dicoumarol. *Biochemistry*, **2006**, 45, 6372-8.
213. Vichai, V.; Kirtikara, K., Sulforhodamine B colorimetric assay for cytotoxicity screening. *Nat. Protocols*, **2006**, 1, 1112-1116.
214. Voigt, W., Sulforhodamine B assay and chemosensitivity. *Methods in molecular medicine*, **2005**, 110, 39-48.
215. Baird, L., et al., Regulatory flexibility in the Nrf2-mediated stress response is conferred by conformational cycling of the Keap1-Nrf2 protein complex. *Proceedings of the National Academy of Sciences of the United States of America*, **2013**, 110, 15259-64.
216. Itoh, K., et al., Keap1 regulates both cytoplasmic-nuclear shuttling and degradation of Nrf2 in response to electrophiles. *Genes to cells : devoted to molecular & cellular mechanisms*, **2003**, 8, 379-91.
217. Lee, Y.-J.; Lee, S.-H., Sulforaphane Induces Antioxidative and Antiproliferative Responses by Generating Reactive Oxygen Species in Human Bronchial Epithelial BEAS-2B Cells. *Journal of Korean Medical Science*, **2011**, 26, 1474-1482.
218. Criddle, D. N., et al., Menadione-induced reactive oxygen species generation via redox cycling promotes apoptosis of murine pancreatic acinar cells. *The Journal of biological chemistry*, **2006**, 281, 40485-92.
219. Anwar-Mohamed, A.; El-Kadi, A. O., Sulforaphane induces CYP1A1 mRNA, protein, and catalytic activity levels via an AhR-dependent pathway in murine hepatoma Hepa 1c1c7 and human HepG2 cells. *Cancer letters*, **2009**, 275, 93-101.
220. Gomez-Lechon, M. J., et al., The use of hepatocytes to investigate drug toxicity. *Methods in molecular biology (Clifton, N.J.)*, **2010**, 640, 389-415.

221. Abdull Razis, A., et al., The naturally occurring aliphatic isothiocyanates sulforaphane and erucin are weak agonists but potent non-competitive antagonists of the aryl hydrocarbon receptor. *Arch Toxicol*, **2012**, 86, 1505-1514.
222. Dinkova-Kostova, A. T., et al., Potency of Michael reaction acceptors as inducers of enzymes that protect against carcinogenesis depends on their reactivity with sulfhydryl groups. *Proceedings of the National Academy of Sciences of the United States of America*, **2001**, 98, 3404-9.
223. Lyss, G., et al., The anti-inflammatory sesquiterpene lactone helenalin inhibits the transcription factor NF-kappaB by directly targeting p65. *The Journal of biological chemistry*, **1998**, 273, 33508-16.
224. Johansson, M. H., Reversible Michael additions: covalent inhibitors and prodrugs. *Mini reviews in medicinal chemistry*, **2012**, 12, 1330-44.
225. Zheng, S., et al., Synthesis, chemical reactivity as Michael acceptors, and biological potency of monocyclic cyanoenones, novel and highly potent anti-inflammatory and cytoprotective agents. *Journal of medicinal chemistry*, **2012**, 55, 4837-46.
226. Chen, Y., et al., Kinetic analyses of Keap1-Nrf2 interaction and determination of the minimal Nrf2 peptide sequence required for Keap1 binding using surface plasmon resonance. *Chemical biology & drug design*, **2011**, 78, 1014-21.
227. Marcotte, D., et al., Small molecules inhibit the interaction of Nrf2 and the Keap1 Kelch domain through a non-covalent mechanism. *Bioorganic & medicinal chemistry*, **2013**, 21, 4011-9.
228. Broad Institute, M., Fluorescence polarization to screen for inhibitors that disrupt the protein-protein interaction between Keap1 and Nrf2 Measured in Biochemical System Using Plate Reader - 2119-01_Inhibitor_Dose_CherryPick_Activity.
http://pubchem.ncbi.nlm.nih.gov/assay/assay.cgi?aid=504540, **2011**.
229. Bertrand, H. C., et al., The design, synthesis and evaluation of triazole derivatives that induce Nrf2 dependent gene products and inhibit the Keap1-Nrf2 protein-protein interaction. UCL School of Pharmacy: **2015**.
230. Vives, E., et al., A truncated HIV-1 Tat protein basic domain rapidly translocates through the plasma membrane and accumulates in the cell nucleus. *The Journal of biological chemistry*, **1997**, 272, 16010-7.
231. Bechara, C.; Sagan, S., Cell-penetrating peptides: 20 years later, where do we stand? *FEBS letters*, **2013**, 587, 1693-702.
232. Lim, K. J., et al., A cancer specific cell-penetrating peptide, BR2, for the efficient delivery of an scFv into cancer cells. *PloS one*, **2013**, 8, e66084.
233. Pocar, P., et al., Molecular interactions of the aryl hydrocarbon receptor and its biological and toxicological relevance for reproduction. *Reproduction (Cambridge, England)*, **2005**, 129, 379-89.
234. Weisberg, E., et al., Second generation inhibitors of BCR-ABL for the treatment of imatinib-resistant chronic myeloid leukaemia. *Nat Rev Cancer*, **2007**, 7, 345-356.
235. Huther, A.; Dietrich, U., The emergence of peptides as therapeutic drugs for the inhibition of HIV-1. *AIDS reviews*, **2007**, 9, 208-17.
236. Potocky, T. B., et al., Cytoplasmic and nuclear delivery of a TAT-derived peptide and a beta-peptide after endocytic uptake into HeLa cells. *The Journal of biological chemistry*, **2003**, 278, 50188-94.
237. Duchardt, F., et al., A Comprehensive Model for the Cellular Uptake of Cationic Cell-penetrating Peptides. *Traffic*, **2007**, 8, 848-866.
238. Steel, R., et al., Anti-inflammatory Effect of a Cell-Penetrating Peptide Targeting the Nrf2/Keap1 Interaction. *ACS medicinal chemistry letters*, **2012**, 3, 407-410.

239. Arkin, M. R.; Wells, J. A., Small-molecule inhibitors of protein-protein interactions: progressing towards the dream. *Nat Rev Drug Discov*, **2004**, 3, 301-17.
240. Wang, F., et al., Identifying target genes of the aryl hydrocarbon receptor nuclear translocator (Arnt) using DNA microarray analysis. *Biological chemistry*, **2006**, 387, 1215-8.
241. Patterson, S.; Wyllie, S., Nitro drugs for the treatment of trypanosomatid diseases: past, present, and future prospects. *Trends in Parasitology*, **2014**, 30, 289-298.
242. Pocar, P., et al., Molecular interactions of the aryl hydrocarbon receptor and its biological and toxicological relevance for reproduction. *Reproduction (Cambridge, England)*, **2005**, 129, 379-389.
243. Ding, W.-X.; Yin, X.-M., Mitophagy: mechanisms, pathophysiological roles, and analysis. *Biological chemistry*, **2012**, 393, 547-564.
244. East, Daniel A., et al., PMI: A ΔΨ(m) Independent Pharmacological Regulator of Mitophagy. *Chemistry & Biology*, **2014**, 21, 1585-1596.
245. Nowakowska, Z., A review of anti-infective and anti-inflammatory chalcones. *European Journal of Medicinal Chemistry*, **2007**, 42, 125-137.
246. Ashida, H., et al., An update on the dietary ligands of the AhR. *Expert Opinion on Drug Metabolism & Toxicology*, **2008**, 4, 1429-1447.
247. Kumar, V., et al., Novel chalcone derivatives as potent Nrf2 activators in mice and human lung epithelial cells. *Journal of medicinal chemistry*, **2011**, 54, 4147-59.
248. Lopez-Velez, M., et al., The study of phenolic compounds as natural antioxidants in wine. *Critical reviews in food science and nutrition*, **2003**, 43, 233-44.
249. Ungvari, Z., et al., Resveratrol confers endothelial protection via activation of the antioxidant transcription factor Nrf2. *American journal of physiology. Heart and circulatory physiology*, **2010**, 299, H18-24.
250. Walle, T., et al., High absorption but very low bioavailability of oral resveratrol in humans. *Drug metabolism and disposition: the biological fate of chemicals*, **2004**, 32, 1377-82.
251. Mayhoub, A. S., et al., Optimizing thiadiazole analogues of resveratrol versus three chemopreventive targets. *Bioorganic & medicinal chemistry*, **2012**, 20, 510-20.
252. Furet, P., et al., Aromatic interactions with phenylalanine 691 and cysteine 828: a concept for FMS-like tyrosine kinase-3 inhibition. Application to the discovery of a new class of potential antileukemia agents. *Journal of medicinal chemistry*, **2006**, 49, 4451-4.
253. Niture, S. K.; Jaiswal, A. K., INrf2 (Keap1) targets Bcl-2 degradation and controls cellular apoptosis. *Cell death and differentiation*, **2011**, 18, 439-51.
254. Tian, H., et al., Keap1: one stone kills three birds Nrf2, IKKbeta and Bcl-2/Bcl-xL. *Cancer letters*, **2012**, 325, 26-34.
255. Li, X., et al., Crystal structure of the Kelch domain of human Keap1. *The Journal of biological chemistry*, **2004**, 279, 54750-8.
256. O'Keefe, E. P., siRNAs and shRNAs: Tools for Protein Knockdown by Gene Silencing. *Materials and Methods*, **2013**, 3.

List of publications

Publications from the thesis work:

Schaap, M. C. A.; Guimarães, A. M. R.; Wilderspin, A. F.; Wells, G. Protocol for a steady-state FRET assay in cancer chemoprevention. *Cancer Chemoprevention*, *Methods Mol. Biol*. **2016**, 1379, 165-179. Ed. Strano, C. Springer, New York.

Bertrand, H. C.; Schaap, M.; Baird, L.; Georgakopoulos, N. D.; Fowkes, A.; Thiollier, C.; Kachi, H.; Dinkova-Kostova, A. T.; Wells, G. The design, synthesis and evaluation of triazole derivatives that induce Nrf2 dependent gene products and inhibit the Keap1-Nrf2 protein-protein interaction. *J. Med. Chem.* **2015**, 58, 7186-7194.

East, D. A.; Fagiani, F.; Crosby, J.; Georgakopoulos, N. D.; Bertrand, H.; Schaap, M.; Fowkes, A.; Wells, G.; Campanella, M. PMI: a $\Delta\Psi_m$ independent pharmacological regulator of mitophagy. *Chem. Biol.* **2014**, 21, 1585-1596.

Schaap, M.; Hancock, R.; Wilderspin, A.; Wells, G. Development of a steady-state FRET-based assay to identify inhibitors of the Keap1-Nrf2 protein-protein interaction. *Prot. Sci.* **2013**, 22, 1812-1819.

Hancock, R.; Schaap, M.; Pfister, H.; Wells, G. Peptide inhibitors of the Keap1-Nrf2 protein-protein interaction with improved binding and cellular activity. *Org. Biomol. Chem.* **2013**, 11, 3553-3557.

Poster abstracts:

Fowkes, A.; Schaap, M.; Bertrand, H.; Thiollier, C.; Kachi, H.; Wells, G. The biological evaluation of small molecule inducers of Nrf2 transcriptional activity that inhibit the Keap1-Nrf2 protein-protein interaction. (presentation at the AACR-NCI-EORTC Molecular Targets and Cancer Therapeutics Meeting, October 2013)